Universität der Bundeswehr München
Fakultät für Elektrotechnik und Informationstechnik
Institut für Hoch- und Höchstfrequenztechnik

Ultra Short Multiband AM/FM/DAB Active Antennas for Automotive Application

Alexandru Negut

Zur Erlangung des akademischen Grades eines

DOKTOR-INGENIEURS
(Dr.-Ing.)

von der Fakultät für Elektrotechnik und Informationstechnik
der Universität der Bundeswehr München genehmigte

DISSERTATION

Tag der Prüfung: 18. November 2011

Vorsitzender des Promotionsausschusses:	Prof. Dr.-Ing. habil. W. Pascher
1. Berichterstatter:	Prof. Dr.-Ing. habil. S. Lindenmeier
2. Berichterstatter:	Prof. Dr.-Ing. habil. U. Barabas

Neubiberg, den 6. Dezember 2011

Acknowledgments

It is with great pleasure to acknowledge the opportunity Prof. Dr.-Ing. habil. Stefan Lindenmeier offered me when he accepted to work out my PhD thesis within the Institute of High Frequency Technology and Mobile Communication, University of the Bundeswehr Munich. I am deeply indebted to him for introducing me to this exciting field and for providing constant guidance and support.

Prof. Dr.-Ing. habil. Udo Barabas is thanked to for being the second reviewer of this thesis.

The vast experience of Apl. Prof. Dr.-Ing. habil. Leopold Reiter in the field of active antennas – but not only – is especially acknowledged, as the knowledge I acquired during this time would have surely been less without his support. I warmly thank him for the fruitful and friendly cooperation.

Long and fruitful discussions with Apl. Prof. Dr.-Ing. habil. Jochen Hopf are gratefully acknowledged, as his rich experience proved invaluable in clarifying many theoretical and practical details.

I also thank Dr.-Ing. Joachim Brose for his kind help whenever it was needed and the electromagnetic simulations contributed to this work.

I wish to express my gratitude to Mr. Oliver Kindt and Mr. Markus Mittermeier, as the realization of the prototypes and of many other mechanical works would not have been possible without their help and commitment. I also thank Mr. Bernd Wahnschaffe especially for his professional help in taking the pictures used throughout this work.

Special thanks to our institute team assistants, Ms. Inge Bajda, Ms. Mariella Ose and Ms. Manuela Wolf, whose help and cooperation proved invaluable in so many cases.

I am indebted to Apl. Prof. L. Reiter, Apl. Prof. J. Hopf and Dipl.-Ing. S. Senega for kindly undertaking the task of reviewing the manuscript and providing valuable feed-back.

All my colleagues have to be thanked to for the extraordinary friendly and fruitful working atmosphere at the institute, which allowed for a fervent experience exchange.

Delphi Delco Electronics Europe GmbH is acknowledged for the support offered to this project and the manufactured prototypes.

Last, but not least, I thank my parents for their trust and constant encouragement. The linguistic suggestions my mother made did help improve the English manuscript and are therefore warmly acknowledged.

Neubiberg, Germany, December 2011 **Alexandru Negut**

Contents

Acronyms List

AC	alternating current
ADR	Astra Digital Radio
AGC	automatic gain control
AM	amplitude modulation
CCHA	capacitive coupled helical antenna
CMOS	complementary metal-oxide-semiconductor
COFDM	coded orthogonal frequency-division multiplexing
DAB	Digital Audio Broadcasting
DC	direct current
DSR	Digital Satellite Radio
DUT	device under test
EMC	electromagnetic compatibility
ESD	electrostatic discharge
FET	field effect transistor
FM	frequency modulation
GaAs	gallium-arsenide
GPS	Global Positioning System
GSM	Global System for Mobile Communications
HEMT	high electron mobility transistor
HIA	high-impedance amplifier

JFET	junction field effect transistor
LNA	low-noise amplifier
LW	long-wave
MESFET	metal semiconductor field effect transistor
MOSFET	metal oxide field effect transistor
MW	medium-wave
PCB	printed circuit board
RF	radio frequency
RMS	root mean square
Si	silicon
SiGe	silicon-germanium
SMD	surface mounted device
SNR	signal-to-noise ratio
SW	short-wave
TMC	Traffic Message Channel
UKW	ultra short wave
VDA	Verband der Automobilindustrie
VHF	very high frequency
VLSI	very large scale integration
VNA	vector network analyzer

Chapter 1

Introduction and Thesis Overview

This thesis embodies the work I have done in the field of automotive active antennas at the Institute of High Frequency Technology and Mobile Communication within the University of the Bundeswehr Munich under the guidance of Univ.-Prof. Dr.-Ing. habil. Stefan Lindenmeier.

The length reduction of rod antennas is nowadays a major concern in the automotive industry. The need for new shorter rods stems from the desire to fulfil the design aesthetics of modern cars and to alleviate the mechanical issues the longer rods have. However, despite the severe length reduction, the short rods have to perform at least as good as the 40 cm long active monopoles usually met nowadays. In this context, the present thesis investigates the possibilities to use for AM, FM and Digital Audio Broadcasting (DAB) broadcast reception in an automotive environment 20 cm long active monopole antennas and 14 cm long active helical elements. Concerning the FM reception, both Japanese and European bands are simultaneously targeted, so that the resulting active antenna does not have to be readjusted.

Electrically very short active antennas are challenging because the very low effective height of the antenna element and its inconvenient antenna impedance with a highly reactive character pose important constrains upon the antenna amplifier. The amplifier has to have high input impedance, which has to be increasingly higher, as the antenna impedance gets also higher. At the same time, the amplifier has to exhibit enough gain and low noise character, in order to achieve good sensitivity. There are also important requirements to be fulfilled concerning its linearity.

A simple 20 cm long monopole is firstly considered as a convenient implementation for AM and FM reception. As it will become clear throughout this work, simply reducing the monopole length does not yield the desired FM performance, even when advanced antenna amplifiers are employed. The main concern is in this case the sensitivity degradation caused by the poor effective height of the antenna and the small antenna capacitance. Nevertheless, in the AM range the measured performance (i.e. output signal-to-noise ratio in this case) achieved by the active antenna developed in the present work is only about 4 dB below the one provided by

the 90 cm long passive monopole. This outstanding result is important because all the antenna elements investigated here perform similarly (from an electrical point of view) in the AM range. As a consequence, the AM amplifier proposed here allows them to be successfully used also for AM reception.

In order to alleviate these disadvantages, a novel antenna structure is used instead. It consists of a helix with capacitive coupling, thus enabling the shaping of the antenna impedance and the improvement of its effective height. This allows for a rod shortening to only about 14 cm. In order to highlight the visual difference thus achieved, Fig. 1.1 compares it to a state of the art 40 cm monopole. It will be shown that only high-input impedance amplifiers are suited to be used together with this type of antennas. In this combination, however, the active antenna exhibits an undesired resonance which has to be compensated by the amplifier. An extensive investigation has the purpose of finding out the best suited amplifier architecture for which design considerations and experimental results are presented and discussed.

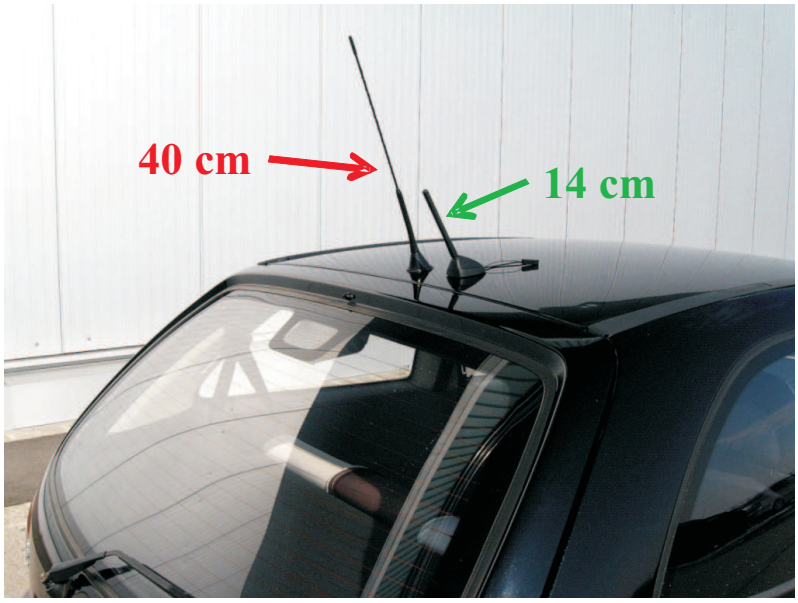

Fig. 1.1: The 14 cm active capacitive coupled helical antenna (CCHA) next to a commercial 40 cm long active monopole, both mounted on the top of a car.

Measurements confirm that the novel ultra-short 14 cm helical active antenna performs better than the 20 cm long active monopole antenna and achieves in average about the same signal level as a passive 90 cm long monopole antenna. The measured sensitivity is comparable to the one attained by 40 cm long active rod antennas and is sustained over the entire European and Japanese FM ranges, as shown in Fig. 1.2. To the best of our knowledge, this is the first time when such sensitivity is achieved with such a short antenna element. Furthermore, this novel active antenna fulfills the linearity requirements and therefore does not need additional automatic gain control circuitry.

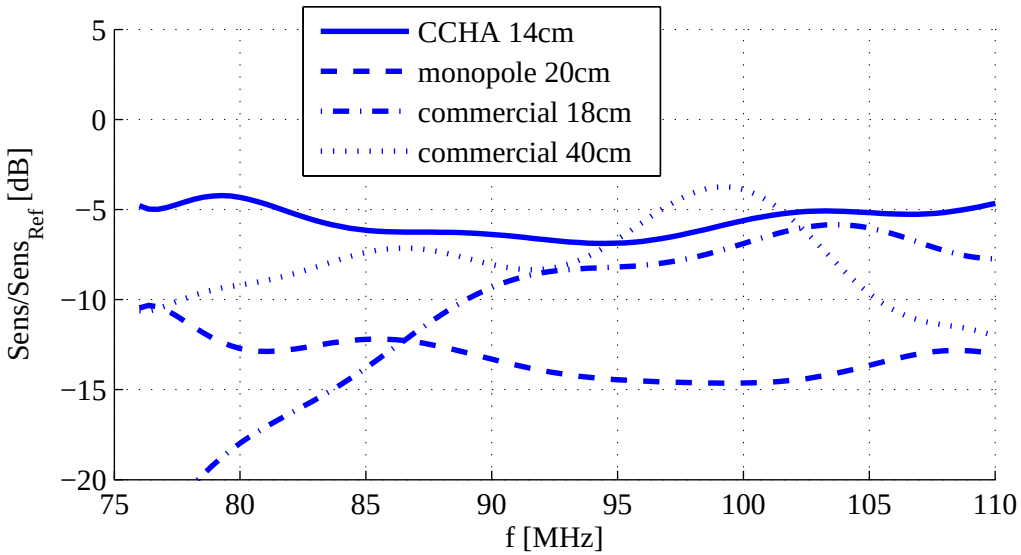

Fig. 1.2: Measured FM sensitivity of different active antennas. Results are referred to the 90 cm long passive reference rod antenna. The 20 cm active monopole and the 14 cm active capacitive coupled helical antenna (CCHA) have been developed throughout this work.

The steady increasing popularity of DAB demands adequate solutions for its reception in cars. As a result the need arises to develop an ultra-short active antenna which has besides AM and FM also DAB capabilities in both Band-III and L-Band. As the 14 cm short capacitive coupled helical structure proves to be a good solution for AM and FM, this work investigates further the possibility to receive also DAB signals with the same antenna. The DAB L-Band does not prove to be an issue, as the rod can be such designed in order to use for the higher frequencies only a small part of it as a $\lambda/4$ monopole; instead, the reception of DAB Band-III signals proves to be much more challenging, as this frequency band is not far enough from the FM one and the amplifier may be subject to undesired FM to DAB conversions. In this context the thesis concentrates on investigating the best suited amplifier topologies for a high performance AM/FM/DAB ultra-short active antenna.

The analysis and the experimental measurements show that a single-transistor FM/DAB amplifier provides good performance but cannot overcome the FM–Band-III intermodulation issue without the use of automatic gain control (AGC) circuitry. It has, however, the advantage of being an ultra-compact solution with low part-count and low demands concerning the input path.

This particular intermodulation issue can be overcome by introducing a separate Band-III amplifier path, while the FM and L-Band can be partly processed together. However, in this approach special care has to be taken in order to separate the FM and DAB-Band-III signals on the input path. The filters required for this task have to introduce little losses and at the same time to mask well enough each path from

the other, so that no additional loading degrades the signal. The implementation proposed in this work successfully manages to split and combine the different signal paths; this, however, at the cost of a lower signal performance in the FM band and lower DAB-Band-III noise performance. In the L-Band such an active antenna provides excellent gain and noise characteristics.

The thesis is structured as follows:

Chapter 1 provides a thesis overview and highlights the achieved results.

Chapter 2 introduces the problematic of radio reception in cars. The broadcasting services addressed in this work (AM, FM and DAB) are briefly presented, in order to highlight their particularities, including the propagation of the corresponding electromagnetic waves. A general discussion concerning the automotive antennas, their antenna amplifiers and the car radio receivers follows, having the purpose of briefly reviewing their development over the last decades. It also introduces the particularities of radio reception in cars.

Chapter 3 reviews basic concepts about short monopole antennas. The most important issues concerning the noise in electronic systems are reminded, as noise is a major limitation factor to the design and use of active receiving systems. The external noise picked-up by an antenna is also discussed. In the end, active antenna theory is reviewed and the performance improvement brought by it when compared to their passive counterparts is highlighted.

Chapter 4 moves the discussion towards the antenna amplifier itself and discusses the parameters and requirements for car active antennas, especially concerning gain, noise and linearity. Two important design considerations, the gate biasing resistor and the noise of different commercial transistors are investigated. A description of the measurement methods employed throughout this work is given.

Chapter 5 explores the possibility to use for automotive AM/FM application a very short only 20 cm long active monopole antenna. The first design investigated consists of a single AM/FM amplifier, which distinguishes itself by simplicity and low costs, but does not succeed in coping with the FM to AM conversion. The second architecture investigated contains two different paths for the AM and FM bands, thus improving the linearity issues. The parameters and the conditions which determine the performance of the designs are investigated and explained and measurement results are presented and discussed.

Chapter 6 introduces an amplifier structure which is optimized to be used with a novel, only 14 cm long thin helical antenna featuring a capacitive coupling. Am-

plifier architectures which flatten the frequency response of the very short resonant antenna are investigated, while maintaining a low noise level and a good linearity. The design analysis and experimental results are shown for the proposed high input impedance amplifier concept which succeeds in coping with the requirements.

Chapter 7 explores the possibilities to extend the use of the ultra-short thin helical antenna featuring a capacitive coupling also to the DAB service in both Band-III and L-Band. An appropriate amplifier architecture is sought for, which is able to manage the nonlinear and filtering issues, while maintaining low noise and good sensitivity. Two different amplifier designs are proposed and their advantages and disadvantages are discussed based on computational analysis and experimental measurements.

Chapter 8 summarizes the conclusions and overviews the results achieved throughout this work.

Appendix A reviews the equivalent noise circuit for two-ports and the concept of optimum noise impedance.

Appendix B overviews the different field effect transistor technologies appliable for the design of ultra short active antennas. Their noise mechanisms and noise models are also discussed.

Chapter 2

State of the Art of Mobile Car Antennas for Radio Reception

Not long after the spread of the commercial radio broadcasting, car owners had the desire to have radio receivers also on the road, so that there were attempts to accommodate domestic radio sets into cars. The first professional devices designed and manufactured especially for automotive applications appeared at the beginning of the '30, like for example the radios from Motorola and Blaupunkt. This was the result of becoming aware of the car environment specific issues, like the lack of space, the need for robust mechanical and electrical designs and the electromagnetic interference.

The first car radios received only amplitude modulation (AM) and had to be powered using vibrators, in order to step-up the low battery voltage to the value required by the vacuum tubes contained in the radio. The following decades brought continuous improvements and changes from vacuum tubes to robust low-voltage discrete transistors and later integrated circuits. The radio-set was upgraded to become a hi-fi audio system, by adding more and more sophisticated audio amplifiers and loudspeaker systems and incorporating cassette players and later CD and MP3 players. The radio receiver itself became multi-service, being able to receive also frequency modulation (FM) and later DAB and satellite radio, while the trend continues towards an even larger service integration.

Present-day car radios are rather complex entertainment systems, which have become standard equipment for cars and can be found in a wide variety from various manufactures. However, a good receiver delivers its best performance only in combination with a good antenna.

In the first decades of car radio history the simple rod antenna about 1 m long played the major role in reception. These antennas offered good performance both in AM and FM; however, such long whips have difficulties in coping with styling requirements, mechanical robustness and wind noise. Simply reducing the rod length brings important performance degradation, because the height reduction decreases proportionally the effective antenna height, increases its impedance and worsens the

obtainable bandwidth. This cannot be overcome as long as the antenna remains passive. Another important issue occurs when the antenna is electrically short and cannot be matched to the cable impedance; in this case there are certain constrains placed on the cable length and thus on the allowed distance between the passive antenna and the radio receiver.

Receiving radio in a mobile environment raises specific difficulties, as the situation is different in comparison to the home reception scenario. These phenomena, like the multipath propagation of the higher frequency waves, had to be first understood and correctly described by mathematical models. With the advances made in the antenna theory and the understanding of the issues involved in the mobile radio reception, new antenna structures had emerged, probably the most important of them being the window-printed type. At first passive, such a structure entirely fulfilled the mechanical automotive requirements, but had poor reception capability.

The major breakthrough came with the development of the active antenna, which approaches the design of the receiving system from a different angle. By connecting an amplifier with high-ohmic input impedance right after the antenna element and thus picking-up the voltage induced in the antenna without drawing power from it, a few delicate issues are being simultaneously overcome: the antenna size can be reduced without degrading its performance, while the impedance matching towards the cable is being alleviated, and so the constrains placed upon the cable length eliminated. Additionally, the mutual coupling between antennas in a compact array is being lowered, so that diversity becomes practical.

Based on these principles, the active version of the window-printed antenna has become very attractive and enjoys commercial success. The active rod antenna and the rear window printed type are nowadays the most common solutions for AM/FM radio reception. The window-printed active antenna is aesthetically superior and meets the automotive mechanical requirements, but it has to be specifically designed for each car type. For low-end cars the rod type antenna is common.

The non-linear issue still remains the major intrinsic drawback of active antennas, as any active device has a non-linear characteristic. The fact that the car travels leads to a very large dynamic range of the signal level picked-up by the antenna, which depends on the distance to different broadcast stations. A variety of large undesired signals may enter the amplifier, because the active antennas are wideband and do not perform any channel selection before the amplifier. Their exposure to intermodulation issues imposes important linearity-requirements for the antenna amplifier. Over the decades this issue has been alleviated by using better transistors and improved circuit techniques, so that the solutions available nowadays enable high linearity performance.

Concerning noise and sensitivity of active antennas, the advances made by the semiconductor devices allowed for a steady performance increase. Besides modern silicon (Si) transistors, the price reduction of high-performance gallium-arsenide (GaAs) devices enabled them to be also used for automotive active antennas.

Despite their simplicity and low price, 1 m long monopole antennas have mechanical disadvantages when it comes to requirements like robustness, low wind-noise, the capability to withstand mechanical stress without breaking and certain safety standards for impact. To this add the aesthetic considerations. As long as shrinking their size was not an option, retractable whip antennas have also been designed and produced, although such a solution increases the overall antenna price, as it adds a considerable amount of mechanics.

With the development of active antennas the rod became shorter, while maintaining a performance comparable to the 1 m long one. 40 cm and later 30 cm antennas mounted on the car roof or on a fender became standard for lower price category cars, for which no window-printed antenna is foreseen. Even today, among the rod antennas, these lengths are very common. The AM reception is active, while for the FM band both passive and active whips can be met.

Nevertheless, the trend for miniaturization doesn't stop here, as there is a strong demand for further reducing the size of car rod antennas as much as possible. This reduction is however dependent on the available amplifier technology. Another way to obtain very short rods is to modify the antenna element itself; for this purpose, special helical structures have recently been introduced, which can be optimized for certain operating bands. Although their manufacturing is basically more complicated, the performance improvement can be significant in comparison to simple monopole antennas. Helical active rods about 20 cm long already equip some cars.

Another trend is represented by the integration of as many services as possible in a single antenna. Traditional rod active antennas are designed for AM and FM reception. However, nowadays there is a steady increasing demand towards DAB, which offers better audio quality and is more suitable to mobile scenarios. Some active antenna modules are designed to accommodate mobile phone signals with the same antenna element as well. It is also aimed to design compact active antenna modules in which the monopole cohabitates with satellite antennas, like for example structures for Global Positioning System (GPS) and digital satellite radio.

Although there is a steady increase of the active antenna complexity, there is a strong demand to lower their prices, while maintaining the high automotive quality standards. This sets certain constrains and trade-offs upon the design, as they will be also highlighted throughout this work.

Next, a brief description of the broadcasting services addressed in this work is given in order to highlight their particularities and the propagation of the corresponding electromagnetic waves. This is followed by a general discussion concerning aspects of radio reception in cars: automotive antennas, antenna amplifiers and car radio receivers. This briefly reviews their development over the last decades and it also introduces the particularities of car radio reception.

2.1 Radio Broadcasting Services

For decades, the car radio sets meant the reception of only AM and FM stations. However, nowadays modern digital services, like DAB and digital satellite radio, add themselves to the traditional radio broadcasting panoply. In Europe, AM and FM radio sets continue to be standard equipment for cars, while DAB is available only in some countries and not as standard option for cars. Next, the characteristics and particularities of the AM, FM and DAB services will be briefly discussed, together with some aspects concerning the propagation of the radio waves in the corresponding bands.

2.1.1 AM Radio Broadcasting

Broadcasting using the AM as a mean of transmitting audio information is popularly called "AM radio" and the radio spectrum commonly used for this services is usually improperly called "the AM band". This interval is divided into three bands, ranging as follows:

- **long-wave (LW)** from 148.5 kHz to 283.5 kHz;
- **medium-wave (MW)** from 526.5 kHz to 1606.5 kHz;
- **short-wave (SW)** from 5.95 MHz to 26.1 MHz. Relevant for car radios is usually only the range between 5.95 MHz and 6.2 MHz.

The AM was the first radio broadcast method and is still in use nowadays. In this technique, the amplitude of the radio frequency (RF) carrier is continuously changed by the instantaneous value (amplitude) of the modulating signal. This results in the *double sideband amplitude modulation*, which means a translation of the modulating spectrum and its mirror image around the RF carrier. If the highest frequency in the modulating signal's spectrum is $f_{\mathrm{m,Max}}$, then the spectrum of the modulated signal has the bandwidth [1]:

$$B_{\mathrm{AM}} = 2 \cdot f_{\mathrm{m,Max}} \tag{2.1}$$

The double sideband amplitude modulation is not very energy and spectrum efficient, because the modulated signal contains the RF carrier (in which most of the energy is concentrated, although it carries no useful information) and the mirror image of the baseband spectrum (thus doubling the required RF bandwidth). More complex amplitude modulation schemes can suppress the carrier (double sideband suppressed carrier amplitude modulation) or even one of the sidebands (single sideband amplitude modulation) in order to increase the power and bandwidth efficiency.

However, for commercial broadcasting the double sideband modulation scheme is used. Due to its simplicity, it even allowed at the beginnings of the radio era the

use of receivers that contained no amplification devices. As the baseband signal is limited to 4.5 kHz in LW and MW (requiring 9 kHz RF bandwidth) and 2.5 kHz in SW, the audio quality is therefore low and improper for high-fidelity transmissions, as for example music channels require. However, the coverage attainable with these frequencies due to ground and skywave propagation and the simplicity of the modulation scheme still hold these services in use.

The diffraction of low frequency waves enables them to follow the curvature of the Earth, so that they can travel up to 1000 km (vertically polarized); this propagation mode is called *groundwave*. However, reflections in the ionosphere allow the propagation of the so called *skywave*, with which even longer distances can be covered. The reflective properties of the ionosphere are a function of the ionization (caused by the solar radiation), the signal frequency (better at lower frequencies) and incidence angle (better at higher angles) [2].

The lower frequency threshold for which skywaves occur is determined by the attenuation in the D-layer of the ionosphere (80 – 100 km altitude), which is larger for lower frequencies. Due to its insufficient ionization, this layer does not have reflective properties. Reflections in the E-layer of the ionosphere (100 – 120 km altitude) take place especially for frequencies below 6 MHz and allow a coverage up to 1500 km. Multiple reflections between the F2-layer (250 – 350 km altitude) and the earth can lead to a coverage of up to 12000 km.

The skywave propagation has the advantage of allowing extremely long-range radio connections, but is a strong function of the day-night cycle, season and latitude. Therefore it poses some constraints concerning reliability. However, the groundwaves still play an important role even in the satellite era, because a single power transmitter can cover large geographic territories. Although, especially in Europe, the AM commercial broadcast stations have lost their importance in favour of the FM ones, the propagation properties of these frequency bands are still important for national broadcast stations and special civil and military communications.

2.1.2 FM Radio Broadcasting

The ultra short wave (UKW)[1] band is a part of the broader very high frequency (VHF) range and is usually (and improperly) denoted as the "FM band", because FM broadcast stations are operating within its range. In Europe the FM band is located between 87.5 and 108 MHz, while in Japan it lies between 76 and 90 MHz. In some countries the "lower FM band" standardized by OIRT[2] and ranging from 65.8 to 74 MHz is still in use.

Frequency modulated signals have better immunity to disturbances that occur on the transmission path and enable the usage of lower emitter powers in comparison to AM [3]. The baseband signal stretches from 30 Hz to 15 kHz, thus offering superior

[1] Abbreviation from the German word "Ultrakurzwelle".

[2] Organisation Internationale de Radiodiffusion et de Télévision.

audio quality in comparison to the AM stations and allowing a proper broadcast of music. In Europe the frequency deviation used for the frequency modulation of the carrier is 75 kHz. The resulting spectrum of the FM signal is infinite, but about 98% of the energy is concentrated in a finite bandwidth, which can be approximated by Carson's rule [1]:

$$B_{\mathrm{FM}} = 2(\Delta f + f_{\mathrm{m,Max}}) \tag{2.2}$$

where Δf is the frequency deviation and $f_{\mathrm{m,Max}}$ the maximum modulation frequency. Although in comparison to AM the FM bandwidth is significantly larger and the receiving equipment is more sophisticated, the improved audio quality made this broadcasting method become over decades the most popular one for commercial purposes and almost synonym with the concept of "radio".

Nowadays the baseband FM channel was extended to include further enhancements, like stereo audio signal, Radio Data System (RDS) signal and Traffic Message Channel (TMC), thus increasing the baseband bandwidth to about 59 kHz. However, the bandwidth of the RF-channel is set in Europe to 150 kHz, so that the 268 kHz wide channel resulting from eq. (2.2) would not fit in. In order to achieve this, the carrier is frequency modulated using a more complex scheme, in which the frequency deviation is pondered across the baseband.

In Europe the channel spacing used for FM is usually 100 kHz. In order to provide sufficient RF-bandwidth for each channel, only a certain number of transmitters can simultaneously broadcast in a given region.

Due to their higher frequency, the UKW waves are usually not reflected by the atmospheric E-layer and do not follow the Earth's curvature, but can still be refracted in the lower atmospheric layers [4]. On the other hand, the frequency is not high enough for a clean line-of-sight propagation, and diffraction does help the UKW waves travel around objects with dimensions comparable with their wave-length – that is, a few meters. The reflection, diffraction and scattering on larger obstacles lead to multipath propagation scenarios, in which the incident waves (to the receiving antenna) have random amplitudes and phases, due to their different propagation paths, although they have the same origin (i.e. the transmitter antenna). The wave superposition at the receiving antenna leads to distortions and interference patterns that can corrupt the demodulated signal.

The multipath scenario can be exactly determined only in particular cases, because it is dependent on geography, vegetation, buildings and other important obstacles existent in the region where the transmitter and the receiver find themselves. When the receiver is mobile, the multipath scenario changes continuously, so that only a statistical analysis is possible.

Unlike the AM service, the FM one is meant to cover smaller areas; in doing so, the frequencies are much often reused.

It is now clear that the mobile FM radio reception is a far more complex problem in comparison to the stationary case, when the receiver finds itself at a fixed position. If the mobile receiver is a car radio, the receiving antenna is mounted at a low

height, while the conductive car body serving as ground has comparable dimensions with the wave-length, thus scattering the waves and impacting upon the antenna's performance. As the car travels, the picked-up signal continuously fluctuates due to the multipath propagation and the scattering on the objects in its immediate vicinity (like other cars).

2.1.3 DAB Radio Broadcasting

The digital radio is the natural result of the trend which made all the communication and entertainment systems migrate from analog to digital. The first commercially available digital radio broadcast in Europe was Digital Satellite Radio (DSR), which started in 1991, and was followed in 1993 by Astra Digital Radio (ADR). Both were satellite services, but were little known and lacked commercial success [5]. With the development of audio compression methods and the coded orthogonal frequency-division multiplexing (COFDM) modulation a new digital radio concept became possible, which efficiently uses the bandwidth, is suited for mobile reception, enables better audio quality than FM and is more resistant to noise and co-channel interference.

DAB was developed at the beginning of the '90s as an European project and was intended to be the replacement for the FM broadcast stations. However, even though the first pilot broadcasts started in 1995 and ever since DAB is widely available in many countries, the service still remains little known and has failed so far to replace FM. According to the World DAB Forum [6] there are 19 countries with regular DAB services (among them Australia, Canada, China, Singapore, South Korea and Taiwan, the rest being European countries) and 16 countries in which tests and trials are being performed. The service has an important commercial success in the United Kingdom (62 million inhabitants), with 85% coverage, about 10 million receivers sold and 446 DAB programs available. Also in Denmark the service enjoys popularity: 90% coverage, 1.5 million receivers at a population of 5.5 million (1^{st} place worldwide at the receiver density), and 18 DAB programs. In Germany (82 million inhabitants), although the coverage reaches 85% and 153 DAB programs are available, there are only about 546,000 receivers.

Compared to the analog broadcasting systems, DAB has a significantly more complex structure. A single DAB RF-channel squeezes together more audio programs and data streams into a so-called DAB multiplex (ensemble) [5].

The audio information (the radio program itself) is first digitalized and then compressed in order to reduce its data rate. The compression uses the lossy algorithms MPEG[3]-1 and MPEG-2 Layer II (also known as MUSICAM[4]), which exploit the psychoacoustic particularities of human hearing to remove both the redundant and the irrelevant information from the audio stream. Depending on the desired audio

[3]Moving Picture Experts Group

[4]Masking Pattern Universal Subband Integrated Coding and Multiplexing

quality, this technique reduces the original data rate from 1.5 Mbps (CD quality) to 32 ... 384 kbps. For mono speech radio 64 kbps may be perceived as sufficient, while for high-fidelity stereo broadcast at least 192 kbps are required.

The DAB multiplex contains a number of compressed audio channels (the radio programs) and a number of data services. The exact structure of this multiplex can be found in the specialized literature ([5], [7]) and is skipped here.

In order to increase the immunity of the transmission against disturbances that occur on the transmission path, the data stream has to be channel coded. This operation, which adds redundancy to the useful information, increases the data rate. DAB has the particularity that every subchannel in the multiplex can have its own amount of channel coding, thus leading to an unequal forward error correction. Prior to modulation, each subchannel is scrambled in order to disperse its spectral power density, and then a convolutional coding is applied. A time interleaving follows, in order to improve the protection against burst errors. The interleaving spreads the bits across 15 frames, so that a systematic delay of 360 ms occurs between transmitter and receiver.

The degree of forward error correction applied to the streams inside a multiplex determines also the number of programs which can be accommodated inside the multiplex and the minimum signal-to-noise ratio (SNR) required for correct reception. Well protected programs need lower SNR at the reception, but require higher data rates, so that fewer programs can be accommodated in the multiplex. Less protected programs require lower data rates – and thus more programs fit inside the multiplex –, but demand higher SNR at the reception.

The data prepared in this way is fed to the COFDM modulator, which uses a number of subcarriers varying between 192 and 1536, whereby each subcarrier is modulated using a $\pi/4$-shift-DQPSK (differential quadrature phase-shift keying) scheme. This means that every COFDM subcarrier carries 2 bits. The COFDM modulation can be seen as some sort of serial-to-parallel conversion: a number of bits from the original serial data stream are simultaneously (parallel) placed on a number of subcarriers. The sum of all these subcarriers constitutes the COFDM symbol. A guard interval a quarter of a symbol long is introduced in the DAB standard after each COFDM symbol. This measure insures immunity against echoes in multipath-propagation scenarios, because intersymbol interference is avoided as long as echoes arriving at the receiver do not exceed the guard interval. Additionally, this measure allows the design of single frequency networks.

There are four DAB modes, which distinguish themselves by the number of COFDM subcarriers available[5]. Since the bandwidth of the DAB signal is always 1536 kHz, it follows that each mode has different COFDM symbol lengths. Long symbols improve the immunity to multipath propagation scenarios, where echoes occur. However, long symbols imply the use of more subcarriers inside the COFDM multiplex, so that the distance between the subcarriers lowers and difficulties may

[5]Number of COFDM subcarriers: Mode I: 1536; Mode II: 384; Mode III: 192; Mode IV: 768.

arise in mobile reception scenarios because of the Doppler Effect.

Together with the error correction and the additional information needed for the receiver configuration, the total data rate of a DAB channel reaches 2.4 Mbps. The net data rate, which regards only the audio and data streams, is in the range of 1.2 ... 1.73 Mbps. A DAB block contains typically between 6 and 8 radio programs.

DAB programs are broadcasted with vertical polarization in the VHF[6] Band III (174 – 240 MHz) and in a portion of the L-Band[7] (1452 – 1492 MHz). As the bandwidth of the DAB block is 1536 kHz wide, it follows that 4 DAB blocks together with some guard band fit into a 7 MHz wide VHF TV channel. Consequently the distance between the centre frequency of two consecutive blocks is 1.75 MHz. Each block inside a VHF channel is denoted with a letter between A and D, while the VHF channels are numbered between 5 and 13 (e.g. 7A, 9C, etc). In L-Band the channels are identified by the letter L followed by a letter between A and W (e.g. LG, LR, etc).

In order to cover large areas, the DAB system allows the use of single frequency networks, in which all broadcast stations casting the same program are using the same operation frequency. These networks are possible due to the properties of the COFDM signals and the guard interval between the symbols: the signals arriving at the receiver from a neighbouring broadcast station are detected as echoes and ignored, if the single frequency network is correctly designed, which means the distance between the broadcast stations and the emitting powers have to be correctly chosen. Such networks represent a very economical use of the radio spectrum, but require a perfect synchronization of all transmitters. This is achieved by using the GPS clock signal for synchronization.

The DAB mode is chosen depending on the application. For single frequency networks covering whole countries mode I in the VHF band is preferred, while for local broadcast stations mode II in the L-Band is chosen. Mode III is intended for the satellite DAB service.

2.2 Car Reception Antennas

A monopole mounted on the car is the simplest and oldest method of receiving radio signals. Nevertheless, the need to make the antenna invisible and to improve its mechanical robustness lead to the development of structures integrated into other parts of the car, like the use of the rear window heater field or the deposition of additional metal wire structures on the other car windows. However, such glass-printed antennas have the disadvantage of requiring careful optimization for each individual car model, thus making them more expensive.

Active windshield antennas, like the one shown in Fig. 2.1(a), entered mass production in 1984 [8]. These structures can be optimized for both polarizations

[6]Frequency range from 30 to 300 MHz.

[7]Frequency range from 1 to 2 GHz.

and exhibit good performance in both AM and FM, but have to disturb as little as possible the visual field of the driver.

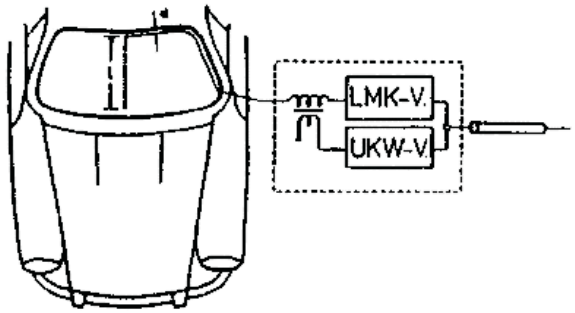

(a) Active AM/FM windshield antenna in the '80s. The antenna amplifier has a two-path architecture.

(b) Active AM/FM antenna integrated in the side mirror.

Fig. 2.1: Examples of antennas mounted in the front part of the car.

The first car active antenna implementation is depicted in Fig. 2.1(b), where the side mirror of a sports car acts as an active monopole antenna with roof capacity.

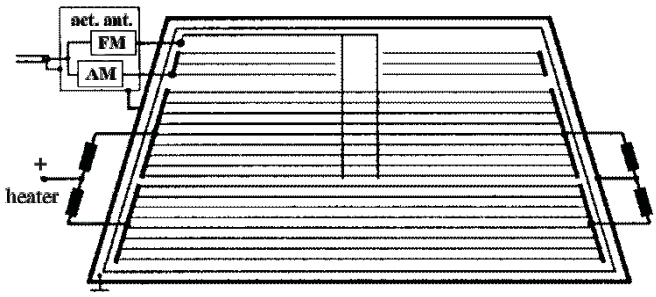

(a) Rear window active AM/FM antenna with the AM structure separated from the heater.

(b) Rear fender AM/FM retractable whip active antenna.

Fig. 2.2: Examples of antennas mounted in the rear part of the car.

Antennas mounted in the front part of the car, regardless their type, are susceptible of picking up the noise generated by the electronic equipment installed in on board, although they have the advantage of a reduced cable length between antenna and radio receiver. The rear mounting positions find themselves in a more "quiet" region of the car, when it comes to noise, but have to be linked by longer cables

to the radio receiver. The importance of the cable length and how active antennas alleviate this issue is later discussed in Section 3.4.

An example of a rear window AM/FM active antenna which is integrated in the window heater is given in [9] and shown in Fig. 2.2(a). In this case, a separate antenna structure is used for AM, in order to avoid the expensive necessity of decoupling the low-frequency AM path from the heater; in FM, due to the higher frequency, the decoupling of the direct current (DC) heater path is much more convenient.

By contrast, a monopole telescopic antenna is shown in Fig. 2.2(b). These models were mounted either on the front or on the rear fender of the car and required additional mechanics in order to make them retractable.

(a) Low-end AM/FM active 40 cm long monopole antenna.

(b) High-end diversity antennas.

Fig. 2.3: Examples of low-end and high-end antenna structures.

Window-printed antennas, especially the rear ones, have additionally the advantage of allowing the cohabitation of more antenna structures on the same glass plate, thus making diversity possible [9] [10] [11]. For example, the high-end solution proposed in Fig. 2.3(b) features not less than 3 FM antennas, 4 TV antennas and one for AM. In addition, GPS and mobile phone antennas are mounted under the small radome on the roof.

FM and TV diversity antenna systems equipped with high-impedance amplifiers can be also integrated into plastic trunk lids, as described in [12]. In addition, the dielectric trunk lid can also host antennas for other services, like AM, mobile phone, GPS and satellite radio.

By contrast, the low-end solution in Fig. 2.3(a) consists of only one AM/FM monopole antenna mounted on the roof. Usual modern whip lengths vary from 40 cm to 20 cm and from the mechanical point of view they are designed to be flexible enough in order to meet certain safety requirements.

Diversity systems employing rod antennas can be imagined in the future, because ultra-short monopole-related structures, like the ones presented in this work, may

be mounted inside a small radome on the roof.

DAB-Band-III reception is possible with the usual 40 cm long rod antennas, as at these frequencies this length corresponds to about $\lambda/4$. For the L-Band a shorter rod is required, only about 5 cm long. Due to the fact that L-Band is far enough from Band-III, the same long AM/FM/Band-III rod can be used for this task, by introducing an inductive structure at the right height, which blocks the higher frequencies and is invisible for the lower ones.

2.2.1 AM Reception in Cars

When an antenna is installed on a car, there will be a certain height between the mounting point and the ground (i.e. earth). While the ground is more or less conductive, the metallic car body is an excellent electrical conductor. As for AM-frequencies the mounting height is much smaller compared to the wavelength, the directivity of the antenna will not be influenced [4]. It can be also shown that h_{eff} is not dependent on the conductivity of the ground (i.e. earth) and is constant for frequencies under 10 MHz. Nevertheless, the effective height will diverge from eq. (3.5).

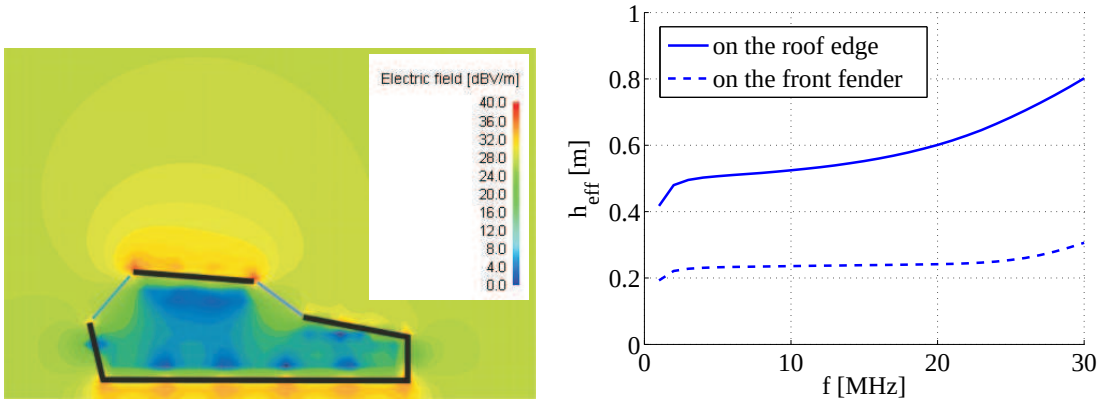

(a) Simulated electric field distribution around the car body.

(b) Calculated effective height of a 20 cm long monopole perpendicularly mounted on the roof and on the fender of the car.

Fig. 2.4: Simulated car placed in the far-field of a 1 MHz transmitter and the calculated effective height of a 20 cm long monopole mounted on it. Courtesy of Dr. J. Brose.

Fig. 2.4(a) depicts the simulated far field of a 1 MHz transmitter around a car body. It can be seen that the electric field concentrates around the metallic edges of the car roof, indicating these spots as the best placement for an antenna. This means also that the effective height h_{eff} of the monopole will be larger than expected from eq. (3.5), as the curves in Fig. 2.4(b) illustrate.

2.2.2 FM and Higher Frequencies Reception in Cars

As pointed out in Section 2.1.2 – and valid also for higher frequencies, the FM wavelength, being comparable to the dimensions of the car body and the surrounding objects, leads to a complex reception scenario. When an antenna is installed on a car, there will be a certain height between the mounting point and the ground (i.e. earth). While the ground is more or less conductive, the metallic car body is an excellent electrical conductor. Because the size of the car body is comparable to the FM wavelength, the behaviour of the electromagnetic field in its proximity is dependent on position, car orientation and frequency. This means that the mounting position of the antenna has a major impact upon the delivered signal.

In Germany, most FM signals are radiated with horizontal polarization, because in this way a better reception for home receiving systems employing roof aerials is achieved[8]. On the other hand, monopole antennas mounted on cars favour vertical polarization, due to their orientation. However, the car's metallic body distorts the electromagnetic field, especially in the vicinity of metal edges, so that vertical electrical components arise. This enables radio reception of horizontally polarized signals with a vertical monopole [4]. That is why the roof edge and the fenders prove to be adequate for mounting vertical rod antennas. By bending the antenna at a certain angle its capability to receive horizontal polarization is additionally improved.

It is interesting to note that the usage of vertical instead of horizontal polarization in a mobile multipath scenario does not bring any advantages to the average FM reception. It can nevertheless slightly improve the reception in some particular cases, like for example in open-field line of sight scenarios. On the other hand, there are other scenarios, like the metropolitan areas, in which the reception is growing worse. Circular polarization seems to bring a slight overall improvement for mobile FM reception [4].

In the past, rod antennas with a length of about 1 m mounted on the front or rear fender of the car were used in combination with tuned radio receivers, owned to the fact they exhibit a resonance in the FM band. Because of the complex car body shape and the parasitic capacitance between antenna element and ground as well, the impedance of the monopole mounted on the car deviates from the theoretical case given by eq. (3.1), so that the antenna length and thickness can be such tailored to achieve a good match to $50\,\Omega$ for the whole FM operating band. Also, their length enables a good AM reception, due to the increased effective height and lower antenna impedance.

Shorter rod antennas, like the 40 cm ones, can be mounted on the roof top, either above the windshield or above the rear shield, thus benefiting from the improved field concentration (Fig. 2.4). Nowadays, the usual mounting position for short rod antennas is on the top of the car, above the rear windshield.

[8] Worldwide, however, also vertical and circular polarizations are being used.

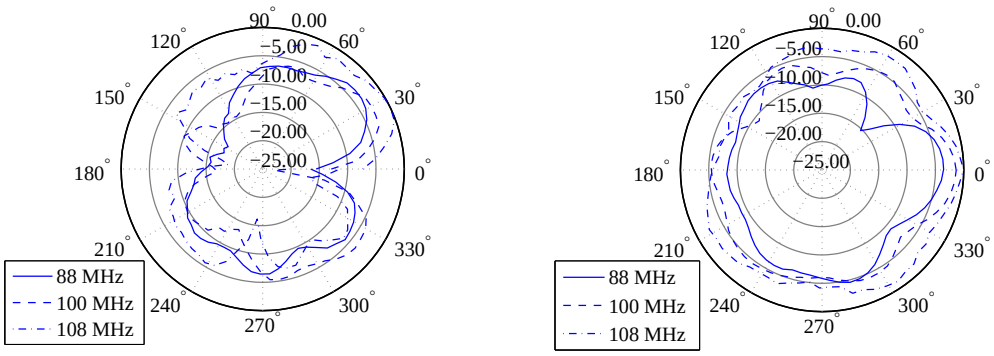

(a) Horizontal.

(b) Vertical.

Fig. 2.5: Measured directivity patterns for horizontal and vertical polarization of a 20 cm active monopole antenna mounted on the roof top of a car above the rear windshield. Values are referred to the maximum of each three curves set. The car's front corresponds to 0°.

Monopoles mounted on an ideal infinite ground plane have for vertical polarization a circular directivity pattern in the azimuth plane. However, the car body is no ideal ground plane, first of all because of its geometry. As a result, the directivity pattern of a rod antenna installed on a car has a complex form which deviates significantly from the circular pattern, as shown in Fig. 2.5 for a 20 cm active monopole mounted on the car roof top above the rear windshield and measured at three different frequencies. Because the car geometry has different impact upon different wave-lengths, the pattern is frequency dependent. The pronounced minima in the horizontal polarization diagram occur at angles at which no properly polarized electric field is available in order to excite the antenna element.

The irregular directivity pattern complicates additionally the mobile radio reception in multi-path propagation scenarios and is important to be known for diversity systems.

2.3 Car Antenna Amplifiers

An active antenna is obtained by connecting a special amplifier directly to the antenna element. This configuration allows the use of significantly shorter antennas without compromising the output SNR, provided that the nonlinear issues inherent to any active device have been alleviated [13] [14].

The amplifiers powering the active antennas have known important developments over the years, as their architecture depends on both the used antenna element and the technical possibilities. Their use allowed for a general size shrinking of the

receiving antennas, the elaboration of more compact antenna arrays[9] and improved the bandwidth [15]. In this context, the car industry fully benefitted from the size reduction (in the case of monopoles) and the possibility to use novel antenna structures (like the window-printed ones) and diversity. The active antennas are also found in applications requiring the embedment of electrically very short antennas into other devices, like for example the FM antenna in a mobile handset [16] [17].

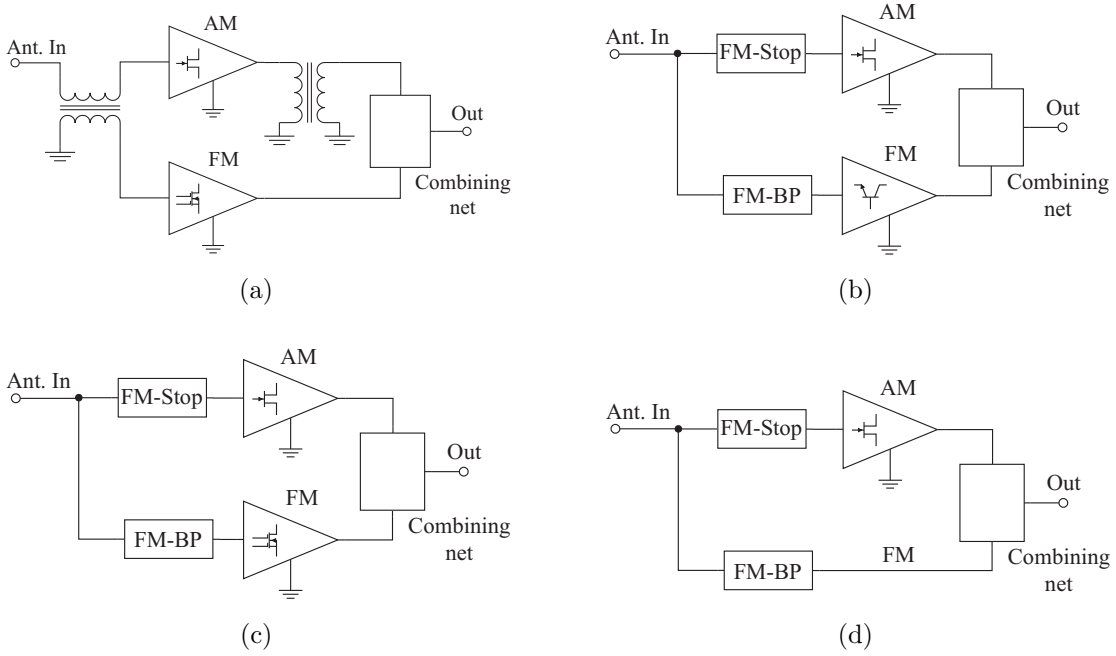

Fig. 2.6: Active rod antenna architectures.

Fig. 2.6 shows some widely used AM/FM active rod antenna architectures. In all cases the AM and the FM signals are amplified separately, in order to avoid FM/AM conversion issues. The first stage of the AM amplifier is built around a Si field effect transistor (FET) connected either as common drain or as common source with some amount of degeneration. The first stage of the FM amplifier consists of either a Si bipolar transistor, a Si double gate metal oxide field effect transistor (MOSFET) or a GaAs FET. There are also commercial versions, like the one in Fig. 2.6(d), which are passive in FM. The two signal paths are usually split and recombined by filters. The configuration in Fig. 2.6(a) has the particularity of employing a resonant transformer at the input. The structure is tuned in FM, whereby the antenna capacitance and the input capacitance of the amplifier are part of the resonant circuit. The AM signal, due to its low frequency, passes the primary winding and is picked-up by the AM amplifier, while the FM signal is transferred from the primary to the secondary resonant circuit.

[9]The high-impedance amplifiers loading the antennas draw virtually no current from the antenna elements, thus lowering their mutual coupling.

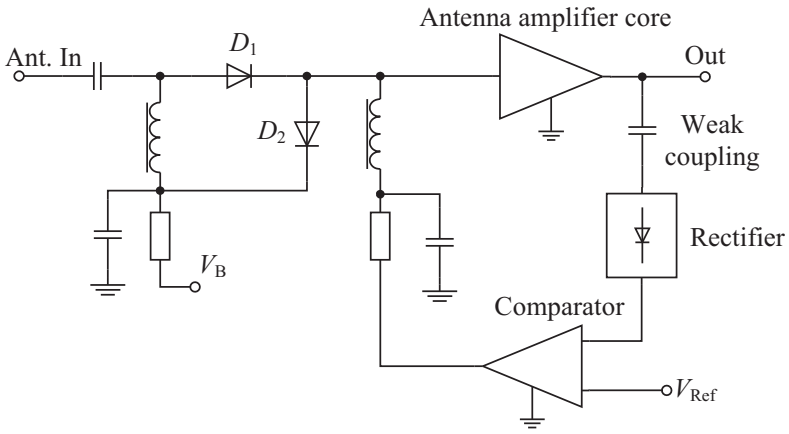

Fig. 2.7: Automatic gain control circuitry.

Over the decades, the noise improvement relied mainly on the advances of the active semiconductor devices. Initial circuits used only Si based transistors, while nowadays lower-noise GaAs devices are also common [18]. However, from the circuit technique point of view, the noise optimization consists basically of minimizing the noise contributed by different components in the amplifier. Noise cancellation techniques [19] are not appropriate for active car antennas, because not only the noise factor has to be optimized, but the output noise level has to be minimized as well[10].

The linearity achievable with antenna amplifiers witnessed during the '70s and the '80s a steady increase [9] [11]. However, modern circuits employing low-noise GaAs active parts tend to have lower non-linear performance.

Some commercial active antennas employ AGC circuitry in order to improve the linearity in the FM range, like the circuit shown in Fig. 2.7. The conduction of the PIN diodes D_1 and D_2 is controlled by a circuit which continuously compares the output signal to a certain reference. When the signal is too strong, D_1 lowers its conduction, while D_2 begins to short-circuit the signal towards ground. In addition, the amplifiers employing dual-gate MOSFETs use the second gate to vary the transconductance of the device, thus controlling the voltage gain of the stage.

This linearity improvement method has the disadvantage of attenuating the entire operating band, not only the strong stations. If, for example, the listener is tuned on a weak station S_1 and, because of the car's movement, station S_2 becomes strong enough in order to activate the AGC, then the entire band will be attenuated, which means that S_1 will become even weaker. In worst case, the weak station becomes impossible to receive any longer.

[10]In addition, the noise cancellation techniques are appropriate for integrated circuits only and for applications where the input impedance is relative low and has to be controlled. The active antenna amplifiers usually require high input impedances, so that the additional capacitance introduced by any further transistor used for noise cancellation is undesired.

AM antenna amplifiers in an integrated version have already been reported in bipolar technology in the '80s [20] and in complementary metal-oxide-semiconductor (CMOS) technology at the beginning of the '90s [21]. These amplifiers use a capacitive negative feed-back loop in order to improve linearity and to obtain a wideband response. Nevertheless, in comparison to their discrete counterparts, these implementations exhibit a higher noise level. An analysis of antenna amplifier configurations using virtually grounded inputs is given in [22].

More recently, integrated circuits are available for the FM band, like the ATR4253 chip from Atmel [23], or the MAX2180 from Maxim [24]. Both chips incorporate the AGC circuitry. However, although these integrated circuits succeed in minimizing the required number of discrete components, they are not suited for the ultra-short antenna elements, or the special helical structures discussed later throughout this work.

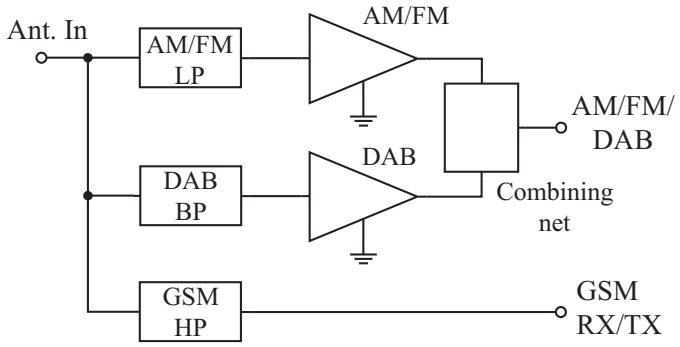

Fig. 2.8: Antenna amplifier architecture including DAB and GSM circuitry.

Sometimes it is required that the antenna element be used also for the Global System for Mobile Communications (GSM) signal. Because in this case both reception and transmission are required and the signal multiplexing is implemented inside the mobile phone, the antenna is used as a passive element, as shown in Fig. 2.8. Therefore, the antenna amplifier(s) for the radio broadcasting services has to be protected against the transmitted GSM signal, which may be very strong. Because GSM is operating in the higher frequency range, there is basically no difficulty to separate it from the AM, FM and Band-III ranges by means of filters. However, the filters employed here have to load as little as possible the other broadcast bands, which is not necessary a trivial task.

The antenna element can be also used for receiving DAB signals, either only one of the band, or both Band-III and L-Band. If the antenna element is a monopole long enough to operate as a $\lambda/4$ one, then a $50\,\Omega$ amplifier can be used for DAB. As shown in Fig. 2.8, filtering measures have to be also taken. Because FM and Band-III are close in frequency, separating them without compromising the AM and FM performance is not an easy task.

2.4 Car Radio Receivers

The dramatic metamorphosis which transformed the original AM car radio into a complex multi-service system brought changes also to the RF front-end, which is in fact the radio part of interest in the present work, because it finds itself in direct connection with the antenna. Car radios have different RF front-ends and tuners for each radio service they have to receive. In order to select a certain band to be listened to, the radio switches the antenna signal to the corresponding RF path.

Old car radios used a selective input for the AM band [4]. The antenna and cable capacitances were tuned-out inductively, whereby the variable elements were adjusted by mechanical means, thus making the assembly large and sophisticated. In order to accommodate long antenna cables, a "shortening" capacitor was introduced in series with the receiver input, so that the total capacitance provided to the selective input circuit in the receiver could be held within certain values specified by the manufacturer; however, such a technique came with sensitivity penalties. As the broadband active antennas for AM developed, the receiver input had no longer to be selective and high impedance inputs became standard. Present-day car radios have a predominant capacitive input impedance in AM with typical values between $10 \ldots 40$ pF.

Also in the FM range, old car radios used selective inputs with variable passive elements that had to be adjusted mechanically. Later developments made it possible to electronically tune the input circuit by using varicap diodes. This made the circuit smaller, more robust and cheaper, but brought additional nonlinear issues, because the diode does no longer behave linear as soon as the signal becomes large enough. The schematic of such an input circuit found in modern car radio receivers is shown in Fig. 2.9(a), where capacitor C_1 and the capacitances of the varicap diodes D_2 and D_3 form the input parallel resonant circuit together with the inductance of the secondary winding of the transformer T. The tuning DC voltage V_{Tune} is supplied to the varicap diodes through R_{D}. The diodes D_2 and D_3 are connected in anti-phase in order to reduce even order distortions.

In order to overcome the nonlinear issues, the radio receivers are provided with AGC circuits, which attenuate the input signal if it becomes too large and overdrives the active devices. In Fig. 2.9(a) for example, the I_{AGC} current controls the conduction of the PIN diode D_1; for too large input signal levels the diode's resistance is progressively reduced, so that the RF signal is eventually short-circuited. The AGC circuit also controls the voltage V_{AGC} applied to the second gate of transistor M_1. This has the effect of controlling the voltage gain brought by the input stage and so prevents overdriving further active stages.

This linearity improvement method has the disadvantage of attenuating the entire operating band, not only the strong stations.

The measured input impedance of such a FM car radio receiver is depicted in Fig. 2.9(b). For this measurement the device was tuned on 100 MHz; as the impedance loop shows, it approaches $50\,\Omega$ at the operating frequency, while presenting a

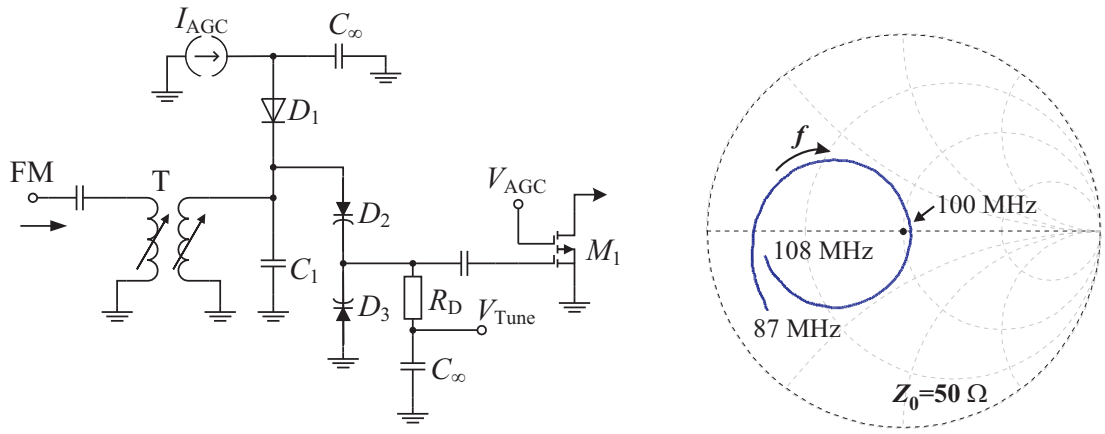

(a) Simplified schematic of the FM input circuit.

(b) Input impedance when the radio is tuned at 100 MHz.

Fig. 2.9: Modern car radio with selective input and automatic gain control: simplified schematic and input impedance of the FM stage.

low impedance otherwise.

There are, however, also radio-sets with broadband 50 Ω FM input impedance. Older FM-radios were designed for 150 Ω input impedance, in order to accommodate the 150 Ω coaxial cable used for connecting the antenna. Such a cable has the advantage of a reduced capacitance per unit length (about 33 pF/m), which is crucial when using passive AM antennas. However, as nowadays active solutions are used for AM, the cheaper and mechanically more convenient 50 Ω cable (having about 100 pF/m capacitance per unit length) has become standard.

From the active antenna designer's point of view, for whom the radio receiver represents the load of the antenna amplifier, it is important to keep in mind that in AM a capacitive load has to be expected, while in FM the load impedance is 50 Ω. Moreover, the characteristics of a resonant impedance, as shown in Fig. 2.9(b), have to be accounted for, in order to prevent unexpected behaviour when a low load is presented to the antenna amplifier.

Car radios have noise figures between 6 dB and 10 dB [4], which lead to receiver noise temperatures between 865 K and 2610 K. Modern car radios implement methods that improve the quality of the audio signal when the reception level is critical. For example, the total amount of noise can be controlled by digitally varying the bandwidth of the intermediate frequency filter. Also, when the signal level is poor, the radio can switch from stereo to mono and can also suppress the higher portion of the audio spectrum, where noise is more likely to be perceived [25]. However, these methods affect also the useful signal, so that a good quality high sensitivity active antenna remains a crucial aspect that cannot be entirely eluded by means of digital signal processing.

Chapter 3

Theory of Active Antennas

Throughout this chapter some concepts about electrically short monopole antennas are reminded, as being a basic configuration for radio reception. In addition, all the antenna elements used throughout this work behave in the AM range similar to simple monopoles.

The most important issues and definitions concerning noise in electronic systems are highlighted as being a major limitation factor to the design and use of active receiving antennas. The noise sources are not only internal to the amplifier, like the thermal noise, shot noise and flicker noise, but also a characteristic of the radio channel, where the disturbances have atmospheric, cosmic and artificial origins.

In the end the active antenna theory is reviewed and discussed and the performance improvement when compared to the passive counterparts is highlighted.

3.1 Short Monopole Antennas

A simple monopole antenna consists of just a wire of length h and thickness d placed perpendicular above an infinite ideal ground plane, as shown in Fig. 3.1.

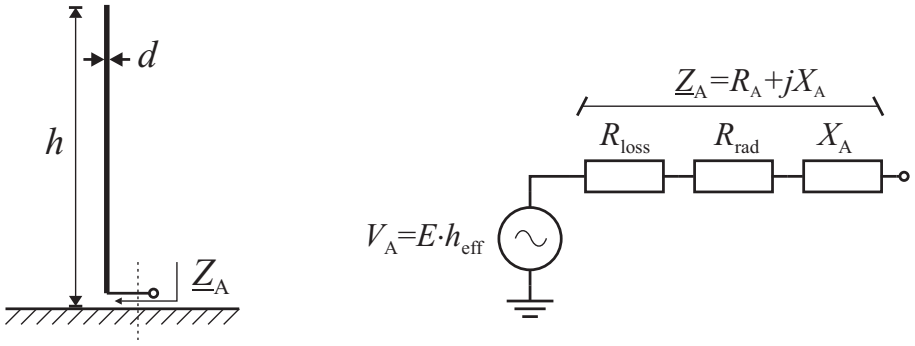

Fig. 3.1: Monopole antenna of height h and thickness d above an infinite ground plane (left) and the corresponding equivalent circuit (right).

The equivalent circuit of such an antenna is also shown in Fig. 3.1. The generator corresponds to the open-circuit voltage induced in the antenna by the electrical field strength E, while $\underline{Z}_\mathrm{A}$ is the impedance seen at the feed point of the antenna [26].

The monopole antenna impedance $\underline{Z}_\mathrm{A}$ is in the general case a complex value which depends on the ratio between length and wavelength h/λ and conductor thickness d. The real part of $\underline{Z}_\mathrm{A}$ consists of the radiation resistance R_rad and the losses resistance R_loss. R_loss incorporates all the losses of the antenna and the power dissipated in it is transformed into heat. The energy dissipated in R_rad is in fact the energy radiated into space. In order to radiate as much as possible from the power delivered by the generator, R_rad should represent the largest part of R_A. The losses in the monopole antenna are frequency, geometry and material dependent and can be usually neglected, as $R_\mathrm{loss} \ll R_\mathrm{rad}$ [26].

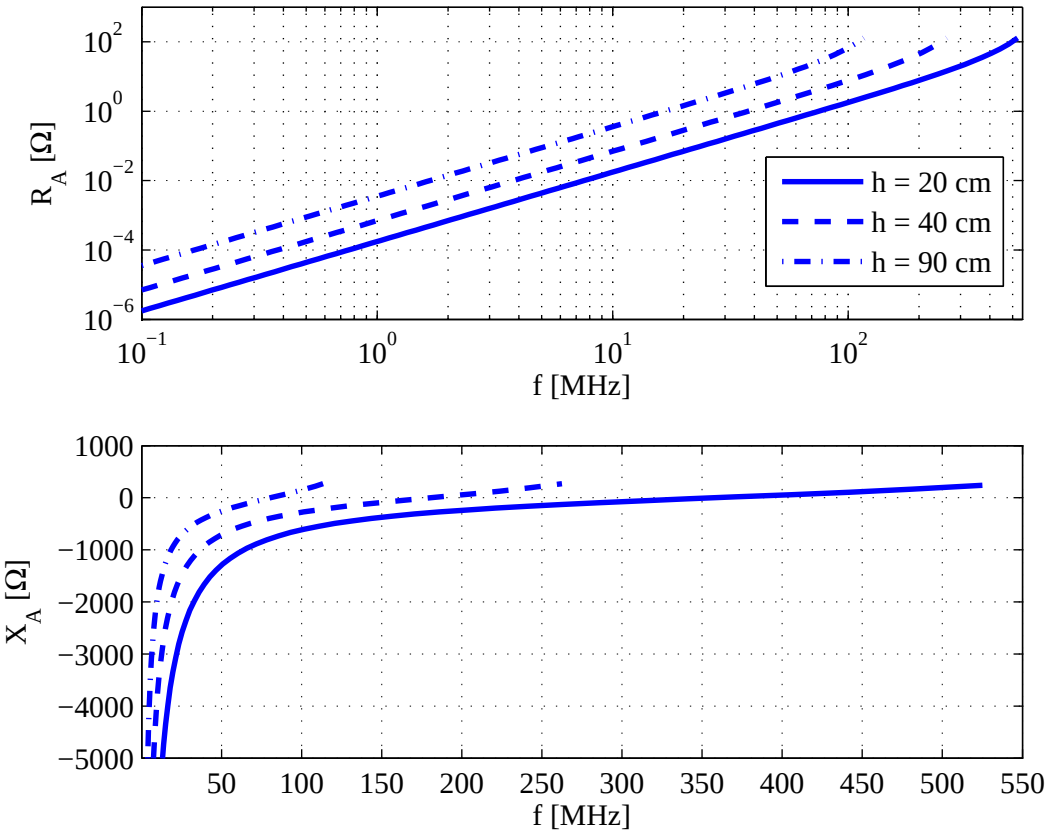

Fig. 3.2: Real and imaginary parts of the antenna impedance $\underline{Z}_\mathrm{A}$ in the case of monopole antennas.

If the length of the monopole is significantly smaller than the wavelength at the operating frequency, then we are discussing about an electrically short monopole

antenna. Neglecting R_{loss}, it can be shown that for such antennas the antenna impedance can be expressed as follows [26]:

$$\begin{aligned}\underline{Z}_{\text{A}} &= 40_{[\Omega]}\left(1-1.32\left(\frac{h}{\lambda}\right)^2\right)\tan^2\left(\pi\frac{h}{\lambda}\right)- \\ &\quad -j\left(\frac{60_{[\Omega]}\left(\ln\left(4\frac{h}{d}\right)-1\right)}{\tan\left(2\pi\frac{h}{\lambda}\right)}-R_1\left(\frac{h}{\lambda}\right)^{\alpha}\right)\end{aligned} \tag{3.1}$$

where $R_1 = 78\,\Omega$ and $\alpha = 1.22$ for $\frac{h}{\lambda} < 0.14$, while $R_1 = 276\,\Omega$ and $\alpha = 1.85$ for $0.14 \leq \frac{h}{\lambda} < 0.25$, and still usable up to a ratio of 0.35. For ratios larger than 0.35 the sinusoidal current distribution in the antenna does not hold any more, even for thin radiant elements [27]. For $h < \lambda/10$ one refers to electrically very short monopole antennas.

Fig. 3.2 plots the real and the imaginary parts of eq. (3.1) as a function of frequency, for three different antenna heights h: 20 cm, 40 cm and 90 cm. All three monopoles have the thickness $d = 3\,\text{mm}$. As it can be seen, the reactive part X_{A} of the antenna impedance is capacitive as long as the antenna is electrically small, while the real part R_{A} is negligible. As h/λ approaches 0.25, the monopole reaches its first series resonance and behaves inductively after that. The equivalent circuit of the electrically very short monopole antenna is depicted in Fig. 3.3, while its antenna capacitance C_{A} is plotted in Fig. 3.4(a).

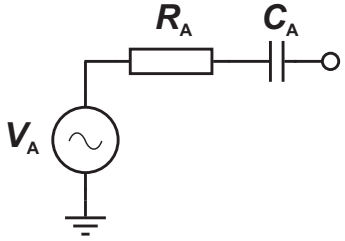

Fig. 3.3: Equivalent circuit of electrically very short monopole antennas.

In the case of AM applications, due to the small antenna capacitance, one can always neglect the real part of the antenna impedance when performing a signal analysis. In FM, the 20 cm and the 40 cm monopoles behave almost entirely capacitive, while the 90 cm monopole resonates in the lower FM range at about 80 MHz.

Fig. 3.4(a) suggests that as long as the condition for electrically very short antennas is satisfied, the antenna capacitance C_{A} is almost frequency independent for a given antenna height h. In this case, using eq. (3.1), the antenna capacitance simplifies to:

$$C_{\text{A,AM}} \simeq \frac{h}{60_{[\Omega]}\left(\ln\left(4\frac{h}{d}\right)-1\right)c} \tag{3.2}$$

where $c \simeq 3\cdot 10^8\,\text{m/s}$ is the speed of light. Equation (3.2) is indeed frequency independent and is plotted in Fig. 3.4(b). The curve can be approximated for hand

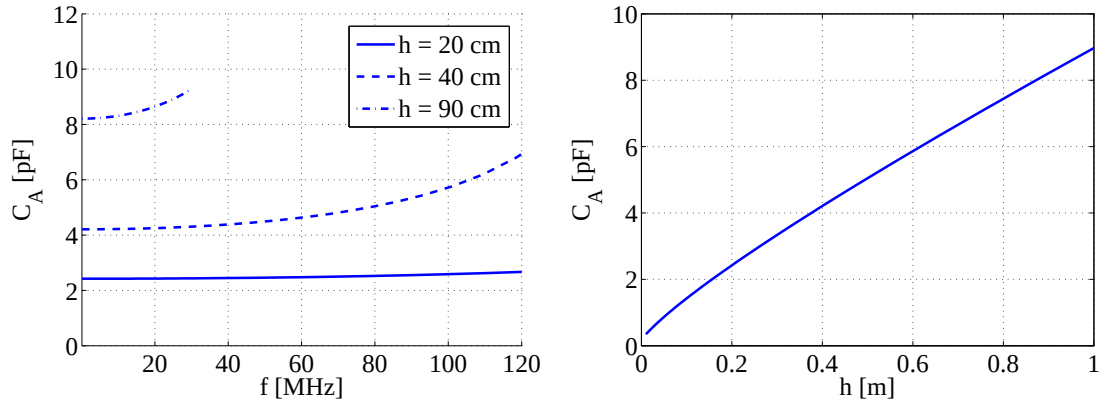

(a) AM and FM range for the 20 and 40 cm monopoles, AM range only (100 kHz to 30 MHz) for the 90 cm monopole.

(b) Input capacitance for variable length h under the assumption of an electrically very short monopole.

Fig. 3.4: Input capacitance of monopole antennas.

calculations with a straight line $C_{\mathrm{A,AM}} \simeq a \cdot h$, where $a = 9\,\mathrm{pF/m}$ is a constant and h is expressed in meter.

The open-circuit voltage induced in the antenna by the electrical field strength E is found to be:

$$V_{\mathrm{A}} = E \cdot h_{\mathrm{eff}} \tag{3.3}$$

where h_{eff} is the effective height of the antenna. The effective height is the height (length) of a monopole with a uniform current distribution I_{eff} along its length, but displaying the same electric field distribution in space as the actual monopole of height h does. If the current distribution along the actual monopole is $I(x)$, then the effective height can be determined from [26]:

$$h_{\mathrm{eff}} = \frac{1}{I_{\mathrm{eff}}} \int_{x=0}^{h} I(x)dx \tag{3.4}$$

When the monopole is electrically very short, a triangular current distribution along its length can be assumed and solving eq. (3.4) one obtains an effective height half the mechanical height:

$$h_{\mathrm{eff}} = \frac{h}{2} \tag{3.5}$$

When the antenna is installed on a car, the effective height will diverge from eq. (3.5), as shown in Fig. 2.4. This is caused by the electric field distribution around the metallic car body.

Observing Fig. 3.5, where the power matching between the antenna and the receiver R_{load} is attempted with the help of a lossy reactance X_{L}, the antenna efficiency η is defined as the ratio between the useful energy – which is dissipated

in R_{rad} – and the total energy – which includes the losses in R_{L}, thus leading to:

$$\eta = \frac{P_{\mathrm{rad}}}{P_{\mathrm{tot}}} = \frac{P_{\mathrm{rad}}}{P_{\mathrm{rad}} + P_{\mathrm{loss}}} = \frac{R_{\mathrm{rad}}}{R_{\mathrm{rad}} + R_{\mathrm{L}}} \tag{3.6}$$

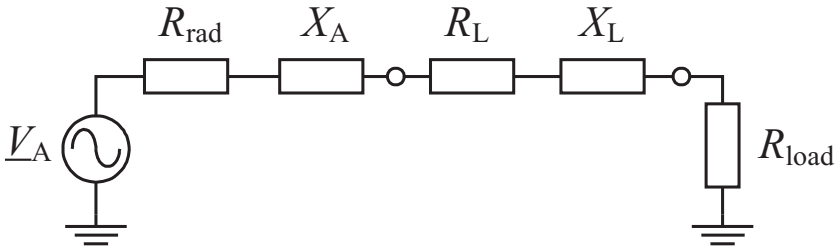

Fig. 3.5: Monopole antenna power matched to a load R_{load}.

The reactance X_{L} is inductive (as the short monopole antenna is capacitive) and has a certain quality factor. As a result, R_{L} can be expressed in terms of loss tangent $\tan\delta_{\mathrm{L}}$:

$$R_{\mathrm{L}} = \omega_0 L \tan\delta_{\mathrm{L}} \tag{3.7}$$

Recalling now the real part of $\underline{Z}_{\mathrm{A}}$ from eq. (3.1), we observe that for short monopoles with $h/\lambda < 0.14$ the term $\left(1 - 1.32\left(\frac{h}{\lambda}\right)^2\right) \simeq 1$, so that:

$$R_{\mathrm{rad}} \simeq 40_{[\Omega]}\pi^2 \left(\frac{h}{\lambda}\right)^2 \tag{3.8}$$

Replacing now (3.7) and (3.8) in (3.6) and using the approximation $C_{\mathrm{A}} \simeq a \cdot h$, we obtain:

$$\eta = \frac{40_{[\Omega]}\pi^2 \left(\frac{h}{\lambda}\right)^2}{40_{[\Omega]}\pi^2 \left(\frac{h}{\lambda}\right)^2 + \frac{\tan\delta_{\mathrm{L}}}{2\pi\frac{c}{\lambda}\cdot a\cdot h}} = \frac{1}{1 + \frac{\tan\delta_{\mathrm{L}}}{80_{[\Omega]}\pi^3 c\cdot a\left(\frac{h}{\lambda}\right)^3}} \tag{3.9}$$

This equation shows that the η decreases with h^3 for a given frequency, which means that the reduction of the monopole's length has dramatic effects on the efficiency. The curve is plotted in Fig. 3.6(a) for $f = 1\,\mathrm{MHz}$ and different $\tan\delta_{\mathrm{L}}$.

The bandwidth attainable with the circuit depicted in Fig. 3.5 can be derived in the same fashion:

$$B = \frac{f}{Q} = \frac{c}{\lambda}\left(80_{[\Omega]}\pi^3 ac\left(\frac{h}{\lambda}\right)^3 + \tan\delta_{\mathrm{L}}\right) \tag{3.10}$$

The equation is plotted in Fig. 3.6(b) and shows that the obtainable bandwidth for a given frequency decreases also with h^3, until it is limited by the inductor losses. The only way to increase the bandwidth of the very short monopole is to introduce

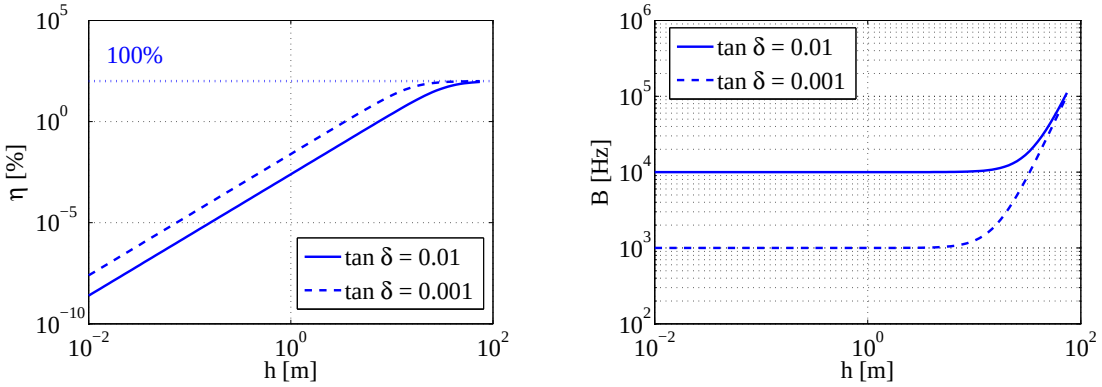

(a) Efficiency. (b) Bandwidth.

Fig. 3.6: Efficiency and bandwidth of a matched monopole for $f = 1\,\mathrm{MHz}$ and different $\tan\delta_\mathrm{L}$.

more losses in the circuit[1] at the expense of the efficiency, and this cannot be an acceptable solution.

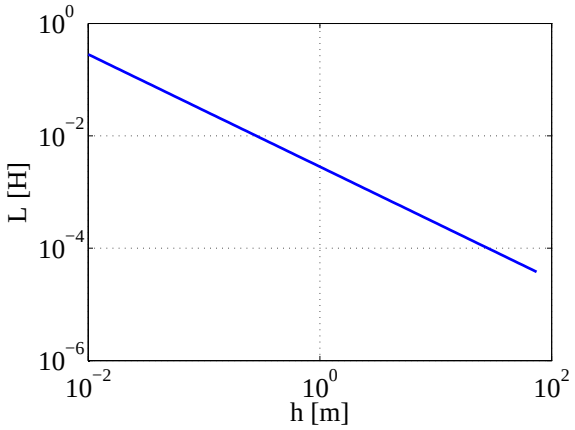

Fig. 3.7: Required inductive for matching a monopole with variable height h at 1 MHz.

The required inductance needed for the power matching of the monopole are plotted at 1 MHz in Fig. 3.7 as a function of height. For example, a 20 cm monopole requires an inductor of about 14 mH.

3.2 Noise in Electronic Systems

Noise in electronic systems is an unwanted and unavoidable phenomenon, which determines the weakest useful signal that can still be processed. Noise cannot be

[1]This shows that even superconductive inductors are not the right approach for this kind of application.

eliminated, but one can design a component or a system in order to minimize its effects.

Since noise is a random process, its instantaneous values are impossible to predict, and the only way to treat it is by use of statistics. The noise has thus a probability distribution associated, which shows with which probability a certain value is to be found at some specific moment. The quadratic mean – or root mean square (RMS) value – of the noise signal plays a very important role for practical use, since it defines an equivalent sinusoidal signal having the same effective value. For an instantaneous noise voltage $v(t)$ the corresponding effective value can be calculated as:

$$V_{\text{eff}} = \sqrt{\overline{v^2(t)}} = \lim_{T\to\infty} \sqrt{\frac{1}{T}\int_0^T v^2(t)dt} \tag{3.11}$$

The noise bandwidth B plays a very important role and is defined differently than signal bandwidth. The noise bandwidth is the area under the power gain curve $G(f)$, divided by the peak gain G_0 [28]:

$$B = \frac{1}{G_0}\int_0^\infty G(f)df \tag{3.12}$$

Thus, the noise bandwidth is larger than the signal 3 dB bandwidth.

Equivalent noise circuits based on the RMS value of the noise are used in order to perform noise analysis in electronic systems. Since noise voltages (or currents) are random processes which do not have predictable amplitudes and phases, they cannot be added using the vector algebra, as one does in the case of sinusoidal signals. Instead, the power has to be summed up.

For example, two uncorrelated noise voltage generators connected in series, having the RMS voltages V_{N1} and V_{N2}, can be replaced by another generator with the voltage:

$$V_{\text{N}} = \sqrt{V_{\text{N1}}^2 + V_{\text{N2}}^2} \tag{3.13}$$

In this case, the new generator's available power is equal to the summed-up available powers of the two original generators.

In the case of a general network, where more uncorrelated voltage and current noise sources act together, the superposition can be used in order to determine the combined effect. To do this, each noise source is supposed of acting alone (all other voltage noise sources are considered short-circuited, while all other current noise sources are considered open-circuited), and the response of the network is determined for this source alone. In the end, the squared individual responses are summed up (superimposed), in order to obtain the total squared response of the network [29]. For example, in the case of a network containing n noise voltage sources, the total noise can be computed as:

$$V_{\text{N}}^2 = |H_1(f)|^2 V_{\text{N1}}^2 + ... + |H_n(f)|^2 V_{\text{N}n}^2 \tag{3.14}$$

where $H_i(f)$ is the voltage transfer function of the i-th noise voltage source. The same applies for noise current sources, taking care to use the corresponding current transfer functions.

3.2.1 Types of Noise

The main types of noise found in electronic components are the *thermal noise*, the *shot noise* and the *flicker (1/f) noise*. Each is next described briefly.

Thermal Noise

The thermal noise is present in any conductor and it is caused by the thermal vibration of the charge carriers. Sometimes it is also referred to as *Johnson* or *Nyquist noise*, since J. Johnson first observed it and H. Nyquist explained its origins [28].

The thermal noise has the characteristics of white noise (and therefore sometimes is also called *white noise*) up to very high frequencies. This holds as long as [29]:

$$\frac{hf}{kT} \cdot \frac{1}{e^{\frac{hf}{kT}} - 1} \simeq 1$$

where $k = 1.38 \cdot 10^{-23}$ J/K is the Boltzmann constant, T is the absolute temperature, f is the frequency and $h = 6.626 \cdot 10^{-34}$ J$\cdot$s is the Planck constant. Errors larger than 1% are first encountered for frequencies above 125 GHz.

The white noise's spectrum shows a constant spectral power distribution over the frequency, which means that, if we consider two bands of equal widths, but situated at two different frequencies, the noise power contained in this bands is also equal. Due to this, the amplitude of the thermal noise can be described with a zero mean Gaussian probability distribution.

Because it is present in any conductive material above 0 K, the thermal noise is the sensitivity limit of any receiving or measuring system. The available thermal noise power is independent of the resistivity of the conductor in which it arises:

$$N_{\text{th}} = kTB \tag{3.15}$$

where B is the bandwidth.

Knowing the available power, one can now calculate the RMS voltage of the equivalent noise generator associated with a resistor of resistance R:

$$V_{\text{R,N}} = \sqrt{N_{\text{th}} \cdot 4R} = \sqrt{4kTBR} \tag{3.16}$$

The equivalent circuits for a noisy resistor can be seen in Fig. 3.8. For the Thevenin representation, the equivalent noise generator has the voltage given by

eq. (3.16), while the resistor is noise-free. Using the Norton theorem, one can transform the voltage source into a current source placed in parallel with the noiseless resistor, and having the RMS current given by:

$$I_{\mathrm{R,N}} = \sqrt{\frac{4kTB}{R}} \tag{3.17}$$

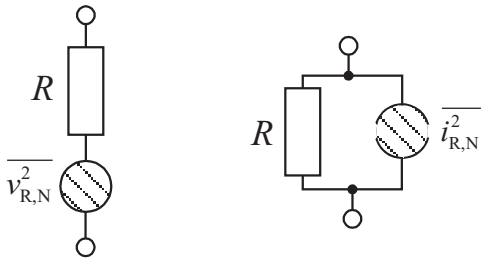

Fig. 3.8: Equivalent circuit of a noisy resistor: Thevenin and Norton configurations.

Besides the thermal noise, resistors also exhibit some amount of *excess noise*, which is uncorrelated to the thermal noise, has a $1/f$ spectrum[2] and is caused by discontinuities in the resistor's structure [30]. Due to their homogeneous structure, metal thin-film resistors have less excess noise in comparison to carbon ones. However, the resistor excess noise tends to be an issue especially at frequencies below 100 kHz, so that this kind of noise is not considered further in this work.

Shot Noise

Shot noise is a phenomenon common to active devices. It originates in the pulsed-character of the current (determined by the discrete nature of the charge carriers, electrons and holes) flowing through a potential barrier, as the one of the *pn*-junction or the charge-free space in a vacuum tube [28].

The shot noise is also a white noise, like the thermal one, and has a Gaussian distributed amplitude. In the noise analysis it is represented by a current source connected in parallel with the junction producing the shot noise, and having the following RMS value:

$$I_{\mathrm{sh}} = \sqrt{2qI_{\mathrm{DC}}B} \tag{3.18}$$

where $q = 1.6 \cdot 10^{-19}\,\mathrm{C}$ is the elementary charge, I_{DC} is the DC current through the potential barrier, and B is the bandwidth.

[2]The RMS voltage of the equivalent excess noise generator associated with a resistor of resistance R can be expressed in a band stretching from f_1 to f_2 as [30]:

$$V_{\mathrm{R,Nex}} = I_{\mathrm{DC}}R \cdot \sqrt{K \ln \frac{f_2}{f_1}}$$

where K is a device dependent constant and I_{DC} is the DC current flowing through the resistor.

Flicker Noise

The flicker or $1/f$ noise, also known as excess noise, low-frequency noise and pink noise, is found both in vacuum tubes and semiconductor devices. In the latter category it is produced by generation and recombination phenomena, caused by impurities and defects. Flicker noise is also found in carbon resistors, due to the granulated-nature of the current path, whereas in metal film resistors it is normally negligible [30].

The spectral power distribution of flicker-noise has in general a $1/f^{\alpha}$ frequency dependence. This means that theoretically the noise would be infinite at DC. Nevertheless, the on-time of the device limits the frequency response.

Since the $1/f$ noise is related to current flow through the device, a general expression for the spectral density of the current generator modeling the flicker can be written as:

$$S_{\mathrm{i,flk}} = K \frac{I_{\mathrm{DC}}^{\beta}}{f^{\alpha}} \tag{3.19}$$

where K, α and β are device related constants, while I_{DC} is the DC current through the device.

Normally a corner frequency f_{c} is defined, setting the frequency above which the thermal noise is predominant, in comparison to flicker noise.

3.2.2 Noise Figure

A signal S_{in} applied at the input of an electric circuit always contains a certain amount of noise N_{in}. The input signal S_{in} as well as the input noise N_{in} are both affected in the same way by the passing through the circuit. If the circuit were noise free, at its output the signal-to-noise ratio SNR_{out} would be the same as the input one SNR_{in}. Nevertheless, all electric circuits are noisy, so that a certain amount of noise is always added to the signal as it passes through the circuit. This means that the output SNR is lower than the input one, as additional noise was contributed by the circuit itself. Based on this, a noise factor F is defined to describe the SNR degradation of a signal as it passes through an electric circuit (Friis' definition) [29]:

$$F = \frac{SNR_{\mathrm{in}}}{SNR_{\mathrm{out}}} \tag{3.20}$$

When expressed in dB, the noise factor F is called noise figure NF:

$$NF = 10 \lg F \tag{3.21}$$

For non-ideal circuits the noise factor F is always larger than 1 (noise figure NF always larger than 0 dB).

The noise factor is a function of the generator impedance $\underline{Z}_{\mathrm{G}}$ presented to the input port of the circuit. It can be shown that there is a generator impedance $\underline{Z}_{\mathrm{G}} = \underline{Z}_{\mathrm{opt}}$ for which F reaches its minimum value (see Appendix A).

For an arbitrary generator impedance $\underline{Z}_{\mathrm{G}}$ other than $\underline{Z}_{\mathrm{opt}}$ the noise factor will always be larger than F_{min}, as shown by the following equation [31]:

$$F = F_{\mathrm{min}} + \frac{R_{\mathrm{n}}}{G_{\mathrm{G}}}\left|\underline{Y}_{\mathrm{G}} - \underline{Y}_{\mathrm{opt}}\right|^2 \tag{3.22}$$

where F_{min} is the minimum noise factor of the two-port, $\underline{Y}_{\mathrm{opt}}$ is the generator admittance at which minimum noise factor occurs, $\underline{Y}_{\mathrm{G}}$ is the generator admittance presented to the input of the two-port, R_{n} is the noise resistance which gives an indication of the sensitivity of noise termination and G_{G} is the real part of the generator's admittance.

An important issue is the noise factor of cascaded two-ports. Knowing the available power gain $G_{\mathrm{a}i}$ of the i-th stage, as well as its noise factor F_i, the total noise factor can be computed as [29]:

$$F = F_1 + \frac{F_2 - 1}{G_{\mathrm{a1}}} + \frac{F_3 - 1}{G_{\mathrm{a1}}G_{\mathrm{a2}}} + \cdots + \frac{F_n - 1}{G_{\mathrm{a1}} \ldots G_{\mathrm{a}n}} \tag{3.23}$$

Here F_i is the noise factor displayed by the i-th stage in the presence of the output impedance of the $(i-1)$-th stage.

Eq. (3.23) shows that the total noise factor F is almost entirely dictated by the noise factor F_1 of the first two-port, when its available power gain G_{a1} is high enough in order to be able to neglect the rest of the terms. Indeed, although the first stage degrades the SNR ratio by F_1 by contributing its own noise, the signal is already amplified at its output. Therefore, the noise contribution of the second stage appears small in comparison to the now amplified signal. In other words the first stage dominates the total noise factor and therefore it is necessary for low-noise applications to minimize F_1 and to maximize G_{a1}.

Passive two-ports display a noise factor equal to their losses [32]. That is why any passive network (such as matching circuits, transmission lines, filters, etc) placed before the first (low-noise) stage of a receiver chain will directly degrade the overall noise factor by the amount of losses present in the passive network.

3.2.3 Noise Temperature

The concept of *noise temperature* can be sometimes used to simplify noise calculations or to describe the circuit noise performance. This is not a physical temperature, but it is defined as the virtual temperature a passive network must have in order to display an available noise power equal to the one of the port to be described, at a certain frequency [29]. For example, one may say that an antenna has a noise temperature of 500 K at a specified frequency. This means that the available noise power at the antenna port is the same as the one of a R_{A} resistance (the real part of the antenna impedance) heated at 500 K.

A noisy two-port can be also described in terms of *effective noise temperature* T_{e}. This is defined as the temperature the source resistance would have, so that the

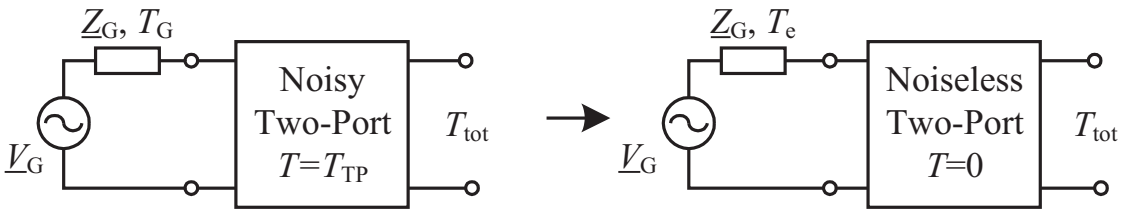

Fig. 3.9: Describing a noisy two-port in terms of effective noise temperature.

noiseless two-port displays the same amount of output noise as the actual two-port [33]. In other words, the noise contributed by the two-port is now no longer seen as the result of an internal cause, but it is externalized and attributed to the source resistance.

Some mathematical manipulation can relate the noise factor F to the effective noise temperature T_e of the two-port [29]:

$$F = 1 + \frac{T_e}{T_0} \tag{3.24}$$

or

$$T_e = (F - 1)T_0 \tag{3.25}$$

where $T_0 = 290\,\mathrm{K}$ is the ambient temperature.

3.3 Radio Channel Disturbances

Not only the noise generated in the receiver itself limits the performance of radio reception, but also the noise picked-up by the antenna, which has atmospheric, cosmic and artificial (man-made) origins. The amount of external noise can be expressed in terms of antenna noise temperature, as detailed in Fig. 3.10.

The noise in the lower frequency range originates mostly from the atmospheric electric discharges, whose electromagnetic waves propagate over large distances and can disturb the radio channel up to frequencies as high as 20 MHz [2]. In Fig. 3.10 the atmospheric noise temperature finds itself in 99% of the cases in the region enclosed by the two curves “atmospheric noise max” and “atmospheric noise min”. The curve “atmospheric noise avg” gives an average value in the LW range which is exceeded in 50% of the cases. This significant dispersion is caused by the large variation of the propagation conditions. This type of noise decreases with frequency and is lower during the day [34].

The man-made noise has an important contribution at higher frequencies and has its origins in industrial equipment, vehicles, etc. In Fig. 3.10 three curves corresponding to three different locations are shown for the man-made noise temperature, that is country side, city side and a serene location. As expected, the metropolitan environment is the noisiest. This noise type is also decreasing with frequency [2].

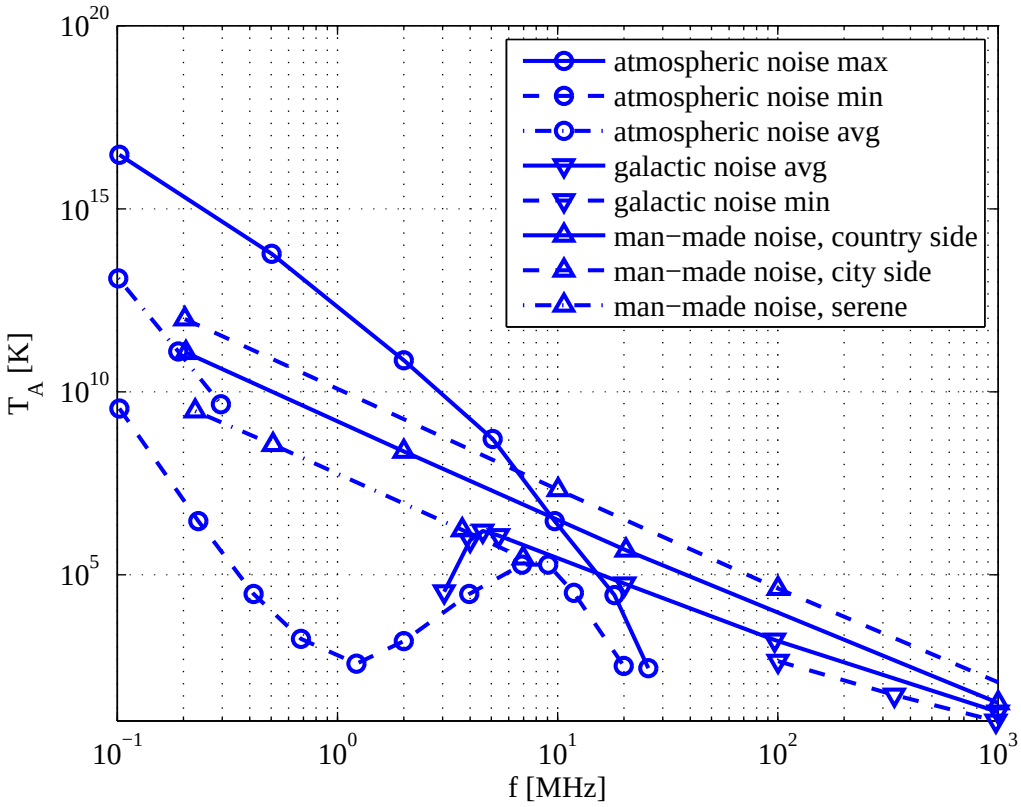

Fig. 3.10: External noise temperature.

When it comes to car radio reception, the car itself is an important source of man-made noise, because the antenna finds itself in the immediate vicinity of noise generators. The disturbances have their origins in the engine ignition pulses, in the power train electronics as well as in all the digital electronic equipment built inside the car. Especially troublesome are components like microprocessors, because they make use of digital signals with abrupt slopes, which exhibit broad spectra and are subject to electromagnetic compatibility (EMC) issues.

The average and the minimum curves are shown in Fig. 3.10 for the cosmic noise, and it can be seen that it becomes important for frequencies higher than 20 MHz. However, at least up to 1000 MHz the country-side man-made noise dominates.

Fig. 3.10 gives the antenna external noise temperature T_{A}, which is a measure of the available external noise power at the antenna feed-point:

$$P_{\mathrm{A,a}} = kT_{\mathrm{A}}B \tag{3.26}$$

where $k = 1.38 \cdot 10^{-23}\,\mathrm{J/K}$ is the Boltzmann constant and B is the bandwidth. Knowing the available power and the real part of the antenna impedance R_{A} given by eq. (3.8), we can now determine the external noise voltage induced in the short

vertical monopole antenna mounted above the ground:

$$V_{\mathrm{A,N}} = \sqrt{4R_{\mathrm{A}}P_{\mathrm{A,a}}} = \sqrt{160\pi^2 k T_{\mathrm{A}} B \left(\frac{h}{\lambda}\right)^2} \tag{3.27}$$

Using this equation and the values given in Fig. 3.10 we can estimate some external noise voltages induced in a 20 cm long monopole antenna element. For all frequencies the country-side man-made noise has been considered for the average value $V_{\mathrm{A,N,avg}}$, while for the minimum value $V_{\mathrm{A,N,min}}$ the serene region man-made noise has been used at 200 kHz and 1 MHz and the average cosmic noise at 100 MHz. The bandwidth is set to 9 kHz in the LW and MW ranges and to 120 kHz in the FM range. The results are summarized in Table 3.1 and give an overview of the required signal voltage that has to be induced in the antenna element in order to achieve a unity SNR, when an ideal noiseless receiver is used.

f [MHz]	$V_{\mathrm{A,N,min}}$ [dBµV]	$V_{\mathrm{A,N,avg}}$ [dBµV]
0.2	-18.6	-5.9
1	-22.9	-8.7
100	-17.4	-9.6

Table 3.1: Minimum and average external noise voltage induced in a 20 cm long monopole antenna. The bandwidth is set to 9 kHz in the LW and MW ranges and to 120 kHz in the FM range.

3.4 Active Antenna Theory of Operation

In a usual reception chain, the antenna element and the receiver are connected together by cables, as shown in Fig. 3.11. In this case we talk about a *passive antenna*, since between the antenna element and the receiver input there are no active circuits which perform amplification. In order to achieve maximum power transfer between the antenna and the receiver regardless the cable length, the receiver input impedance has to equal the cable characteristic impedance $\underline{Z}_0$, while the antenna impedance $\underline{Z}_{\mathrm{A}}$, if it deviates from $\underline{Z}_0$, has to be matched to this value. The presence of the matching network and the cable between the antenna and the receiver leads to a degradation of the signal-to-noise ratio, because these passive elements are lossy. Assuming for them an insertion loss a_{L} ($a_{\mathrm{L}} < 1$) and using eq. (3.23) and (3.25) we get the noise temperature of the passive receiving system $T_{\mathrm{sys,passive}}$:

$$T_{\mathrm{sys,passive}} = \frac{T_{\mathrm{rec}}}{a_{\mathrm{L}}} + T_0 \left(\frac{1}{a_{\mathrm{L}}} - 1\right) \tag{3.28}$$

where T_{rec} is the receiver noise temperature. The total noise temperature has to include the antenna noise temperature T_{A} as well:

$$T_{\mathrm{tot,passive}} = T_{\mathrm{A}} + T_{\mathrm{sys,passive}} \tag{3.29}$$

Even if the receiving system were noise-free, the external noise represents the lower limit of the achievable sensitivity. On the other hand, the receiver noise temperature T_{rec} is further "inflated" by the losses in the passive elements.

The matching circuit can be used as long as the antenna impedance $\underline{Z}_{\mathrm{A}}$ can be matched in the whole operating band without much difficulty and too many losses to the cable impedance $\underline{Z}_0$ (usually $50\,\Omega$), as the case is for $\lambda/4$ antennas. Nevertheless, as we have seen in section 3.1, the short and very short monopole antennas used for radio reception in cars display capacitive impedances for which the matching is very difficult, if not impossible, because of very small radiator bandwidth. Furthermore, very complex circuits would be required for matching impedances for applications with large percentage bandwidth (like AM for instance) [13]. Insufficient matching between antenna and cable leads to a transformation of $\underline{Z}_{\mathrm{A}}$, which is dependent on the cable's length l. As a consequence in practice, in applications with large percentage bandwidth the right impedance cannot be presented this way to the receiver. A way to avoid this issue is to use matching circuits which can be tuned for each frequency to be received, but this means a significant increase in complexity.

The receiver noise factor and, as a consequence, its noise temperature T_{rec} is a function of the source impedance, as explained in Section 3.2.2. In order to optimize its noise performance, noise matching instead of power matching should be performed and the cable's output should provide an impedance as close as possible to the receiver's $\underline{Z}_{\mathrm{opt}}$. However, $\underline{Z}_{\mathrm{opt}}$ is usually a complex value, while $\underline{Z}_0$ is real, so either an additional matching network must be used between cable and receiver, or the cable itself is used as a matching element. Both solutions are not practical for applications with large percentage bandwidth, because they require matching networks having an arbitrary complexity. Additionally, controlling the cable length can be impossible, especially for automotive applications. Therefore, when a cable is required, power matching is not avoidable.

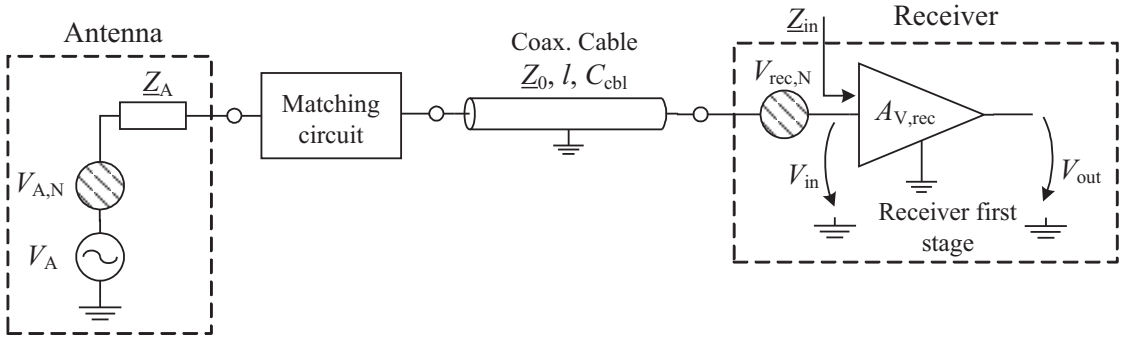

Fig. 3.11: Passive antenna receiver chain.

Let us now assume the case depicted in Fig. 3.12, which describes a reception chain using an *active antenna*: the antenna element is directly connected to an amplifier, which further drives the cable and the receiver input. The antenna amplifier

(here also denoted as *buffer*) has the voltage gain $A_{\mathrm{V,buf}}$, input impedance $\underline{Z}_{\mathrm{in,buf}}$, output impedance $\underline{Z}_{\mathrm{out,buf}}$ and the input referred noise voltage $V_{\mathrm{buf,N}}$.

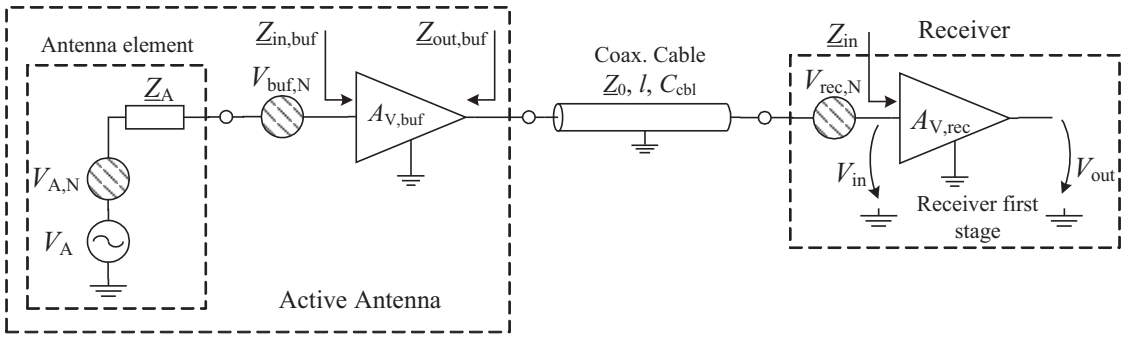

Fig. 3.12: Active antenna receiver chain.

Since now there are no other passive elements between the antenna element and the antenna amplifier (buffer), the noise temperature of the active antenna can be written as:

$$T_{\mathrm{aa}} = T_{\mathrm{A}} + T_{\mathrm{buf}} \tag{3.30}$$

where T_{buf} is the noise temperature of the buffer. If the buffer's gain is high enough, then the noise contribution of the cable and of the receiver can be neglected (eq. (3.23)) and T_{aa} approximates the total noise temperature of the active receiver chain:

$$T_{\mathrm{tot,active}} \simeq T_{\mathrm{aa}} \tag{3.31}$$

Since the output SNR is of importance for receiving systems, it is important to determine the frequency range for which a certain SNR can be maintained within certain limits. This frequency range is denoted as the *noise bandwidth* and can be defined as the domain in which the noise temperature of the active receiving chain reaches the double of its minimum value [13]:

$$T_{\mathrm{tot,active}} \leq 2 \cdot T_{\mathrm{tot,active,min}} \tag{3.32}$$

Both T_{A} and T_{buf} are frequency dependent: the antenna noise temperature varies as shown in Fig. 3.10, while the buffer's noise factor (and noise temperature, as a consequence) as given by eq. (3.22). If for a limited operating range the frequency dependence of T_{A} is small in comparison to the dependence of T_{buf}, then $T_{\mathrm{tot,active}}$ becomes:

$$T_{\mathrm{tot,active}} = T_{\mathrm{A}} + T_{\mathrm{buf,min}} + \frac{T_0 R_{\mathrm{n}}}{G_{\mathrm{A}}} \left| \underline{Y}_{\mathrm{A}} - \underline{Y}_{\mathrm{opt}} \right|^2 \tag{3.33}$$

where $T_{\mathrm{buf,min}}$ is the minimum noise temperature of the buffer achievable at $\underline{Y}_{\mathrm{opt}}$. As a result, the minimum noise temperature of the active receiver chain is:

$$T_{\mathrm{tot,active,min}} = T_{\mathrm{A}} + T_{\mathrm{buf,min}} \tag{3.34}$$

It follows that for the 3 dB noise bandwidth we have:

$$\frac{T_0 R_\mathrm{n}}{G_\mathrm{A}} \left| \underline{Y}_\mathrm{A} - \underline{Y}_\mathrm{opt} \right|^2 \leq T_\mathrm{A} + T_\mathrm{buf,min} \tag{3.35}$$

By adequately modifying for noise temperature eq. (A.10) and (A.11), this condition can be "graphically expressed" in the Smith chart as a circle, representing the impedance boundary of the noise bandwidth. This circle encloses the area which contains the antenna impedances $\underline{Z}_\mathrm{A}$ for which the noise bandwidth condition is satisfied. Knowing the frequency dependence of $\underline{Z}_\mathrm{A}$, the noise bandwidth can now be determined.

It is important to note that condition (3.35) becomes more and more permissive as T_A increases. The physical explanation relies on the fact that the additional noise contributed by the buffer has to increase continuously in order to double the minimum noise temperature $T_\mathrm{tot,active,min}$. This implies that the antenna impedance is allowed to travel further and further away from $\underline{Z}_\mathrm{opt}$ without significantly increasing the additional noise. As a result, the noise bandwidth becomes always larger as T_A increases[3].

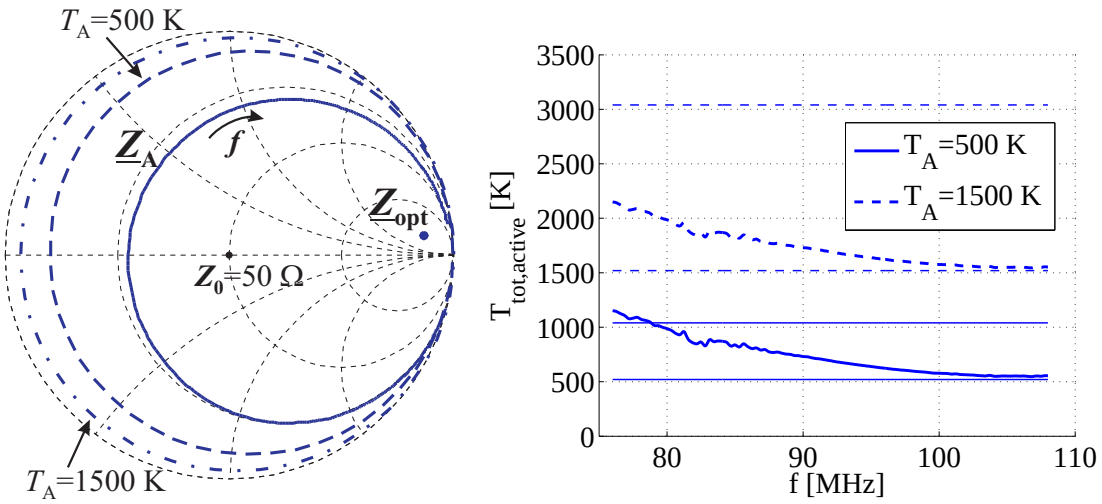

(a) Constant noise temperature circles for the 3 dB noise bandwidth and antenna impedance $\underline{Z}_\mathrm{A}$.

(b) Active antenna noise temperature. The lower and upper temperatures of the noise bandwidth are marked for each T_A.

Fig. 3.13: Simulated total noise temperature circles and the total noise temperature of an active antenna for two different external noise temperatures T_A in the FM range.

In Fig. 3.13 is given an example in the FM range, when a resonant antenna structure similar to the one presented in Chapter 6.1 is used in combination with

[3]Mathematically this can also be observed in eq. (A.11), where the noise circle radius increases towards unity (which implies an almost complete covering of the Smith chart) as F_min gets larger.

an ATF33143 transistor. Two antenna temperatures T_A have been considered and the corresponding 3 dB noise bandwidth circles are plotted in the Smith chart in Fig. 3.13(a). The lower temperature value (500 K) corresponds to the minimal cosmic radiation, while the larger one (1500 K) to the average cosmic radiation[4]. As expected, the 1500 K circle is larger than the 500 K one. The optimum noise impedance $\underline{Z}_{opt}$ and the antenna impedance $\underline{Z}_A$ are plotted on the same chart. Because the buffer's minimum noise temperature $T_{buf,min} \simeq 20\,K$ is low in comparison with T_A, the noise circles are considerably wide and cover almost entirely the Smith chart. Impedance $\underline{Z}_A$ lies almost entirely inside the $T_A = 500\,K$ circle and completely inside the $T_A = 1500\,K$ circle, as the plot in Fig. 3.13(b) shows.

Using a passive antenna and a lossless cable and matching network ($a_L = 1$), the total system noise temperature (eq. (3.29)) in the scenario with $T_A = 500\,K$ is 1365 K, when using a good receiver with 865 K noise temperature. In contrast, the active system reaches the minimum value (eq. (3.34)) of 520 K, which means about 4.2 dB improvement when it comes to SNR.

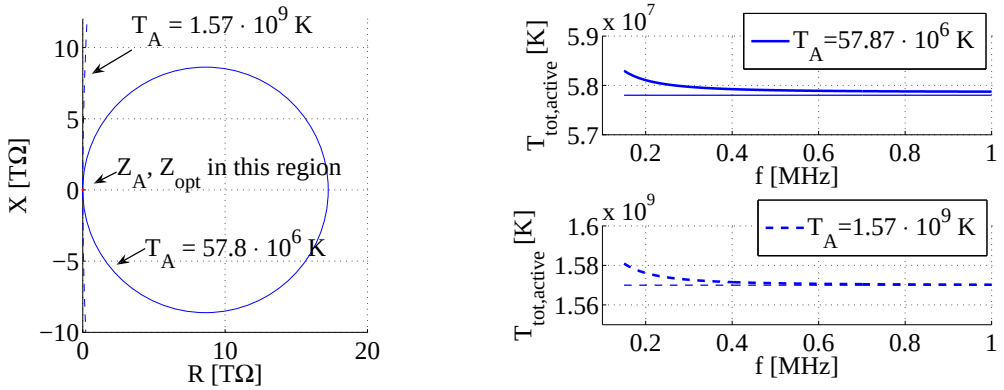

(a) Constant noise temperature circles for the 3 dB noise bandwidth and antenna impedance $\underline{Z}_A$.

(b) Active antenna noise temperature. The lower temperature of the noise bandwidth is marked for each T_A.

Fig. 3.14: Simulated total noise temperature circles and the total noise temperature of a 20 cm long active antenna for two different external noise temperatures T_A in the AM range.

In Fig. 3.14 is given an example in the AM range, when a 20 cm long simple monopole antenna is used together with a SST310 transistor. This time, because of the extremely high external noise temperature in the AM range, the representation of the noise bandwidth circles in the Smith chart proves to be irrelevant: the circles are so wide, that graphically there is no distinction any more between the circles and the border of the chart itself. That is why a Cartesian representation in the

[4]The considered antenna noise temperatures represent rather a worst case, since the man-made noise has usually higher values.

impedance plane is preferred. After some algebraic manipulations we get the circles' equation:

$$\left(R_{\mathrm{A}} - \left(R_{\mathrm{opt}} + \frac{|Z_{\mathrm{opt}}|^2(T - T_{\mathrm{tot,active,min}})}{2R_{\mathrm{n}}}\right)\right)^2 + (X_{\mathrm{A}} - X_{\mathrm{opt}})^2 = \\ = \frac{|Z_{\mathrm{opt}}|^2(T - T_{\mathrm{tot,active,min}})}{R_{\mathrm{n}}}\left(R_{\mathrm{opt}} + \frac{|Z_{\mathrm{opt}}|^2(T - T_{\mathrm{tot,active,min}})}{4R_{\mathrm{n}}}\right) \tag{3.36}$$

where $\underline{Z}_{\mathrm{A}} = R_{\mathrm{A}} + jX_{\mathrm{A}}$ and $\underline{Z}_{\mathrm{opt}} = R_{\mathrm{opt}} + jX_{\mathrm{opt}}$.

Two antenna temperatures T_{A} have been considered and the corresponding 3 dB noise bandwidth circles were plotted in the impedance plane in Fig. 3.14(a). The lower temperature value ($57.8 \cdot 10^6$ K) corresponds to the man-made noise in the serene regions at 1 MHz, while the larger one ($1.57 \cdot 10^9$ K) to the country-side man-made noise at 1 MHz. The $1.57 \cdot 10^9$ K circle is so large in comparison to the $57.8 \cdot 10^6$ K one, that it is only partially plotted. Even so, the $57.8 \cdot 10^6$ K circle is also extremely large, and the impedance goes well into the TΩ range. As a result, $\underline{Z}_{\mathrm{opt}}$ and $\underline{Z}_{\mathrm{A}}$ cannot be properly plotted. More information is given by Fig. 3.14(b), where the noise temperature is plotted as a function of frequency. For both T_{A} the total noise temperature $T_{\mathrm{tot,active}}$ lies within the 3 dB noise bandwidth. It is also interesting to notice that these external temperatures are for 1 MHz; for lower frequencies T_{A} and the noise bandwidth get even larger.

As long as the external noise T_{A} dominates the buffer's noise $T_{\mathrm{buf,min}}$ the noise bandwidth is significantly larger than the power bandwidth for electrically short antenna elements (which have very small real part antenna impedances R_{A}) [13]. This is the normal case at low frequencies, thus allowing the use of electrically very short antennas for reception without performing power matching.

A useful active antenna design relation can be devised by calculating the SNR in Fig. 3.12. The calculation is performed for the AM range, but it offers useful indications in FM as well.

The very short monopole active antenna is connected by a cable to a receiver with input impedance $\underline{Z}_{\mathrm{in}}$. For the AM frequency range for which the cable length l is much smaller than $\lambda/4$ the cable behaves capacitively and is represented in Fig. 3.12 by the C_{cbl} capacitance. The $V_{\mathrm{A,N}}$ noise source sums up both the own noise of the antenna and the noise picked-up from the atmosphere. Since the thermal noise contributed by R_{A} is negligible, only the external noise given by eq. (3.27) counts. $V_{\mathrm{rec,N}}$ is the input referred noise of the first receiver stage, evaluated for the source impedance connected to it, while $A_{\mathrm{V,rec}}$ is its voltage gain.

The SNR at the output of the first receiver stage can be computed after some algebraic manipulations, in which it is assumed that $\underline{Z}_{\mathrm{in}} \to \infty$, as most car radios have a high input impedance in AM much higher than the cable reactance:

$$\left.\frac{V_{\mathrm{out,S}}^2}{V_{\mathrm{out,N}}^2}\right|_{\mathrm{active}} = \frac{|A_{\mathrm{V,buf}}|^2 V_{\mathrm{A}}^2 \left|\frac{\underline{Z}_{\mathrm{in,buf}}}{\underline{Z}_{\mathrm{A}}+\underline{Z}_{\mathrm{in,buf}}}\right|^2 \left|\frac{j\underline{X}_{\mathrm{cbl}}}{\underline{Z}_{\mathrm{out,buf}}+j\underline{X}_{\mathrm{cbl}}}\right|^2}{|A_{\mathrm{V,buf}}|^2 \left(V_{\mathrm{A,N}}^2 + V_{\mathrm{buf,N}}^2\right) \left|\frac{\underline{Z}_{\mathrm{in,buf}}}{\underline{Z}_{\mathrm{A}}+\underline{Z}_{\mathrm{in,buf}}}\right|^2 \left|\frac{j\underline{X}_{\mathrm{cbl}}}{\underline{Z}_{\mathrm{out,buf}}+j\underline{X}_{\mathrm{cbl}}}\right|^2 + V_{\mathrm{rec,N}}^2} \tag{3.37}$$

where $\underline{X}_{\mathrm{cbl}} = 1/(\omega C_{\mathrm{cbl}})$ is the reactance of the cable capacitance.

As expected, equation (3.37) shows that if the receiver were noise-free, the output SNR would be lower than in the passive case, since now we have an additional noise source – that is, the antenna amplifier. It also shows that, in the realistic case of a noisy receiver, the SNR degradation due to $V_{\mathrm{rec,N}}$ is much more pronounced if there is a strong voltage division between $\underline{Z}_{\mathrm{A}}$ and $\underline{Z}_{\mathrm{in,buf}}$ and between $\underline{Z}_{\mathrm{out,buf}}$ and $\underline{X}_{\mathrm{cbl}}$.

The first voltage division shows that the buffer has to have high input impedance $\underline{Z}_{\mathrm{in,buf}}$ in order to pick-up as much signal as possible from the antenna element. When compared to the passive case (where ca buffer is missing), this is an important improvement: $\underline{X}_{\mathrm{cbl}}$ is a function of the cable length – which is further dependent on the car configuration. This length can vary between 1.5 m and 6 m, which means a cable capacitance[5] between 50 pF and 600 pF. When compared to the antenna capacitance values C_{A} depicted in Fig. 3.4(a), it is easy to see that the signal is strongly attenuated by this voltage division.

The second voltage division shows that the buffer has to be able to drive the capacitive loading represented by the cable[6]. This means that the buffer has to have a low output impedance $\underline{Z}_{\mathrm{out,buf}}$.

Being able to improve the delivered SNR by means of active antennas implies also that it is possible to decrease the antenna size, while preserving the SNR. The extent to which this reduction is possible is a strong function of the amplifier's technology.

3.5 Summary

Electrically very short monopoles are antennas whose physical length is lower than a tenth of the operating wavelength. In this case, the current distribution along the monopole is triangular and the antenna impedance is mainly capacitive. It has been shown that power matching is not possible for electrically very short monopole antennas because of the drastic decrease of both efficiency and attainable bandwidth. These aspects, together with the low effective height, do not allow the combination of these antennas with conventional reception techniques for broadband radio reception.

Noise in electronic systems is an unavoidable phenomenon, which impairs the reception of weak radio signals. Besides the external noise picked-up by the antenna, the main noise types found in the active antenna circuit are the thermal noise, the shot noise and the flicker noise. However, the active antenna concept, which in the presence of external noise gives up power matching between antenna and amplifier, allows for the design of broadband reception elements optimized for output signal-

[5] For cables with 50 Ω characteristic impedance the capacitance per unit length can be assumed to be about 100 pF/m, while for 150 Ω cables this capacitance can be assumed to be about 33 pF/m.

[6] There are some radio receivers which have 50 Ω input impedance also in AM. In this case the buffer output has to be matched to 50 Ω.

to-noise ratio. This principle makes possible for the electrically very short monopole antennas to be effectively used for broadband radio reception.

Chapter 4

Critical Design Issues of Automotive Active Antennas

The previous chapter focused on the sensitivity topic in the context of noisy radio reception and the improvement achievable with the help of active antennas. The discussion moves now to the antenna amplifier itself and its design issues, like the selection of proper active devices, noise minimization and linearity.

As we shall shortly see, the biasing technique of active devices used for active antenna amplifiers plays an important role for the noise performance. Only field effect transistors are suited for high-impedance antenna amplifiers and a comparison between different commercial available types is made in order to pick-up the best suited device. As the noise performance is the main classification criterion, the noise characteristics of the transistors are obtained experimentally, so that the resulting noise models are best suited for the frequency range and the application intended in this work.

Finally, as every practical circuit has to be characterized experimentally, the measurement techniques of different important parameters are discussed, like the noise performance, the linearity or the field measurements.

4.1 Gate Biasing Resistor Noise

The gate or base of any transistor has to be biased. This is achieved by connecting a DC current conducting element to the transistor's gate or base, such as a resistor or an inductor. In the AM range the inductors prove to be impractical, since very large values are required in order not to short-circuit the signal path; instead, resistors are used for biasing. Because of the large value required, only FET devices can be used, due to their very small gate leakage current. Besides their relative low input impedance, bipolar transistors also have significant base currents, so important

voltages may fall upon the biasing resistor, making their use impractical[1].

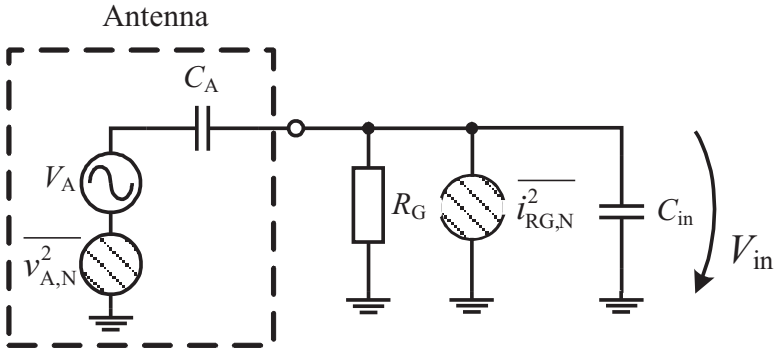

Fig. 4.1: Noise at the amplifier's input.

The noise contributed by such a gate biasing resistor (further denoted as R_G) requires a special analysis. Fig. 4.1 depicts schematically the input circuit of the amplifier, with C_{in} the input capacitance of the amplifier, C_A the antenna capacitance and the thermal noise of the resistor R_G described by the parallel noise current source $\overline{i^2_{RG,N}}$:

$$\overline{i^2_{RG,N}} = \frac{4kT_0B}{R_G} \tag{4.1}$$

The thermal noise voltage produced by the resistor reaches the transistor's gate through the voltage divider (which also behaves like a low-pass filter) formed by R_G itself and $C_A + C_{in}$. This means that the noise contribution of R_G is frequency dependent. In this case, the noise voltage $\overline{v^2_{in,RG,N}}$ contributed by R_G alone at the amplifier's input can be written as:

$$\overline{v^2_{in,RG,N}} = \frac{4kT_0BR_G}{1 + R_G^2 \cdot \omega^2 \left(C_A + C_{in}\right)^2} \tag{4.2}$$

which is frequency dependent, as already hinted. Analyzing (4.2) we find that the input noise voltage exhibits a maximum in respect to R_G:

$$\frac{\partial \overline{v^2_{in,RG,N}}}{\partial R_G} = 0 \Rightarrow R_{G0} = \frac{1}{\omega \left(C_A + C_{in}\right)} \tag{4.3}$$

This means that there is a worst-case choice for R_G, in which the input noise voltage will have a peak, and which must be avoided. As shown, this critical value R_{G0} is frequency dependent and gets larger, as the frequency decreases.

[1]For example, for 30 mA collector current and $\beta = 100$, the base current is $300\,\mu A$. If the application requires $100\,k\Omega$ for the biasing resistor, the DC-voltage upon this resistor would be as high as 30 V.

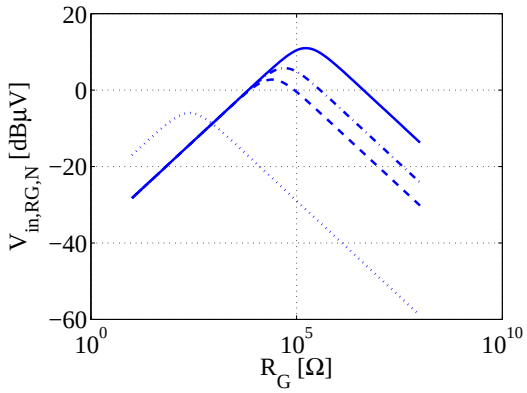

(a) Noise voltage contributed by R_G at the amplifier's input.

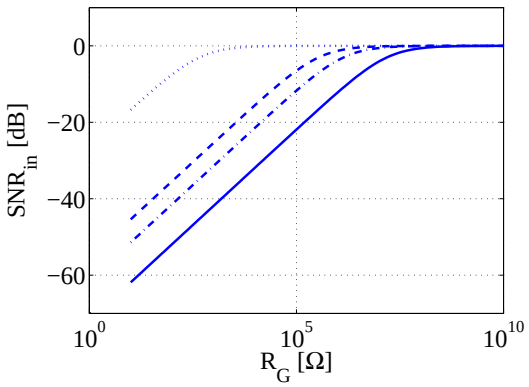

(b) Signal-to-noise ratio at the amplifier's input when $SNR_A = 1$ and $\overline{V_{A,N}^2}$ has an arbitrary value.

Fig. 4.2: Noise performance vs. R_G at three different AM operating frequencies: – 150 kHz,–· 500 kHz, - - 1 MHz, and one FM operating frequency: · · 100 MHz. The considered bandwidth is 9 kHz in AM and 120 kHz in FM.

Figure 4.2(a) depicts the input noise voltage curves calculated with eq. (4.2) for three different AM frequencies (9 kHz bandwidth) and one FM frequency (120 kHz bandwidth). $C_A = 3.3\,\text{pF}$ and $C_{in} = 3\,\text{pF}$ for all considered cases. The peak predicted by (4.3) can be seen for each considered frequency. As expected, the value of R_{G0} decreases, as f increases. For $f = 150\,\text{kHz}$ the worst-case value for R_G is $R_{G0} = 168.4\,\text{k}\Omega$, while for $f = 1\,\text{MHz}$ one obtains $R_{G0} = 25.3\,\text{k}\Omega$. At 100 MHz $R_{G0} = 252.6\,\Omega$ is obtained.

We shall now investigate the influence of R_G upon the input SNR. In Fig. 4.1 the useful signal voltage V_{in} at the amplifier's input can be written as:

$$V_{in} = V_A \frac{\omega R_G C_A}{\sqrt{1 + \omega^2 R_G^2 (C_A + C_{in})^2}} \tag{4.4}$$

The noise voltage $\overline{v_{in,N}^2}$ at the amplifier's input is contributed by the antenna and the R_G resistor and it can be expressed as:

$$\overline{v_{in,N}^2} = \frac{\overline{v_{A,N}^2} \cdot \omega^2 R_G^2 C_A^2 + 4kT_0 B R_G}{1 + \omega^2 R_G^2 (C_A + C_{in})^2} \tag{4.5}$$

where $\overline{v_{A,N}^2}$ is the noise contributed by the antenna. As the SNR at the antenna port can be expressed as:

$$SNR_A = \frac{V_A^2}{\overline{v_{A,N}^2}} \tag{4.6}$$

the SNR at the amplifier's input can now be written using (4.4) and (4.5):

$$SNR_{\mathrm{in}} = \frac{V_{\mathrm{in}}^2}{\overline{v_{\mathrm{in,N}}^2}} = SNR_{\mathrm{A}} \frac{1}{1 + \frac{4kT_0B}{\overline{v_{\mathrm{A,N}}^2} \cdot \omega^2 R_{\mathrm{G}} C_{\mathrm{A}}^2}} \tag{4.7}$$

Unlike the input noise voltage $\overline{v_{\mathrm{in,N}}^2}$, eq. 4.7 does not display any peaks, but asymptotically tends towards SNR_{A} when $R_{\mathrm{G}} \to \infty$, as shown in Fig. 4.2(b) for three different AM frequencies and one FM frequency, $SNR_{\mathrm{A}} = 1$ and an arbitrary value for $\overline{v_{\mathrm{A,N}}^2}$.

This discussion highlights the importance of the R_{G} value, which should be chosen as large as possible. The lowest frequency for which the amplifier has to work represents the worst case, so the dimensioning of R_{G} should be made for this case. Nevertheless, as (4.7) shows, beyond a certain R_{G} value there is little improvement in the input SNR. The tendency indicated by (4.2) has also to be taken into account in order to reach the output noise level target.

4.2 Noise of Different Commercial Transistors

As the active device plays the major role in the output SNR of an active antenna, this sections evaluates the noise of some commercial FET transistors and compares their performance and suitability for the automotive active antenna use.

Bipolar transistors are not suited to be used in amplifiers for high-impedance antennas, because they exhibit a significant base-emitter shot noise current source. The effect of this noise source gets very pregnant at low frequencies, where the antenna impedance $\underline{Z}_{\mathrm{A}}$ is also very high. Even the silicon-germanium (SiGe) transistors, although they feature very low flicker noise, prove to be unsuitable for the active antenna use when the antenna element has high impedance. Additionally, bipolar transistors have significant base currents and relative low input impedance at low frequencies, which cannot be fully compensated by means of circuit techniques.

FET transistors are suited for active antenna application, due to their intrinsic high input impedance character and their very low gate-source noise current source.

The noise characteristics of the investigated transistors has been obtained experimentally, because the simulation models and the information provided in the datasheets for the high frequency GaAs devices proved to be poor in the lower frequency range. The measurements were performed in the range between 100 kHz and 300 MHz by measuring the output noise voltage in two situations: the first when the transistor's AC input is short-circuited, so that only the drain noise current source $I_{\mathrm{D,n}}$ contributes noise to the output, and the second when a $50\,\Omega$ impedance is presented to the transistor's AC input. In both cases the noise contributed by the other passive elements in the circuit was deembedded.

Four transistors have been experimentally investigated:

- **SST310** – Si junction field effect transistor (JFET) manufactured by Linear;

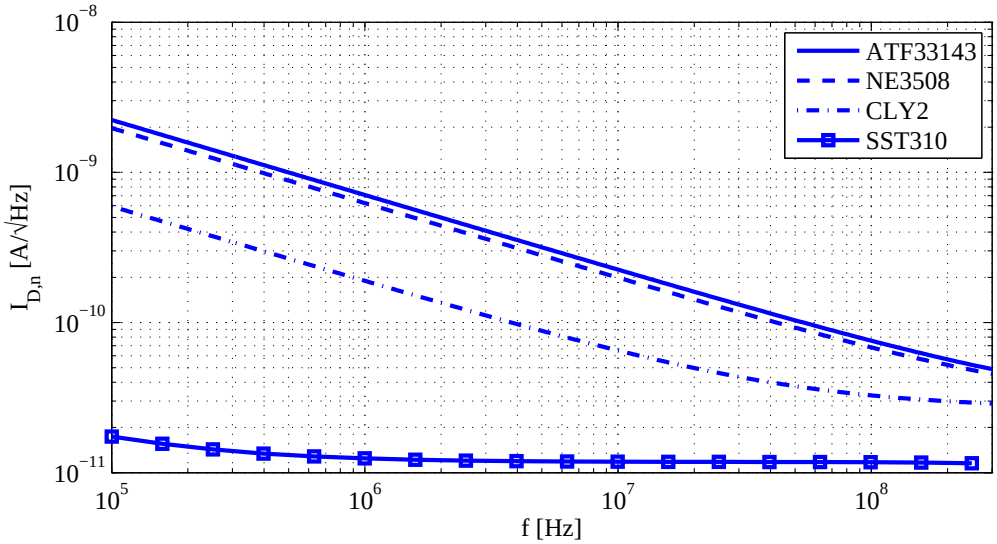

Fig. 4.3: Drain noise current vs. frequency for different commercial transistors.

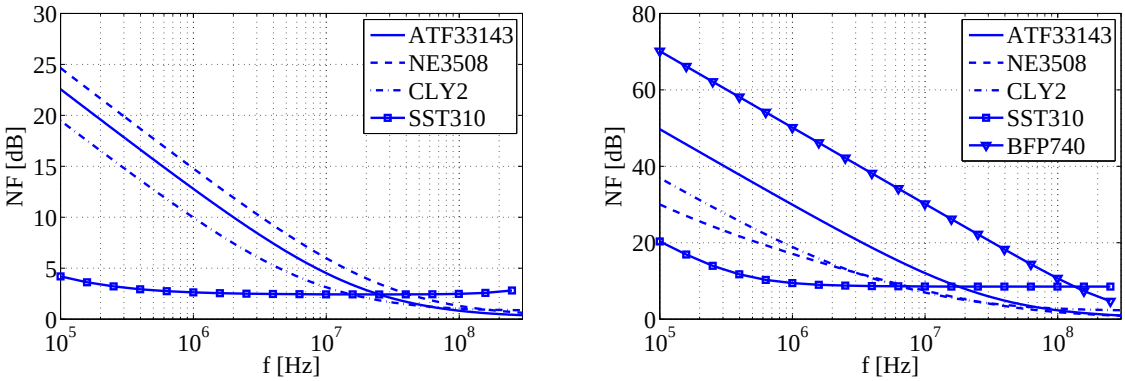

(a) Noise figure in a 50 Ω system.

(b) Noise figure with 50 Ω + 3.3 pF source impedance.

Fig. 4.4: Noise figure vs. frequency for different commercial transistors.

- **CLY2** – GaAs metal semiconductor field effect transistor (MESFET) manufactured by TriQuint;
- **ATF33143** – GaAs high electron mobility transistor (HEMT) manufactured by Agilent;
- **NE3508** – GaAs HEMT manufactured by NEC.

Eq. (B.6) and eq. (B.12) have been fitted on the measured data and the parameters P, K and α shown in Table 4.1 have been found to provide acceptable results. Regarding the shot noise component of the gate noise current, Table 4.1 lists also

the measured values of the gate leakage current I_G. As expected, the GaAs transistors have higher values than the Si device. Also, because the NE3508 transistor can handle lower drain currents than the ATF33143 and the CLY2 transistors, its area is also smaller and thus I_G is lower. Alone the ATF33143 has a very high I_G, which also strongly varies from sample to sample, thus complicating the design in some situations.

Fig. 4.3 shows the drain noise current source $I_{D,N}$ determined experimentally. The GaAs devices exhibit the highest noise values and an ascending trend towards lower frequencies. Also, the HEMT devices have higher noise currents when compared to the MESFET. In contrast, the Si device features lower noise at low frequencies. This comparison is nevertheless insufficient, because it does not account for the transconductance g_m of each active device, and so the achievable gain. This is shown in Fig. 4.4(a), where the noise figure NF in a $50\,\Omega$ system is depicted. This time the Si device exhibits a better performance only at low frequencies, while for the higher ones the GaAs transistors are superior. As expected from the device theory, the HEMTs feature the lowest noise figure at high frequencies.

In Table 4.1 it can be seen that the g_m of the SST310 transistor, typical for Si JFET devices, is very low, which means that the achievable gain is also low. As long as the noise current of the Si JFET at low frequencies is significantly lower than the one of the GaAs devices, the noise figure is also lower. However, at higher frequencies, where the noise current of the GaAs transistors becomes smaller, their gain advantage is observable also in the noise figure, which drops below 1 dB.

Transistor	I_D [mA]	g_m [mS]	r_o [Ω]	P	K	α	I_G [nA]
SST310	30	16	1270	0.55	$1.70 \cdot 10^{-15}$	1.30	< 1
CLY2	40	121	74	1.06	$1.14 \cdot 10^{-12}$	0.76	50
NE3508	30	215	71	0.40	$3.60 \cdot 10^{-11}$	1.00	6
ATF33143	40	322	67	0.10	$5.36 \cdot 10^{-12}$	0.39	1000

Table 4.1: Comparison of different transistors.

Fig. 4.4(b) depicts the noise figure of the transistors when the source is a 3.3 pF capacitance, a usual value for short monopole antennas. In the FM range and above, of all the GaAs transistors the HEMTs feature the lowest noise figure. The noise figure attainable with a BFP740 SiGe bipolar transistor from Infineon is also shown for comparison. As expected, it brings by far the largest amount of noise, because of the unfortunate combination between the source impedance and its intrinsic input noise current source.

As a conclusion, the Si JFET is the best solution for AM applications, while the GaAs devices are the right choice for the FM, Band-III and further for the L-Band operation.

4.3 Important Parameters and Requirements

4.3.1 Embedding the Antenna Impedance into the Simulation

The correct design of an active antenna implies a close correlation between antenna and amplifier and in the simulations the amplifier has to be provided with the correct antenna impedance $\underline{Z}_{\mathrm{A}}$. Antenna impedances can be embedded into simulations either by using an adequate antenna dummy circuit, or by using measured data. The simulation port impedance, usually $50\,\Omega$, has to be transformed without losses into the measured $\underline{Z}_{\mathrm{A}}$, so that the port's power is preserved. This can be done using an adequate non-dissipative two-port, which can be calculated from the measured data.

The S-parameter matrix $\mathbf{S}$ of a passive, reciprocal and non-dissipative two-port has to satisfy the condition [35]:

$$\mathbf{S}^* \cdot \mathbf{S} = \mathbf{U} \tag{4.8}$$

where $\mathbf{U}$ is the unity matrix. From this condition the relations between the magnitudes of each component are:

$$|\underline{S}_{11}|^2 + |\underline{S}_{21}|^2 = 1 \tag{4.9}$$
$$|\underline{S}_{12}|^2 + |\underline{S}_{22}|^2 = 1 \tag{4.10}$$

while the phase relation is obtained from:

$$\underline{S}_{11}\underline{S}_{21}^* + \underline{S}_{12}\underline{S}_{22}^* = 0 \tag{4.11}$$

Additionally, because the two-port is symmetrical, we know that $\underline{S}_{11} = \underline{S}_{22}$ and $\underline{S}_{21} = \underline{S}_{12}$. This leads to the following S-parameter matrix for the antenna two-port:

$$\mathbf{S} = \begin{bmatrix} |\underline{S}_{11}| \cdot e^{j\varphi_{11}} & \sqrt{1 - |\underline{S}_{11}|^2} \cdot e^{j(\varphi_{11} \pm \pi/2)} \\ \sqrt{1 - |\underline{S}_{11}|^2} \cdot e^{j(\varphi_{11} \pm \pi/2)} & |\underline{S}_{11}| \cdot e^{j\varphi_{11}} \end{bmatrix} \tag{4.12}$$

As a result, measuring the antenna reflection coefficient $\underline{S}_{11}$ is enough for calculating the corresponding non-dissipative symmetric two-port. The phase ambiguity of $\underline{S}_{21}$ and $\underline{S}_{12}$ is not important for this application.

4.3.2 Field Measurements

The signal performance of a car antenna in the VHF band can be evaluated only when the antenna is mounted on the car. Because of the metallic car body and the signal wavelength, the electromagnetic field is no longer uniform in the car's proximity, and the antenna directivity pattern becomes a frequency dependent function of the car body geometry and mounting position.

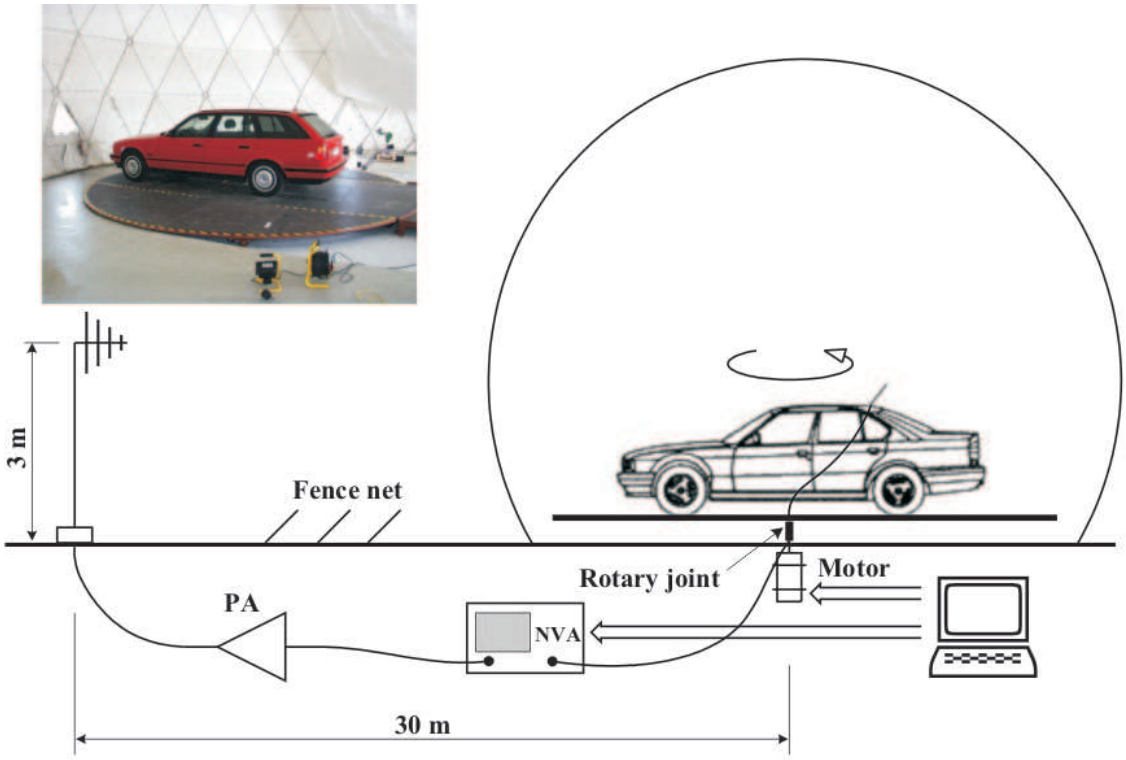

Fig. 4.5: Simplified set-up for the field measurement (drawing not to scale).

In order to evaluate all these parameters and the signal performance, field measurements are done with the active antenna mounted on a car. The usual mounting position of short rod antennas is on top of the car, above the rear windshield. The car is placed on a turntable which is installed in a radome in order to protect the measuring equipment from the weather. A logarithmic periodic antenna, about 3 m high, is mounted about 30 m away from the radome and radiates the RF signal towards the car, as shown in Fig. 4.5. The radiated waves can be either horizontally or vertically polarized. In order to avoid ground reflections and maintain constant (± 1 dB) the field intensity in the car's vicinity, a metal fence net is mounted between the emitting antenna and the turntable. The emitting antenna and the receiving one (i.e. the car antenna) are connected to a vector network analyzer (VNA), so that the transmission $\underline{S}_{21}$ between the two antennas is measured. A broadband RF power amplifier (PA) is inserted between the VNA and the logarithmic periodic antenna, in order to compensate for the cable and free space propagation losses.

Because the free space propagation loss is unknown and dependent on poor controllable parameters like the car position on the turntable, the measurement has to be referred to a certain reference, which in this case is a 90 cm long passive monopole antenna mounted on a front fender of the car. The VNA and the turntable are both controlled by a computer, and a full frequency sweep is performed every 5° during

the rotation. Because of the car body's influence, the directivity is also frequency dependent and this can be observed for both polarizations in the frequency variation of the signal level (Fig. 2.5). The software computes the frequency dependent antenna directivity, as well as the (rotation) averaged frequency characteristic. In the latter case the antenna directivity is accounted for by averaging the values for each frequency point for a complete car rotation, thus obtaining an estimate of the overall antenna performance.

4.3.3 Noise of Active Antennas

Section 3.4 already gave an insight of the importance of the noise issue in active antennas, while Section 3.2 treated the main noise sources occurring in an antenna amplifier. Now we have to set the design goals and describe the measurement methodology.

Required Noise Performance

The noise performance of a two-port is mainly evaluated in terms of noise factor. However, this is usually done in a $50\,\Omega$ system, for which the measurement equipment is also foreseen. An active antenna, on the other hand, is not a two-port which can be connected to a standard measurement equipment, since its input port is the antenna element itself. It is of course possible to measure only the antenna amplifier, but this brings little knowledge when the noise source of standard measurement equipment is $50\,\Omega$ matched. Indeed, the actual antenna impedance may wander far from $50\,\Omega$ (as for example $\underline{Z}_\mathrm{A}$ of a short monopole does), while the amplifier's noise figure is a strong function of the source impedance (Eq. (3.22)). Such non-$50\,\Omega$ measurements can be performed with special equipment containing expensive impedance tuners, which is unfortunately unavailable in common laboratories.

Another way of measuring the noise figure in a non-$50\,\Omega$ environment is by inserting an additional two-port between the noise source and the device under test (DUT), so that the DUT is provided with the actual antenna impedance $\underline{Z}_\mathrm{A}$ (antenna dummy). However, this method is not accurate, since $\underline{Z}_\mathrm{A}$ can be seldom precisely modeled, while the losses in this antenna dummy have to be determined as well. Nevertheless, such an approach is used in this work for rough estimates of the design performance during the development phase, as no other technique is available.

The noise factor describes the SNR degradation of a signal as it passes through an electric circuit (eq. (3.20)), but it offers no direct information about the *noise level* at the circuit's output. It is of course possible to calculate the output noise voltage from the noise factor, but this computation requires an accurate measurement of the noise factor and precise information about the available gain of the DUT, the source impedance and the actual T_A. Therefore a much more convenient way is to

directly measure the output noise voltage with the help of a test receiver, as detailed in the next section.

The output noise voltage is a very important parameter for active antennas, because the noise level further delivered toward the radio receiver has to be kept below certain values. The Verband der Automobilindustrie (VDA) organization [36] issued recommendations concerning these noise levels and the bandwidth to be measured in, which are highlighted in Table 4.2 for the AM and FM bands.

Range	LW	MW	SW	FM-J	FM-ECE
$V_{\text{out,N}}$ [dBµV]	-1	-6	-6	-5	-5
B [kHz]	9	9	9	120	120

Table 4.2: Maximum allowable output noise voltage and the corresponding bandwidth.

As we shall see, the output noise level will be a main issue along this work. Common modern low noise amplifiers (LNA) usually exhibit outstanding noise factors, but with very high output noise voltages due to their high gain values. Therefore, in this work we are concerned to fulfill the requirements listed in Table 4.2, rather than optimizing the noise factor alone.

Noise Measurement

In order to avoid the pick-up of unwanted signals, like radio channels or industrial interferences, the noise measurements have to be performed under controlled conditions, in shielded chambers or even anechoic chambers, if available.

A rapid way to determine the noise performance of an active antenna – useful especially in the development phase, when measurements are often required after try-and-error design changes – is to use an antenna dummy instead of the actual antenna element, so that the antenna amplifier (DUT) "sees" the correct impedance at its input port. The DUT and the antenna dummy circuit are placed in a shielded box, as Fig. 4.6(a) illustrates. The output noise voltage $V_{\text{out,N}}$ is measured with the help of a test receiver, which finds itself outside the shielded enclosure.

The actual car radios have high input impedance in the AM range. As this is not achievable with a standard 50 Ω test receiver, an additional buffer having about 7 pF input capacitance is used for the AM noise measurements, as shown in Fig. 4.6(a). A long coaxial cable connects the DUT to the buffer, as also is the case in the car. For the lab measurements a 2.5 m long 50 Ω cable was used, which means about 250 pF capacitive loading for the antenna amplifier.

An anechoic chamber provides both shielding and absorption of the electromagnetic waves. Therefore in this case the antenna amplifier can be evaluated together with the antenna element, as Fig. 4.6(b) shows. The active antenna is mounted on a metal grounded plate, which has to be large enough in order to behave like a valid ground plane for the considered frequency range. Because of its wavelength, the AM

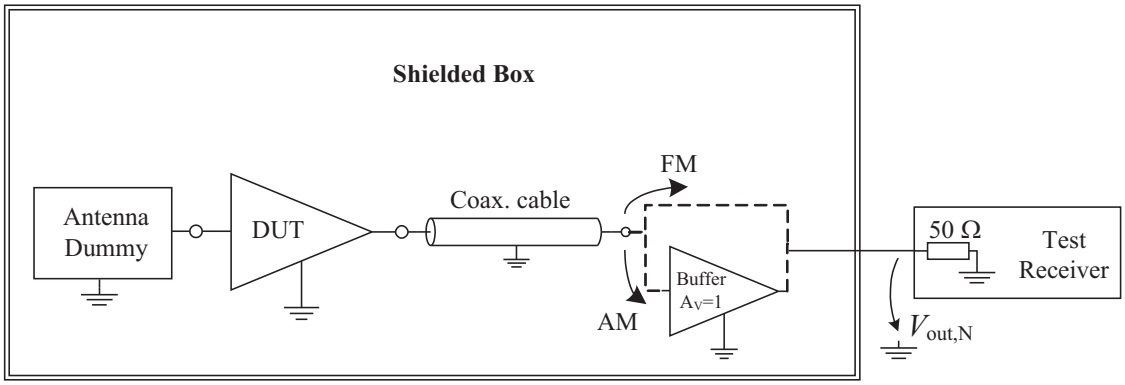

(a) Noise measurement in the shielded box.

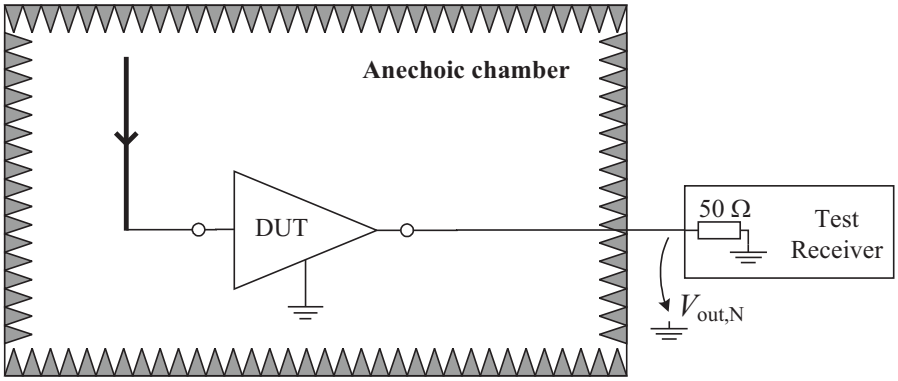

(b) Noise measurement in the anechoic chamber.

Fig. 4.6: Noise measurement in the lab.

range is not evaluated in this way, the shielded box approach being preferred. The output noise voltage $V_{\mathrm{out,N}}$ is measured by a test receiver, which is placed outside the anechoic chamber.

4.3.4 Sensitivity

The sensitivity of an electronic system shows the minimal still detectable signal in the presence of noise. For radio receivers, the sensitivity is related to the minimum SNR which can still be correctly demodulated. In the case of the active antennas presented in this work, the sensitivity will be defined for a unity SNR at the active antenna's output.

The FM sensitivity of an active antenna is measured in the anechoic chamber and is referred to the sensitivity achievable under the same conditions with a passive 90 cm long rod antenna (reference antenna). To do this, an FM modulated signal is radiated by an emitting antenna placed in the anechoic chamber, as shown in Fig. 4.7. The emitting power is chosen in such a way, that the measured an-

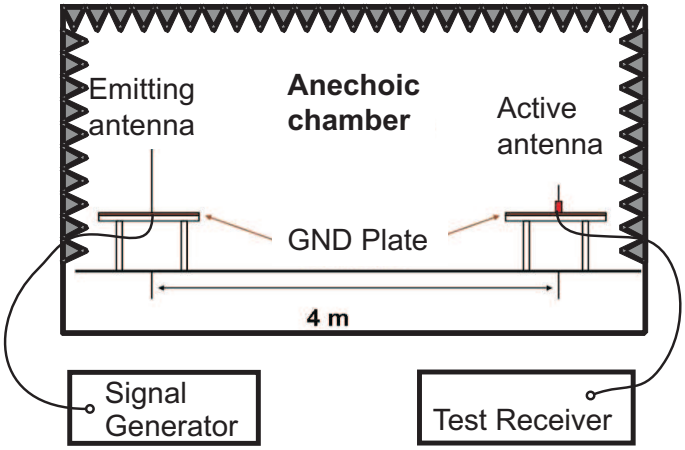

Fig. 4.7: Set-up for measuring the FM sensitivity in the anechoic chamber.

tenna (active or passive) output signal power equals its output noise power. Since the results for the active antenna are referred to the ones obtained with the reference rod, the particularities of the measuring arrangement (like cable attenuations, propagation attenuation, etc.) are accounted for.

4.3.5 Non-linear Effects

A circuit is said to behave linear when its output is a linear function of its input. This is normally the case when the small-signal conditions are fulfilled. However, how small small may be is a matter of the circuit's particular structure.

Active devices naturally have nonlinear characteristics, as for instance eq. (B.1) shows. Therefore, large input signals lead to distorted outputs. Such nonlinear transfer functions can be handled mathematically by employing power series (which is a more simplistic method, as the output does not take into account the time history of the input) or Volterra series [37], the latter being the general approach which also takes "memory " effects into account. Using the power series, the amplifier's output can be expressed as an infinite series:

$$v_{\text{out}} = a_1 v_{\text{in}} + a_2 v_{\text{in}}^2 + a_3 v_{\text{in}}^3 + \ldots + a_n v_{\text{in}}^n \tag{4.13}$$

where v_{in} is the input voltage, while a_i are coefficients characterizing the amplifier and are frequency and bias dependent. Only the first term represents the linear gain, while all the other ones generate higher order distortions.

As a consequence of the non-linear characteristic of the amplifier, an one-tone input signal $v_{\text{in}} = V_{\text{in}} \cos(\omega t)$ will result in an output signal containing harmonics, i.e. signals situated on the multiples of the fundamental frequency ω. Truncating the series to the third order, we get:

$$v_{\text{out}} = \frac{1}{2} a_2 V_{\text{in}}^2 + \left(a_1 V_{\text{in}} + \frac{3}{4} a_3 V_{\text{in}}^3 \right) \cos(\omega t) + \frac{1}{2} a_2 V_{\text{in}}^2 \cos(2\omega t) + \frac{1}{4} a_3 V_{\text{in}}^3 \cos(3\omega t) \tag{4.14}$$

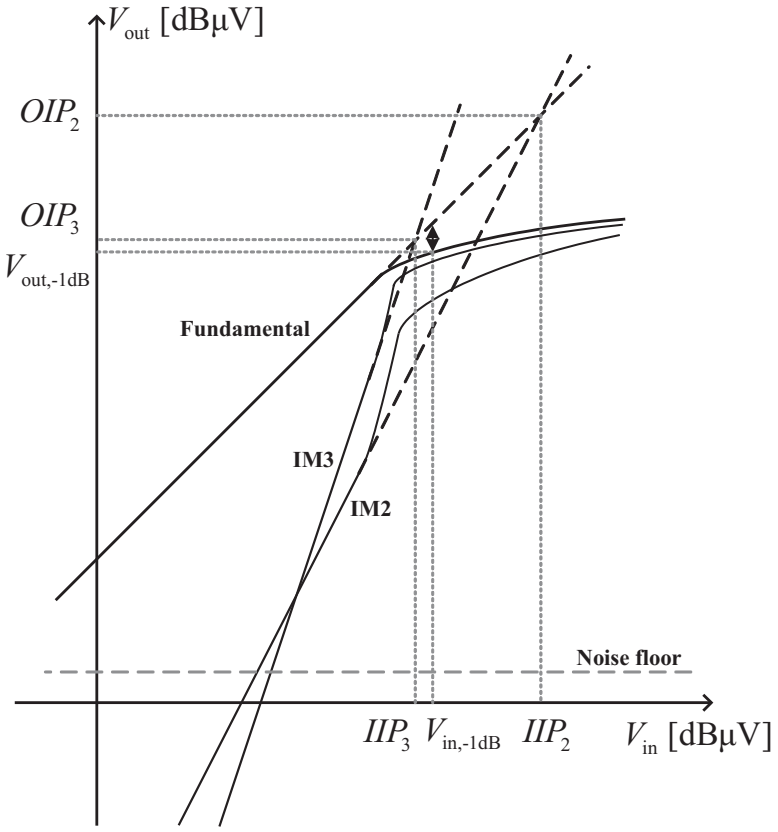

Fig. 4.8: Amplifier large-signal input-output characteristic.

As this equation shows, also the third order non-linearity contributes to the output fundamental tone and above a certain input level V_{in} the output fundamental tone will no longer follow linearly the input signal, but will saturate. The power (or voltage) level at which the actual fundamental output signal is 1 dB lower than the ideal linear output level is designated as the *1 dB compression point*, as shown in Fig. 4.8. As long as the amplifier is operated well below the compression point, the power series can be truncated to the third order distortion.

The situation gets more complicated when the input signal consists of two tones, $v_{\text{in}} = V_{\text{in},1}\cos(\omega_1 t) + V_{\text{in},2}\cos(\omega_2 t)$. In this case, applying eq. (4.13) we obtain a complex output spectrum, in which new tones are generated on frequencies of the general form $\pm m\omega_1 \pm n\omega_2$, with m and n being integer values. These tones are called *intermodulation products* and can be very troublesome, especially when they occur inside useful signal bands. The order of the intermodulation products is given by $m + n$.

When plotting the second and third order intermodulation products as a function of the input in a double logarithmic scale, as shown in Fig. 4.8, well below the compression point the 2nd order IM product has the slope 2:1 (40 dB/dec), while

the 3rd order one has the slope 3:1 (60 dB/dec). The fundamental gain has in this region the slope 1:1, which means that the IM products grow faster as the input level increases. Also, the 1 dB compression point gets lower as more than one tone is being applied at the amplifier's input [32].

By extrapolating the linear curves above the compression point (dotted lines in Fig. 4.8), the IM curves intersect the fundamental gain at the intercept points IP2 and IP3, respectively. These points are theoretical, which means they cannot be measured directly, as they occur in a region where the amplifier is already in saturation. The input intercept point (IIP) shows the input power at which the intermodulation tones would equal the fundamental ones; the reached output level is denoted as the output intercept point (OIP).

In practice the input signal has usually a complex spectrum, since it carries information. As a result of the amplifier's nonlinearities, the output spectrum contains regrowth sidebands[2], which consist of the generated intermodulation products. The n^{th} order sideband is n-times wider than the useful signal bandwidth [37], which means that it "invades" the adjacent channels.

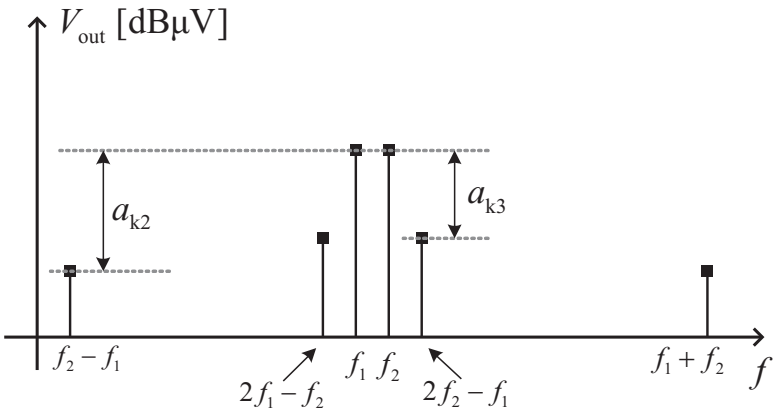

Fig. 4.9: Output spectrum.

Coming back to the two-tone case, it provides us with a practical way of measuring the linearity performance of an amplifier. Fig. 4.9 shows an output voltage spectrum containing the fundamental tones and the 2nd and 3rd order intermodulation products. We define the intermodulation distance a_{k} as the ratio expressed in dB of the fundamental tone to the intermodulation tone:

$$a_{\text{k}} = 20 \log \left(\frac{V_{\text{out,1}}}{V_{\text{out,k}}} \right) \tag{4.15}$$

If the amplifier were ideally linear, the intermodulation distance a_{k} would be infinite.

[2]Also denoted as *adjacent channel power* (ACP).

Required Linearity Performance

The linearity requirements posed on the active antenna are determined by the fact that the car may travel through areas with very strong electromagnetic field, as is the case in the vicinity of powerful radio broadcast transmitters. Active antennas have the particularity of being wideband, which means that large undesired signals may enter the amplifier, as no channel selection occurs before the amplifier [14]. If the amplifier is not linear enough, the strong signals produce intermodulation, which may interfere with the desired channels.

In the AM range both 2nd and 3rd order intermodulation products are important, since all of them fall inside the AM band. In the FM range only the 3rd order intermodulation products fall inside the FM band. However, the 2nd order intermodulation products generated by FM signals will affect both AM and DAB-Band-III ranges. Therefore they have to be also taken into account if the active antenna is to cover these services too.

The VDA issued recommendations concerning the minimal linearity the active antenna should exhibit in AM and FM in the case of a two-tone input signal [36]. For amplifiers without automatic gain control these requirements are defined for the case when the output signal level at each fundamental tone reaches 110 dBµV. For DAB there is so far no VDA recommendation; however, the industrial practice requires at least 50 dB intermodulation distance when the output signal level at each fundamental tone reaches 100 dBµV. These values are gathered in Table 4.3.

	AM	FM	DAB
a_{k2} [dB]	50	80	50
a_{k3} [dB]	50	60	50

Table 4.3: Minimal linearity for active antennas without automatic gain control (V_{out} = 110 dBµV for AM/FM and V_{out} = 100 dBµV for DAB). DAB value is not specified by the VDA; value complies with industrial practice.

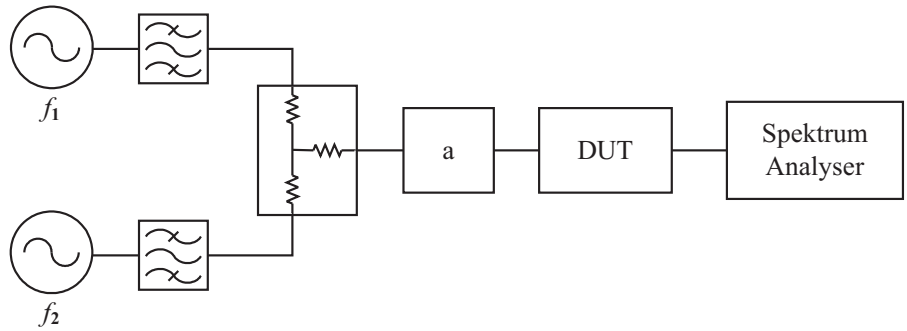

Fig. 4.10: Experimental setup for linearity measurements.

Linearity Measurement

The experimental setup for linearity measurements is depicted in Fig. 4.10. The two input tones f_1 and f_2 supplied by signal generators are band-pass filtered in order to avoid an undesired mutual coupling between the two generators. A power combiner adds the two signals and then an attenuator follows, which both improves the impedance matching toward the DUT and can also be used to vary the input level. The DUT's output signal is fed to a spectrum analyser, where the intermodulation levels can be read. Care has to be taken in order not to overdrive the spectrum analyser's input stage, as it contributes distortions on its own. Therefore, for high level output DUT signals the spectrum analyser's internal attenuator has to be set to higher values, in order to protect the input stage. On the other hand, when measuring low amplitude tones, this attenuation has to be lowered, in order not to drown the signal into the noise floor. Also, the bandwidth of the internal intermediate frequency filter can be reduced in order to decrease the measuring equipment noise and therefore improve its sensitivity. Thus the linearity measurement requires an elaborate compromise between attenuation and sensitivity.

4.4 Summary

The gate biasing resistor plays a very important role for the noise performance of the amplifier used for electrically very short antennas. The amount of noise picked-up by the transistor is a function of both the resistor value and the capacitances surrounding it, so that the resistor has to be dimensioned for the lowest operating frequency. As a general design rule, its value should be chosen as large as practically possible.

Special requirements have also to be met concerning the noise performance of the transistor used in the first stage of the antenna amplifier. The noise parameters of the transistors compared in this work have been experimentally measured and it has been concluded that Si JFETs, due to their low flicker noise, are more appropriate for AM applications, while for FM, DAB-Band-III and DAB-L-Band the GaAs devices are preferred. When compared to standard simulation models, the resulting noise models are more accurate in describing low frequency noise effects.

Active antennas have to achieve certain requirements concerning noise, signal level and linearity. In order to determine these, a combination of laboratory and field measurements is used. A 90 cm long passive monopole antenna usually serves as a reference.

Chapter 5

High-Impedance Amplifiers for Monopole Antennas

Nowadays, for AM/FM radio reception, the rod type antenna is common for low-end cars. Initially a 90 cm long passive monopole was used, but although displaying good performance it had an inconvenient length. As we have seen in Section 3.1, a height reduction of the monopole antenna decreases proportionally its effective height, increases its impedance and worsens the obtainable bandwidth and efficiency. These effects in combination with conventional amplifier technology lead to a severe SNR reduction both in AM and FM. The undesired side effects can be overcome by the use of the active antenna principle, as shown in Section 3.4. Therefore, in the past decades 40 cm long active rod antennas mounted on the car roof (above the windshield or the rear window) or on a fender have become the usual choice. They provide good performance in both frequency bands comparable to a 90 cm whip antenna and have a low cost. The amplifier usually consists of two distinct paths, one for AM and one for FM. Nevertheless, there is a strong demand for further reducing the size of car rod antennas as much as possible in order to meet nowadays styling requirements, to minimize wind noise and exposure to vandalism, as well as to increase their robustness and inconspicuousness.

Recently antennas have been introduced, which can alleviate these shortcomings in FM, due to special helical structures. Nevertheless, their manufacturing is more complicated than the one of simple thin monopole antennas. Moreover, such antennas behave in the AM range just like simple thin monopole structures do. Therefore our investigation starts with a thin 20 cm monopole active antenna[1], in order to determine the achievable performance in combination with modern amplifier techniques. As we shall see, such simple antenna elements impose high demands on the high-impedance amplifier in order to deliver a comparable performance.

The performance of two high-impedance amplifier architectures is investigated and presented. The first design consists of a single transistor AM/FM amplifier,

[1]This length is chosen as a result of previous research.

while the second contains two different paths for the AM and FM bands. The parameters and the conditions which determine the performance of the designs are investigated and explained and measurement results are presented and discussed.

5.1 The 20 cm Long Rod Antenna

A monopole antenna element made of brass with 20 cm length and 3 mm diameter will be further used. In the AM range, according to the calculations detailed in Section 3.1, the antenna has a predominant capacitive $\underline{Z}_{\mathrm{A}}$, consisting of a capacitance $C_{\mathrm{A}} \simeq 2.4\,\mathrm{pF}$ and a negligible real part R_{A}. If the monopole is mounted on an infinite conductive plane, the theoretical effective height h_{eff} is 10 cm, as eq. (3.5) indicates. However, in reality, when the antenna is mounted on a car, h_{eff} is a function of the car geometry and the mounting position, as Fig. 2.4(b) depicts for the case of a VW Golf car. In this particular case, the calculated h_{eff} is larger than 40 cm in the AM range when the antenna is placed on the roof edge, which is a considerable deviation from eq. (3.5). Nevertheless, this discrepancy occurs in a positive way, since it shows, in fact, that the AM radio reception will be improved when the antenna is mounted on a car.

The analysis in Section 3.1 points out how difficult it is to reach the required bandwidth using a short monopole antenna and inductive matching (provided that the inductors are feasible). Fortunately, impedance matching is not needed either in AM or FM, as the situation can be overcome by using the active antenna principle [38] [11], already described in Section 3.4. According to it, the antenna design combines the antenna feed-point directly with an amplifier. Instead of drawing power from the antenna, the amplifier is optimized for a high input impedance in order to pick up as much as possible from the antenna voltage and then drive the radio receiver.

5.2 The Active Antenna Amplifier

Recalling eq. (3.37), the input capacitance C_{in} of the amplifier is to be designed as low as possible in order to achieve a good sensitivity, while the amplifier should be able to drive the cable and the radio receiver. Other requirements which have to be taken into account are the output noise voltage and the linearity, as discussed in Sections 4.3.3 and 4.3.5. For determining the sensitivity, the 90 cm passive monopole antenna will be used as reference.

Unfortunately the stated requirements are contradictory, as we shall next see, and the amplifier topology has to be chosen to allow for the alleviation of these compromises. The amplifier should display high gain, because the voltage induced in the antenna element is very small. On the other hand, a high gain also produces a high output noise level. The high impedance signal source seen by the amplifier (i.e.

the antenna impedance $\underline{Z}_\mathrm{A}$) requires that the amplifier exhibits a low parallel input noise current source. In this case field-effect transistors have to be used instead of bipolar ones. The use of FETs also helps achieving high input impedance. The high linearity requirements indicate that the use of a transistor in common source topology is inappropriate and some kind of feedback should be used to increase its linearity.

In order to achieve a high input impedance, only two feedback configurations are possible: the series-series and the series-parallel. The first one can be implemented as a degenerated common source stage, while the latter one as a common drain stage, as depicted in Fig. 5.1. While the common drain circuit features excellent linearity properties and high input impedance, it achieves no voltage gain [39]. The voltage gain of the degenerated common source stage can be adjusted by modifying the amount of feedback; nevertheless, such a stage has a larger input capacitance, caused by the Miller effect.

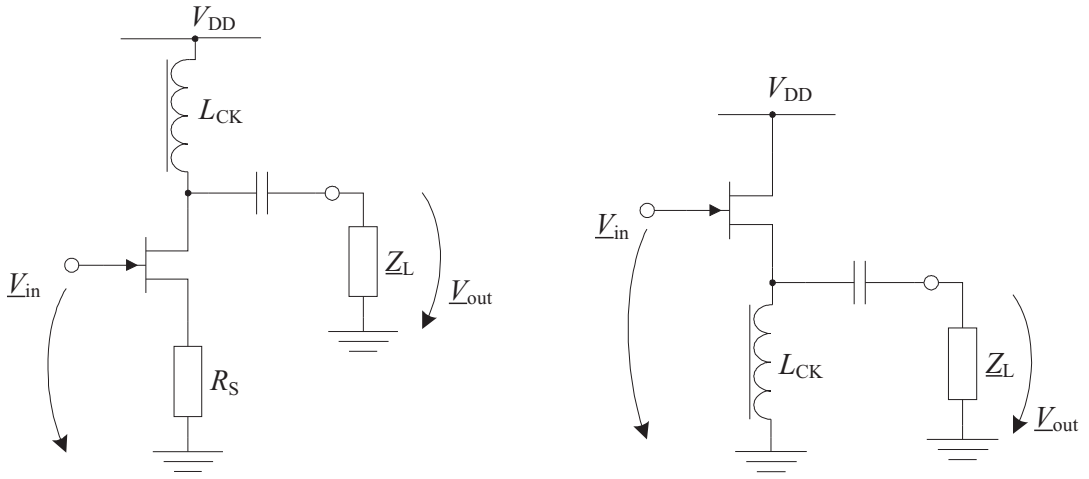

(a) Series-series feedback.

(b) Series-parallel feedback.

Fig. 5.1: AC schematics of series-series feedback stage and series-parallel feedback stage.

The need of voltage gain indicates that the common drain stage alone is not sufficient. In this case the voltage gain has to be reached either with the help of a transformer, or with a second gain stage. Nevertheless, as the introduction of a transformer or a second gain stage will complicate the design, a one-stage implementation is preferred.

Another important aspect is the question of whether a single stage can be used for both AM and FM bands. The trouble is, the amplifier has to be extremely linear in order to avoid FM to AM conversions – that is, strong FM stations produce 2$^\mathrm{nd}$ order intermodulation products which may fall in the AM range. In order to avoid this, the car manufacturers require that the active antennas have to achieve in the FM range at least 80 dB 2$^\mathrm{nd}$ order intermodulation distance a_k2. If a single transistor

AM/FM amplifier does not prove to be feasible, then a two-path version has to be investigated, in which the AM and FM signals are processed by two different amplifiers interconnected by means of filters.

5.3 Single Transistor AM/FM Antenna Amplifier

As already mentioned, a degenerated common source amplifier stage will be used, because it offers the possibility to control the voltage gain. In the case of active antenna amplifiers the natural transistor choice is a FET, since it features high-input impedance and very small input parallel noise current source. A high and over frequency sustainable transconductance value g_m is desired in order to be able to achieve the required gain and linearity. The simplified small signal equivalent circuit of such a topology is shown in Fig. 5.3.

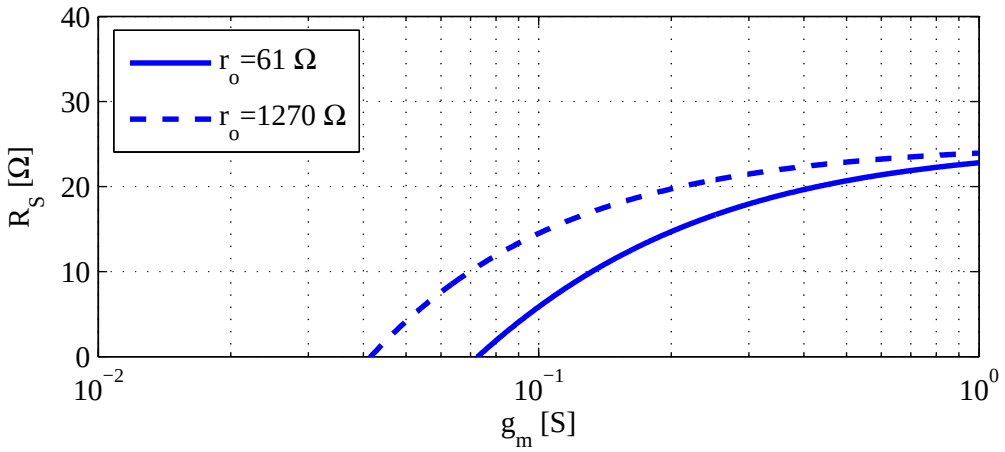

Fig. 5.2: Required degeneration resistance R_S as a function of the transconductance g_m, when $|\underline{A}_\mathrm{V}| = 2$ and $\underline{Z}_\mathrm{L} = 50\,\Omega$.

Neglecting the capacitances and inductances associated with a FET transistor (as their influence is small in the FM range when $\underline{Z}_\mathrm{L} = 50\,\Omega$), the voltage gain $\underline{A}_\mathrm{V}$ of a common source stage with resistive degeneration (Fig. 5.1(a)) can be written as:

$$\underline{A}_\mathrm{V} = \frac{\underline{V}_\mathrm{out}}{\underline{V}_\mathrm{in}} = -\frac{r_\mathrm{o} g_\mathrm{m}}{r_\mathrm{o}\,(1 + g_\mathrm{m} R_\mathrm{S}) + \underline{Z}_\mathrm{L} + R_\mathrm{S}} \underline{Z}_\mathrm{L} \tag{5.1}$$

where $\underline{Z}_\mathrm{L}$ is the load impedance, R_S the degeneration resistance, r_o the output resistance of the transistor and g_m its transconductance. The degeneration increases both the linearity and the input impedance of the stage; however, a resistive degeneration has the disadvantage of contributing noise to the circuit, but it offers a wider frequency response.

Usually $\underline{Z}_\mathrm{L}$ and r_o are known, so the need arises to determine R_S and g_m for a certain $|\underline{A}_\mathrm{V}|$. Fig. 5.2 depicts the degeneration resistance R_S as a function of the

transconductance g_m for two different r_o values, when $|\underline{A}_V| = 2$ and $\underline{Z}_L = 50\,\Omega$. This voltage gain value has been chosen because it offers a satisfactory compromise between gain and output noise voltage, as we shall later see. The g_m value for which $R_S = 0$ corresponds to the normal common source stage. For transconductances lower than this, physically incorrect negative R_S values are required. Indeed, no higher voltage gains can be obtained than those achieved by the common source configuration. For transconductances above the value required by the common source the R_S value rises asymptotically to about $25\,\Omega$, which means that for high enough g_m values the gain is dictated by the feedback only, and not by the basic amplifier.

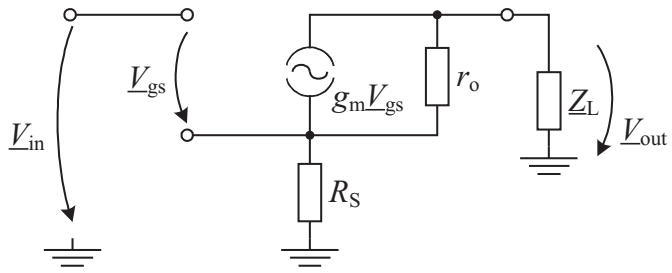

Fig. 5.3: Simplified AC small-signal equivalent circuit of the common source stage with resistive degeneration.

The curves depicted in Fig. 5.2 show that for a transistor with at least $1270\,\Omega$ output resistance (such as the SST310 JFET or the BF998 MOSFET) the minimum required g_m is about 43 mS, in order to achieve a voltage gain of 2 with a $50\,\Omega$ load. In the case of a transistor with only $61\,\Omega$ output resistance (such as the ATF33143 HEMT) the minimum required g_m is about 78 mS.

Transistor	I_D [mA]	g_m [mS]	r_o [Ω]	C_{GS} [pF]	C_{GD} [pF]	C_{DS} [pF]
SST310 (Si JFET)	30	16	1270	4.83	1.55	1
BF998 (Si MOSFET)	20	28	100k	2.1	0.025	1.1
NE3508 (GaAs)	30	215	71	0.46	0.32	0.05
ATF33143 (GaAs)	50	267	61	2.1	0.45	0.08

Table 5.1: Comparison of different transistors.

A comparison between the transconductance of different transistor types is shown in Table 5.1. The SST310 JFET and the BF998 MOSFET are Si based transistors used for RF applications. The NE3508 and the ATF33143 are GaAs FETs normally intended for microwave applications. It can be easily seen that the g_m of GaAs devices is by far superior. Coming back to the discussion regarding Fig. 5.2, it is now clear that neither the SST310 JFET nor the BF998 MOSFET have enough transconductance to achieve the required gain even in a common source configuration, not to mention the possibility to be able to use a degeneration. A solution

is the parallel connection of more transistors, but this dramatically increases the input capacitance of the stage. On the other hand, the high g_m value of the GaAs transistors allows for about 16 Ω degeneration.

The flicker noise exhibited by transistors can affect the AM range, especially at the lower frequencies. As discussed in Section 4.2, the Si JFETs normally have low flicker noise, while the GaAs devices a rather high value, which stretches up even almost to the FM range, thus complicating the design of the amplifier in the AM band. Nevertheless, since the Si JFETs have unfortunately an insufficient transconductance, they are not suited for the AM/FM application. We shall see next how the low-frequency noise issue of the GaAs device can be alleviated.

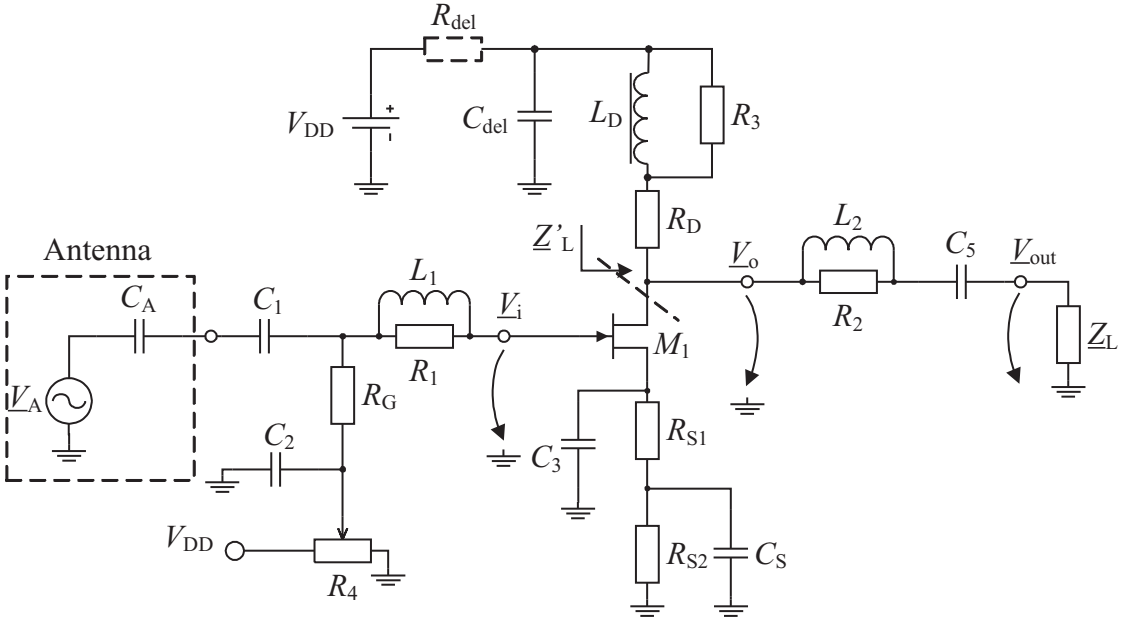

Fig. 5.4: Schematic of the single transistor AM/FM antenna amplifier.

Fig. 5.4 depicts the schematic of the AM/FM antenna amplifier. The antenna is replaced by its equivalent circuit consisting of the voltage source $\underline{V}_A$ and the antenna capacitance C_A. Capacitors C_1, C_2 and C_5 are DC blocks and can be considered short-circuits for the entire AM/FM operating range.

Resistor R_G biases the transistor gate, while potentiometer R_4 helps setting the gate voltage. However, due to the low drain-source breakdown voltage of modern HEMTs, there are some precautions to be taken when powering the circuit, because the transient regime occurring until the correct bias point settles may result in large V_{DS}. The required supply voltage V_{DD} is higher than $V_{DS,max}$, so that if the gate voltage rises too slowly in comparison to the supply voltage, an overvoltage may drop on the transistor and damage it. According to the absolute maximum ratings in the datasheets [40] [41], the ATF33143 transistor has $V_{DS,max} = 5.5\,V$, while the

NE3508 has $V_{\mathrm{DS,max}} = 4.0\,\mathrm{V}$. As a consequence, the time constant of the R_4–C_2 group has to be such chosen, that the gate voltage rises fast enough. In the case of the NE3508 transistor an additional delay is introduced by the R_{del}–C_{del} group, so that the drain voltage rises slower.

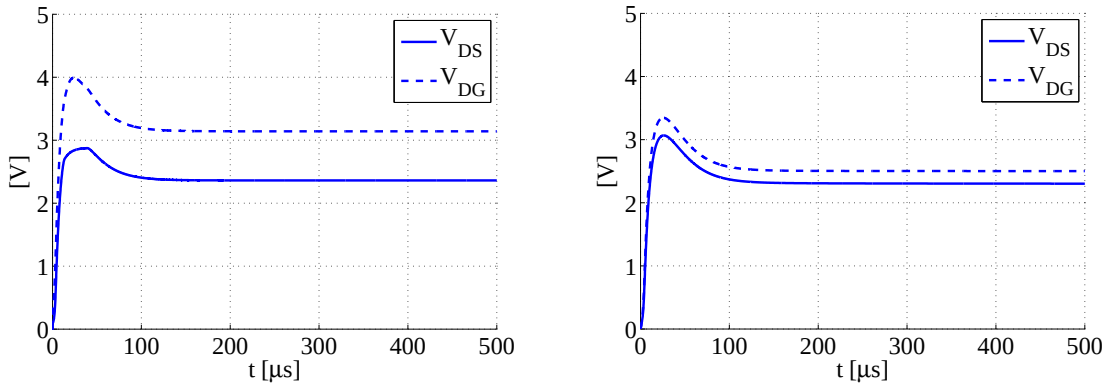

(a) ATF33143 circuit.

(b) NE3508 circuit.

Fig. 5.5: Simulated drain-source and drain-gate voltages during the start-up transient regime.

The simulated start-up transients are shown for both transistors in Fig. 5.5 for the complete circuit. The R_{del} resistor is present only for the NE3508 circuit. As it can be seen, both circuits ensure a safe start-up.

The L_1–R_1 and L_2–R_2 groups ensure the stability of the stage and are such dimensioned to have a minimal impact upon the working range. The resistors R_{S1} and R_{S2} and the capacitors C_3 and C_{S} form together a frequency dependent source degeneration. Resistors R_{D} and R_3 together with inductor L_{D} shape the frequency dependence of the total load $\underline{Z}'_{\mathrm{L}}$ provided to the transistor.

In an actual car environment a long coaxial cable connects the antenna amplifier with the radio receiver. The usual radio receivers have $50\,\Omega$ input impedance in the FM range and a capacitive high input impedance in the AM range. In Fig. 5.7 the high-ohmic character of the receiver in AM is symbolized by the path containing the unity gain buffer; the other path represents the FM one. The coaxial cable used to connect the active antenna to the receiver has the characteristic impedance $\underline{Z}_{\mathrm{C}}$ and the length l.

5.3.1 Design in the FM Range

In choosing the voltage gain of the stage, a trade-off has to be made between sensitivity, output noise level and linearity. In order to compensate for the reduced voltage $\underline{V}_{\mathrm{A}}$ excited by the electrical field in the small antenna and the voltage division indicated by eq. (3.37), the first choice would be to increase the amplifier gain. Nevertheless, the output noise voltage of the amplifier is increasing as its gain

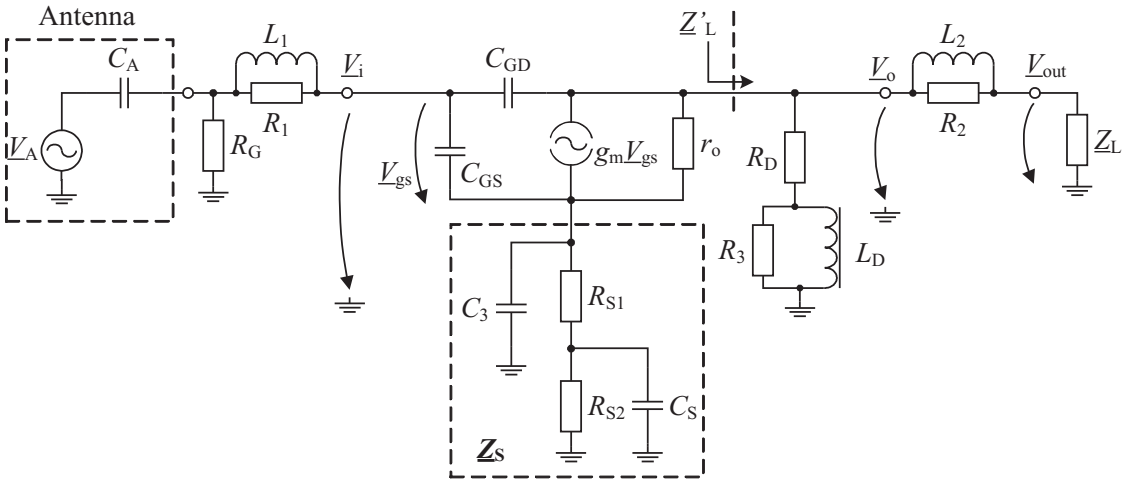

Fig. 5.6: AC small signal equivalent circuit of the single transistor AM/FM antenna amplifier.

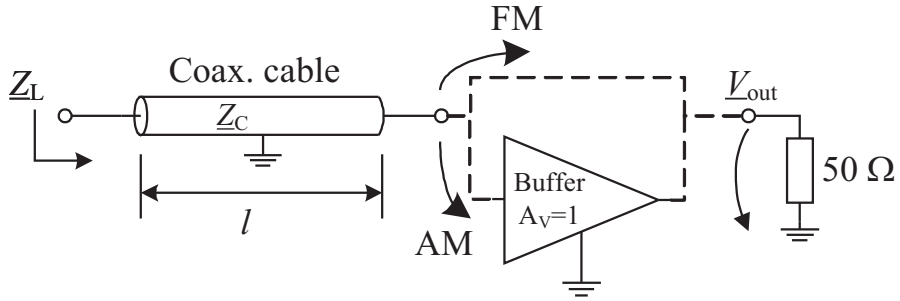

Fig. 5.7: Load $\underline{Z}_L$ seen in the AM and FM ranges by the antenna amplifier.

increases. Linearity is a function of the amount of negative feed-back, which again impacts on the gain.

The AC small signal equivalent circuit of the amplifier in Fig. 5.4 is shown in Fig. 5.6. Recalling eq. (5.1) in the case of the degenerated common source stage in Fig. 5.4 and neglecting the high-frequency effects, the voltage gain $\underline{V}_o/\underline{V}_i$ can be written as:

$$\underline{A}_{V,csd} = \frac{\underline{V}_o}{\underline{V}_i} \simeq -\frac{g_m r_o \underline{Z}_L}{r_o\,(1 + g_m \underline{Z}_S) + \underline{Z}_L + \underline{Z}_S} \tag{5.2}$$

where g_m is the transistor's transconductance, r_o its output resistance, $\underline{Z}_S$ the degeneration impedance and $\underline{Z}_L$ the load impedance. The output resistance r_o cannot be neglected in eq. (5.2) because of its relative small value in the case of HEMT transistors.

For this application, a broadband solution is required, so a resistive degeneration $\underline{Z}_S = R_S$ rather than an inductive one has to be employed, although a resistor contributes noise to the circuit. Nevertheless, the amount of output noise is decreasing

together with the voltage gain when R_S is increasing[2]. This behaviour is depicted in Fig. 5.9(a), where the simulated output noise voltage is plotted versus R_S at 100 MHz and 120 kHz bandwidth. As it can be seen, degenerations larger than 5 Ω result in output noise voltages lower than −5 dBμV.

With the current values of L_2 and R_2 and for $\underline{Z}_L = 50\,\Omega$, the load $\underline{Z}'_L$ seen by the transistor is about $(67 + j21)\,\Omega$. The influence of the degeneration resistor upon the voltage gain $A_V = |\underline{V}_o/\underline{V}_i|$ and the antenna voltage gain $A_{V,T} = |\underline{V}_o/\underline{V}_A|$ is depicted for the ATF33143 circuit in Fig. 5.8 at 100 MHz. Both gains decrease with the increase of R_S.

A voltage gain $|\underline{A}_V| = 3$ of the amplifier core is considered sufficient in practice and applying eq. (5.2) we get $R_S \simeq 16\,\Omega$. Using this value for R_S in the design, the simulations indicate an output noise voltage $V_{out,N} = -6.6\,\text{dB}\mu\text{V}$, thus leaving enough room for the practical realization to achieve the targets.

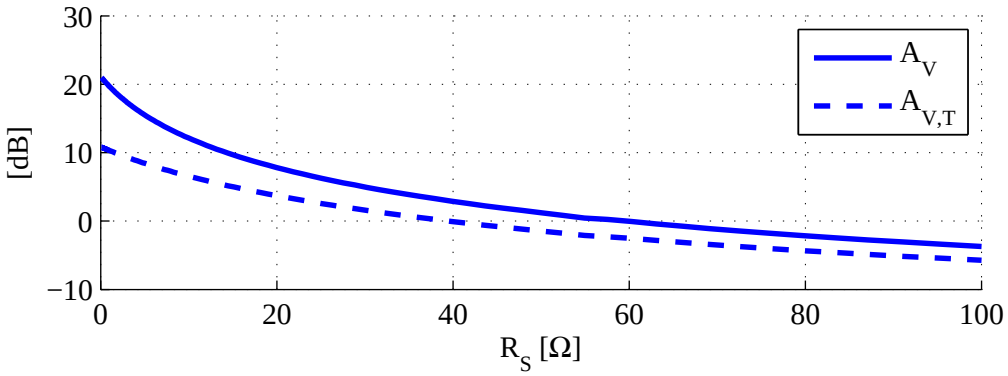

Fig. 5.8: Simulated FM voltage gain at 100 MHz.

The input impedance of the degenerated common source stage is also affected by the degeneration:

$$\underline{Z}_{in,csd} \simeq \underline{Z}_S + \underline{Z}_{GS}\,(1 + \underline{Z}_S g_m) + \frac{1}{j\omega C_{GD}\left(1 - \underline{A}_{V,csd}\right)} \tag{5.3}$$

where $\underline{Z}_{GS}$ is the gate-source impedance derived in the small signal model. The last term in the equation stands for the Miller effect. Considering $\underline{Z}_{GS} = \frac{1}{j\omega C_{GS}}$ and a resistive degeneration $\underline{Z}_S = R_S$, the input impedance can be rewritten as:

$$\underline{Z}_{in,csd} \simeq R_S + \frac{1}{j\omega C_{GS}}\,(1 + g_m R_S) + \frac{1}{j\omega C_{GD}\left(1 - \underline{A}_{V,csd}\right)} \tag{5.4}$$

Due to the negative feedback the input impedance is enlarged, which means the equivalent gate-source capacitance is lower by a factor of $1 + g_m R_S$, as eq. (5.4) shows. This is a desired effect, since the smallest possible input capacitance is desired.

[2] R_S will further describe the total resistive degeneration. The actual configuration including R_{S1}, R_{S2} and C_S will be later detailed.

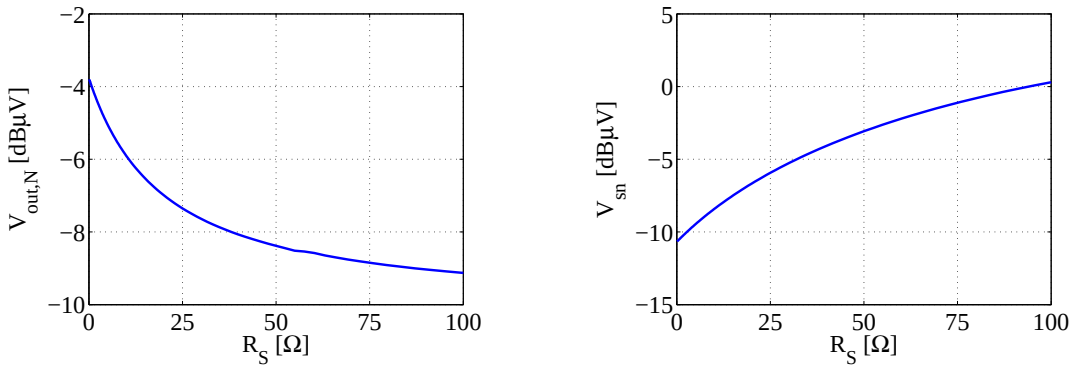

(a) Simulated FM output noise voltage for 120 kHz bandwidth.

(b) FM sensitivity.

Fig. 5.9: Simulated FM output noise voltage and sensitivity at 100 MHz with $\underline{Z}_\mathrm{A}$ connected at the amplifier's input.

The dotted curve in Fig. 5.8 shows the antenna voltage gain $A_{\mathrm{V,T}} = |\underline{V}_\mathrm{o}/\underline{V}_\mathrm{A}|$, which is lower than A_V due to the capacitive voltage division at the amplifier's input. Although A_V increases when R_S decreases, $A_{\mathrm{V,T}}$ has a milder increase, because the input capacitance gets also larger as the feedback diminishes and the Miller effect increases. This increase of the input capacitance exacerbates the input capacitive voltage division and thus softens the ascent of $A_{\mathrm{V,T}}$.

The increase in the degeneration resistance results in a decrease of the sensitivity. In Fig. 5.9(b) is plotted the required input signal for achieving a unity SNR at node V_o at 100 MHz. This is a measure of the sensitivity and it can be seen that it degrades rapidly as the degeneration R_S increases: for 0 Ω there are only −10.6 dBμV necessary at the input for an output signal voltage equal to the output noise voltage, but for 16 Ω there are already −7.4 dBμV input voltage required, which means about 3 dB sensitivity degradation.

In the case of the ATF33143 transistor and for the current design, the input reflected C_GS is lowered from 2.1 pF to about 0.3 pF. The Miller effect contributes about 1.6 pF to the input capacitance, so the total input capacitance C'_in of the amplifier core sums up 1.9 pF. It is expected that the practical realization will add at least 0.5 pF parasitic capacitance at the input node, caused by the layout parasitics[3]. For $C_\mathrm{A} = 3.3$ pF, the input voltage attenuation is therefore about 4.7 dB.

The series-series negative feedback enlarges also the output impedance of the stage:

$$\underline{Z}_\mathrm{out,csd} \simeq r_\mathrm{o} + \underline{Z}_\mathrm{S}\,(1 + g_\mathrm{m} r_\mathrm{o}) \tag{5.5}$$

In this particular design the output drain resistance is increased to 434 Ω. This effect is not desired here, so an impedance matching circuit is required at the amplifier's

[3]The amount of additional capacitance may be even larger if electrostatic discharge (ESD) protection is added.

output.

Another important issue is the linearity of the stage. The degeneration value being set by the gain and noise constrains, Fig. 5.10 shows for both ATF33143 and NE3508 transistors the 2nd and 3rd order intermodulation distances as a function of I_D, when the input tones are located on 100 and 101 MHz. These quantities are determined for 110 dBµV output level of each fundamental tone.

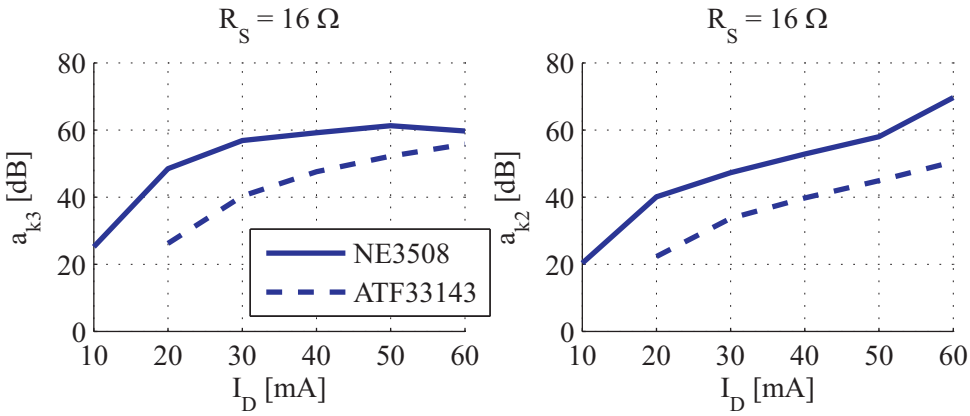

Fig. 5.10: Simulated FM intermodulation distance of the single transistor AM/FM antenna amplifier vs. drain current evaluated for 110 dBµV output voltage level of each fundamental tone; $f_1 = 100$ MHz, $f_2 = 101$ MHz.

The left plot in Fig. 5.10 shows the impact of the drain current upon the 3rd order linearity of the stage when $R_S = 16\,\Omega$. As it can be seen, a drain current of about 40 mA ensures a 3rd order intermodulation distance of about 60 dB in the case of the NE3508 transistor, while for the ATF33143 one the linearity tends to improve for higher currents. The right plot in Fig. 5.10 depicts the impact of the drain current upon the 2nd order linearity of the stage. In this case the linearity tends to improve for both transistors by increasing the drain current.

The most important hint provided by the results shown in Fig. 5.10 is concerning a_{k2}. As already explained, the 2nd order intermodulation products generated in the FM band may fall into the AM range. For the considered example with $f_1 = 100$ MHz and $f_2 = 101$ MHz, one of the 2nd order intermodulation product is on 1 MHz, so inside the AM band. In fact, in the case of real FM signals, because the FM channels are wider than the AM ones, a number of consecutive AM channels are disturbed.

In the case of the NE3508 transistor, even for 60 mA the reached a_{k2} value is only 70 dB, which is unfortunately insufficient compared to the usual industrial practice which requires at least 80 dB. For $I_D = 50$ mA only 58 dB are expected. For the ATF33143 transistor a_{k2} is only about 50 dB for 60 mA drain current and about 45 dB for 50 mA drain current. This result shows that the single transistor AM/FM antenna amplifier is not suited for the automotive application – unless additional measures for increasing its linearity are considered, such as the automatic

gain control.

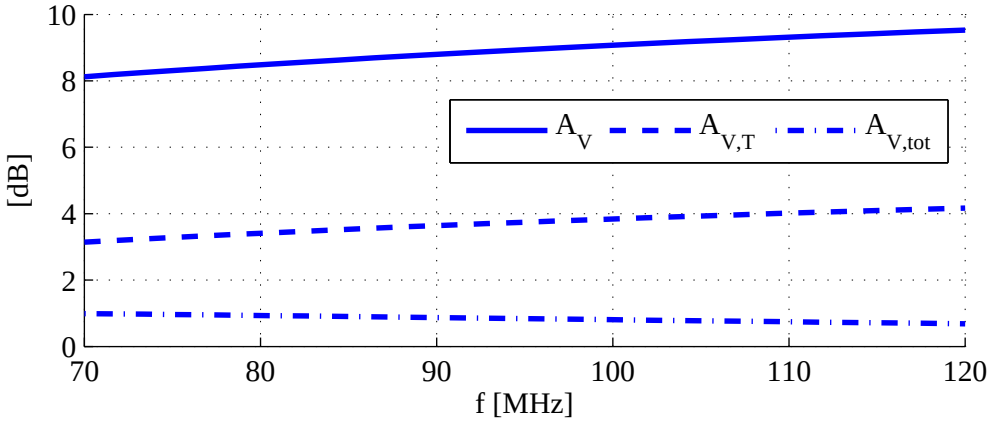

(a) Simulated FM voltage gain.

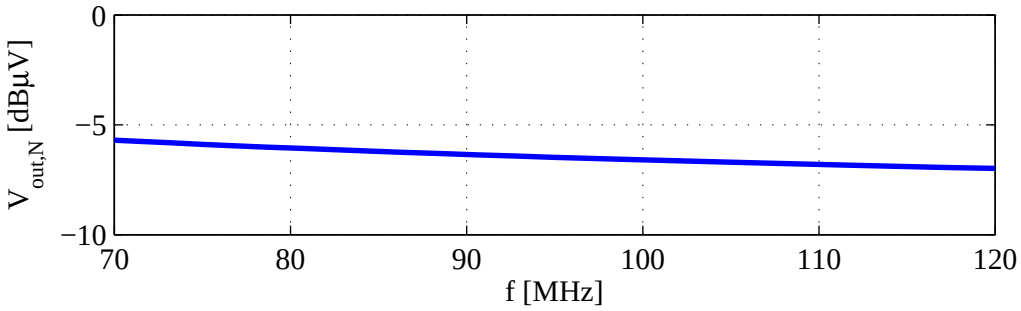

(b) Simulated FM output noise voltage for 120 kHz bandwidth, with $\underline{Z}_\mathrm{A}$ connected at the amplifier's input.

Fig. 5.11: Simulated FM gain and output noise voltage for $R_\mathrm{S} = 16\,\Omega$.

As the current has to be maintained at a reasonable level, the NE3508 transistor will be further operated at 40 mA drain current, while the ATF33143 one at 50 mA. Both transistors are biased at $V_\mathrm{DS} = 2.5\,\mathrm{V}$. The simulated frequency characteristic of the antenna amplifier is shown in Fig. 5.11(a) for $R_\mathrm{S} = 16\,\Omega$. The voltage gain $A_\mathrm{V} = |\underline{V}_\mathrm{o}/\underline{V}_\mathrm{i}|$ is the gain of the amplifier core, while $A_\mathrm{V,T} = |\underline{V}_\mathrm{o}/\underline{V}_\mathrm{A}|$ is the antenna voltage gain and $A_\mathrm{V,tot} = |\underline{V}_\mathrm{out}/\underline{V}_\mathrm{A}|$ is the total voltage gain (including the stability networks). Fig. 5.11(b) displays the simulated output noise voltage in the FM range.

5.3.2 Design in the AM Range

The first design issue in the AM range is the significant flicker noise of the HEMT transistor. The only way to decrease the output noise level is to sufficiently suppress the voltage gain of the stage.

As already shown in Section 4.1, the value of the gate biasing resistor R_G plays an important role in the noise behaviour of the circuit. The critical value depends

on the operating frequency, antenna capacitance C_A and input capacitance C_{in}. For the analysis the lowest operating frequency (150 kHz) represents the worst case. Nevertheless, C_{in} is not known yet, since its value depends on the final amplifier configuration. For an initial solution we shall assume $C_{in} = 1\,\text{pF}$ and applying eq. (4.3) we get the value of the gate biasing resistor which contributes the maximum amount of input noise $R_{G0} = 246\,\text{k}\Omega$. As a consequence, R_G has to be significantly higher than R_{G0}. Nevertheless, a comment has to be made here: since the transistor noise is anyway very high in the LW range, the noise contribution of R_G becomes less obvious. This means that one gets little advantage by choosing extremely high R_G values. Due to practical reasons, we shall further consider $R_G = 10\,\text{M}\Omega$; increasing R_G to $20\,\text{M}\Omega$ brings little advantage concerning noise, while even higher values become difficult to employ.

In the AM range the radio receiver has high input impedance, so that the load the antenna amplifier sees is dominated by the cable capacitance (Fig. 5.7). The voltage gain of the stage can be reduced by both increasing the degeneration resistance and by decreasing the load impedance, as eq. (5.2) indicates. Reducing the voltage gain by means of degeneration only is not a practical solution for the AM range where the load impedance is high, since large degeneration values are required in order to be comparable with Z_L. That is why the degeneration has to be combined with a reduction of the load impedance. This is illustrated in Fig. 5.12 for the ATF33143 circuit, where the sweep of R_S alone in the considered range produces almost no changes upon the voltage gain and the output noise voltage.

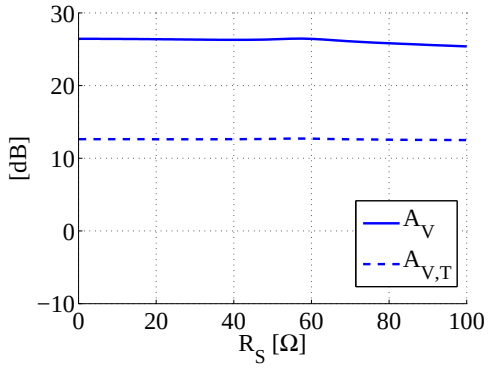

(a) Voltage gain.

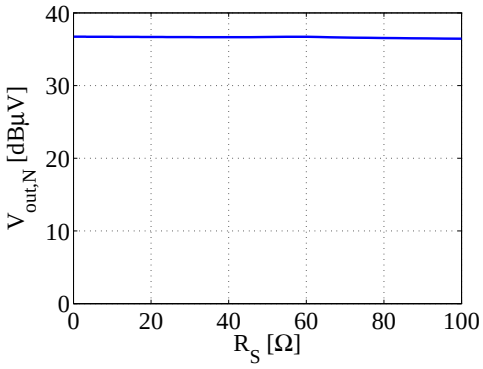

(b) Output noise voltage for 9 kHz bandwidth.

Fig. 5.12: Simulated AM voltage gain and output noise voltage vs. R_S at 150 kHz for the ATF33143 circuit, with $\underline{Z}_A$ connected at the amplifier's input.

Given this, a sweep of the load impedance provided to the transistor is performed instead. This is depicted for both ATF33143 and NE3508 transistors in Fig. 5.13 at 150 kHz for $R_S = 57\,\Omega$. The two transistors offer almost identical voltage gains, since both have high enough transconductance values g_m. Nevertheless, as expected,

the NE3508 transistor features significantly lower noise in the LW range.

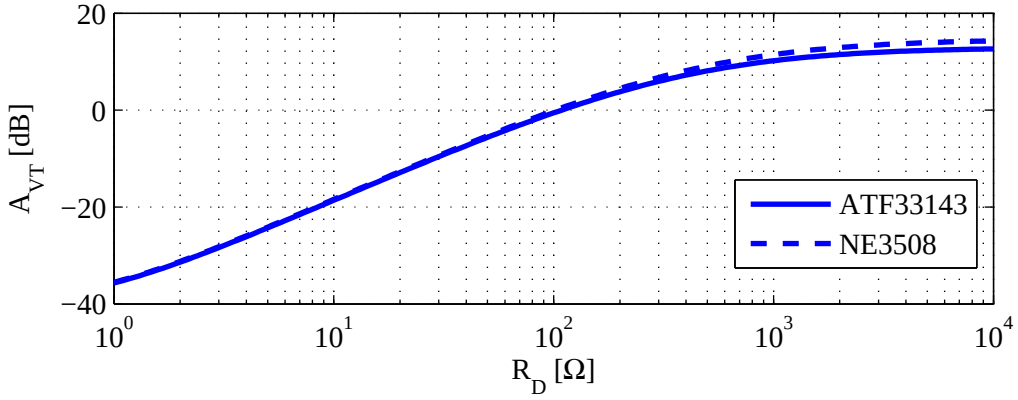

(a) Antenna voltage gain.

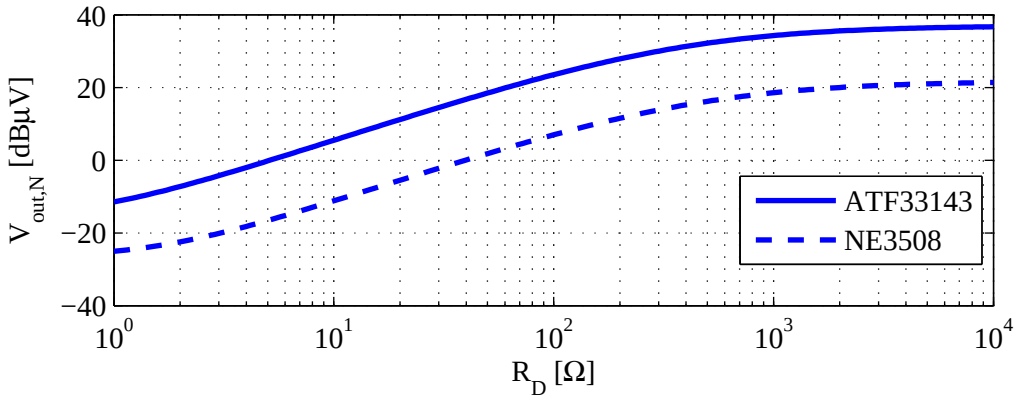

(b) Output noise voltage for 9 kHz bandwidth.

Fig. 5.13: Simulated AM antenna voltage gain and output noise voltage vs. R_D at 150 kHz, with $\underline{Z}_\mathrm{A}$ connected at the amplifier's input and $R_\mathrm{S} = 57\,\Omega$.

In Fig. 5.4 capacitor C_S can be such dimensioned that resistor R_S1 acts only in the FM range, while for the AM range R_S2 adds its contribution. Similarly, inductor L_D has to short-circuit R_3 in the AM range (thus decreasing the drain impedance), while allowing R_3 to fully act in the FM range. In this way, frequency dependent degeneration and load impedances are achieved.

The simulated noise curve at 150 kHz for the ATF33143 transistor (Fig. 5.13(b)) suggests that the load should be only about $4\,\Omega$ in order to achieve the required noise level. Such a low value practically means short-circuiting the receiver's input and gain and sensitivity can no longer be expected from the active antenna. The NE3508 transistor reaches the required noise level at a load of about $35\,\Omega$ (Fig. 5.13(b)).

As the long-wave range is not a critical one – at least not for the most listeners – a higher output noise level will be accepted, so that the voltage gain is less affected.

For 30 Ω load impedance the output noise level of the NE3508 circuit will be about −2.1 dBμV, while the antenna voltage gain will be about −9.3 dB. For the same configuration, the output noise level of the ATF33143 circuit is expected to be about 14.5 dBμV.

The severe voltage gain decrease is required only for the LW range, where the noise level is high. For the MW and SW bands the voltage gain can be increased without compromising the output noise level. Referring back to Fig. 5.4 and recalling the results from Section 5.3.1, following values are now employed for the AM/FM amplifier: $R_{S1} = 16\,\Omega$, $R_{S2} = 41\,\Omega$, $R_D = 30\,\Omega$, $C_S = 1\,\text{nF}$, $R_3 = 910\,\Omega$ and $L_D = 820\,\text{nH}$. Capacitor $C_3 = 8\,\text{pF}$ is introduced for stability considerations, in order to provide the transistor's source with a high-frequency short-circuit.

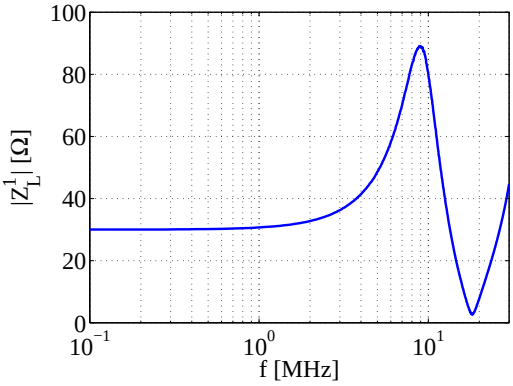

(a) Load $|\underline{Z}'_L|$ seen by the transistor in AM.

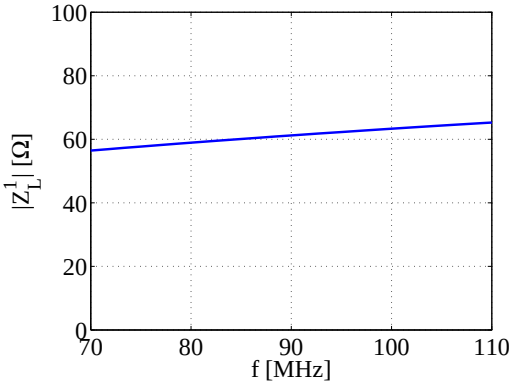

(b) Load $|\underline{Z}'_L|$ seen by the transistor in FM.

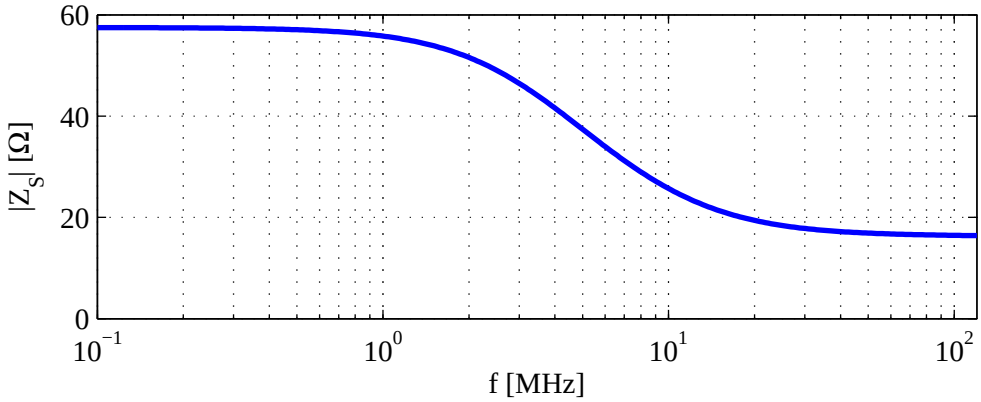

(c) Degeneration applied to the stage.

Fig. 5.14: Simulated values of the load and degeneration applied to the stage in the AM and FM range.

The magnitude of the degeneration impedance is plotted in Fig. 5.14(c) for the whole AM and FM ranges. The magnitude of the load impedance $|\underline{Z}'_L|$ seen by the transistor, when the cable and radio receiver are connected, is depicted in

Fig. 5.14(a) and (b). In the AM range a radio receiver with high input impedance has been considered, connected with a 2.5 m long 50 Ω cable[4] to the active antenna, in which case the cable capacitance dominates. At higher frequencies the cable transforms the receiver's input impedance due to the impedance mismatch between the receiver and the cable; as a result, for a certain frequency range (which depends on the cable's length) a low impedance value will be presented to the active antenna. In Fig. 5.14(a) this is the case for frequencies around 18 MHz. This explains why for frequencies higher than 10 MHz a 50 Ω receiver is more appropriate. In the FM range a 50 Ω radio receiver has been considered. The small impedance increase which can be seen in Fig. 5.14 (b) is caused by the output stability network.

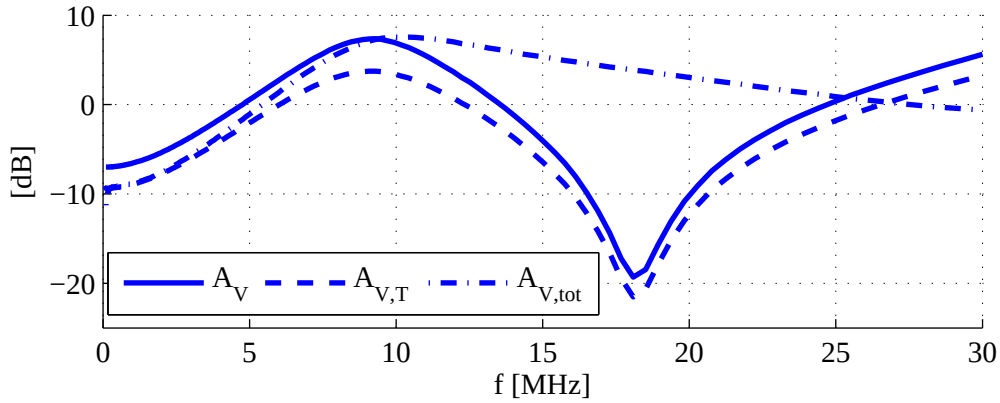

(a) Voltage gain for the NE3508 circuit.

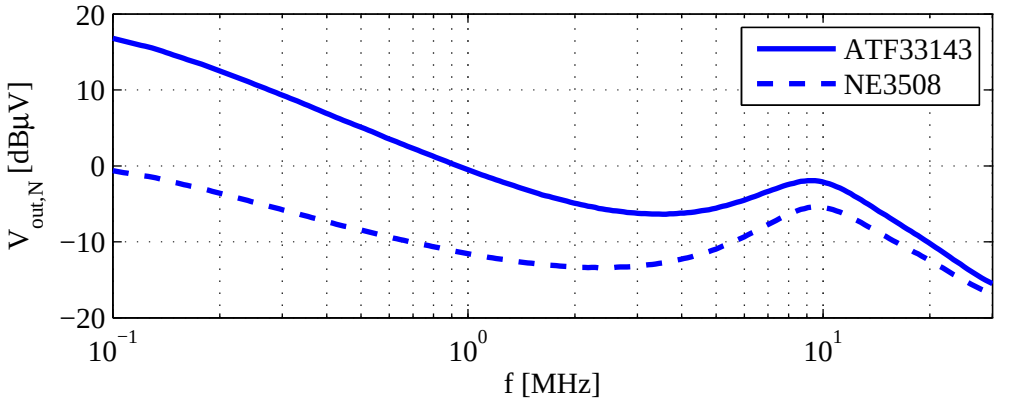

(b) Output noise voltage for 9 kHz bandwidth.

Fig. 5.15: Simulated AM voltage gain and output noise voltage for $R_{S1} = 16\,\Omega$, $R_{S2} = 41\,\Omega$, $R_D = 30\,\Omega$, $L_D = 820\,\text{nH}$, with $\underline{Z}_A$ connected at the amplifier's input.

The simulated frequency characteristic of the antenna amplifier (NE3508 circuit)

[4]This cable length has been chosen in order to introduce an average capacitive loading for the active antenna in the AM range.

is shown in Fig. 5.15(a) for the proposed solution. The voltage gain $A_V = |\underline{V}_o/\underline{V}_i|$ is the gain of the amplifier core, while $A_{V,T} = |\underline{V}_o/\underline{V}_A|$ is the antenna voltage gain and $A_{V,tot} = |\underline{V}_{out}/\underline{V}_A|$ is the total voltage gain (including the 2.5 m cable and the 7 pF buffer). The frequency characteristic of the ATF33143 circuit is not shown, being very similar to the presented one. Fig. 5.15(b) displays the simulated output noise voltage in the AM range for both circuits. As expected, the NE3508 circuit has superior noise performance in the whole AM band.

In the case of the NE3508 transistor and for the current design at 150 kHz, C_{GS} is lowered from 0.46 pF to about 0.04 pF. The Miller effect contributes about 0.46 pF to the input capacitance, so the total input capacitance C'_{in} of the amplifier core sums up 0.5 pF. It is expected that the practical realization will bring at least 0.5 pF parasitic capacitance at the input node, caused by the layout parasitics. For $C_A = 3.3\,\text{pF}$, the input voltage attenuation is therefore about 2.3 dB. For frequencies lower than 6 MHz, this result is confirmed by the A_V and $A_{V,T}$ curves in Fig. 5.15(a).

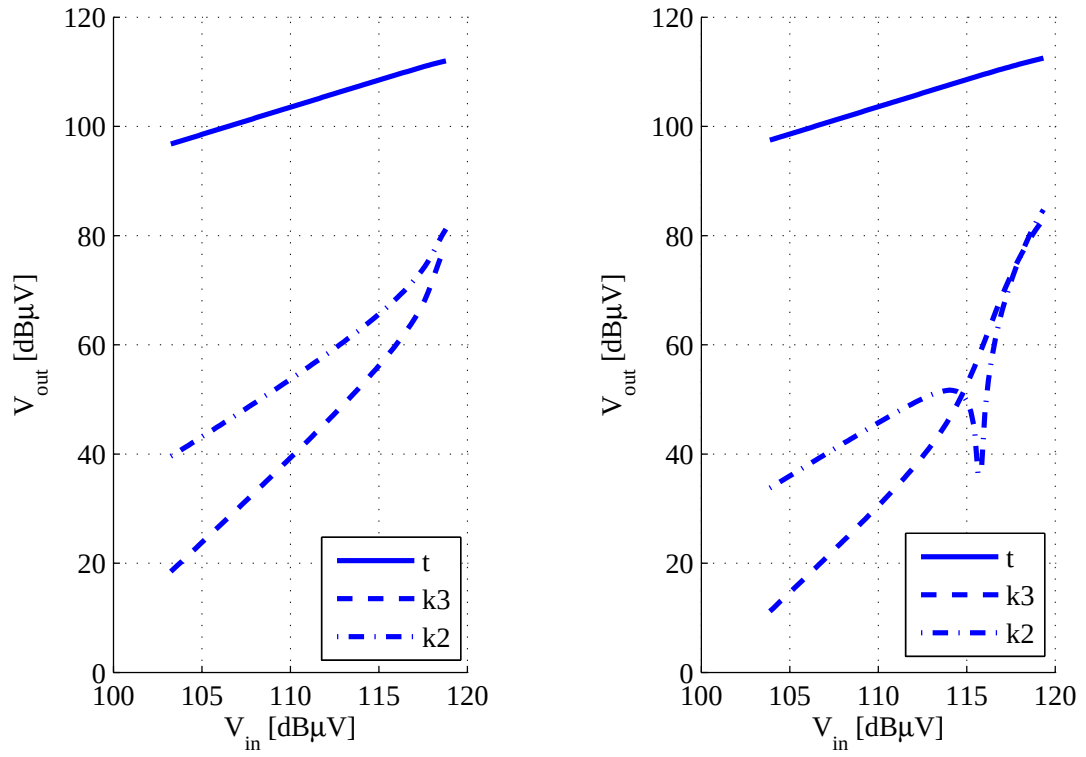

(a) ATF33143 circuit, 50 mA drain current.

(b) NE3508 circuit, 40 mA drain current.

Fig. 5.16: Simulated intermodulation performance for $f_1 = 1\,\text{MHz}$ and $f_2 = 1.2\,\text{MHz}$.

The simulated 3rd and 2nd order intermodulation performance is shown in Fig. 5.16 for both transistor circuits when $f_1 = 1\,\text{MHz}$ and $f_2 = 1.2\,\text{MHz}$. The ATF33143 circuit achieves for 50 mA drain current $a_{k3} = 47\,\text{dB}$ and $a_{k2} = 39\,\text{dB}$ for $110\,\text{dB}\mu\text{V}$

output level, while the NE3508 circuit reaches for 40 mA drain current $a_{k3} = 46\,\mathrm{dB}$ and $a_{k2} = 52\,\mathrm{dB}$ for the same output level.

5.3.3 Stability Considerations

As already mentioned in the previous paragraphs, L_1–R_1 and L_2–R_2 serve the stability purpose. Next this subject is brought into discussion, as the same approach is used also for the other circuits proposed throughout this work.

The stability of a circuit can be evaluated by inspecting the stability factors k and B [31]:

$$k = \frac{1 - |\underline{S}_{11}|^2 - |\underline{S}_{22}|^2 + |\underline{\Delta}|^2}{2 \cdot |\underline{S}_{12}\underline{S}_{21}|} \tag{5.6}$$

$$B = 1 + |\underline{S}_{11}|^2 - |\underline{S}_{22}|^2 - |\underline{\Delta}|^2 \tag{5.7}$$

where $\underline{\Delta} = \underline{S}_{11}\underline{S}_{22} - \underline{S}_{12}\underline{S}_{21}$. Unconditional stability requires $k > 1$ and $B > 0$. This condition has to be fulfilled for the largest possible frequency range, as the circuit might oscillate also outside the operating band. A way to achieve unconditional stability is to load resistively the circuit at the input and/or output, although this procedure has to be carefully considered in order to minimally interfere with the signal behaviour in the operating band.

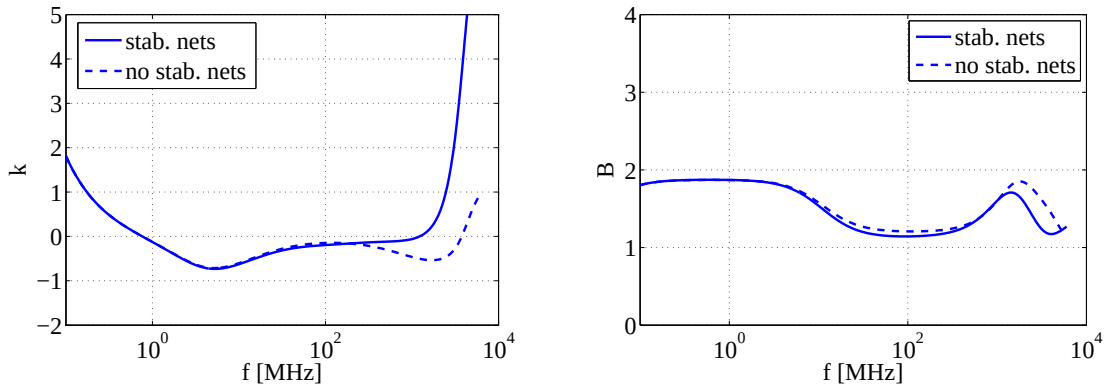

(a) Simulated stability factor k. (b) Simulated stability factor B.

Fig. 5.17: ATF33143 circuit. Simulated stability factor curves, with and without stability networks.

As it can be seen in Fig. 5.17 for the ATF33143 circuit, without stability networks only the B factor fulfills the required condition, while k indicates a region of potential instability. Unfortunately this region includes also the operating bands, which makes the use of resistive loading difficult to apply. In the general case of a high impedance amplifier, connecting a resistor in parallel to the input will degrade both signal and noise performance, as it decreases the input impedance value and it contributes additional noise (Section 4.1). Connecting a resistor in series with the

input interferes less with the signal (at least as long as it has a moderate value), but contributes a certain amount of noise. At the output both possibilities (resistor in parallel or in series) degrade the signal performance.

Achieving unconditional stability inside the operating bands is therefore very difficult, if not impossible without seriously compromising the performance. On the other hand, a potentially instable circuit might very well function as long as the instability region is limited and no "dangerous" impedances are presented as terminations to the circuit. This approach, combined with experimental results, will be used throughout this work for stabilizing the antenna amplifiers.

Unconditional stability will be aimed only outside the operating band, at high frequencies. It should be noted that the GaAs transistors used throughout this work have high cut-off frequencies, which expose the circuits also to potential high frequency instabilities. Experience has shown that good stability is achieved for this kind of application by connecting resistors in series with the input and the output of the antenna amplifier. An inductor is placed in parallel to the resistor used for loading, so that the resistor is short-circuited for low frequencies (including the operating band) and starts to act only at higher frequencies (L_1–R_1 and L_2–R_2 in Fig. 5.4).

The stability factors in the presence of the stability networks can be seen in Fig. 5.17 for $L_1 = 1.5\,\mathrm{nH}$, $R_1 = 100\,\Omega$, $L_2 = 56\,\mathrm{nH}$ and $R_2 = 43\,\Omega$. The networks have no to little effect in the lower frequency range, but improve the stability for the higher frequencies. This solution proves valuable in practice, as it does not affect the in-band performance.

5.3.4 Experimental Results

The two circuits (ATF33143 and NE3508) have been realized on standard FR4 boards, as Fig. 5.18 shows. The design of the layout concentrated on minimizing the parasitic effects which could lead to high-frequency instabilities. The ground plane has been removed from beneath the input node, in order to minimize the input capacitance of the circuit.

Frequency Characteristic

The frequency characteristic is measured in the lab by inserting the 3.3 pF capacitor representing the antenna impedance between the signal generator and the amplifier's input. In Fig. 5.19 the simulated and measured total voltage gain curves $A_{\mathrm{V,tot}} = |\underline{V}_{\mathrm{out}}/\underline{V}_{\mathrm{A}}|$ are shown for both circuits in the AM range, when a 2.5 m 50 Ω coaxial cable is connected between the amplifier's output and the high-ohmic buffer (having about 7 pF input capacitance), as described in Fig. 5.7. A good agreement between measurement and simulation can be observed in the entire AM range. As expected, the two circuits have almost similar gain performance.

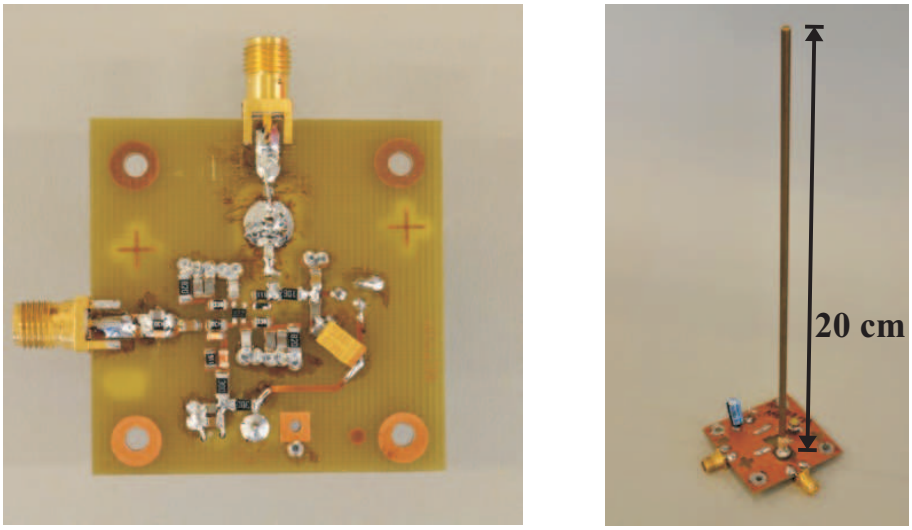

Fig. 5.18: Realized NE3508 circuit.

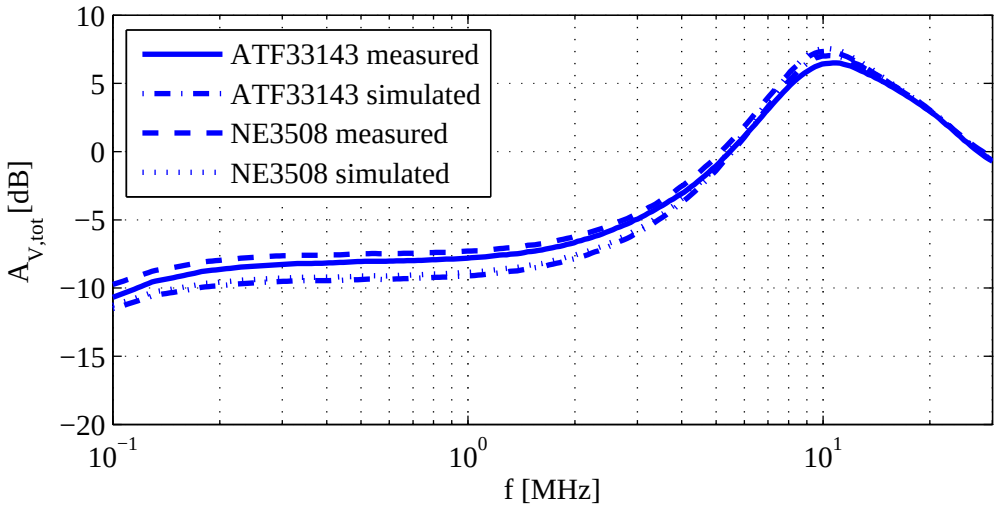

Fig. 5.19: Simulated and measured frequency characteristic in the AM range in the presence of $\underline{Z}_{\mathrm{A}}$.

The lab measurement in the FM range is performed with the 50 Ω load directly connected to the amplifier's output, while at its input the 3.3 pF capacitor is present as before. In Fig. 5.20 the simulated and measured total voltage gain curves $A_{\mathrm{V,tot}} = |\underline{V}_{\mathrm{out}}/\underline{V}_{\mathrm{A}}|$ are shown for both circuits in the FM range. The simulation proves to be somewhat more pessimistic when compared to the measurement, probably in terms of input capacitance; nevertheless the agreement is good for both circuits.

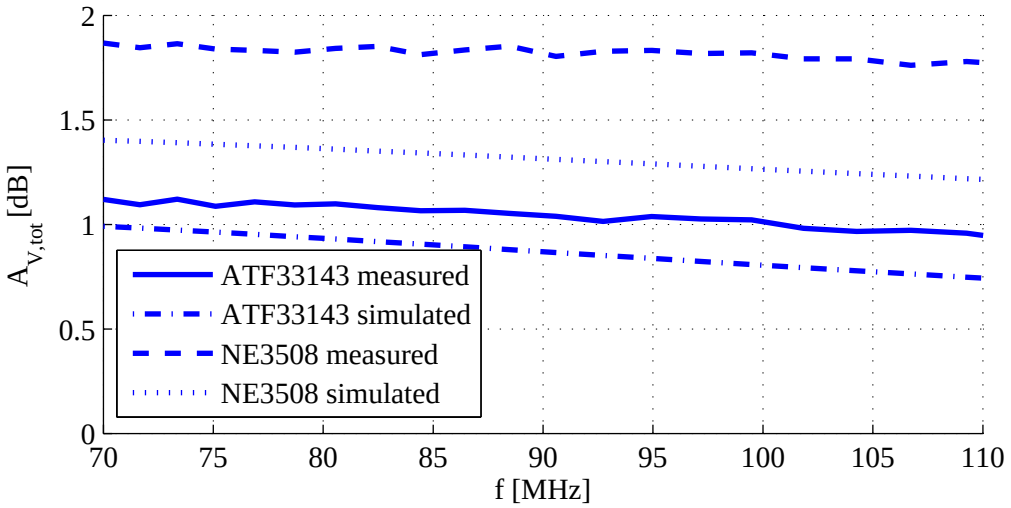

Fig. 5.20: Simulated and measured frequency characteristic in the FM range in the presence of $\underline{Z}_{\mathrm{A}}$.

Noise Performance

The noise is measured in the lab as described in Section 4.3.3, with the 3.3 pF capacitor representing the antenna impedance connected at the amplifier's input. The output noise voltage curves, simulated and measured for 9 kHz bandwidth, are shown in Fig. 5.21 for both circuits in the AM range. The antenna amplifier's output is loaded with the long coaxial cable and the high-ohmic buffer.

The high gate leakage current of the ATF33143 transistor makes the use of large gate biasing resistors R_{G} difficult. Experimental results show that the intermodulation performance is severely degraded when $R_{\mathrm{G}} = 10\,\mathrm{M\Omega}$, probably because of the gate leakage current modulation which in turn produces important voltage drops across R_{G}. Because of this the resistor value is decreased to only 2 MΩ. The simulations do not show a significant noise worsening in the AM range because the output noise level is already high anyway.

Fig. 5.21 reveals important differences between measurement and simulation in the case of the ATF33143 circuit. The simulation seems to have overestimated the output noise level because of the assumption of a too high gate leakage current.

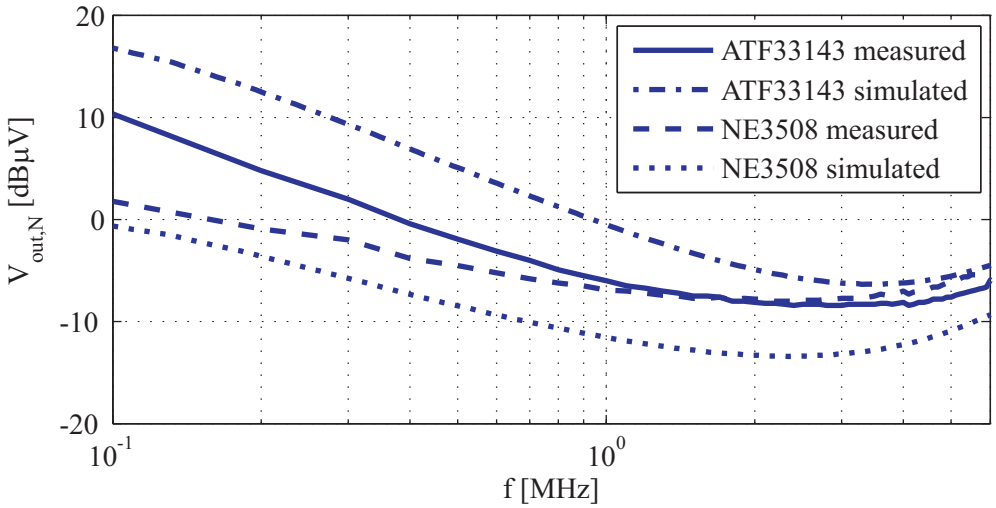

Fig. 5.21: Simulated and measured output noise voltage $V_{\mathrm{out,N}}$ in the AM range for 9 kHz bandwidth with $\underline{Z}_{\mathrm{A}}$ connected.

Nevertheless, the gate leakage current appears to strongly vary from device to device, so a correct prediction concerning the associated shot noise is difficult to make.

The measurement indicates about 7 dBµV output noise at 150 kHz, while levels lower than −6 dBµV are first reached at about 1 MHz. This indicates that the ATF33143 circuit is not appropriate for AM operation, or at least not without seriously compromising the sensitivity.

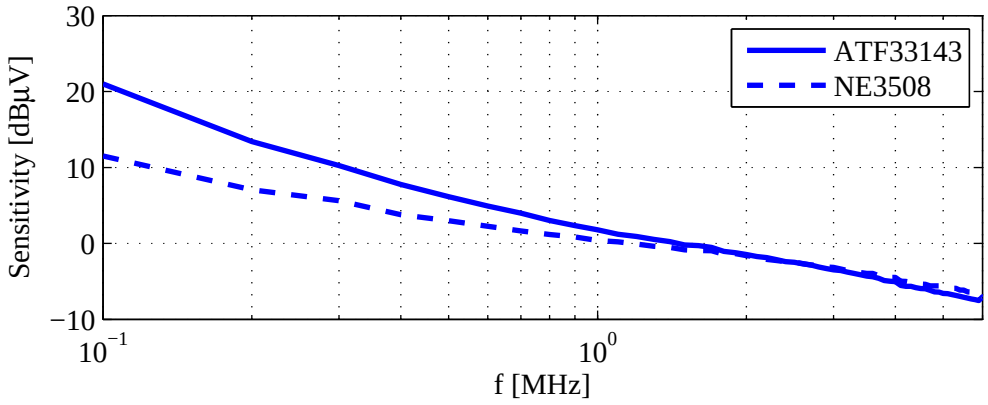

Fig. 5.22: Measured antenna voltage V_{A} for unity output SNR in the AM range.

In the case of the NE3508 circuit the noise model proves to be a little too optimistic. The measured values are well below those recorded with the ATF33143 circuit in the LW range. At 150 kHz the output noise voltage is about 0.2 dBµV, while for frequencies above 750 kHz the noise level drops below −6 dBµV. Even if the circuit did not achieve the recommended output noise level in the whole AM

range, it still features an acceptable performance.

Based on the measured data, the calculated sensitivity (defined for a unity output SNR) is depicted in Fig. 5.22. As expected, the NE3508 circuit features better sensitivity in the LW and MW bands.

The lab measurement in the FM range is performed with the 50 Ω load directly connected to the amplifier's output, while at its input the 3.3 pF capacitor is present as before. In Fig. 5.23 the simulated and measured output noise voltage curves are shown for both circuits in the FM range.

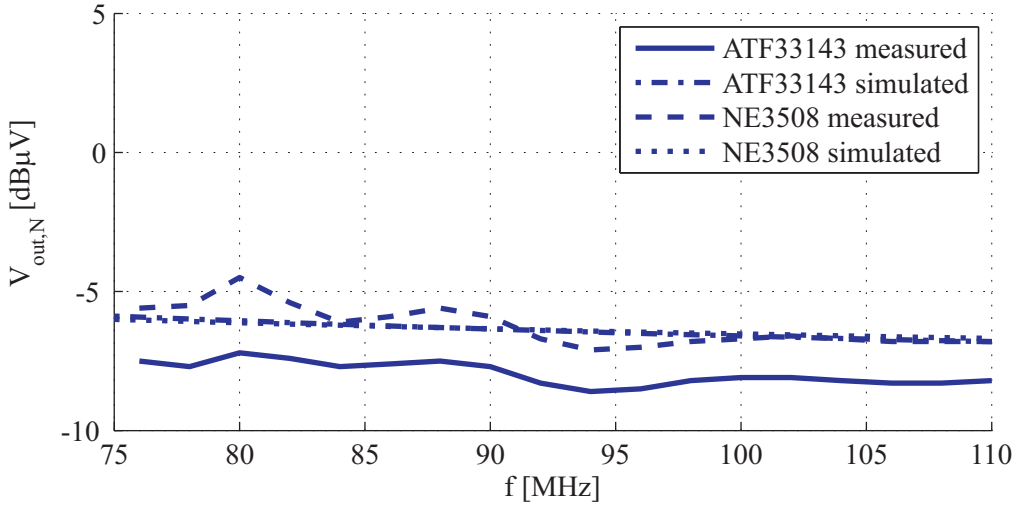

Fig. 5.23: Simulated and measured output noise voltage $V_{\mathrm{out,N}}$ in the FM range with $\underline{Z}_{\mathrm{A}}$ connected, $B = 120\,\mathrm{kHz}$.

Again, for the ATF33143 circuit the noise level has been somewhat pessimistically anticipated. The measured value is about 1 dB below the simulated one. For both Japanese and European band the output noise level is below $-7.2\,\mathrm{dB\mu V}$. For the NE3508 circuit a good agreement between measurement and simulation can be observed. For the European band the output noise level is lower than $-5.6\,\mathrm{dB\mu V}$, while for the most part of the Japanese one it is below $-5.4\,\mathrm{dB\mu V}$.

The calculated sensitivity (defined for a unity output SNR and based on the measured data) is displayed in Fig. 5.24 and it can be seen that the ATF33143 circuit performs about 1 dB better than the NE3508 one.

Linearity

The measured 3rd and 2nd order AM and FM intermodulation performance is shown in Fig. 5.25 for the NE3508 transistor circuit alone. A comparison between the intermodulation distances achieved by both circuits is given in Tab. 5.2 for 110 dBµV output level. In the FM range, the input tones are located at $f_1 = 99\,\mathrm{MHz}$ and $f_2 =$

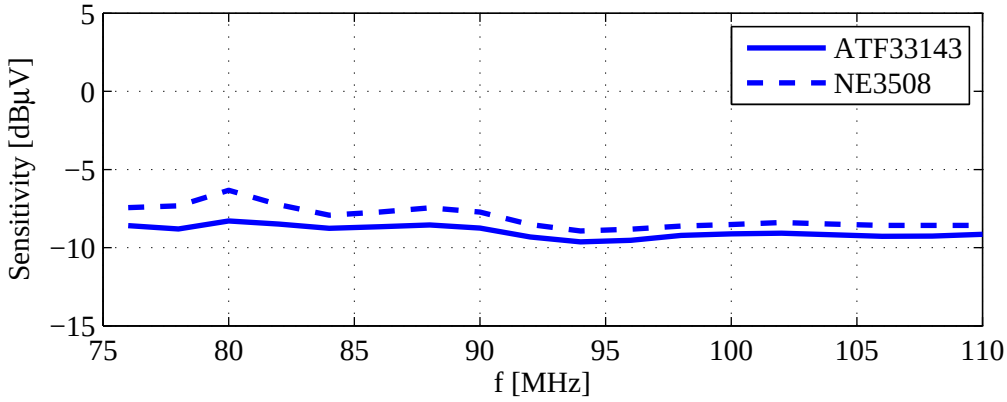

Fig. 5.24: Measured antenna voltage V_A for unity output SNR in the FM range.

101 MHz. Both circuits fail to accomplish at least 80 dB 2rd order intermodulation distance, thus exposing themselves to FM-AM conversion issues.

Circuit	a_{k3} [dB]	a_{k2} [dB]
NE3508	49	62
ATF33143	48	44

Table 5.2: FM intermodulation performance (110 dBµV output level).

In AM, as depicted in Fig. 5.25(b), the NE3508 circuit achieves $a_{k3} = 49$ dB and $a_{k2} = 43$ dB, which can be considered satisfactory.

5.3.5 Discussion

The discussed single path AM/FM antenna amplifier has the advantage of a simple structure that makes use of only one transistor, thus reducing costs. It achieves a good gain in combination with the 20 cm long monopole antenna, but it has only modest sensitivity and linearity performance. The linearity issue can be improved by means of automatic gain control, which implies a more expensive solution. The sensitivity issue has to be accepted as part of the low-cost antenna amplifier. Due to this impairments the design is no longer optimized (for example, by adding an output matching network), but serves as a starting point for further improved antenna amplifier architectures.

5.4 Two Path AM/FM Antenna Amplifier

As we have seen, a one-transistor low-noise stage cannot be designed linear enough in order to prevent FM-AM conversions. Without employing automatic gain control

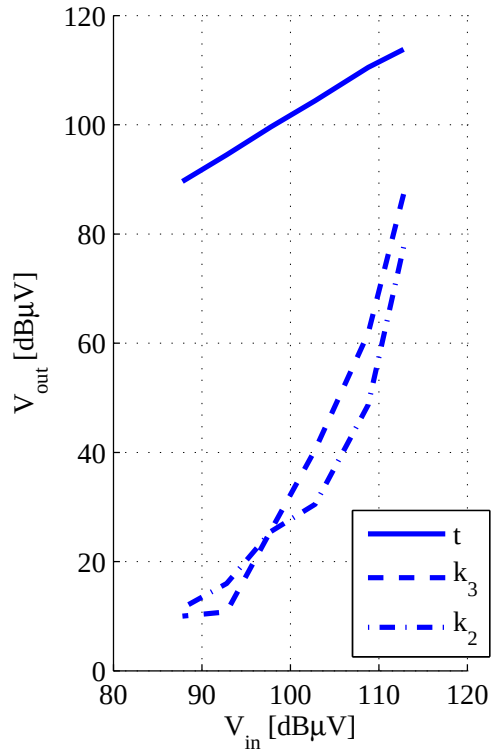

(a) Linearity in the FM range for $f_1 = 99\,\text{MHz}$ and $f_2 = 101\,\text{MHz}$.

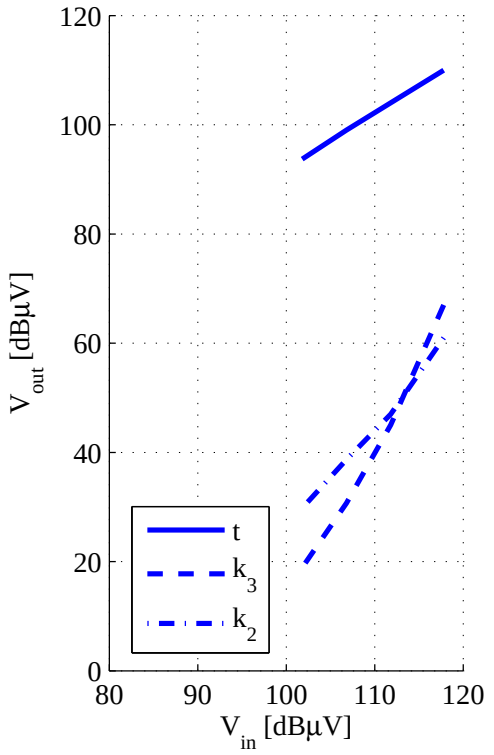

(b) Linearity in the AM range for $f_1 = 1.1\,\text{MHz}$ and $f_2 = 1.3\,\text{MHz}$.

Fig. 5.25: NE3508 circuit. Measured 3rd and 2nd order linearity.

circuitry, sufficient 2nd order intermodulation distances cannot be achieved with a single amplifier stage, at least not without sacrificing other important parameters such as the noise behaviour. Therefore the need for a two-path amplifier arises, in which the AM and FM bands are processed individually [42]. Another reason explaining why to have a two-path amplifier is the flicker-noise, which requires the use of low $1/f$-noise transistors for the AM range. Unfortunately, these devices have insufficient transconductance to be successfully used for the FM amplifier also, as already illustrated in Section 5.3.

In Fig. 5.26 the schematic of the two-path AM/FM active antenna is presented. The AM and FM signals are processed separately by two specialized low-noise amplifiers with high input impedance and high linearity. C_{par} sums up the parasitic capacitances that arise on the input path of the amplifier.

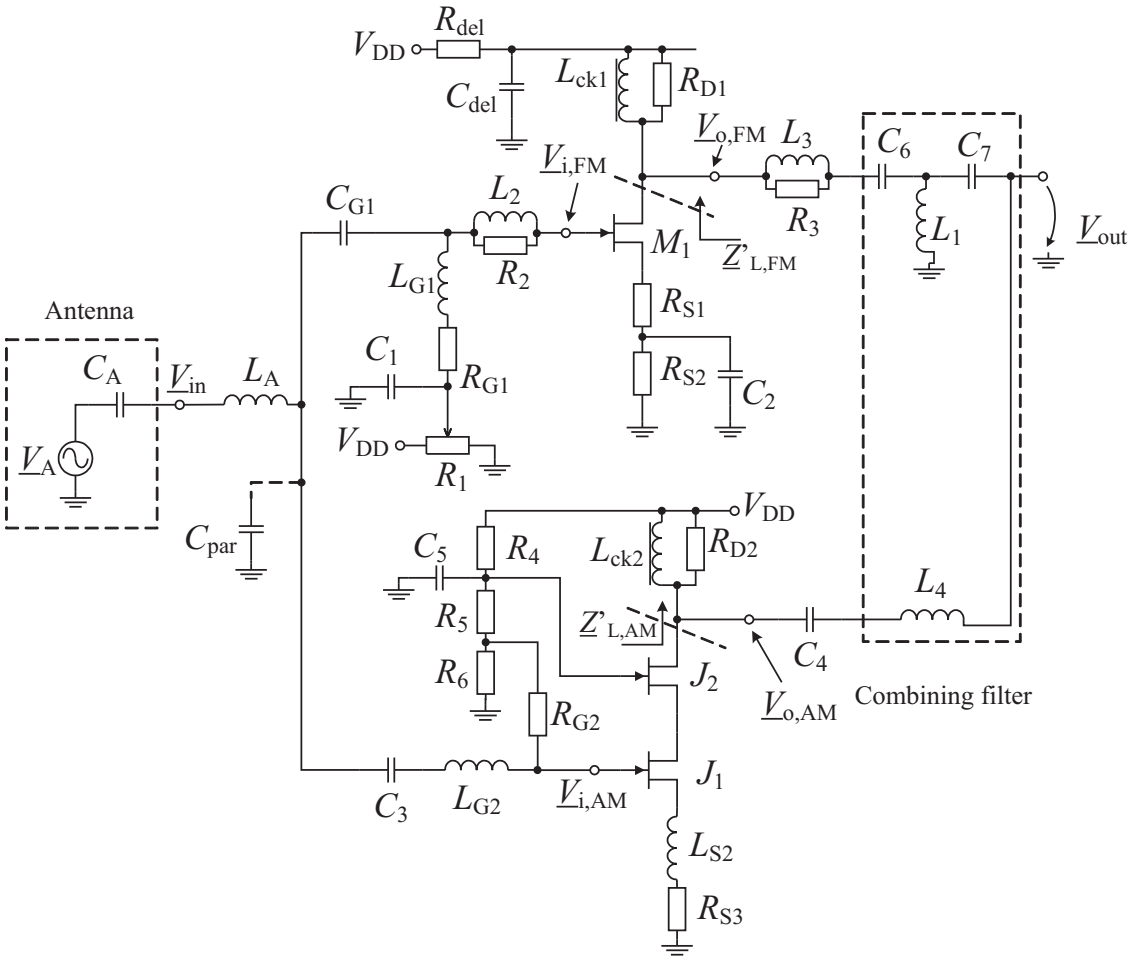

Fig. 5.26: Schematic of the two-path AM/FM active antenna.

5.4.1 FM Amplifier

The FM amplifier consists of one amplifying stage equipped with an ATF33143 GaAs HEMT transistor M_1 and has a similar structure as the one described in Section 5.3. As already discussed, this transistor type has excellent noise-figure and transconductance and achieves good linearity, but because of its high flicker noise, it is not suited for low frequency AM range. For this reason, the AM amplifier is built around a Si JFET cascode stage realized with J_1 and J_2, as explained later.

Because in this implementation the AM signal is processed by a different amplifier, the degeneration and load of the FM stage have no longer to be a function of frequency.

In Fig. 5.26 R_{del} is used for lowering the voltage supply of the FM amplifier. Together with C_{del} it also creates a delay in the start-up transient. L_{ck1} saves DC voltage headroom and acts like a choke inductor in FM range, while R_{D1} has a sufficient high value, so that it can be neglected in respect to a 50 Ω load. The gate

biasing voltage is set by the R_1 potentiometer, while the DC negative feedback is given by the R_{S1} and R_{S2} resistors. C_1 and R_1 also have to address the start-up transient issue in a similar manner to the one already discussed for the single-transistor AM/FM amplifier. L_{G1} and R_{G1} have no impact on the biasing, since the gate leakage current is small enough. As already discussed in Section 5.3, the transistor is biased at a relative large drain current $I_D = 50\,\text{mA}$ in order to improve its linearity.

The decoupling capacitors C_1 and C_2 can be considered short-circuits for the entire FM operating range. The L_2–R_2 and L_3–R_3 groups ensure the stability of the stage and are such dimensioned to have a minimal impact upon the working range.

The FM circuit in Fig. 5.26 displays some important differences when compared to the circuit in Fig. 5.4:

- the large gate biasing resistor has been replaced by the L_{G1} – R_{G1} combination, since the stage is no longer required to work in the AM range. For FM the impedance of L_{G1} is high enough in order to neglect its effect, while R_{G1} attenuates the resonance caused by L_{G1} together with the surrounding capacitances;

- in the AM range, $L_{G1} = 4.7\,\mu\text{H}$ and $C_{G1} = 10\,\text{pF}$ form a high-pass "noise filter", which prevents the induced gate noise current source of M_1 from degrading the noise of the AM path [43]. C_{G1} is carefully chosen in order not to introduce too much capacitance in the AM path. On the other hand, the capacitance value must be high enough to avoid a too strong signal loss in FM;

- the high-pass T-filter C_6–L_1–C_7 placed at the amplifier's output matches the output impedance of the FM stage to $50\,\Omega$ and also blocks the AM signal from entering the FM path.

As already described in Section 5.3, the trade-off between sensitivity, output noise level and linearity has to be made when choosing the voltage gain of the stage. The voltage gain value and the linearity are attained with the help of the resistor R_{S1}. Using eq. (5.2) and the results from Section 5.3.1, R_{S1} is chosen to be $16\,\Omega$, thus achieving a voltage gain of the FM core $A_{V,FM} = |V_{o,FM}/V_{i,FM}| \simeq 3$ (for $50\,\Omega$ load) and a simulated output noise voltage $V_{out,N} \simeq -6.6\,\text{dB}\mu\text{V}$ at 100 MHz, with $\underline{Z}_A$ connected and in the absence of the output matching network.

Without the matching network, the output return loss in the FM range is lower than –8 dB, as shown in Fig. 5.27. The high-pass T-matching network has to cover both Japanese and European FM bands. By realizing a good impedance match at one frequency, as the dash-dotted curve in Fig. 5.27 shows, the network becomes narrowband and fails to cover the whole FM range. Capacitors C_6 and C_7 have to be large enough for the lower Japanese band to be able to pass through, while they have to be small enough in order to block the AM signals. By lowering the total quality factor of the network a broadband solution is reached, in which the return

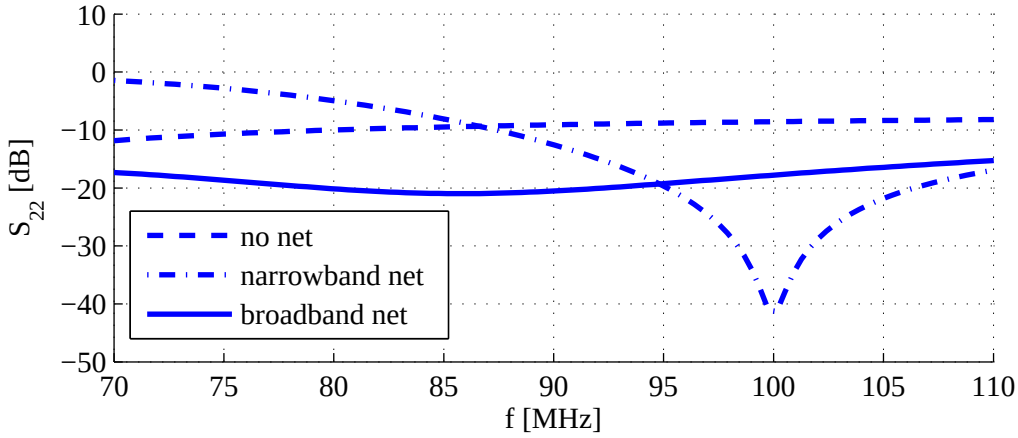

Fig. 5.27: Simulated output return loss of the FM stage with different output matching networks.

loss is lower than –15.7 dB in the entire Japanese and European bands (solid curve in Fig. 5.27).

At 100 MHz, due to the impedance transformation performed by the matching network, the transistor sees a load $|Z'_{\mathrm{L}}| \simeq 110\,\Omega$ and applying eq. (5.2), we get a core voltage gain of about $|A_{\mathrm{V}}| \simeq 4.5 = 13\,\mathrm{dB}$. This impacts on the Miller effect affecting C_{GD} and thus on the input capacitance of the stage. The Miller effect contributes now about 2.2 pF to the input capacitance, while the degeneration lowers C_{GS} from 2.1 pF to about 0.3 pF. In this case, the input capacitance of the FM core $C'_{\mathrm{in,FM}}$ is estimated to be about 2.5 pF. For the two-path amplifier, due to the more complicated layout and the loading imposed by the AM stage, it is assumed that the practical realization contributes at least 1 pF parasitic capacitance, so that $C_{\mathrm{in}} \simeq 3.5\,\mathrm{pF}$ and the input voltage attenuation is about 6.3 dB.

In order to overcome the gain loss caused by C_{G1} and the loading brought by the AM amplifier, the inductor L_{A} is introduced to partially tune out the antenna capacitance. Its value could be chosen to produce a resonance at the amplifier's input, but in this situation the bandwidth would be severely limited. Furthermore, the output noise voltage would increase very much at the resonance frequency, making the amplifier inappropriate for active antenna use. By choosing $L_{\mathrm{A}} = 470\,\mathrm{nH}$ the resonance occurs out of FM band, at about 172 MHz. In spite of this, $A_{\mathrm{V,tot}}$ will be improved, as Fig. 5.28 shows.

5.4.2 AM Amplifier

For the AM amplifier, the JFET transistor SST310 is preferred due to its low flicker-noise and low price. This transistor has quite large gate-source and gate-drain capacitances ($C_{\mathrm{GS}} \simeq 4.8\,\mathrm{pF}$ and $C_{\mathrm{GD}} \simeq 1.6\,\mathrm{pF}$), so that a significant input signal attenuation is expected when compared to the single-transistor AM/FM amplifier,

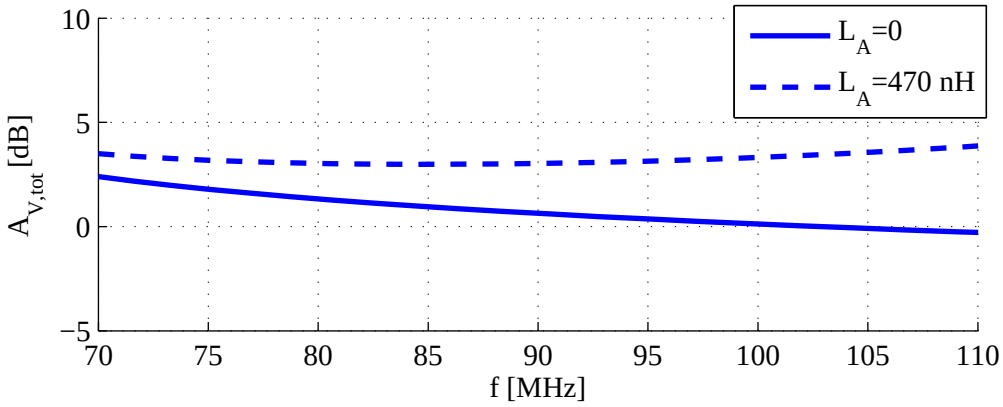

(a) Voltage gain $A_{\mathrm{V,tot}} = |\underline{V}_{\mathrm{out}}/\underline{V}_{\mathrm{A}}|$.

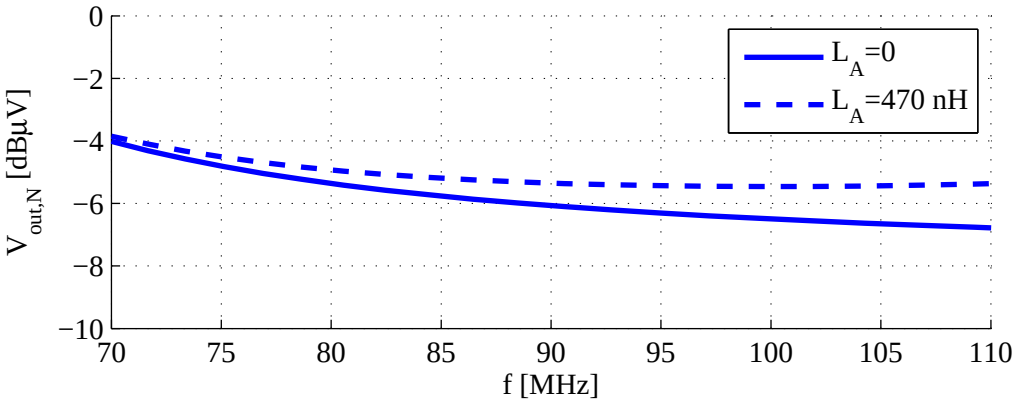

(b) Output noise voltage for 120 kHz bandwidth.

Fig. 5.28: Simulated FM voltage gain and output noise voltage with and without L_{A}.

where the HEMT transistors exhibited very low input capacitances. In order to alleviate this issue, a degenerated cascode stage is used for the AM path. The degeneration reduces the equivalent gate-source capacitance and improves linearity, while the cascode topology minimizes the Miller effect.

The AM amplifier in Fig. 5.26 consists of the J_1 and J_2 cascode stage. Resistance R_{S3} improves linearity and input impedance of the stage. The inductance L_{S2} improves linearity and input impedance in the FM range, so that the stage will not contribute to undesired distortions of the output signal. L_{ck2} is a choke inductor for AM range and saves DC voltage headroom, while R_{D2} sets the voltage gain of the stage, because the AM amplifier has a high-impedance load (formed by the cable and the high-ohmic radio receiver). The gates of J_1 and J_2 are biased with the help of the voltage divider $R_4 - R_5 - R_6$. The gate resistor R_{G2} ensures the high resistance required for low noise in the AM range. As already explained, its value should be as high as possible, but for practical reasons is limited to 20 MΩ.

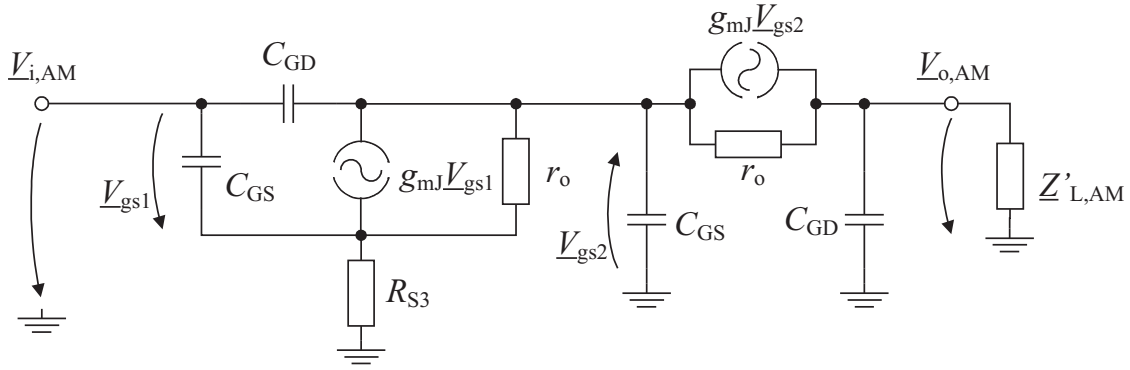

Fig. 5.29: AC small-signal equivalent circuit of the AM stage.

The JFET transistors are biased with 30 mA, which leads to a transconductance g_{mJ} of about 16 mS. The AC small-signal equivalent circuit of the AM cascode is shown in Fig. 5.29. For the degeneration resistance $R_{S3} = 56\,\Omega$ a small amount of DC voltage is consumed and the C_{GS} of J_1 is reduced from about 4.8 pF to about 2.5 pF. We shall now estimate the voltage gain $A_{V,J1}$ of J_1 taking into consideration the cascode topology. The load "seen" by J_1 towards J_2 is about $1/g_{mJ} \simeq 62.5\,\Omega$ due to the common base connection of J_2. Applying eq. (5.2) for the degenerated J_1 stage when $r_o \simeq 1270\,\Omega$, we get $A_{V,J1} \simeq -0.5$. As a result, the Miller effect adds about 2.4 pF to the input capacitance $C'_{in,AM}$ of the stage, thus summing up to about 4.9 pF.

As we have seen in Section 5.4.1, the presence of C_{G1} adds to the total input capacitance, so that:

$$C_{in,AM} = C'_{in,AM} + C_{G1} + C_{par} \tag{5.8}$$

For $C_{par} = 1\,\text{pF}$ we get $C_{in,AM} \simeq 16\,\text{pF}$, so that the input voltage attenuation is about 15.3 dB.

Combining now the voltage gain of the degenerated common source (eq. (5.2)) with the voltage gain of the common base circuit:

$$A_{V,cb} = \frac{(g_m r_o + 1)\,\underline{Z}'_{L,AM}}{\underline{Z}'_{L,AM} + r_o} \tag{5.9}$$

we get the voltage gain of the cascode stage:

$$A_{V,cas} = -\frac{\underline{Z}'_{L,AM} g_m r_o (g_m r_o + 1)}{\underline{Z}'_{L,AM} + 2r_o + R_S(g_m r_o + 1)^2 + g_m r_o^2} \tag{5.10}$$

We shall now estimate the required antenna amplifier gain which achieves the same output signal level as the 90 cm long monopole antenna connected to the same antenna amplifier:

$$A_V = \frac{h_{90}}{h_{20}} \cdot \frac{C_{A,90}}{C_{A,20}} \cdot \frac{C_{A,20} + C_{in,AM}}{C_{A,90} + C_{in,AM}} \simeq 10.1 = 20.1\,\text{dB} \tag{5.11}$$

where $C_{A,90} \simeq 10\,\text{pF}$ is the antenna capacitance of the 90 cm monopole.

Introducing now the voltage gain value in eq. (5.10) and considering $\underline{Z}'_{L,AM}$ real, the required load is found to be $Z'_{L,AM} \simeq 1280\,\Omega$. In the actual circuit the load $\underline{Z}'_{L,AM}$ the transistor J_2 sees can be set by adjusting the drain resistor R_{D2}. As the gain vs. R_{D2} curves plotted in Fig. 5.30(a) show, there is a good agreement between the hand-calculated value and the simulation for the considered frequency (150 kHz).

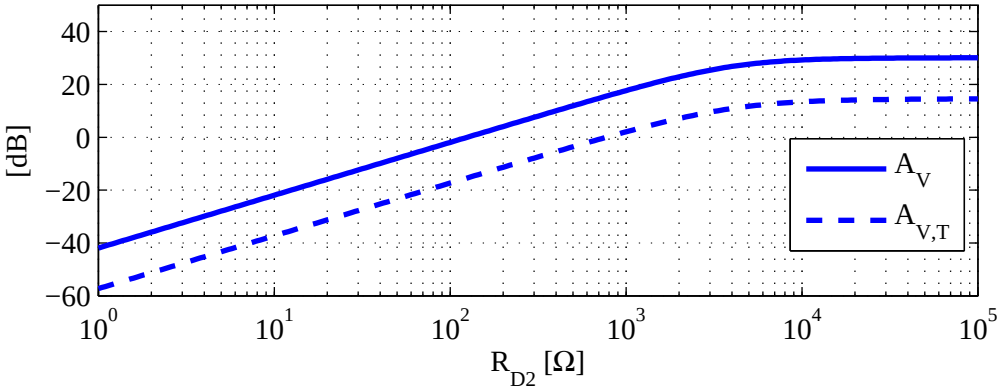

(a) Voltage gain.

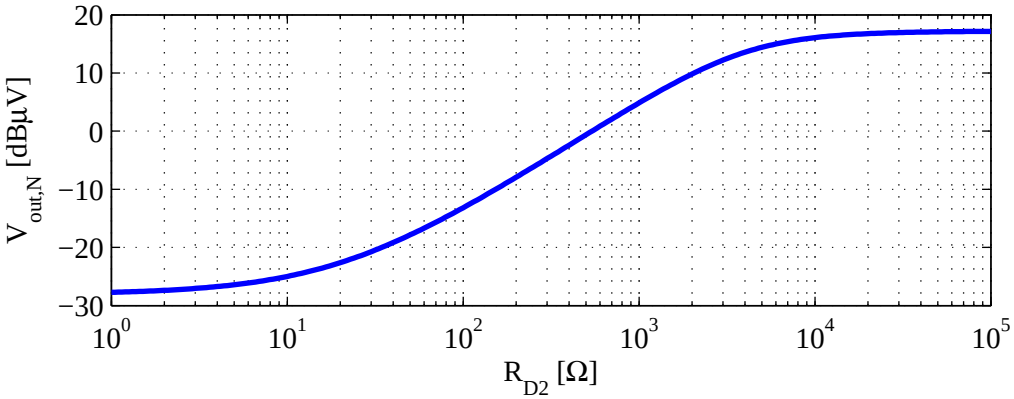

(b) Output noise voltage for 9 kHz bandwidth.

Fig. 5.30: Simulated AM voltage gain and output noise voltage at 150 kHz, with $\underline{Z}_A$ connected at the amplifier's input.

The simulated output noise voltage for the proposed core gain (20.1 dB) is nevertheless too high, about 6.6 dBμV for 9 kHz bandwidth. Simulations show that $R_{D2} = 470\,\Omega$ brings the output noise level below $-1\,\text{dB}\mu\text{V}$. In order to provide some room for the practical realization, the output noise voltage will be further reduced to about $-4\,\text{dB}\mu\text{V}$, which corresponds to $R_{D2} = 330\,\Omega$ and the core voltage gain $A_V \simeq 8.4\,\text{dB}$.

Analyzing now the noise contributed by R_{G2} in Fig. 5.31, doubling the value of

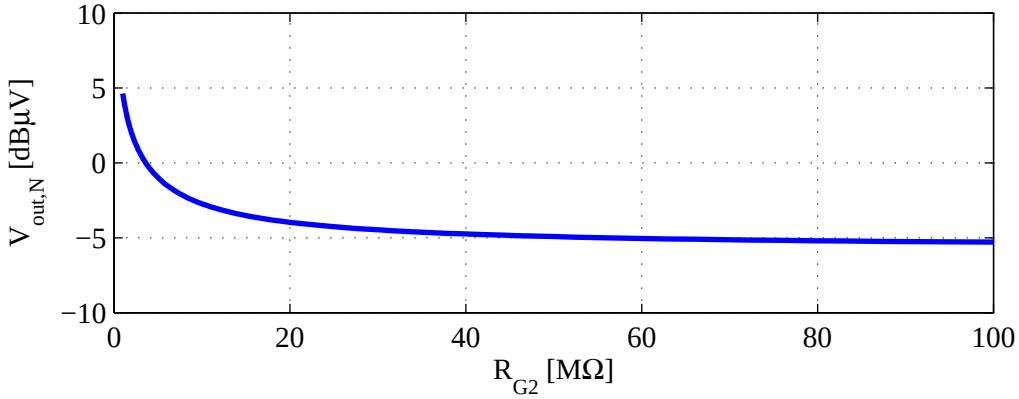

Fig. 5.31: Simulated AM output noise voltage at 150 kHz vs. gate biasing resistor R_{G2}, with $\underline{Z}_A$ connected at the amplifier's input.

R_{G2} from 20 MΩ to 40 MΩ brings only a minor improvement in the output noise voltage of about 0.7 dB. As a result, 20 MΩ are considered sufficient.

For the practical implementation we choose the choke $L_{ck2} = 1\,\text{mH}$, providing sufficient high impedance even in the LW range; larger inductance values are impractical because of size and cost considerations.

The output impedance $\underline{Z}_{out,AM}$ of the AM stage is dominated by the $L_{ck2} - R_{D2}$ group, which means that its value is rather large. Stages exhibiting large output impedances are not well suited for driving large capacitive loads. Indeed, the low-pass filter formed by $\underline{Z}_{out,AM}$ and the capacitance C_{cbl} of the cable connecting the antenna amplifier to the high-impedance receiver introduces a pole which may fall into the operating range. In our case, for which $\underline{Z}_{out,AM} \simeq R_{D2} = 330\,\Omega$ and $C_{cbl} \simeq 250\,\text{pF}$, the pole occurs at:

$$f_t = \frac{1}{2\pi R_{D2} C_{cbl}} \simeq 1.9\,\text{MHz} \tag{5.12}$$

This means that the present AM design can be used for covering the usual AM broadcasting bands, from 150 kHz to about 6 MHz. For better performance an appropriate buffer stage with low output impedance can be added, capable of driving the capacitive load. The same solution can be employed for further covering the AM band up to 30 MHz. This improvement increases nevertheless the circuit complexity.

The simulated total voltage gain $A_{V,tot} = |\underline{V}_{out}/\underline{V}_A|$ and the output noise voltage $V_{out,N}$ are plotted in Fig. 5.32. The gain curve exhibits the pole predicted by eq. (5.12) at lower frequencies, where the coaxial cable can be considered as a capacitive load. At higher frequencies, as already explained in Section 5.3.2, the cable transforms the receiver's input impedance, so that the gain has a minimum. The simulated output noise voltage (when the amplifier source impedance equals the antenna impedance $\underline{Z}_A$) is lower than $-4\,\text{dB}\mu\text{V}$ in LW band and below $-5.5\,\text{dB}\mu\text{V}$

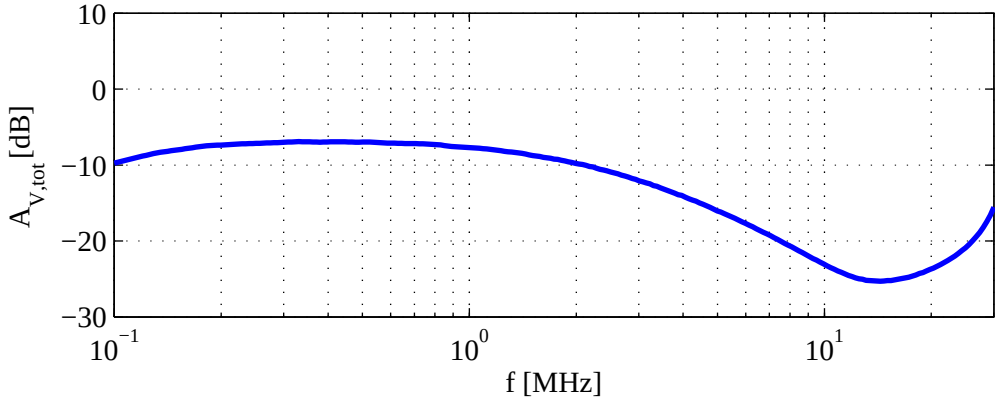

(a) AM total voltage gain $A_{V,tot} = |\underline{V}_{out}/\underline{V}_A|$.

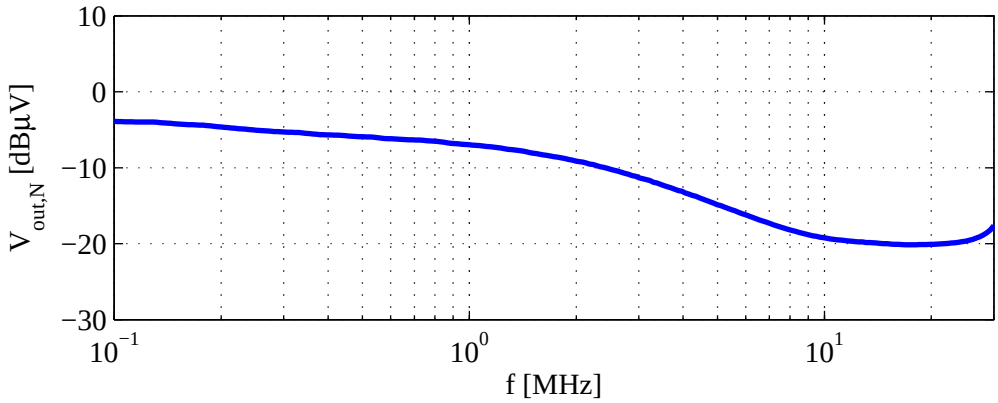

(b) AM output noise voltage for 9 kHz bandwidth.

Fig. 5.32: Simulated AM total voltage gain and output noise voltage, with $\underline{Z}_A$ connected at the amplifier's input.

in the MW range.

5.4.3 Combining the AM and FM Amplifiers

The two amplification paths have now to be such combined, that the interference between them is minimized. The amplifiers' separation is achieved by means of filters, as further described.

FM Input

The high-pass filter $C_{G1} - L_{G1}$ blocks the AM signal from entering the FM amplifier, while preventing the large low-frequency noise of the FM amplifier from intruding the AM path. The FM input is thus protected against the intrusion of strong AM signals which can produce unwanted nonlinear effects. The filter has to add

a minimal capacitive loading to the input node, in order not to degrade the AM performance, while in the FM range it has to avoid impairment of the FM signal. In the AM range (up to 6 MHz) inductor $L_{G1} = 4.7\,\mu H$ together with resistor $R_{G1} = 330\,\Omega$ exhibit a much lower impedance than capacitor $C_{G1} = 10\,pF$ does, so that the capacitive loading contributed by the filter can be approximated with C_{G1}.

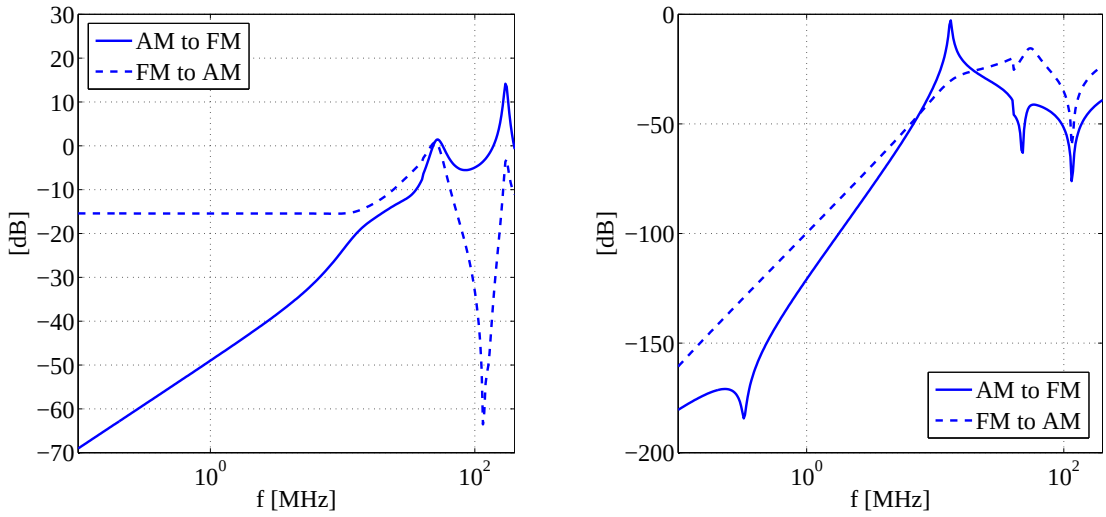

(a) Input. (b) Output.

Fig. 5.33: Input and output simulated AM-to-FM and FM-to-AM transfer.

The transfer function between the antenna and the input of the FM amplifier $\left|\underline{V}_{i,FM}/\underline{V}_A\right|$ (Fig. 5.34) is plotted solid in Fig. 5.33(a), where one can see that for frequencies below 30 MHz the attenuation is at least 12 dB, while for frequencies below 6 MHz the attenuation is at least 31 dB.

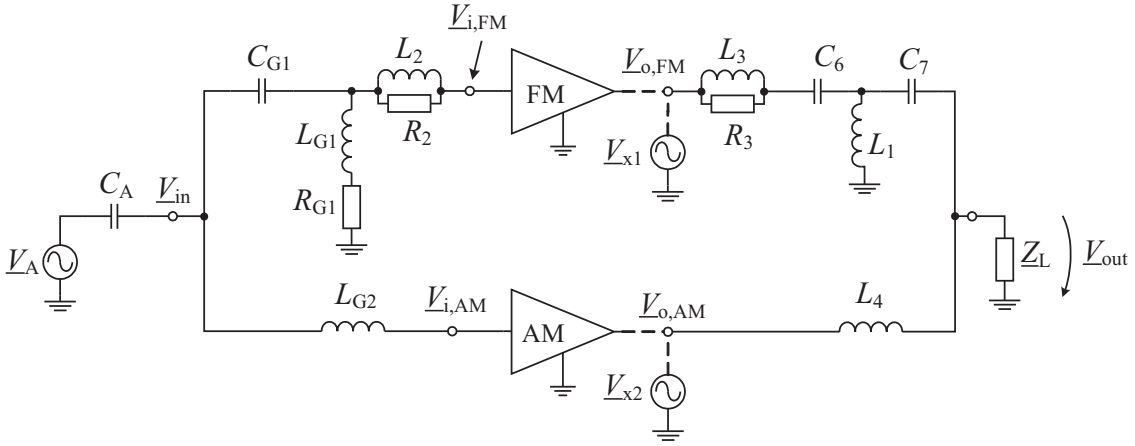

Fig. 5.34: Simulation setup for determining the transfer functions between the two amplifiers.

AM Input

Also the AM input has to be protected against the intrusion of strong FM signals which can produce unwanted nonlinear effects. In this case, inductor $L_{G2} = 4.7\,\mu\text{H}$, together with the input capacitance of the AM stage forms a low-pass filter, which reduces the FM signal well before it reaches the input of the AM amplifier. The transfer function between the antenna and the input of the AM amplifier $\left|\underline{V}_{\text{i,AM}}/\underline{V}_{\text{A}}\right|$ (Fig. 5.34) is dashed plotted in Fig. 5.33(a), where one can see that for frequencies above 76 MHz the attenuation is at least 17 dB. Inductor L_{G2} represents also a choke for the FM signal, so that the input capacitance of the AM stage does not load the input node.

AM and FM Output

The output signals of the two amplifiers are combined by means of filters. The high-pass T-filter at the output of the FM path blocks the AM signal and also matches the output impedance of the FM stage to $50\,\Omega$. The inductor $L_4 = 4.7\,\mu\text{H}$ prevents the FM signal from entering the AM path.

In order to determine the transfer function between the output of the AM amplifier and the output of the FM one $\left|\underline{V}_{\text{o,FM}}/\underline{V}_{\text{o,AM}}\right|$, the output of the AM amplifier is disconnected and replaced by a test voltage source $\underline{V}_{\text{x2}}$, as shown in Fig. 5.34. The load $\underline{Z}_{\text{L}}$ is frequency dependent, being high-ohmic up to 40 MHz and $50\,\Omega$ onwards. The resulting transfer function is plotted solid in Fig. 5.33(b), where it can be seen that for frequencies below 6 MHz the attenuation is at least 54 dB.

For determining the transfer function between the output of the FM amplifier and the output of the AM one $\left|\underline{V}_{\text{o,AM}}/\underline{V}_{\text{o,FM}}\right|$, a similar procedure is employed with the help of $\underline{V}_{\text{x1}}$, as shown in Fig. 5.34. The resulting transfer function is dashed plotted in Fig. 5.33(b), and it can be seen that for frequencies above 76 MHz the attenuation is at least 24 dB.

Linearity

The inductance $L_{S2} = 680\,\text{nH}$ provides an additional degeneration in the FM range, so that the linearity and input impedance of the AM amplifier increase and the stage does not contribute to undesired distortions.

The simulated 2^{nd} and 3^{rd} order linearity of the amplifier in AM and FM ranges is illustrated in Fig. 5.35. Table 5.3 highlights the intermodulation distances reached for $110\,\text{dB}\mu\text{V}$ fundamental output signal level. Simulations indicate that this circuit architecture is not subject to undesired FM-AM conversion issues.

5.4.4 Experimental Results

Fig. 5.36 depicts the practical realization of the new active antenna. The printed circuit board (PCB) form has been adapted with respect to a commercial active

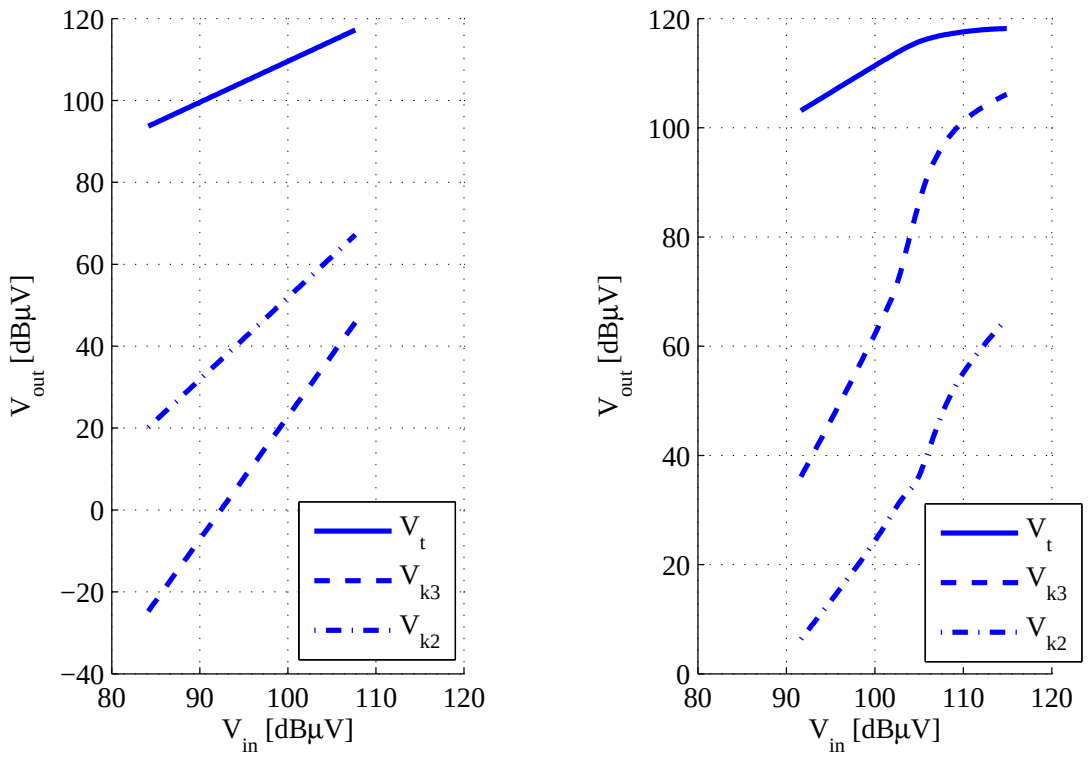

(a) AM. (b) FM.

Fig. 5.35: Simulated 2nd and 3rd order linearity.

Range	a_{k3} [dB]	a_{k2} [dB]
AM	86	57
FM	52	89

Table 5.3: Intermodulation performance (110 dBµV output level).

antenna. The layout design aimed at optimizing the high-frequency behaviour of the circuit, which could lead to instabilities. Also, care is taken in order to minimize the parasitic capacitances of input traces, also by removing the ground plane underneath the input node. The antenna is mounted directly on the amplifier PCB, thus avoiding other undesired capacitive loading which may occur at the input node. The antenna has a usual bend angle $\alpha = 60°$.

Frequency Characteristic

The realized antenna amplifier has L_A connected at the input, as already explained. The measurements show that the amplifier has about 18.5 pF input capacitance in AM range and 4.4 pF in FM range. These values are larger than expected, but

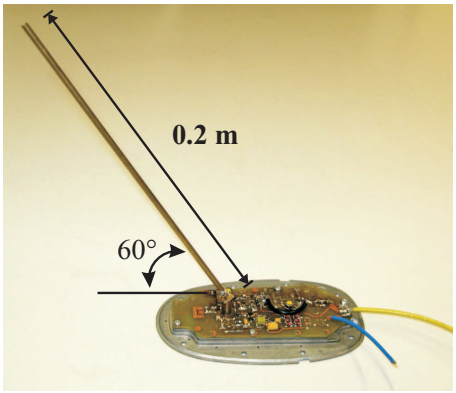

Fig. 5.36: Realized 20 cm long monopole active antenna.

nevertheless close to them, especially in AM. In Fig. 5.37 is depicted the measured total voltage gain in FM, $A_{V,tot} = |\underline{V}_{out}/\underline{V}_A|$. Its value is lower than expected due to the higher input capacitance.

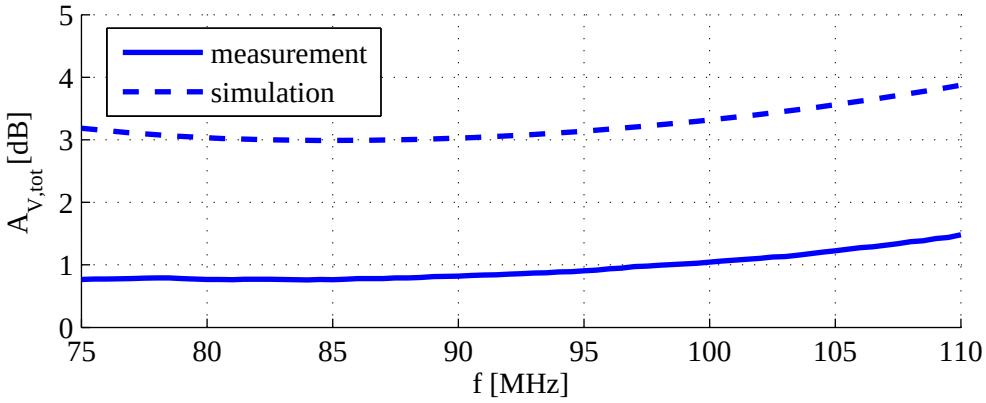

Fig. 5.37: Simulated and measured total FM voltage gain $A_{V,tot} = |\underline{V}_{out}/\underline{V}_A|$.

When measuring the AM-performance of the active antenna in the lab, the amplifier is placed in a shielded box, using the antenna equivalent circuit as the source impedance for the amplifier. A coaxial cable and a high-impedance buffer connect the active antenna to the 50 Ω receiving equipment, thus emulating the AM radio receiver input impedance. In Fig. 5.38 the measured total voltage gain $A_{V,tot} = |\underline{V}_{out}/\underline{V}_A|$ is depicted for AM range. When compared to the simulations, the total gain value is lower due to the higher input capacitance.

Field measurements are also performed with the new active antenna mounted on top of a car, above the rear windshield, as it is normally placed. The car is placed on a turntable, as detailed by the measurement procedure described in Section 4.3.2.

Fig. 5.39 depicts the ratio between the signal delivered by the new 20 cm active monopole antenna and the signal delivered by the 90 cm passive reference antenna, in the whole FM range, for both horizontal and vertical polarizations.

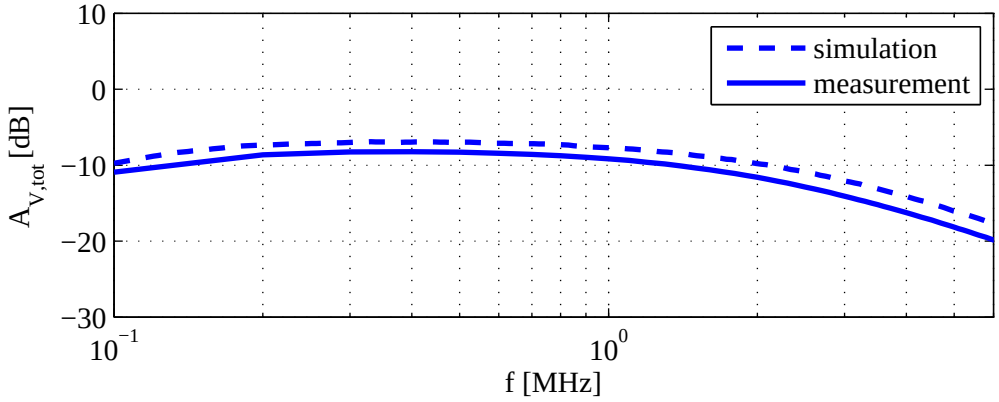

(a) Total AM voltage gain $A_{\mathrm{V,tot}} = |\underline{V}_{\mathrm{out}}/\underline{V}_{\mathrm{A}}|$.

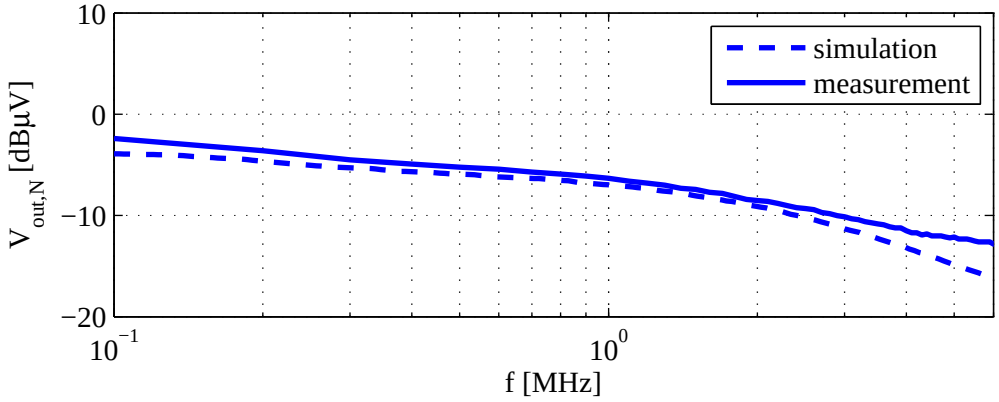

(b) AM output noise voltage for 9 kHz bandwidth.

Fig. 5.38: Simulated and measured total AM voltage gain and output noise voltage.

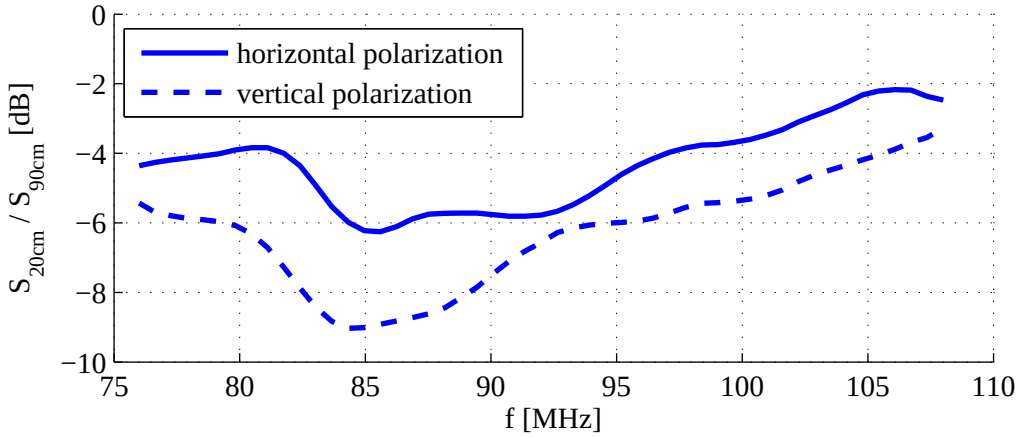

Fig. 5.39: Field measurement in the FM range showing the ratio between the signal delivered by the new 20 cm active antenna and the signal delivered by the reference antenna, when both are mounted on a car.

The field measurements in the AM range are performed in the valleys of the Bavarian mountainous regions, where the man-made noise is low. The 20 cm active antenna and the 90 cm passive rod reference antenna are mounted in the same way as described for the FM measurements. For both antennas, the output signal is measured on a broadcast station at 801 kHz frequency and the noise at 850 kHz in an unallocated AM frequency. Thus the ratio of the output SNR of the 20 cm monopole active antenna to the output SNR of the reference antenna is found to be –4.1 dB. This result shows that despite the drastic shortening of the new active antenna, its output SNR is only about 4 dB beneath the SNR provided by the passive reference. With analog AM-broadcast, a difference of 4 dB in SNR is only audible in a direct A/B comparison.

Noise Performance

The measured FM output noise voltage $V_{\mathrm{out,N}}$ is depicted in Fig. 5.40 and is determined in an anechoic chamber, with the 20 cm long rod antenna connected to the amplifier. For the Japanese FM range, the output noise level is lower than $-5\,\mathrm{dB\mu V}$, while for the European range it is below $-6\,\mathrm{dB\mu V}$. The discrepancy between simulation and measurement is attributed mainly to the poor noise modelling of the HEMT transistor in FM range. Nevertheless, the experimental values are found to be satisfactory.

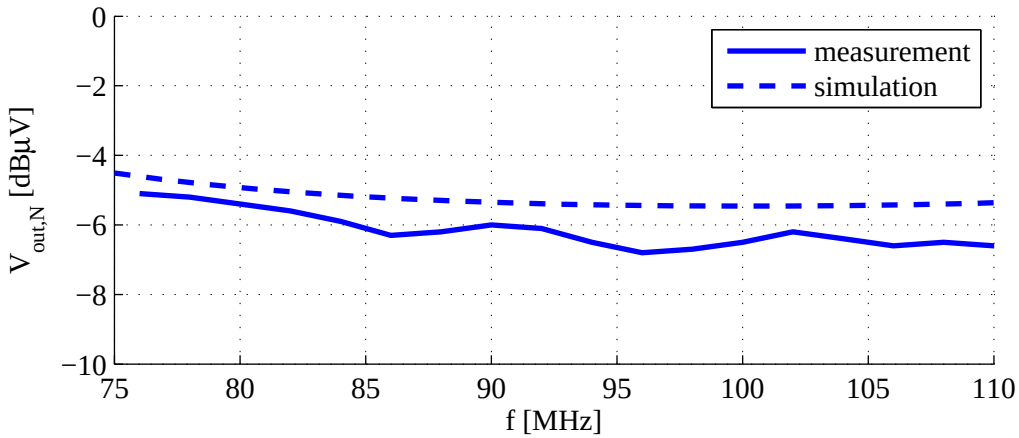

Fig. 5.40: Simulated and measured FM output noise voltage for 120 kHz bandwidth and $\underline{Z}_{\mathrm{A}}$ connected.

The sensitivity of the new active antenna is also measured in the anechoic chamber with the experimental setup explained in Section 4.3.4 and is referred to the sensitivity achievable under the same conditions with a passive 90 cm long rod antenna (reference antenna). As expected, the results depicted in Fig. 5.41 show that the sensitivity of the new 20 cm active antenna is beneath the one of the reference

rod, in average 12 dB for the Japanese FM range and 14 dB for the European FM range.

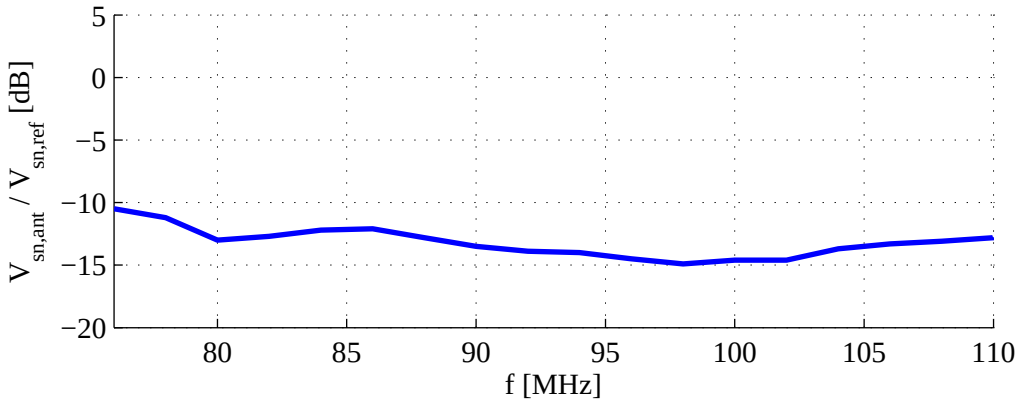

Fig. 5.41: Measured sensitivity of the 20 cm long active antenna. Result is referred to the 90 cm long passive reference rod antenna. All antennas are mounted on a ground plane.

The measured AM output noise voltage $V_{\mathrm{out,N}}$ is depicted also in Fig. 5.38 and shows a good agreement with the simulations in the long and medium wave ranges, accomplishing the VDA recommendations. In the short wave range, the output noise voltage of the active antenna becomes comparable with the noise of the receiving system, thus making the results inaccurate.

Linearity

The linearity of the amplifier is measured in the lab, by supplying two tones at the input and measuring the output signal levels for the fundamental input frequencies and the 2nd and 3rd order intermodulation products.

Fig. 5.42(a) depicts the 3rd order intermodulation products for FM. The two input tone frequencies are 99 and 103 MHz and a_{k3} is found to be 52 dB. Due to the less excitation (as a result of the short monopole), the measured a_{k3} value is satisfactory. For the measurement of the FM-to-AM conversion the two input tone frequencies are 99 and 101 MHz, so that the lower 2nd order intermodulation product falls near the MW band, and $a_{\mathrm{k2}} = 83\,\mathrm{dB}$ is found.

The linearity of the AM amplifier is also measured in the lab under the same conditions as the FM amplifier and Fig. 5.42(b) and 5.42(c) depict the 3rd and 2nd order intermodulation products. For AM, the two input tone frequencies are located on 1.1 and 1.3 MHz and a_{k3} is found to be 62 dB, while a_{k2} is 64 dB. In the case of the AM measurements, it should be noted that the buffer is connected at the output of the antenna amplifier, in order to load it with a high-impedance. This buffer will also contribute to the non-linear behaviour and the intermodulation distances shown above are degraded by its presence. When measured alone for the same fundamental

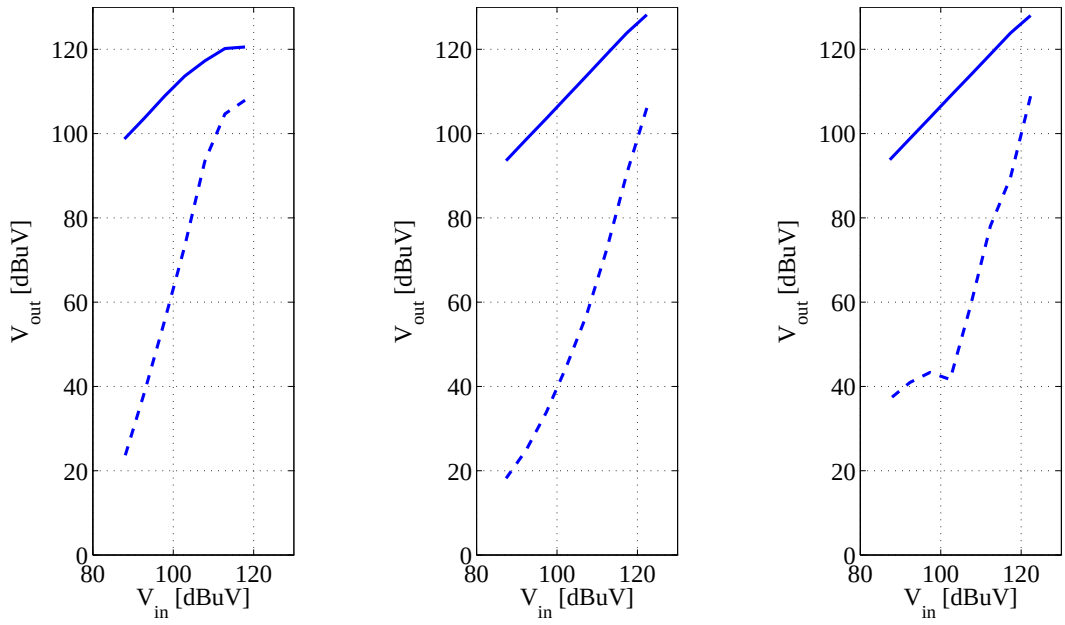

(a) FM a_{k3}. (b) AM a_{k3}. (c) AM a_{k2}.

Fig. 5.42: Measured 2nd and 3rd order intermodulation products in AM and FM range.

tones, the buffer has $a_{k3} = 66\,\text{dB}$ and $a_{k2} = 70\,\text{dB}$, so values larger but comparable with the ones exhibited by the combination of DUT with the buffer. Therefore, the buffer's linearity influence upon the final result cannot be considered negligible.

5.5 One-Path Amplifier vs. Two-Path Amplifier

The gain, noise, sensitivity and linearity performance of the two amplifier architectures (one-path and two-path respectively) can now be compared. In the case of the one-path amplifier only the NE3508 circuit has been considered, since it offers better results in the AM range.

In Fig. 5.43 the measured total gain of both designs is shown. The one-path amplifier has a larger gain in the AM range, especially in the SW band, and can easily drive its load. In the FM range, due to its lower input capacitance, the one-path amplifier exhibits about 1 dB more gain than its two-path counterpart.

Fig. 5.44 compares the measured output noise voltage of the two architectures. In the AM range, the two-path amplifier features almost overall a lower output noise level than the one-path design does. In the FM range the two circuits are similar.

Based on the measured data presented so far, the calculated sensitivity (defined for a unity output SNR) is depicted in Fig. 5.45. In the LW band the two-path amplifier reaches a better sensitivity. In the MW and SW bands the one-path amplifier is superior, due to its significant larger gain. In the FM range the one-

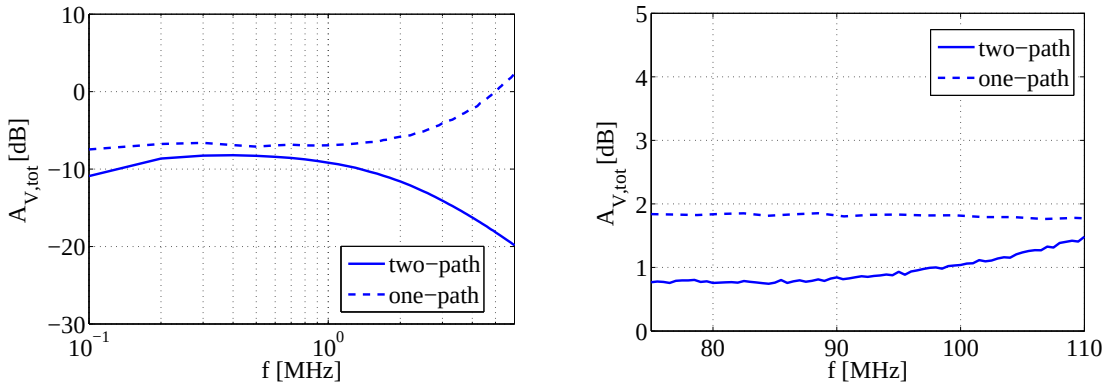

(a) AM range. (b) FM range.

Fig. 5.43: Comparison between the measured total voltage gain achieved by the one-path amplifier and the two-path amplifier in both AM and FM range.

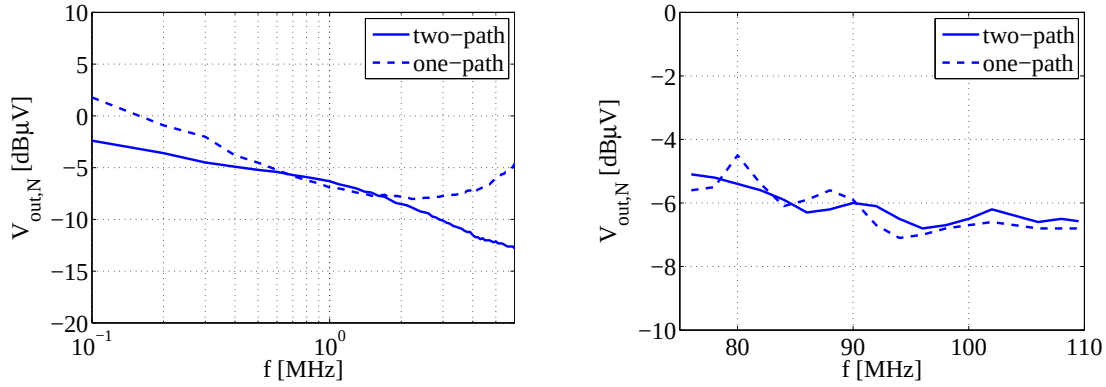

(a) AM range. (b) FM range.

Fig. 5.44: Comparison between the measured output noise voltage achieved by the one-path amplifier and the two-path amplifier in both AM and FM range.

path amplifier is a little bit better compared to the two-path design, due to its larger gain at approximately the same output noise level.

In the case of the linearity, there are differences between the two circuit architectures, as detailed in Tab. 5.4. The two-path architecture has overall a better linear behaviour, especially in AM. Also, the FM-AM conversion issue has been alleviated.

5.6 Effects in the AM Range when Further Reducing the Monopole Height

Decreasing the monopole height h impacts upon the input signal of the active antenna by the simultaneous reduction of the voltage V_A induced in the antenna el-

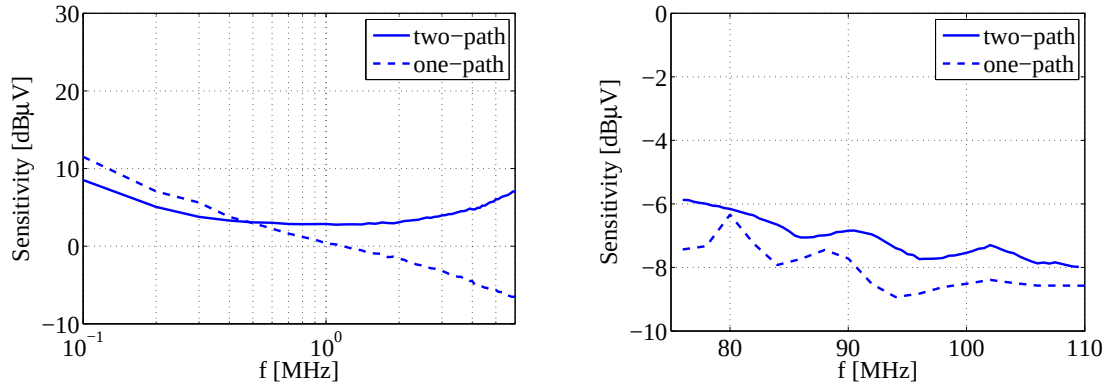

(a) AM range.

(b) FM range.

Fig. 5.45: Comparison between the sensitivities achieved by the one-path amplifier and the two-path amplifier in both AM and FM range. Curves based on measured data.

Circuit	AM	AM	FM	FM
	a_{k3} [dB]	a_{k2} [dB]	a_{k3} [dB]	a_{k2} [dB]
one-path	43	49	49	62
two-path	62	64	52	83

Table 5.4: Comparison between the measured intermodulation performance achieved by the one-path amplifier and the two-path amplifier in both AM and FM range (110 dBµV output level).

ement (as a result of the decreasing effective height h_{eff}) and the antenna capacitance C_{A}:

$$V_{\text{in,active}} = V_{\text{A}} \cdot \frac{C_{\text{A}}}{C_{\text{A}} + C_{\text{in}}} = E \cdot h_{\text{eff}} \cdot \frac{1}{1 + \frac{C_{\text{in}}}{ah}} \tag{5.13}$$

where a is a constant expressed in pF/m, E is the electric field strength and h_{eff} is the effective height of the antenna. In practice the measurement results are referred to a passive 90 cm reference monopole antenna, in order to eliminate the necessity of determining E and the exact value of h_{eff}.

Fig. 5.46 shows the results obtained in a field measurement performed at 801 kHz by sweeping the height of the active antenna. The measured data is referred to the ones obtained with a 90 cm passive reference monopole antenna. A 3 m long 50 Ω cable connects the active antenna to the test receiver, while for the passive reference a 4.5 m long 150 Ω cable is used. As it can be seen, using the AM amplifier discussed in Section 5.4.2 allows the reduction of h to about 6.5 cm, while still delivering the same signal as the 90 cm passive reference.

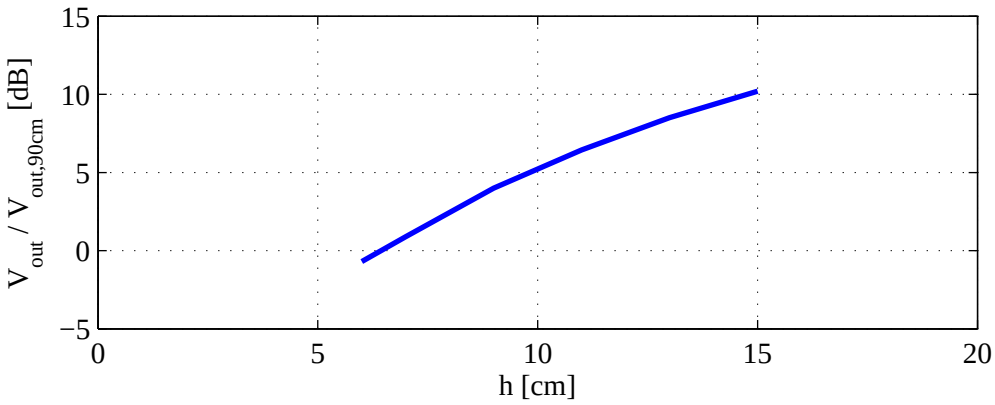

Fig. 5.46: Field measurement at 801 kHz showing the ratio of the receiver voltage when using an active monopole antenna of height h to the receiver voltage when using the 90 cm passive reference monopole.

5.7 Summary

This chapter explored the possibility to shrink the size of a simple monopole active antenna to only 20 cm, while maintaining its performance to satisfactory levels. Because the length shrinking of the monopole antenna decreases its antenna capacitance and effective height, special measures have to be taken when designing the antenna amplifier, in order to preserve the reception quality.

Two high-impedance amplifier designs have been investigated for this purpose. The first design is an attempt to implement a low-cost solution with only one transistor operating both in AM and FM broadcast bands. When compared to the two-path version, this solution features superior gain and partly superior sensitivity in both AM and FM, but it is noisier in the AM band and it fails to be linear enough. Its most severe limitation is the FM-AM conversion, which cannot be held at a sufficiently low value, since both bands are processed by the same transistor.

The two-path amplifier performs well in both broadcast bands and it also features sufficient linearity. The price paid is its higher complexity, because each band is processed separately by two specialized amplifier paths, which are optimized for low-noise, high input impedance and low distortion.

The two-path active antenna has been investigated in the laboratory as well as in field tests, after being mounted onto a car. As expected, the measurement results of the very short active antenna with the length of 20 cm are for both AM and FM range below the performance achievable with a common 90 cm long passive whip antenna. Nevertheless, in the AM range the measured performance (i.e. output signal-to-noise ratio in this case) achieved by this active antenna is only about 4 dB below the one provided by the 90 cm long passive monopole. This outstanding result is important, because also the antenna elements investigated further on in this work perform similarly (from an electrical point of view) in the AM range. As

a consequence, the combination with the AM amplifier proposed here allows them to be used also for AM reception.

Chapter 6

High-Impedance Amplifiers for Short Helix Active Antennas

In the last years 30 cm and 20 cm long antennas have been more and more common in order to meet the nowadays styling requirements. As shown in Chapter 5, decreasing the length of a simple monopole to only 20 cm requires a high-performance high-impedance low-noise amplifier and the overall achieved performance is merely satisfactory in comparison to a 90 cm long passive rod antenna. This is because the antenna effective height is drastically reduced and the diminished voltage excited in the antenna element cannot be sufficiently amplified in order to compensate for this, because of output noise and linearity constraints.

In order to alleviate these issues, helical antenna structures operating in normal mode are used, being known to be well suited for miniaturization, while maintaining a good performance level [44]. Their resonant character can result in more convenient impedance and improves the effective height, but the very sharp resonance makes their employment in broadband applications, such as radio reception, difficult.

In [45] an amplifier structure is introduced which is optimized to be used with a novel, only 14 cm long, thin helical antenna featuring a capacitive coupling. The proposed high-impedance amplifier (HIA) concept flattens the frequency response of the very short resonant antenna, while maintaining a low noise level and a good linearity. The design has been realized and the measurements show that the new 14 cm active antenna has comparable sensitivity with state of the art 40 cm long active monopole antennas. Field measurements indicate good performance in comparison to the common passive rod antennas of 90 cm length, both in AM and FM range.

6.1 Short Capacitive Coupled Helix Antenna

As already shown in Chapter 5, simply shrinking the length of a monopole will only decrease its effective height h_{eff} and its antenna capacitance C_{A}. As a result, not

much performance can be expected from this approach.

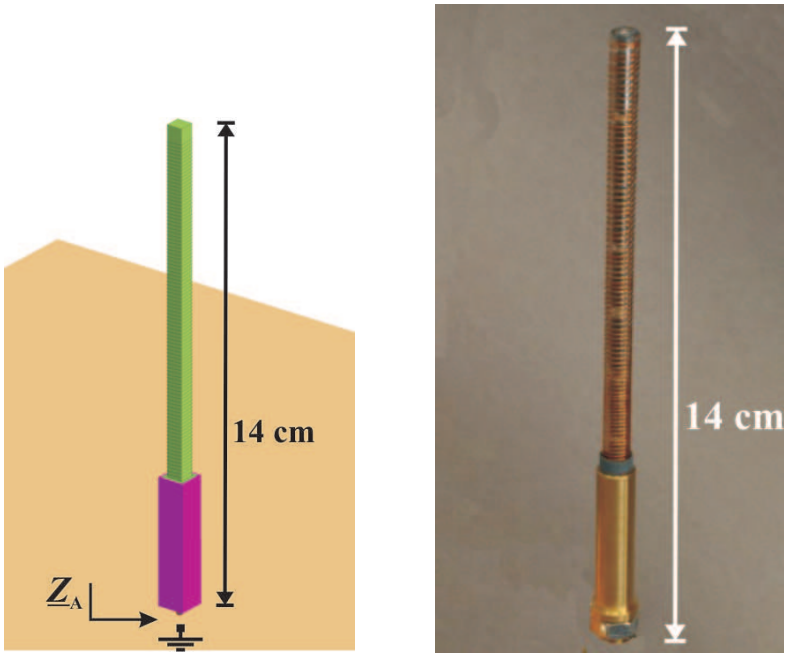

(a) Simulation model. (b) Realized element.

Fig. 6.1: Capacitive coupled helix antenna (CCHA).

A better solution to reduce the rod size is to use a helical structure. In this case, the current distribution along the antenna element is improved, being no longer triangular, but resembling more the current distribution of a $\lambda/4$ monopole. This results in higher radiation resistance and improved effective height. These antenna elements exhibit a resonant antenna impedance $\underline{Z}_A$, which can be such tailored to wander through more convenient regions of the Smith chart.

The active antenna design presented in this chapter is based on a novel capacitive coupled helical antenna (CCHA) only 14 cm long developed at the Institute of High Frequency Technology and Mobile Communication, University of the Bundeswehr Munich [45]. This antenna element consists of a copper helix with constant pitch, wound on a flexible dielectric tube. The lower end of the helix, insulated by a thin dielectric layer, is inserted in a cylindrical metal socket without having any galvanic contact with it. The helix structure and the socket are thus capacitively coupled. The antenna model used for the electromagnetic simulation and a realized lab sample are depicted in Fig. 6.1. A parallelepiped form instead of a cylindrical one is used for the FEKO[1] simulation in order to avoid numerical difficulties [46].

Because of the resonant character of the antenna structure, its antenna impedance is also resonant. The antenna element itself exhibits a series self-resonance f_S

[1]Commercial full-wave electromagnetic field simulator.

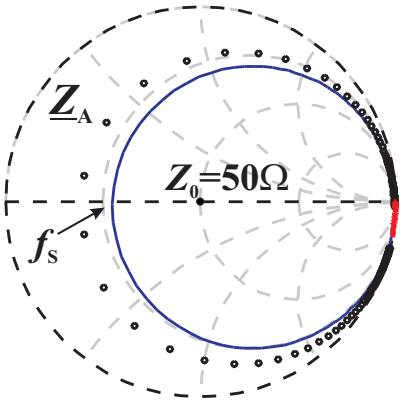

Fig. 6.2: Measured (–) and FEKO simulated (∘) CCHA (14 cm long) impedance $\underline{Z}_A$ in the FM range. Antenna impedance of a 20 cm simple monopole is plotted in red.

and a parallel one $f_{P,A}$. The series one is mainly determined by the combination of the helix inductance L_A and the capacitive coupling C_A, while the parallel one is mainly caused by L_A and the interwinding capacitance C_P.

The full-wave electromagnetic FEKO simulation offers good agreement with the measured antenna impedance (Fig. 6.2), although the simulated real part proves to be smaller than in reality [46]. For comparison, the antenna impedance of a 20 cm simple monopole is also shown in Fig. 6.2.

The series resonance frequency f_S was tailored for this application to be about 93.4 MHz, so inside the European FM band, while $\underline{Z}_A$ at resonance is about 19 Ω. The measured high quality factor of the antenna $Q \simeq 66$ proves to be troublesome, allowing for only about 1.4 MHz bandwidth around f_S, which is too narrow to cover the whole FM range in combination with state of the art antenna amplifiers.

The effective height h_{eff} of the CCHA is also frequency dependent, as the simulation in Fig. 6.3 shows. In comparison to a simple monopole antenna with the same length, the CCHA exhibits a larger h_{eff} for frequencies higher than about 78 MHz. The h_{eff} resonance occurs at the parallel self-resonant frequency of the antenna.

At low frequencies the CCHA element behaves like a simple monopole antenna, having a measured antenna capacitance C_A of about 2.7 pF.

Given the antenna impedance, it is in practice not possible to match it to the receiver for the entire operating range without significant losses. This issue can be overcome by employing the active antenna principle, as further discussed. In the following we investigate the requirements for the antenna amplifier.

6.1.1 Connecting the Helical Antenna to a 50 Ω Amplifier

Fig. 6.4 depicts a passive matching network connecting the CCHA to a 50 Ω amplifier. The network is designed to provide an output return loss $|\Gamma_{match,out}|$ lower than –10 dB with a ripple of only 2 dB in the whole Japanese and European bands,

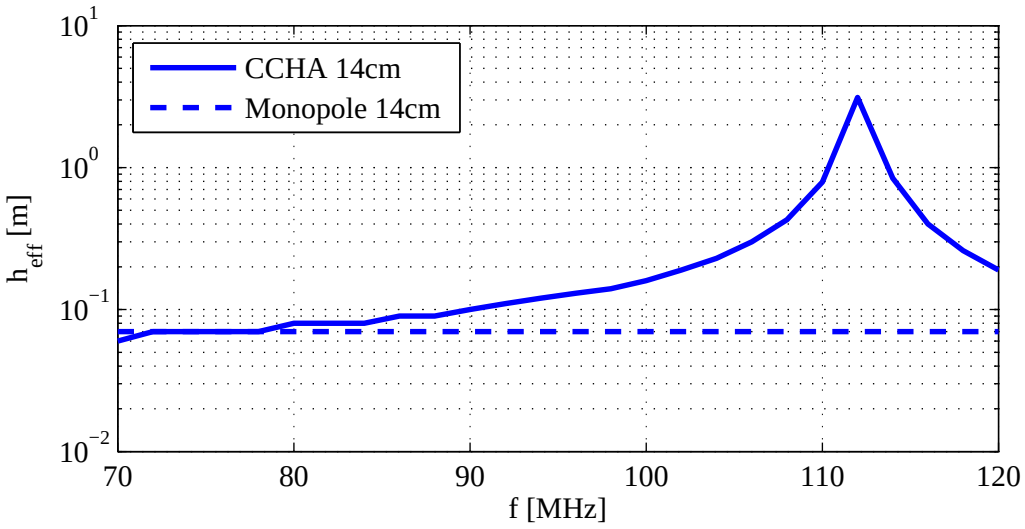

Fig. 6.3: Simulated effective height of the 14 cm long CCHA in comparison to the simple monopole antenna. Ideal ground plane considered.

as can be seen simulated in Fig. 6.5(a). The values shown in Fig. 6.4 resulted from numeric computations and are intended only for the theoretical analysis. The resonant circuits L_1–C_1 and L_2–C_2 have each the quality factor $Q_1 = Q_2 = 1.4$, while L_3–C_3 has $Q_3 = 39$. The transformer and the amplifier are considered ideal.

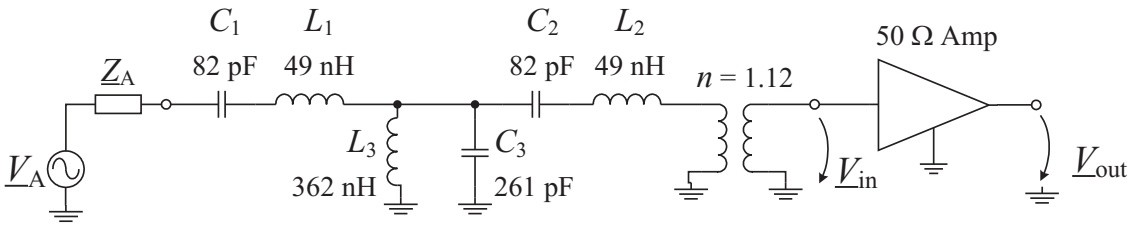

Fig. 6.4: CCHA antenna element matched to a 50 Ω amplifier. Resonant circuits quality factors: $Q_1 = Q_2 = 1.4$, $Q_3 = 39$.

Although a remarkably good matching can be achieved in theory, the noise figure of the passive matching network shown in Fig. 6.5(b) shows the price it has to be paid for it: $NF > 16.8$ dB for the entire operating band. This confirms the fact that the matching of the CCHA is associated with large losses, especially at the band edges where $\underline{Z}_\mathrm{A}$ is highly reactive.

Also the ratio between the voltage $\underline{V}_\mathrm{in}$ which arises at the input of the amplifier and the voltage $\underline{V}_\mathrm{A}$ induced in the antenna and solid plotted in Fig. 6.7 reveals the drawback of the approach: there is a significant voltage attenuation that occurs especially in the regions where the antenna behaves mainly capacitive or inductive, so that a severe degradation of the SNR is expected.

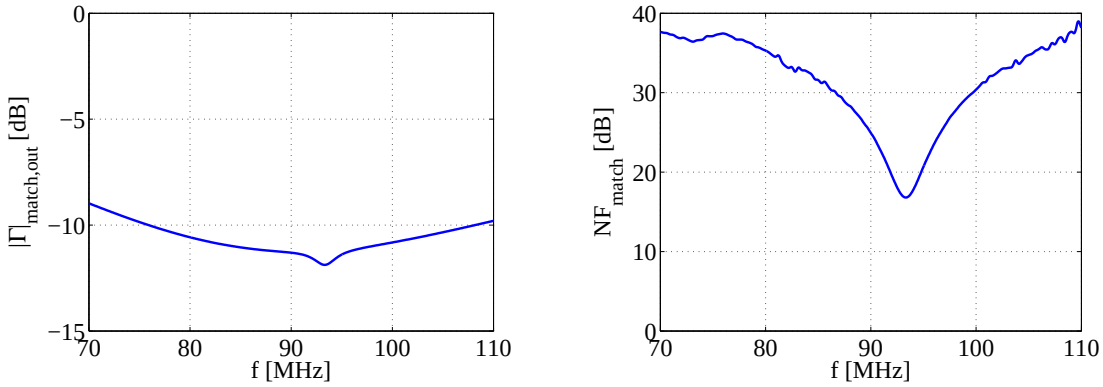

(a) Reflection coefficient at the output of the matching network.

(b) Noise figure of the matching network.

Fig. 6.5: Output reflection coefficient and noise figure of the passive matching network.

6.1.2 Connecting the Helical Antenna to a High-Impedance Amplifier

As the use of the new CCHA with a 50 Ω amplifier proves to be impractical, we investigate the possibility to use instead a high-impedance amplifier with mainly capacitive input impedance (Fig. 6.6) for covering the entire FM band from 76 MHz to 108 MHz. High-impedance amplifiers are well known for their usage in combination with small antenna elements where impedance matching is not recommended [38], and their advantages have already been discussed in Section 3.4.

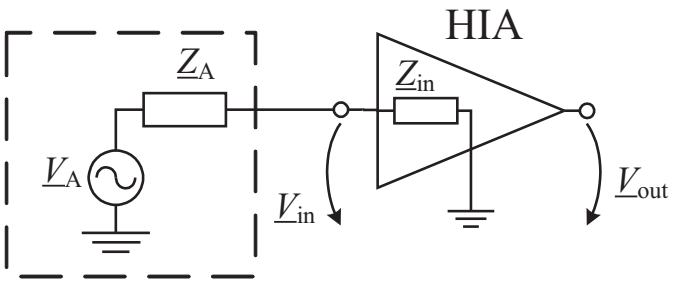

Fig. 6.6: HIA connected to the CCHA antenna element.

For frequencies much below f_S the antenna impedance is capacitive, so that in combination with the amplifier's input capacitance C_{in} a frequency-independent capacitive voltage divider arises. Above f_S the antenna impedance is inductive and a parallel resonance occurs in combination with C_{in}, which transforms the antenna open-loop voltage $\underline{V}_A$ and thus increases the amplifier's input voltage $\underline{V}_{in}$, resulting in a sharp voltage peak. This parallel resonance frequency will be denoted with f_P and occurs with the realized antenna element at about 106 MHz, which is inside the

European FM frequency band, if the HIA has $C_{\text{in}} \simeq 2\,\text{pF}$. The bandwidth around f_{P} is about 1.9 MHz. The transfer function between $\underline{V}_{\text{A}}$ and $\underline{V}_{\text{in}}$, dashed plotted in Fig. 6.7, has its peak value of about 18.7 dB, while the value at the lower edge of the FM band (76 MHz) is only about –11 dB, thus resulting in an overall ripple of about 30 dB.

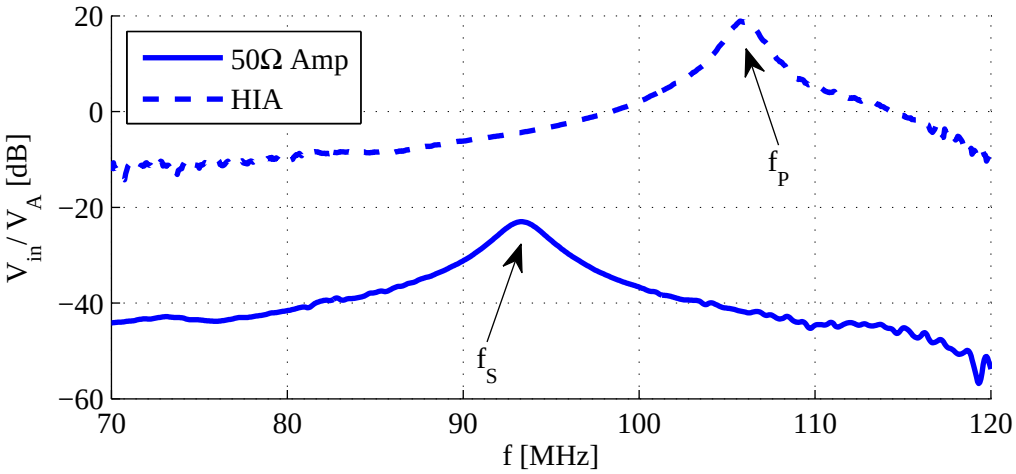

Fig. 6.7: Ratio between the amplifier input voltage $\underline{V}_{\text{in}}$ and CCHA antenna voltage $\underline{V}_{\text{A}}$ as a function of frequency, for a 50 Ω amplifier and a HIA.

Important comments have to be made about the noise behaviour. At f_{P} the real part of the impedance of the resonant circuit is very large and, consequently, the antenna noise voltage and the input signal $\underline{V}_{\text{in}}$ are also large. As a result, the input SNR of the HIA is almost frequency independent, but the amplifier's noise contribution degrades the output SNR in a frequency dependent fashion, since the noise figure of the HIA is a function of $\underline{Z}_{\text{A}}$.

These considerations lead to the necessity to investigate the possibilities to flatten the frequency response and the noise characteristic of an active CCHA, in order to fulfill the requirements imposed on automotive applications.

6.2 Amplifier for a Short Capacitive Coupled Helix Antenna

Besides the requirements detailed in Chapter 5 concerning the amplifier's input impedance, noise and linearity, the use of a CCHA assumes that the amplifier flattens the overall frequency response. The lower FM band has to be amplified, while the parallel resonance caused by the antenna has to be suppressed. For this, an amplifier configuration has to be chosen, which allows for selective voltage amplification. Nevertheless, this alone can be difficult to achieve, since components with high-quality

factors are required and the noise and linearity performance have to be maintained at a good level. Next a few amplifier topologies will be investigated and discussed.

6.2.1 Amplifier Employing a Transformer

The required gain can be obtained using common drain stages for good linearity and a transformer to boost-up the voltage level. Such a topology is shown in Fig. 6.8, where the two transistors are field-effect type, while the transformer is ideal and has a transforming ratio n. Impedances $\underline{Z}_\mathrm{P}$ and $\underline{Z}_\mathrm{S}$ are used to tailor the frequency selective characteristic of the amplifier.

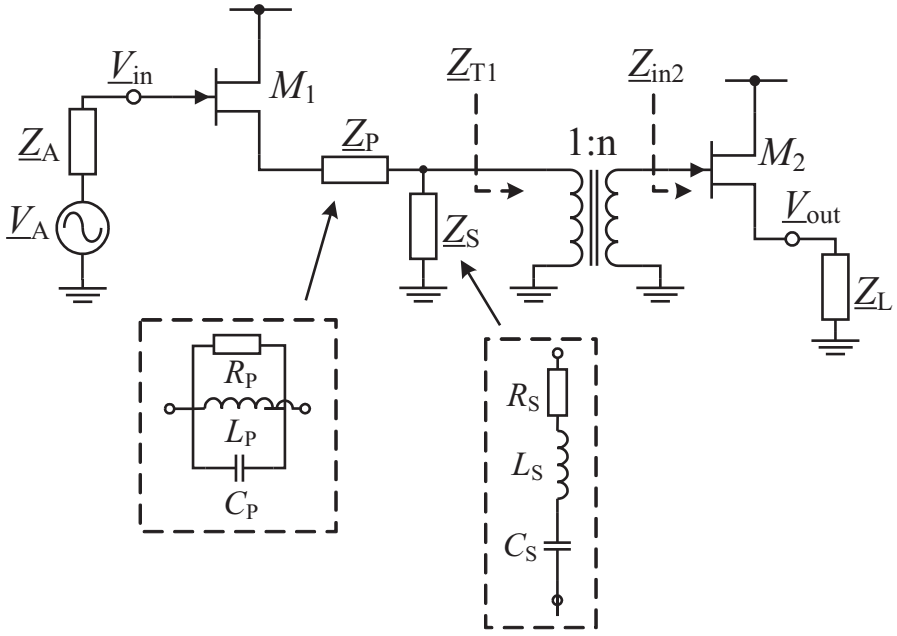

Fig. 6.8: AC schematic of an amplifier topology employing transformer.

Following the signal flow, the voltage gain $\underline{A}_\mathrm{V} = \underline{V}_\mathrm{out}/\underline{V}_\mathrm{in}$ can be computed as:

$$\underline{A}_\mathrm{V} = \frac{n \cdot \underline{A}_\mathrm{V2}\,(\underline{Z}_\mathrm{T1}||\underline{Z}_\mathrm{S})}{\underline{\alpha} + \frac{1}{g_\mathrm{m1}} + \frac{\underline{\alpha}}{g_\mathrm{m1}}\left(\frac{1}{r_\mathrm{o1}} + \frac{1}{\underline{Z}_\mathrm{gs1}}\right)} \tag{6.1}$$

where:

$$\underline{\alpha} = \underline{Z}_\mathrm{P} + \underline{Z}_\mathrm{T1}||\underline{Z}_\mathrm{S}$$

$$\underline{Z}_\mathrm{T1} = \frac{\underline{Z}_\mathrm{in2}}{n^2}$$

$$\underline{Z}_\mathrm{in2} = \left(\underline{Z}_\mathrm{gs2} + (r_\mathrm{o2}||\underline{Z}_\mathrm{L}) \cdot \left(1 + \underline{Z}_\mathrm{gs2} g_\mathrm{m2}\right)\right)||\underline{Z}_\mathrm{gd2}$$

$$\underline{A}_\mathrm{V2} = \frac{g_\mathrm{m2}}{g_\mathrm{m2} + \frac{1}{\underline{Z}_\mathrm{L}} + \frac{1}{\underline{Z}_\mathrm{gs2}} + \frac{1}{r_\mathrm{o2}}}$$

$\underline{Z}_{\mathrm{gd2}}$ is the gate-drain impedance of M_2, $\underline{Z}_{\mathrm{gs1}}$ and $\underline{Z}_{\mathrm{gs2}}$ are the gate-source impedances of M_1 and M_2 respectively, while r_{o1}, r_{o2} and g_{m1}, g_{m2} are their output resistance and transconductance, respectively, as the small-signal equivalent circuit in Fig. 6.9 shows. The transformer is considered ideal.

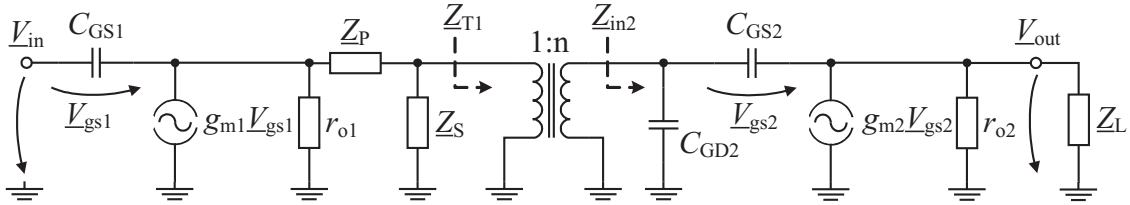

Fig. 6.9: AC small-signal equivalent circuit of the amplifier topology employing a transformer.

Now we have to define the goals for the total voltage gain $\underline{A}_{\mathrm{V,tot}} = \underline{V}_{\mathrm{out}}/\underline{V}_{\mathrm{A}}$ by observing the dashed curve in Fig. 6.7. We shall consider it satisfactory if $A_{\mathrm{V,tot}} \simeq 0\,\mathrm{dB}$ at 76 MHz and $A_{\mathrm{V,tot}} \simeq 10\,\mathrm{dB}$ at f_{P}, which means a ripple of 10 dB. In terms of A_{V}, this means 10 dB gain at 76 MHz and –10 dB gain at f_{P}.

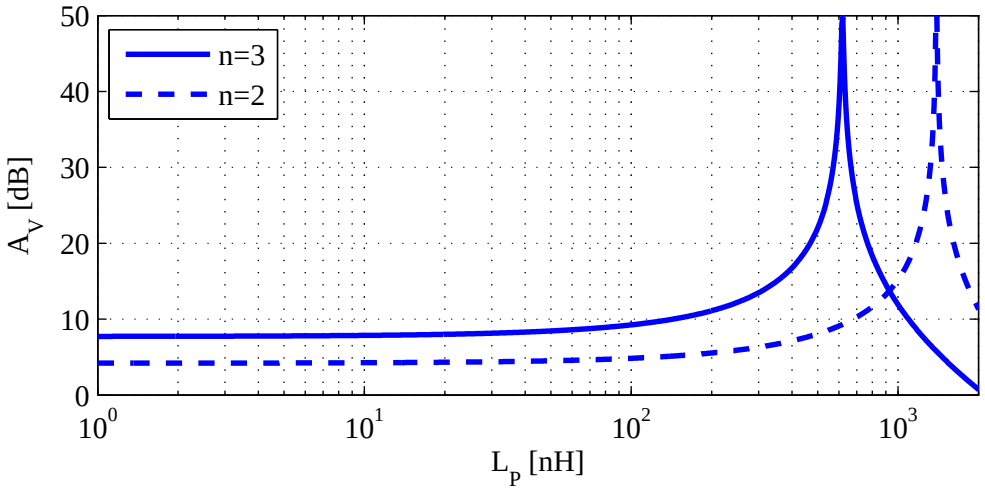

Fig. 6.10: Amplifier voltage gain vs. L_{P} at 76 MHz.

We start by removing $\underline{Z}_{\mathrm{S}}$ from the circuit, which leads to the necessity of $\underline{Z}_{\mathrm{P}}$ being a parallel resonant circuit consisting of L_{P}, C_{P} and R_{P}. At resonance $\underline{Z}_{\mathrm{P}}$ exhibits its maximum value, so A_{V} reaches its minimum. At the band edge $\underline{Z}_{\mathrm{P}}$ has to allow for voltage amplification.

At the lower band edge the parallel resonant circuit finds itself in the inductive region. Considering the resonance frequency fixed $f_0 = f_{\mathrm{P}}$ (by adjusting C_{P} permanently in order to keep the resonance frequency at f_{P}) and neglecting R_{P}, the

impedance $\underline{Z}_\mathrm{P}$ can be expressed as:

$$\underline{Z}_\mathrm{P} = j\frac{\omega L_\mathrm{P}}{1-\frac{\omega^2}{\omega_0^2}} \tag{6.2}$$

Using now eq. (6.1) we can plot the amplifier's voltage gain at 76 MHz, as shown in Fig. 6.10 for $n = 2$ and $n = 3$. Inductor L_P has been swept up to only about 2 µH, which is the value for which the resonance at f_0 requires $C_\mathrm{P} \simeq 1\,\mathrm{pF}$. Smaller capacitance values are considered too impractical to be used in the design. As Fig. 6.10 shows, when using a transformer with $n = 3$ there are 144 nH required for achieving $A_\mathrm{V} = 10\,\mathrm{dB}$, and 680 nH when employing the $n = 2$ transformer.

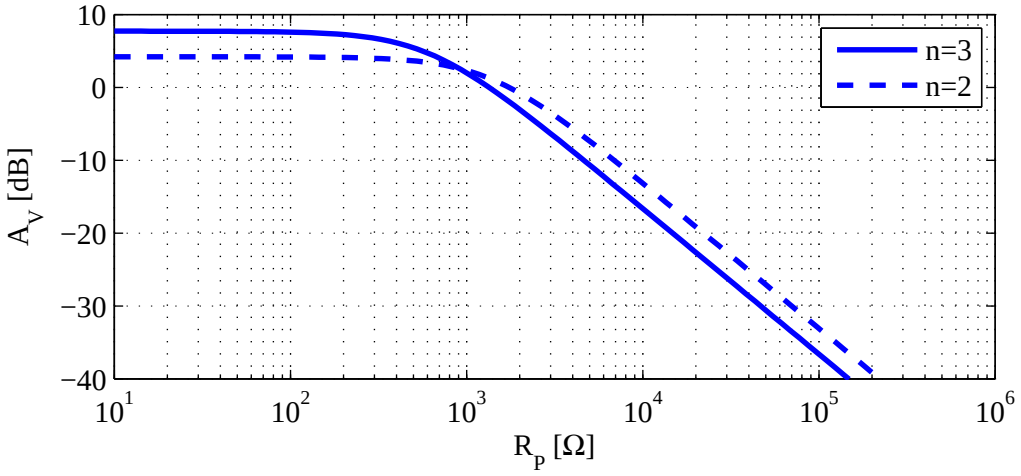

Fig. 6.11: Amplifier voltage gain at f_P vs. R_P.

Having now determined L_P and implicitly C_P, we can compute the required R_P in order to sufficiently attenuate f_P. Using eq. (6.1) we can now plot the amplifier's voltage gain at f_P for the case $\underline{Z}_\mathrm{P} = R_\mathrm{P}$, as shown in Fig. 6.11 for $n = 2$ and $n = 3$. We find that the circuit employing the $n = 3$ transformer requires $R_\mathrm{P} \simeq 4.75\,\mathrm{k\Omega}$ in order to reach $A_\mathrm{V} = -10\,\mathrm{dB}$, while the one using the $n = 2$ transformer requires $R_\mathrm{P} \simeq 6.8\,\mathrm{k\Omega}$.

These R_P values are large and show that the quality factor of the L_P inductor has to be high. For example, $L_\mathrm{P} = 144\,\mathrm{nH}$ and $R_\mathrm{P} = 4.75\,\mathrm{k\Omega}$ imply $Q_\mathrm{P} \simeq 50$. On the other hand, when employing the $n = 2$ transformer, for which $L_\mathrm{P} = 680\,\mathrm{nH}$ and $R_\mathrm{P} = 6.8\,\mathrm{k\Omega}$, only $Q_\mathrm{P} \simeq 15$ is required. Capacitor C_P has been considered ideal along this analysis.

The trouble is, in this approach a new resonance occurs at the input node of the transformer, between the capacitive part of the transformer input impedance $\underline{Z}_\mathrm{T1}$ and the inductive region of $\underline{Z}_\mathrm{P}$. This resonance falls inside the useful band, as the simulation in Fig. 6.12 illustrates. It can also be shown that the noise level is dramatically increased at this resonance. A way to avoid this is reducing the amount

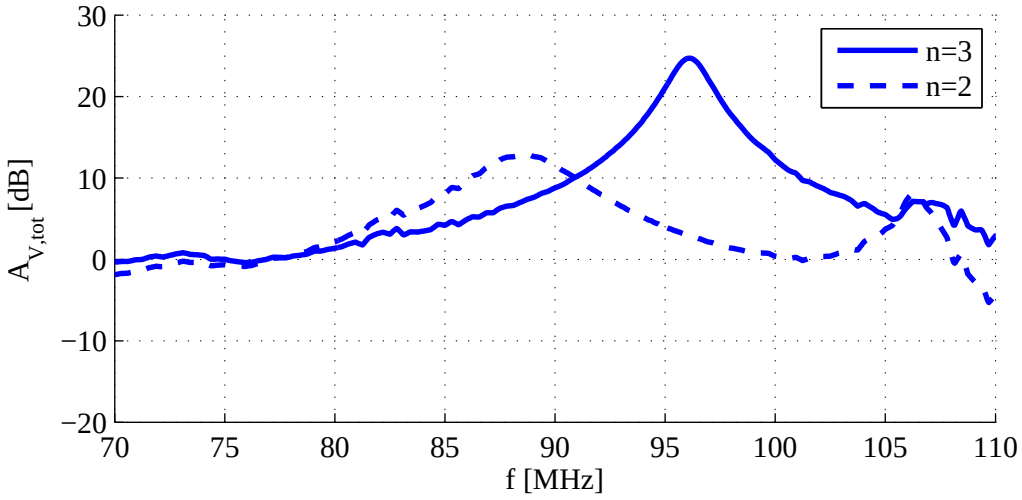

Fig. 6.12: Total voltage gain $A_{\mathrm{V,tot}} = |\underline{V}_{\mathrm{out}}/\underline{V}_{\mathrm{A}}|$ of the amplifier employing transformer.

of L_{P}, so that the resonance moves outside the FM band, although this reduces the amount of gain attainable at lower frequencies, as Fig. 6.10 shows. Assuming this trade-off can be accepted, the impact upon the quality factor Q_{P} is next investigated.

The parallel resistance R_{P} of the $\underline{Z}_{\mathrm{P}}$ resonant circuit is determined by the amount of attenuation the amplifier has to introduce at f_{P}, so it is independent of the values of L_{P} and C_{P}. As:

$$Q_{\mathrm{P}} = \frac{R_{\mathrm{P}}}{\omega_0 L_{\mathrm{P}}} \tag{6.3}$$

it becomes obvious that the smaller L_{P} gets, the larger Q_{P} has to become. This can be very difficult to achieve in practice. For example, we have previously calculated that we need a 144 nH inductor with a quality factor of 50. Commercial surface mounted device (SMD) 150 nH inductors (the closest standard value) have quality factors of about 40 or even 30 at 100 MHz [47], [48]. Achieving higher quality factors implies the use of air-coils, but these have the disadvantage of a smaller inductance. The inductance decrease is increasing the necessary quality factor, so overall there is no way out of this vicious circle. For example, a self-wound air-coil with 12 nH inductance has a quality factor of about 60. Nevertheless, in order to accomplish the requirements imposed by this application ($R_{\mathrm{P}} = 4.75\,\mathrm{k\Omega}$), a quality factor of about 594 is required. On the other hand, relaxing the quality factor results in an insufficient attenuation of the antenna resonance, which means a larger overall ripple.

There is also another reason why not to increase too much the quality factor of $\underline{Z}_{\mathrm{P}}$. If the resonance becomes too sharp, then it will no longer be able to compensate the broader antenna resonance.

This brief analysis points out the necessity to increase the complexity of the frequency-shaping network, in order to decrease the requirements imposed to the

individual components. The influence of $\underline{Z}_S$ implemented as a series resonant circuit is next taken into account.

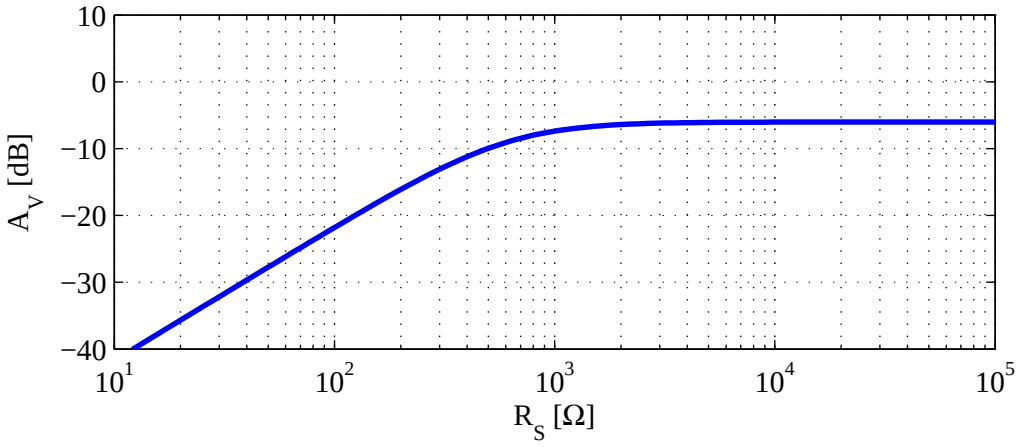

Fig. 6.13: Amplifier voltage gain vs. R_S at f_P for $n = 3$.

The first step is to reduce the quality factor of $\underline{Z}_P$ to a practical value of only 30, which results in $R_P \simeq 2.88\,\mathrm{k\Omega}$. From Fig. 6.11 we find that only 6 dB attenuation are now possible.

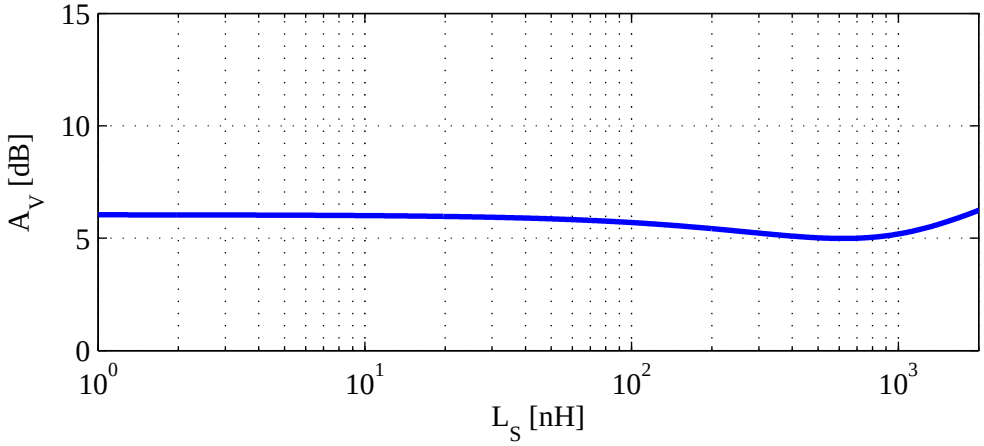

Fig. 6.14: Amplifier voltage gain vs. L_S at 76 MHz for $n = 3$.

Using now eq. (6.1) we can plot the amplifier's voltage gain at f_P, as shown in Fig. 6.13 for $n = 3$. As expected, large R_S values have no influence on the circuit, while small ones allow for a significant attenuation. For 10 dB additional attenuation $R_S = 498\,\Omega$ is required. Because R_S is so large, the quality factor of $\underline{Z}_S$ is now very small[2] and the values of L_S and C_S have only a negligible influence upon A_V, as

[2]Inductor L_S has been swept up to only about 2 µH, which is the value for which the resonance

the sweep of L_S performed at 76 MHz in Fig. 6.14 shows. As a consequence, in this approach we find $\underline{Z}_S = R_S$.

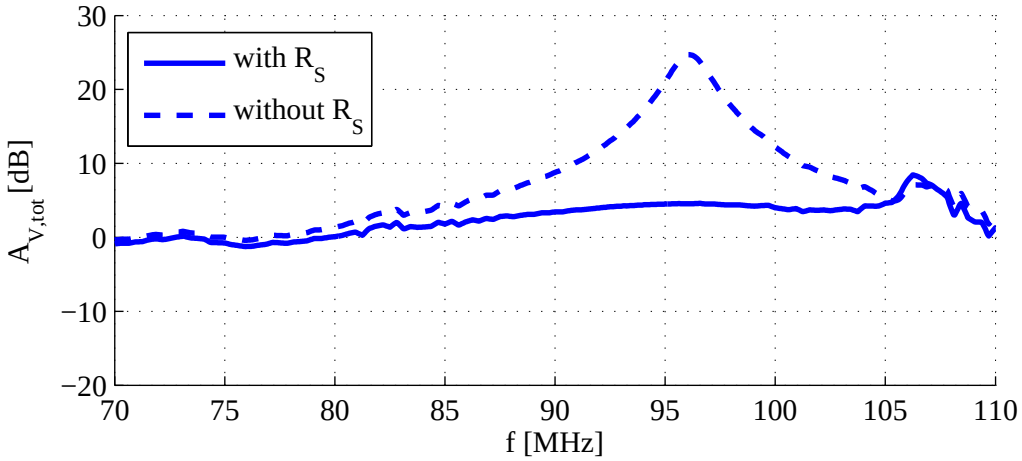

Fig. 6.15: Total voltage gain of the amplifier employing the $n = 3$ transformer, with and without $\underline{Z}_S$.

Additionally, the parallel connected resistor R_S significantly attenuates now the resonance occurring between $\underline{Z}_P$ and $\underline{Z}_{T1}$, as it can be seen in Fig. 6.15. The output noise level shown in Fig. 6.16 is also flattened, but its level is in average unacceptable high, being overall larger than 1 dBµV.

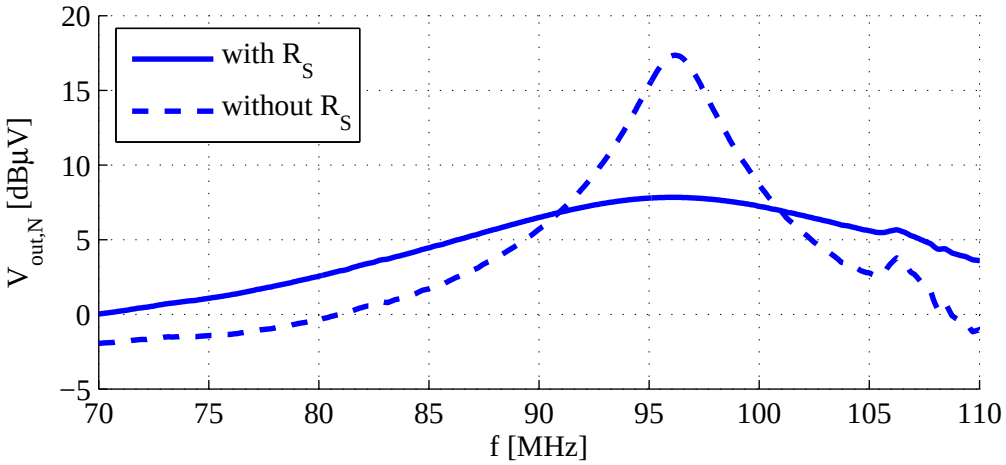

Fig. 6.16: Output noise voltage in 120 kHz bandwidth of the amplifier employing the $n = 3$ transformer, with and without $\underline{Z}_S$.

Although the total transfer function $|\underline{V}_{out}/\underline{V}_A|$ can be well equalized by this

at f_0 requires $C_S \simeq 1$ pF. Smaller capacitance values are considered too impractical to be used in the design.

circuit topology and a ripple of only about 5 dB is achieved, the very high output noise level makes this approach unusable for a FM active antenna application. The version employing the $n = 2$ transformer suffers from the same high output noise level.

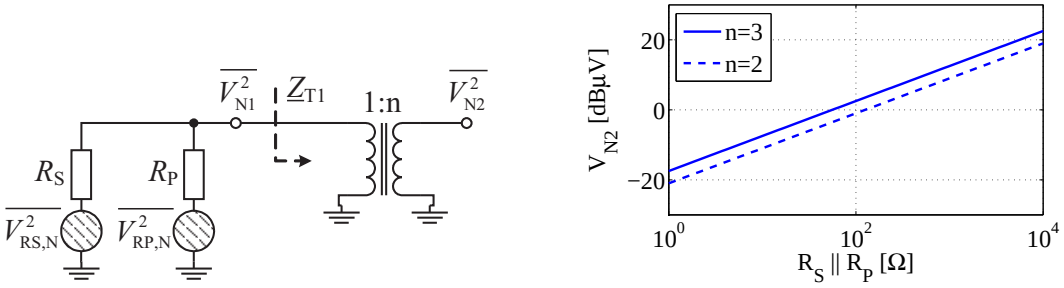

(a) Equivalent circuit for the noise analysis of the equalizing network at resonance.

(b) Noise voltage at the transformer's output.

Fig. 6.17: Noise analysis of the equalizing network at resonance.

In fact, the output noise voltage issue is the main drawback of this architecture. A brief analysis shows that the main noise source inside the amplifier is the equalizing network itself. As the output impedance of the first common-drain stage is low (Fig. 6.8), we can simplify the noise analysis of the equalizing network as shown in Fig. 6.17(a), whereas at resonance R_S and R_P appear in parallel. The input impedance in the second common-drain stage is high and although the transformer decreases its value by a factor n^2, the impedance $\underline{Z}_{T1}$ reflected to the primary is still high enough, so that it can be considered that the transformer picks-up the entire noise voltage generated by the resistors. As a consequence, as long as $R_S||R_P \ll Z_{T1}$, using eq. (3.16) we get:

$$V_{N1} = \sqrt{4kTB\,(R_S||R_P)} \tag{6.4}$$

The voltage is further boosted by the transformer, so that $V_{N2} = n \cdot V_{N1}$. The noise voltage at the transformer's output is shown in Fig. 6.17(b) for both transformation ratios, when the equivalent circuit depicted in Fig. 6.17(a) is used. Assuming that the second common-drain stage has a unity voltage gain and no noise contribution, $R_S||R_P$ has to be lower than 18 Ω for $n = 3$ and lower than 41 Ω for $n = 2$, in order to keep the output noise voltage lower than -5 dBμV. It is of course possible to use such small values for R_S in order to suppress the noise, but this would also supress the total active antenna gain.

In the case of the complete circuit, the transistors and the antenna element contribute additional noise. Comparing with the values of R_S and R_P needed for a flat decent gain, it is now obvious that this kind of amplifier topology is not suited for combination with a CCHA. The practical realization of such circuits has been analyzed and the experimental results have been discussed in [49].

Replacing the transformer with a gain stage like the degenerated common source as described in [49] does not solve the noise issue, since the output of the equalizing network is again picked-up by a high-impedance stage.

6.2.2 Architecture Common Drain – Common Base

As we have so far seen in this chapter, picking-up the signal from the equalizing network with a high-input impedance stage is leading to a few difficulties:

- When using $\underline{Z}_\mathrm{P}$ alone (Fig. 6.8) a high quality factor is required in order to make the voltage division between the network and the transformer's input effective. Nevertheless, high quality factors can be impractical and can result in a too narrowband compensation;
- A new resonance occurs between the equalizing network and the capacitive impedance seen toward the second stage;
- The transformer picks-up almost all the thermal noise generated in the equalizing network and then boosts-up its level.

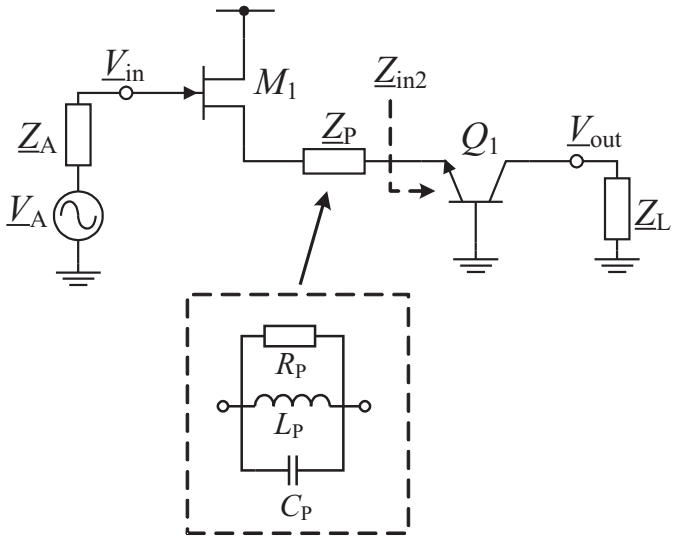

Fig. 6.18: AC schematic of the amplifier employing a common base stage.

These issues suggest the replacement of the transformer and the second common drain stage with a low-input impedance gain stage, like the common base. In this case only a parallel resonant circuit connected in series ($\underline{Z}_\mathrm{P}$ in Fig. 6.18) should be sufficient in order to flatten the frequency characteristic. The first highly-linear common drain stage ensures the high-impedance character of the amplifier, but the voltage gain is lower than 1. The common base stage takes over the output current

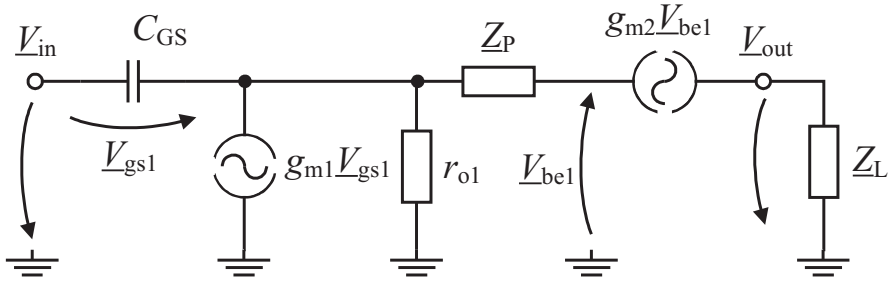

Fig. 6.19: AC small-signal equivalent circuit of the amplifier employing a common base stage.

of the first stage, due to its low input impedance. This stage is capable of high voltage gain, while maintaining low noise and good linearity.

The voltage gain $\underline{A}_{\text{V}} = \underline{V}_{\text{out}}/\underline{V}_{\text{in}}$ of the circuit in Fig. 6.18 can be approximated using the small-signal equivalent circuit given in Fig. 6.19:

$$\underline{A}_{\text{V}} = \frac{\underline{Z}_{\text{L}}}{\underline{Z}_{\text{P}}\left(1+\frac{1}{g_{\text{m1}}r_{\text{o1}}}\right)+\frac{1}{r_{\text{o1}}g_{\text{m1}}g_{\text{m2}}}+\frac{1}{g_{\text{m1}}}+\frac{1}{g_{\text{m2}}}+\frac{1}{\underline{Z}_{\text{gs}}g_{\text{m1}}g_{\text{m2}}}} \tag{6.5}$$

where r_{o1} is the output resistance of M_1, $\underline{Z}_{\text{gs}}$ its gate-source impedance, and g_{m1}, g_{m2} are the transconductances of M_1 and M_2, respectively. The output resistance r_{o2} and the base-emitter impedance $\underline{Z}_{\text{be}}$ of Q_1 have been neglected.

At the lower band edge the parallel resonant circuit finds itself in the inductive region. Considering the resonance frequency fixed $f_0 = f_{\text{P}}$ and neglecting R_{P}, the impedance $\underline{Z}_{\text{P}}$ is given by eq. (6.2). Using now eq. (6.5) we can plot the amplifier's voltage gain at 76 MHz, as shown in Fig. 6.20(a). The maximum amount of amplification, 17.7 dB, is achieved for $Z_{\text{P}} \to 0$, while 10 dB voltage gain are reached when $L_{\text{P}} = 13.7\,\text{nH}$. Having now determined L_{P} and implicitly C_{P}, we can compute the required R_{P} in order to sufficiently attenuate f_{P}. Using eq. (6.5) we can now plot the amplifier's voltage gain at f_{P} for the case $\underline{Z}_{\text{P}} = R_{\text{P}}$, as shown in Fig. 6.20(b), and we find that the circuit requires $R_{\text{P}} \simeq 260\,\Omega$ for $A_{\text{V}} = -15\,\text{dB}$. This corresponds to a quality factor of about 28, which is a reasonable value.

The total FM voltage gain $A_{\text{V,tot}}$ is depicted in Fig. 6.21 for the $\underline{Z}_{\text{P}}$ determined before[3]. This circuit architecture basically allows a well flattened frequency characteristic.

If we now assume that R_{P} is the only noise source in the circuit, use the same approximations as in eq. (6.5) and consider the output impedance of the first common-

[3]The unsmooth appearance of the curve has its origins in the measured antenna impedance $\underline{Z}_{\text{A}}$ embedded into the simulation: the impedance has been measured using a VNA and is therefore not accurate in the region corresponding to a magnitude of the reflection coefficient close to 1.

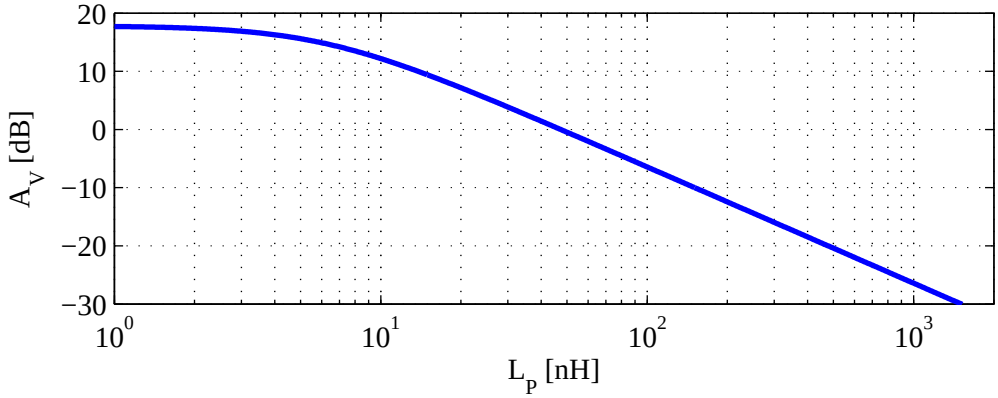

(a) Amplifier voltage gain vs. L_{P} at 76 MHz.

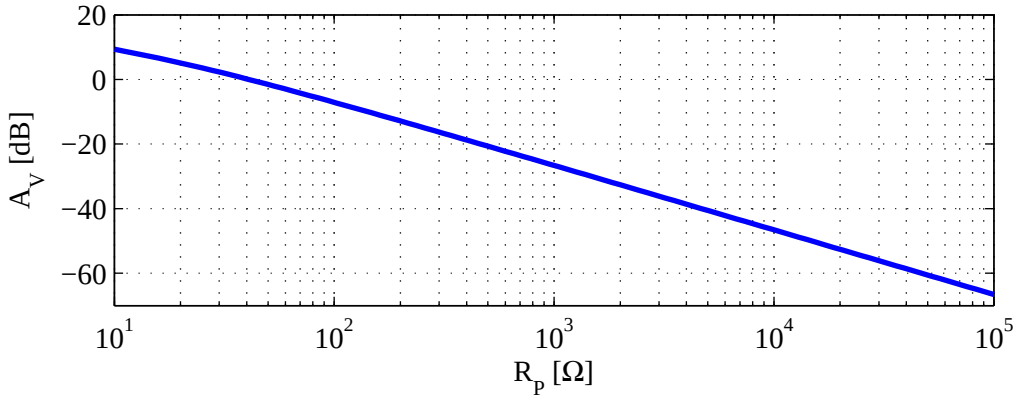

(b) Amplifier voltage gain vs. R_{P} at f_{P}.

Fig. 6.20: Amplifier voltage gain vs. L_{P} and R_{P}.

drain stage to be negligible, then the output noise voltage is:

$$V_{\mathrm{out,N}} = \sqrt{4kTBR_{\mathrm{P}}} \cdot \frac{g_{\mathrm{m2}} Z_{\mathrm{L}}}{g_{\mathrm{m2}} R_{\mathrm{P}} + 1} \tag{6.6}$$

and is plotted in Fig. 6.22. After a broad peak at small R_{P} values the output noise level gets smaller as R_{P} gets larger, which is the opposite trend when compared to the transformer circuit. This means that this topology is basically not endangered by the increase of the quality factor of the equalizing network, at least as far as the output noise voltage is concerned. For the R_{P} value previously derived we get $V_{\mathrm{out,N}} \simeq -17.3\,\mathrm{dB\mu V}$. To this is added the noise contribution of the transistors and antenna element, as we shall see later.

So far we have seen that this FM amplifier topology is theoretically able to achieve the design requirements of an active CCHA. We investigate further the practical considerations and the realization of the new active antenna.

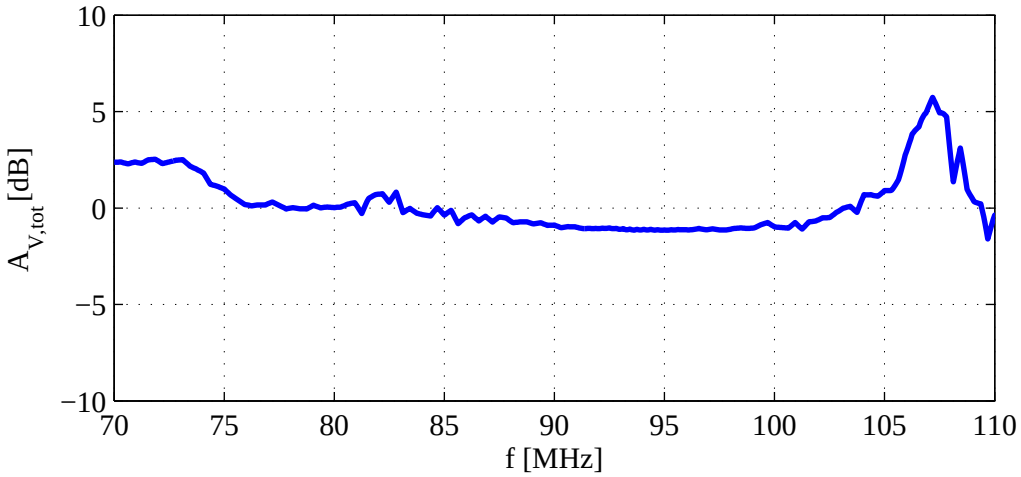

Fig. 6.21: Simulated total FM voltage gain of the CD-CB amplifier.

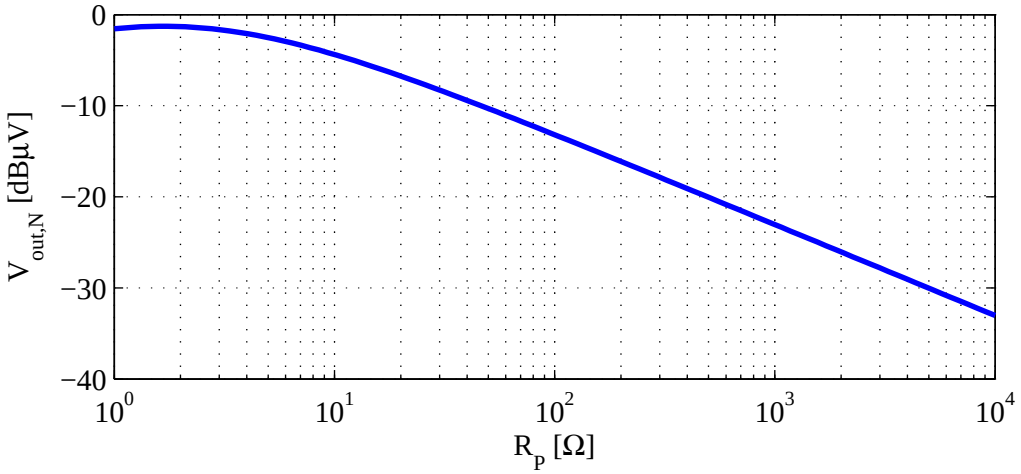

Fig. 6.22: Simulated output noise voltage for 120 kHz bandwidth if R_P is the only noise source in the circuit.

Fig. 6.23 shows the schematic of the proposed AM/FM amplifier. For reasons already explained in Chapter 5 concerning the FM-AM conversion and noise, the AM and FM signals are amplified separately by two specialized amplifiers. The antenna element is replaced by its equivalent circuit consisting of the voltage source $\underline{V}_\mathrm{A}$ and the antenna impedance $\underline{Z}_\mathrm{A}$. The capacitance C_par sums up the capacitive parasitic effects which occur on the input path of the amplifier, including ESD protection. This implementation makes use of the BAV99 switching diodes [50] for the ESD protection, which come in pairs in the same package. The capacitance thus added is lower than 1.5 pF.

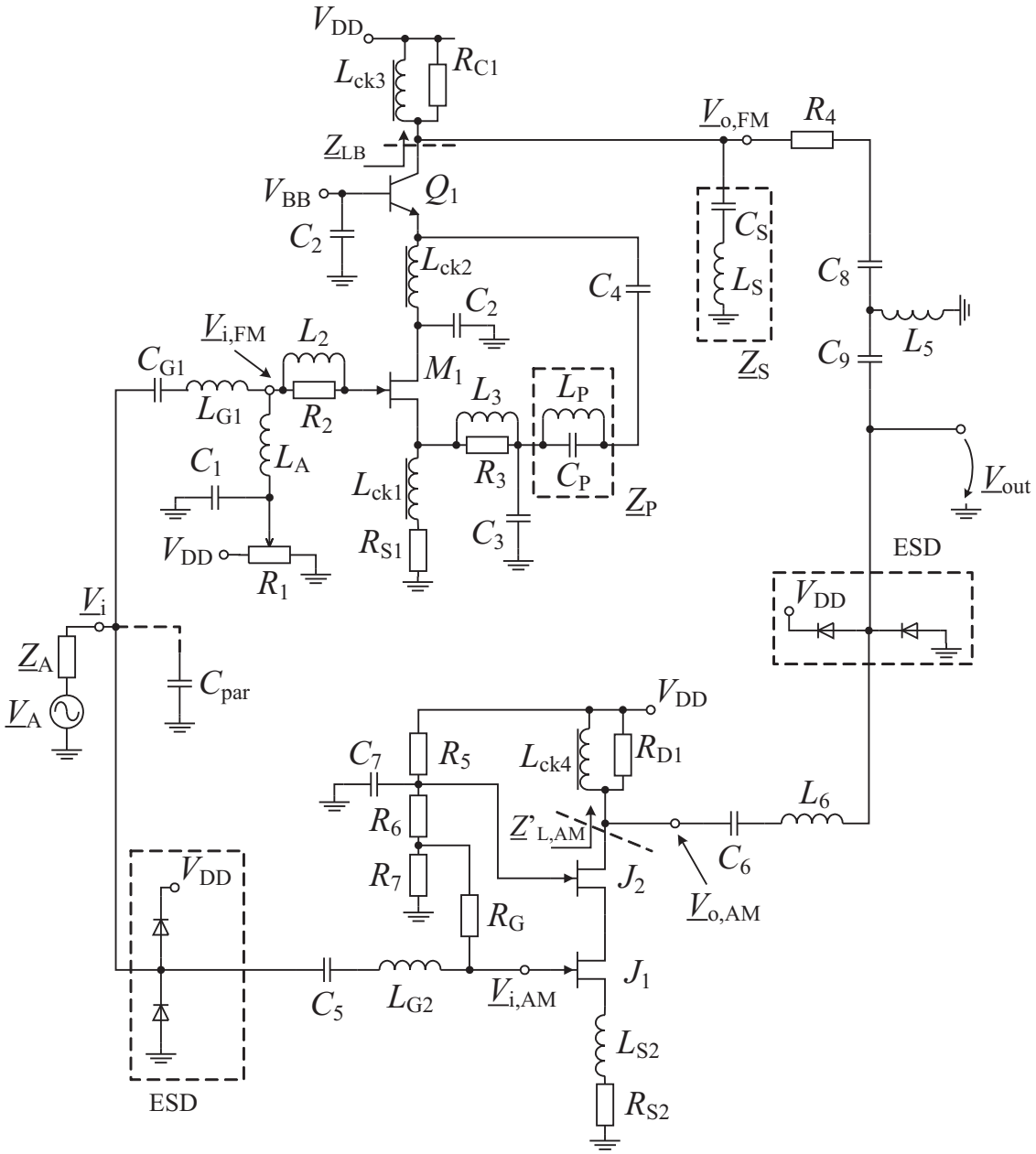

Fig. 6.23: Schematic of the two-path AM/FM amplifier for CCHA.

FM Amplifier

The FM path implements the architecture described in Fig. 6.18 and consists of a GaAs HEMT transistor M_1 (type NE3508 [41]) connected as source follower and a bipolar transistor Q_1 (type BFQ19 [51]) employed in common base. Due to their higher price, the number of GaAs devices to be used in the design is restricted, so a low-cost BFQ19 bipolar transistor is preferred in the second stage, where the

requirements are more relaxed.

In order to save DC current in the FM stage in Fig. 6.23, the drain current of M_1 is being reused for Q_1. Inductor L_{ck1} acts like a choke in FM range, while R_{S1} together with the gate biasing voltage set by potentiometer R_1 determine the drain current – and implicitly the bias current of both transistors. The start-up transient voltages are shown in Fig. 6.24. In this schematic, the bipolar transistor takes over the high voltage until the FET begins to conduct. The bipolar is not endangered, as it has higher breakdown voltages $V_{CE,max} = 15\,V$ [51].

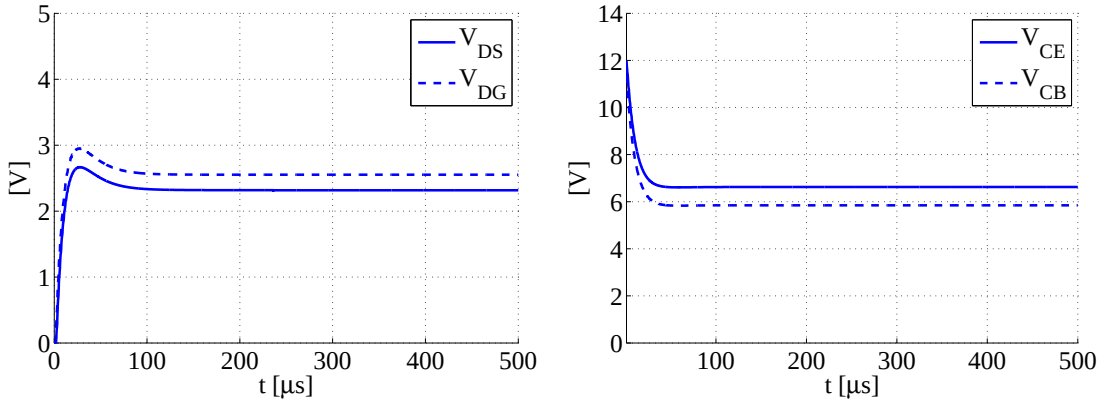

(a) NE3508. (b) BFQ19.

Fig. 6.24: Simulated start-up transient for both transistors in the FM amplifier.

The L_2–R_2 and L_3–R_3–C_3 groups ensure the stability of the common drain stage and are such dimensioned to have a minimal impact upon the working range.

L_{ck2} and L_{ck3} in the second FM stage act like choke inductors, while the base voltage V_{BB} is set by a potentiometer not shown in the figure. L_{ck2} and C_2 are separating the two stages in AC, providing a ground connection for the drain of M_1 and a choke for the emitter of Q_1. R_{C1} can be neglected in respect to the load. R_4 ensures the stability of the common base stage and has a minimal impact upon the working range.

The decoupling capacitors C_1, C_2 and C_4 can be considered short-circuits for the entire FM operating range. The role of L_A, L_P–C_P and L_S–C_S will be explained later.

There is not much room in choosing the voltage gain, because the load $\underline{Z}_{LB}$ is fixed and g_{mQ} depends on the collector current – which, in turn, is chosen for good linearity. The high-pass T-matching network C_8–L_5–C_9 has to cover both Japanese and European FM bands. Capacitors C_8 and C_9 have to be large enough for the lower Japanese band to be able to pass through, while they have to be small enough in order to block the AM signals.

Because of the L_3–R_3 stability network, $\underline{Z}_P$ in eq. (6.5) has now to be replaced with $L_3||R_3 + L_P||C_P$. Capacitor C_3 can be ignored for the hand-calculations. The

stability network changes quantitatively the conditions imposed to L_P and C_P. The maximum attainable voltage gain in the absence of the flattening network $\underline{Z}_{FNW} = 0$ and for $\underline{Z}_{LB} = 50\,\Omega$ is $\left|\underline{A}_{V,FM}\right| \simeq 2.7$. This suggests a decreasing of L_P for more gain at 76 MHz; nevertheless, inductors with small inductance values tend to have low quality factors of just 20 or even below ([47], [48]), which decrease the attenuation effectiveness at resonance. That is why $L_P = 12\,\text{nH}$ is kept and $Q \simeq 33$ is aimed, which represents a good trade-off between the gain at the lower band edge and the attenuation achievable at resonance. In practice C_P is trimmed in order to obtain the right resonance. The total voltage gain and the output noise level (for 120 kHz bandwidth) thus resulting are dashed plotted in Fig. 6.25. As it can be seen, $\underline{Z}_P$ strongly attenuates the sharp antenna resonance, which can still be seen falling inside the FM band. Overall a gain ripple of about 9 dB is reached. In order to compensate this peak, the quality factor of $\underline{Z}_P$ should ideally be about the same as that of the antenna's. Unfortunately, such high quality factors cannot be attained in practice with usual components; as a result, the resonance is not sufficiently attenuated.

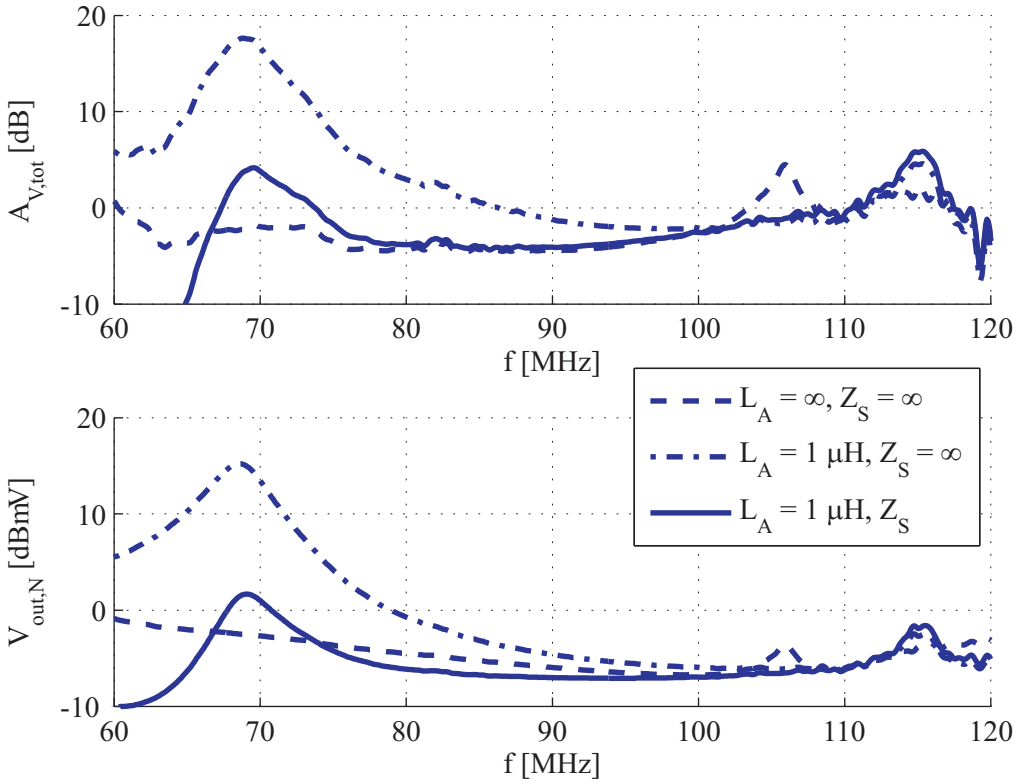

Fig. 6.25: Effect of the equalizing network, if the signal source has $\underline{Z}_A$ impedance. Top: simulated total FM voltage gain $A_{V,tot} = |\underline{V}_{out}/\underline{V}_A|$; Bottom: simulated FM output noise voltage for 120 kHz bandwidth.

In order to alleviate these shortcomings, an inductor L_A is connected in parallel with the amplifier's input. Its task is to push the parallel antenna resonance out of the FM band and obtain a flattened frequency response, as the dashed-dotted curve in Fig. 6.25 depicts. Also, a new resonance occurs below the FM range, at about 68 MHz. Now, as the sharp resonance lies outside the FM band at about 115 MHz, the requirements posed on the quality factor of the $\underline{Z}_P$ flattening network have been relaxed, but a small price still has to be paid, namely the necessity to attenuate the lower resonance as well. This is necessary because the output noise voltage $V_{out,N}$ rises fast toward the lower FM band edge, as the dashed-dotted noise curve in Fig. 6.25 shows. This is accomplished by inserting an additional network $\underline{Z}_S$ consisting of the series resonant circuit L_S–C_S connected in parallel with the amplifier's output. However, the new flattening network is much more practical than the one required in the absence of the transforming network. The resulting total FM voltage gain and the output noise level are solid plotted in Fig. 6.25. Noise levels below $-5\,\mathrm{dB\mu V}$ are expected for the entire FM range.

Additionally, similar to L_{G1} in Fig. 5.26, the transforming inductor L_A has the task of preventing the gate noise current source of M_1 from degrading the noise performance of the AM stage. This isolation between the two stages helps also avoid the undesired interferences between strong AM signals and the FM path.

AM Amplifier

Since in the AM range the CCHA behaves itself like a simple monopole antenna with capacitive impedance, the same AM amplifier as the one described in Section 5.4.2 is used for this active antenna too. Inductor L_{G1} has been introduced in addition to the schematic in Fig. 5.26 to tune out the capacitance $C_{G1} = 10\,\mathrm{pF}$ in the FM range.

In comparison to the case when the longer 20 cm monopole antenna is used, the employment of the CCHA for the AM band lowers overall the total gain for about 1 dB, while the output noise rises especially in the LW range for about 1 dB.

Combining the AM and FM Amplifiers

The interference issue between the AM and FM paths has been discussed in detail in Section 5.4.3. For the CCHA active antenna the AM-to-FM and FM-to-AM transfer functions are plotted in Fig. 6.26.

The transfer function between the antenna feed-point (V_i) and the input of the FM amplifier is solid plotted in Fig. 6.26(a), where one can see that for frequencies below 6 MHz the attenuation is at least 40 dB. The transfer function between the antenna feed-point and the input of the AM amplifier is dashed plotted in Fig. 6.26(a) and the attenuation is at least 14 dB for frequencies above 76 MHz.

The transfer function between the output of the AM amplifier and the output of the FM one is solid plotted in Fig. 6.26(b), where it can be seen that for frequencies

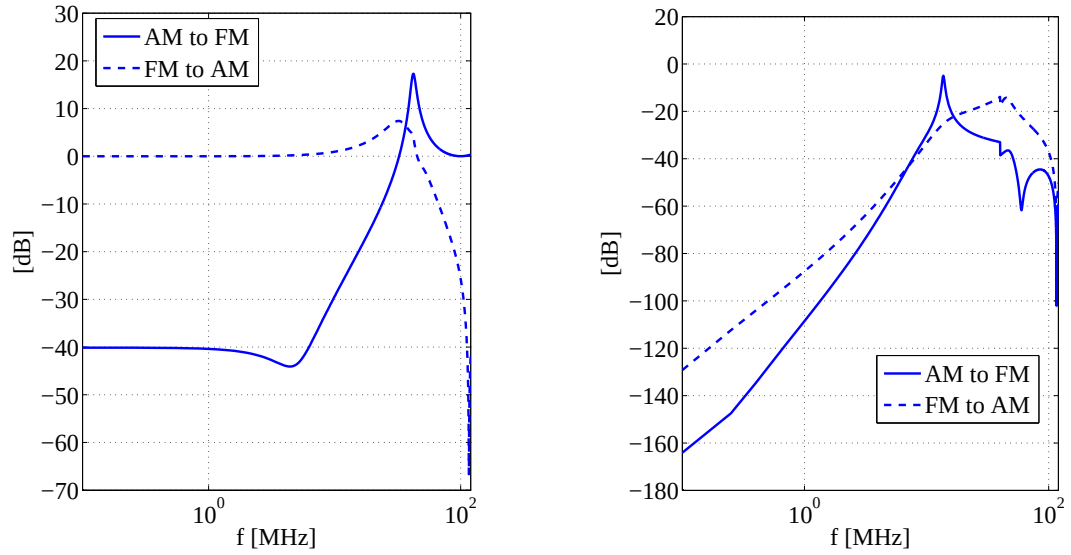

(a) Input. (b) Output.

Fig. 6.26: Simulated AM-to-FM and FM-to-AM transfer.

below 6 MHz the attenuation is at least 50 dB. The transfer function between the output of the FM amplifier and the output of the AM one is dashed plotted in Fig. 6.26(b), and the attenuation is at least 27 dB for frequencies above 76 MHz.

Linearity

The simulated 2nd and 3rd order linearity of the amplifier in AM and FM ranges is illustrated in Fig. 6.27. Table 6.1 highlights the intermodulation distances reached for 110 dBµV fundamental output signal level. Simulations indicate that this circuit architecture is not subject to undesired FM-AM conversion issues, while achieving a good 3rd order intermodulation distance.

Range	a_{k3} [dB]	a_{k2} [dB]
AM	84	55
FM	66	126

Table 6.1: Simulated intermodulation performance (110 dBµV output level).

6.2.3 Experimental Results

The realization of the proposed AM/FM active antenna is depicted in Fig. 6.28. The complete circuit is supplied at 12 V and the transistors are operated with a current

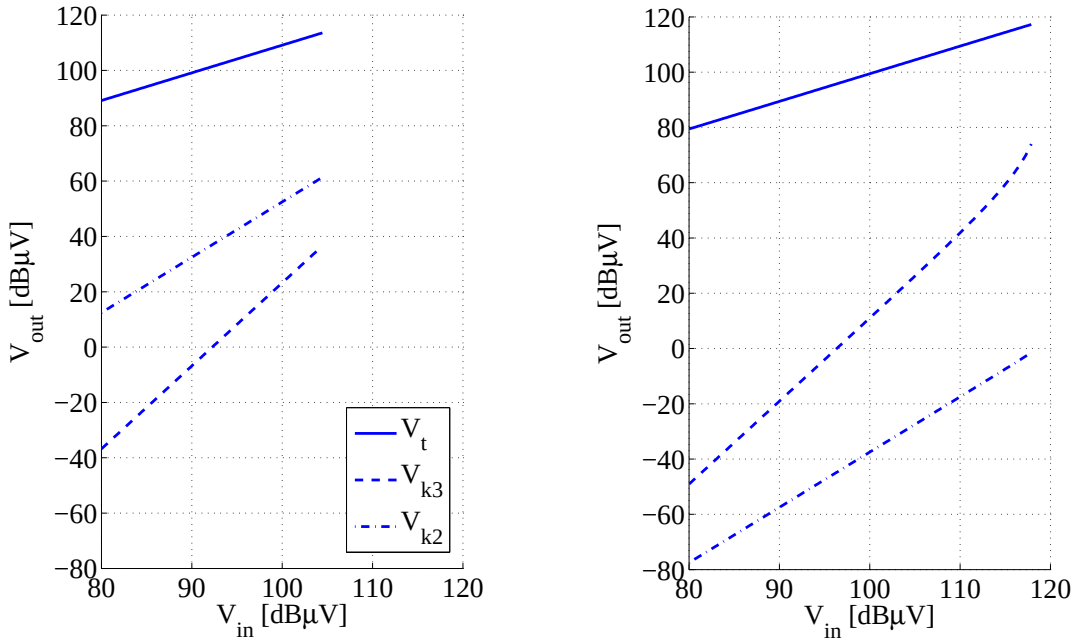

(a) AM. (b) FM.

Fig. 6.27: Simulated 2nd and 3rd order linearity.

of about 30 mA. The antenna element, bent at a usual angle $\alpha = 60°$, is mounted directly on the amplifier PCB, in order to avoid additional capacitive loading at the input node. The layout design was aimed to minimize any parasitic capacitance of the input node and to ensure in general the circuit's stability.

The antenna element is an industrial prototype with a structure similar to the lab version shown in Fig. 6.1(b).

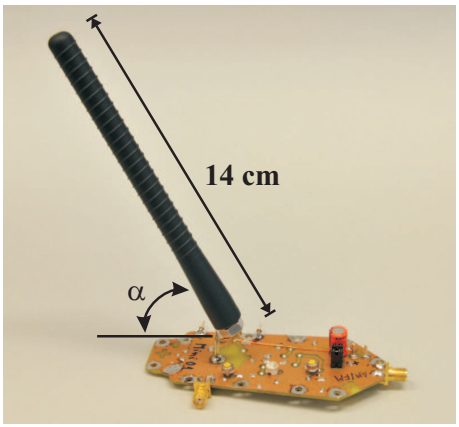

Fig. 6.28: Realized 14 cm long CCHA antenna mounted on the amplifier PCB.

Frequency Characteristic

The voltage gain of the amplifier $A_V = |\underline{V}_{out}/\underline{V}_i|$ measured alone in the lab is plotted in Fig. 6.29, together with the simulation result for comparison. The experimental results fit the simulations well.

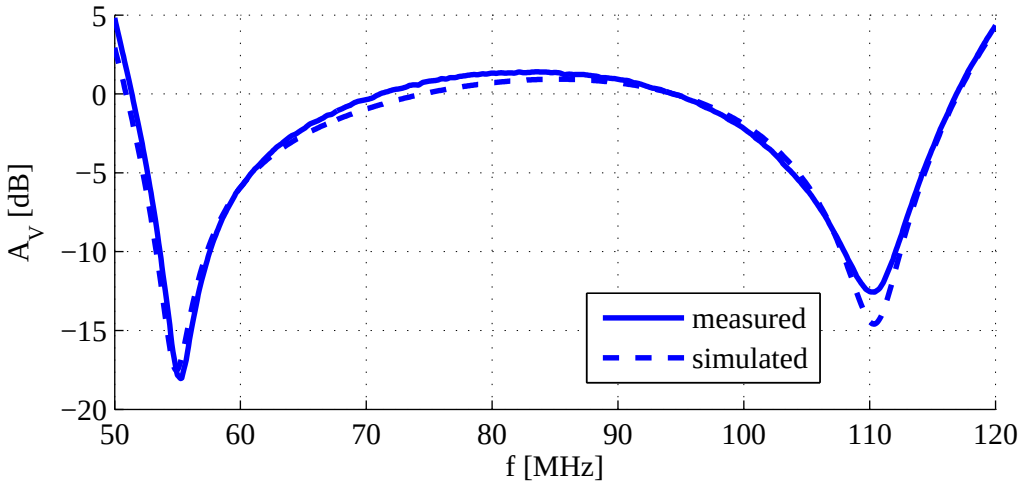

Fig. 6.29: FM Voltage gain of the amplifier alone $A_V = |\underline{V}_{out}/\underline{V}_i|$, measurement and simulation.

In order to evaluate the signal performance, field measurements are done with the active antenna mounted on top of a car, above the rear windshield. The car is placed on a turntable, as detailed by the measurement procedure described in Section 4.3.2. The results plotted in Fig. 6.30 show for both polarizations the ratio of the signal delivered by the new design to the signal delivered by the 90 cm passive reference antenna. Although its length is significantly shorter, for the horizontal polarization the active CCHA delivers in average the same signal as the reference.

Noise Performance

The measured FM output noise voltage $V_{out,N}$ is depicted in Fig. 6.31 and is determined in an anechoic chamber, with the 14 cm long CCHA connected to the amplifier. For the Japanese FM range, the output noise level is lower than $-5\,\mathrm{dB\mu V}$, while for the European range it is below $-6.5\,\mathrm{dB\mu V}$, thus achieving the VDA recommendations. The experimental values are found in good agreement with the simulations, as the comparison in Fig. 6.31 shows.

A comparison between the simulated and measured noise figure *NF* is shown in Fig. 6.32(b). The simulation was performed using the measured antenna impedance $\underline{Z}_A$ as the source impedance for the amplifier, while for the measurement the CCHA equivalent circuit was employed. The measurement poses some practical difficulties, caused by the losses in the equivalent antenna circuit and the low gain of the active

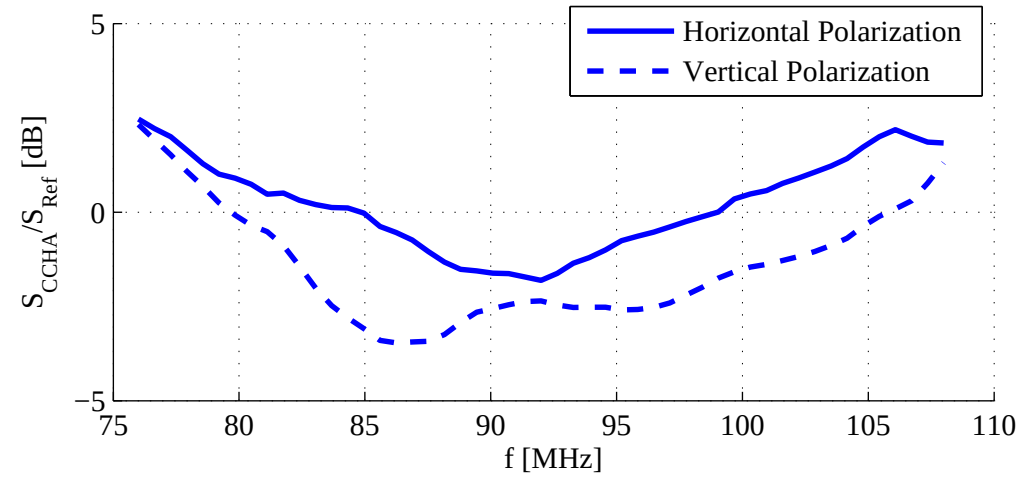

Fig. 6.30: Field measurement in the FM range showing the ratio between the signal delivered by the tested active antenna and the signal delivered by the reference antenna, when both are mounted on a car.

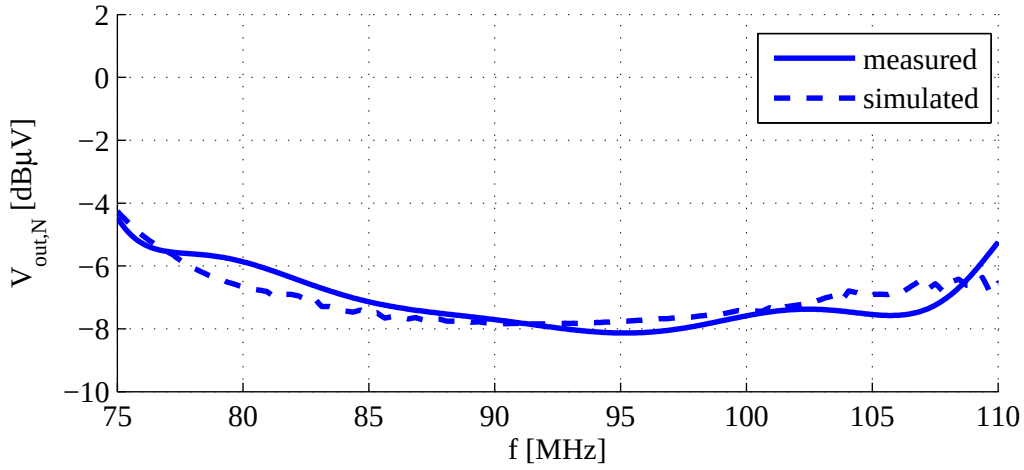

Fig. 6.31: Simulated and measured FM output noise voltage for 120 kHz bandwidth and $\underline{Z}_{\mathrm{A}}$ connected.

antenna. Because a low gain DUT affects the measurement accuracy when using the Y-factor Method [52], an additional low-noise amplifier (LNA) is inserted after the "active antenna" in order to boost the total gain, as shown in Fig. 6.32(a). Recalling that the noise figure of passive two-ports equals their insertion loss [32], so that $F_1 = 1/G_1$, and using eq. (3.23), we get:

$$F_2 = \frac{F}{F_1} - \frac{F_3 - 1}{F_1 \cdot G_{12}} \tag{6.7}$$

where G_{12} is the available power gain of the "active antenna". There are several

uncertainties affecting this measurement originating from the experimental setup, like for example the LNA noise factor F_3, which is a function of the antenna amplifier output impedance and is therefore difficult to estimate. To this add the uncertainties of the Y-factor method itself, so that the experimental curve shown in Fig. 6.32(b) is not considered very accurate; nevertheless, it gives an estimate of the *NF* and its tendency and is in reasonable agreement with the simulation.

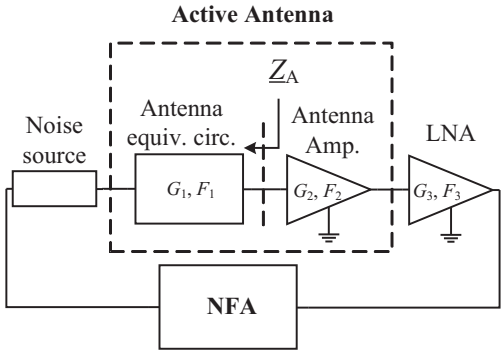

(a) Experimental setup for *NF* measurement.

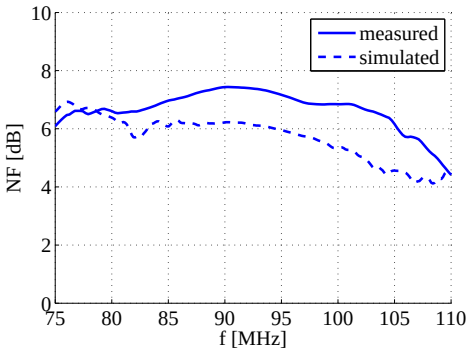

(b) Simulated and measured FM noise figure of the 14 cm active CCHA.

Fig. 6.32: Noise figure measurement of the 14 cm active CCHA.

The antenna impedance $\underline{Z}_A$, as Fig. 6.2 shows, wanders far from the optimum noise impedance required by the amplifier, so that the mismatch in eq. (3.22) is accordingly large, leading to the increased noise figure.

The sensitivity of the new active antenna is also measured in the anechoic chamber with the experimental setup explained in Section 4.3.4 and is referred to the sensitivity achievable under the same conditions with a passive 90 cm long rod antenna (reference antenna). The results depicted in Fig. 6.36 show that the sensitivity of the 14 cm active helix antenna is in average 5.5 dB for the Japanese FM range and 6 dB for the European FM range beneath the one of the reference rod. This sensitivity is significantly better than the one achievable with the 20 cm long active monopole.

Linearity

The linearity of the amplifier is measured in the lab and the frequency behaviour of the antenna impedance $\underline{Z}_A$ is accounted for by connecting an equivalent circuit at the amplifier's input. In this way, the overall frequency response of the measured circuit is flattened and very similar to the actual complete active antenna.

For the FM band, the two input tone frequencies are 96 and 98 MHz and the 3rd order intermodulation product is shown in Fig. 6.33. The intermodulation distance a_{k3} is evaluated to be 64 dB. The intermodulation distance of the 2nd order inter-

modulation product which falls into the AM band, causing the FM-AM conversion, is measured to be 84 dB.

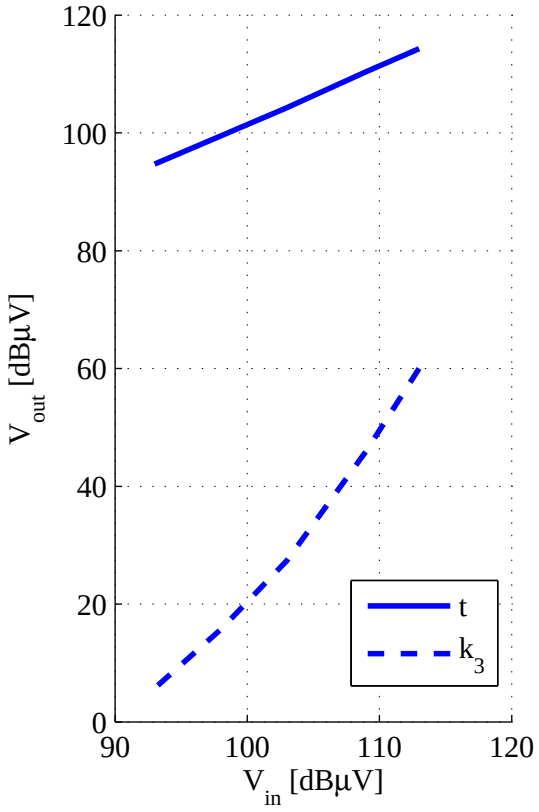

Fig. 6.33: Measured 3rd order intermodulation products in FM range.

6.2.4 Comparison between the Active Capacitive Coupled Helical Antenna and other Active Antennas

The performance of the 14 cm active CCHA will be next compared to the performance achievable with commercial active antennas, as well as with the 20 cm active monopole described in the previous chapter. The commercial antennas considered here are a 18 cm long active helix and a 40 cm long active monopole.

In Fig. 1.1 the visual impact of the new 14 cm short active antenna can be evaluated by direct comparison to a 40 cm long active monopole, which is a common antenna for low-end cars[4]. The achievable aesthetic advantage is obvious.

A comparison between the signal levels delivered by the tested antennas for horizontal polarization is shown in Fig. 6.34. For this measurement they were mounted

[4]Also passive 40 cm long monopoles are common for FM reception in low-end cars.

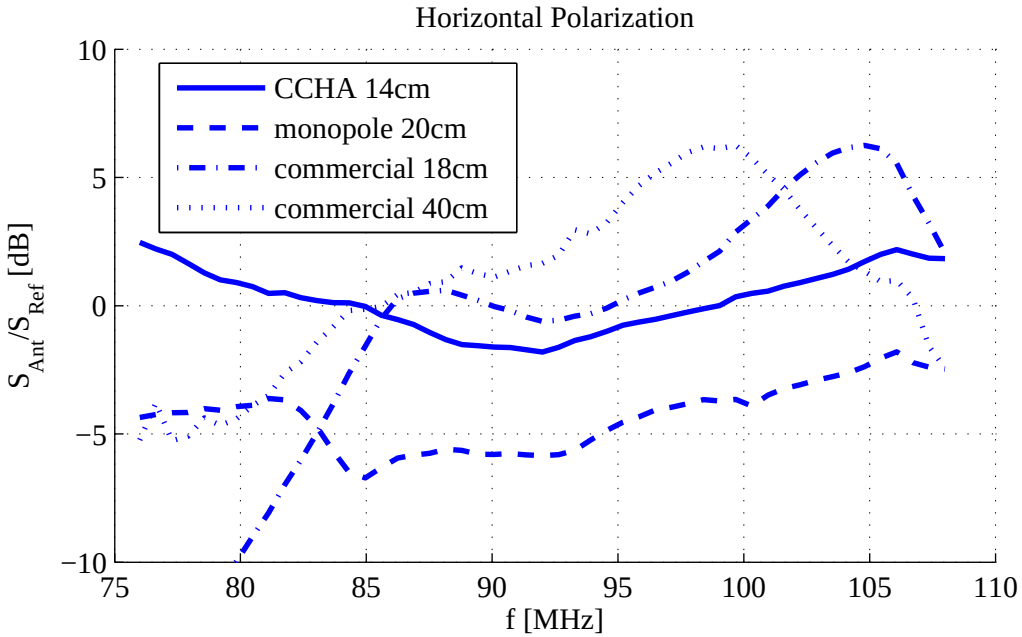

Fig. 6.34: Field measurement in the FM range showing the ratio between the signal delivered by the tested active antennas and the signal delivered by the reference antenna, when both are mounted on a car.

on a car, as described in Section 4.3.2. The active 14 cm CCHA delivers about 5 dB more signal than the active 20 cm monopole, although its length is significantly shorter. The 18 cm commercial active helix has a slightly better signal pick-up in the ECE range, but with an increased ripple and it is not intended to cover the Japanese band as well. The active 40 cm commercial monopole exhibits the best signal pick-up in the ECE range, especially due to its increased length, although with an increased ripple. It also enables a partial covering of the Japanese band.

Fig. 6.35 is showing a comparison between the output noise levels delivered by the tested active antennas. The lowest output noise voltage is achieved by the 40 cm commercial active monopole. In the ECE band the 14 cm CCHA exhibits similar results; nevertheless, the noise gets higher in the Japanese band, but remains overall in the "green" area. The 20 cm active monopole has a higher output noise level, while the one of the 18 cm commercial active helix fluctuates between large and small values.

The comparison of the measured sensitivity is performed in Fig. 6.36. Again, despite its length, the 20 cm active monopole is more than 5 dB less sensitive than the active 14 cm CCHA is. The sensitivity of the commercial 18 cm active helix is below the CCHA in the ECE range, while for the Japanese one it is not at all suited. Only the 40 cm commercial monopole has a small region in which it is more sensitive than the CCHA. The broadband character of the active CCHA is again to be noticed.

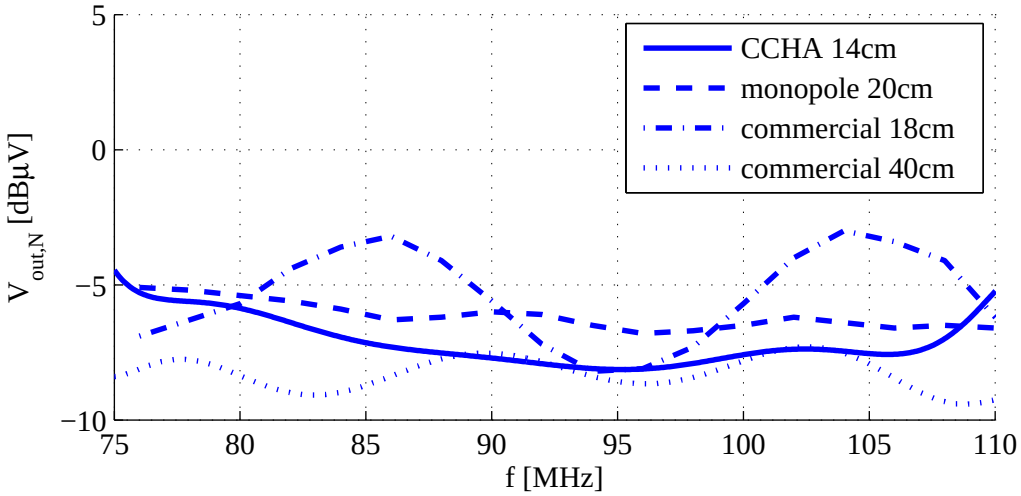

Fig. 6.35: Measured FM output noise voltage of different active antennas for 120 kHz bandwidth.

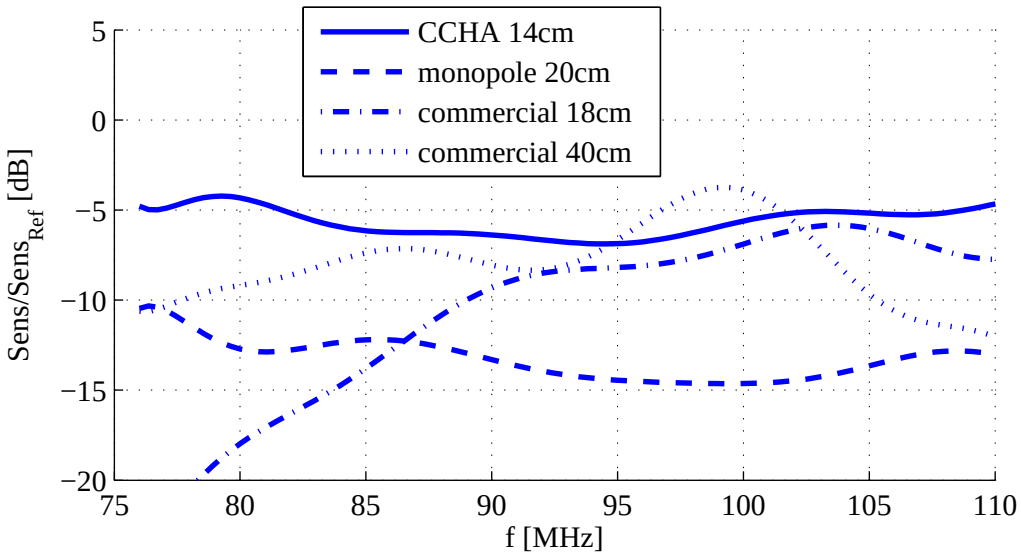

Fig. 6.36: Measured FM sensitivity of different active antennas. Results are referred to the 90 cm long passive reference rod antenna.

6.3 Summary

The possibilities to use a novel 14 cm long capacitive coupled helical antenna (CCHA) for AM and FM reception have been investigated in this chapter. Such a resonant antenna structure produces very sharp resonances and is therefore difficult to use in broadband applications. It has been shown that the required performance can be attained in combination with a high-impedance amplifier. Two HIA architectures have been investigated and discussed and it has been shown that a common-drain–common-base topology can flatten the antenna frequency characteristic, while being optimized for low noise and low distortion. As a result, the new active antenna can be used for automotive application in both AM and FM bands.

The active antenna has been investigated in the laboratory as well as in field tests, after being mounted onto a car. Despite its drastic length reduction, the novel ultra-short 14 cm helical active antenna is able to perform even better than a 20 cm long active monopole antenna. When compared to a common 90 cm long passive rod antenna, the ultra-short CCHA active antenna delivers in average about the same signal level, while maintaining a low output noise level. It also fulfills the linearity requirements and therefore does not require additional automatic gain control circuitry. Its measured sensitivity is for both AM and FM range below the sensitivity achievable with the 90 cm passive rod antenna, but comparable with the one achieved by 40 cm long active monopole antennas. To the best of our knowledge, this is the first time when such sensitivity is achieved with such a short antenna element.

Chapter 7

Short Helix Active Antennas for DAB

Regular DAB digital radio services are nowadays available in many countries all over the world and the coverage is expected to increase in the future [6]. Also, there is the prospect of DAB eventually replacing the currently used FM, in some countries this transition being already planned. Therefore, the need to receive in cars also DAB programs is entirely justified.

In order to keep the costs and the number of antennas mounted on the car low, an active antenna has to be developed that is capable of receiving all three services: AM, FM and DAB, whereby DAB is broadcasted in both VHF-Band-III and L-Band, as detailed in Section 2.1.3. This means that both the antenna element and the antenna amplifier have to be suited for the task.

This chapter explores the possibilities to extend the use of the capacitive coupled helical antenna (CCHA) element also for the Band-III and L-Band and to develop an appropriate amplifier architecture. As we shall further see, the latter goal does not prove to be trivial, because of nonlinear issues and filtering difficulties.

7.1 Short Capacitive Coupled Helix Antenna for DAB

The CCHA element described in Chapter 6.1 can be easily modified in order to be appropriate for DAB reception.

The DAB L-Band has the centre frequency at 1472 MHz and 40 MHz bandwidth (2.7% percent bandwidth), thus being a narrowband application. A $\lambda/4$ monopole antenna has in this case about 5 cm height, which means that the cylindrical metal socket in Fig. 7.1(a) can serve as the L-Band antenna element. The large inductance of the helix does not load the L-Band antenna and the measured antenna impedance $\underline{Z}_{\mathrm{A}}$ can be seen in Fig. 7.1(b), where the centre value is $(39 + j58)\,\Omega$.

(a) Realized element.

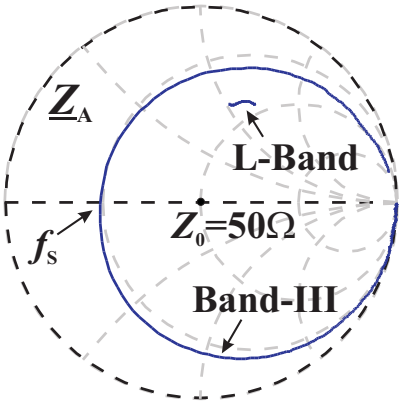

(b) Measured CCHA impedance $\underline{Z}_A$ in both Band-III and L-Band.

Fig. 7.1: Realized DAB-CCHA element and measured impedance.

The helix structure can be such tuned to obtain the series resonance f_S in the Band-III. The measured antenna impedance $\underline{Z}_A$ shown in Fig. 7.1(b) has $f_S \simeq 195\,\text{MHz}$, so inside the DAB band, while $\underline{Z}_A$ at resonance is about $16\,\Omega$. The measured high quality factor of the antenna $Q \simeq 44$ allows for only about 4.4 MHz bandwidth around f_S, which is too narrow to cover the whole Band-III.

In FM the CCHA element has now a capacitive behaviour, about 3.1 pF. The character of $\underline{Z}_A$ in both FM and Band-III ranges indicates that an antenna amplifier with high input impedance has to be used. In doing so, the antenna element poses in FM the difficulties highlighted in Chapter 5 and in Band-III those discussed in Chapter 6. For the L-Band there is no need for a high-input impedance amplifier, because the antenna impedance has a "reasonable" value. In AM the antenna element behaves like a simple monopole with the antenna capacitance of about 2.3 pF.

Connecting the HIA to the DAB CCHA element, as shown in Fig. 6.6, we obtain the parallel resonance f_p depicted in Fig. 7.2 at about 229 MHz, so inside the operating band. This means that the frequency characteristic has to be flattened in the Band-III, while for the FM band a simple broadband HIA is enough.

7.2 Single-Transistor FM/DAB Antenna Amplifier

Fig. 7.3 depicts a single transistor, ultra-compact amplifier for the FM/DAB bands, this approach having the advantage of the low part-count. One more amplifier path has to be added for AM, as the one described in the previous chapters. The antenna

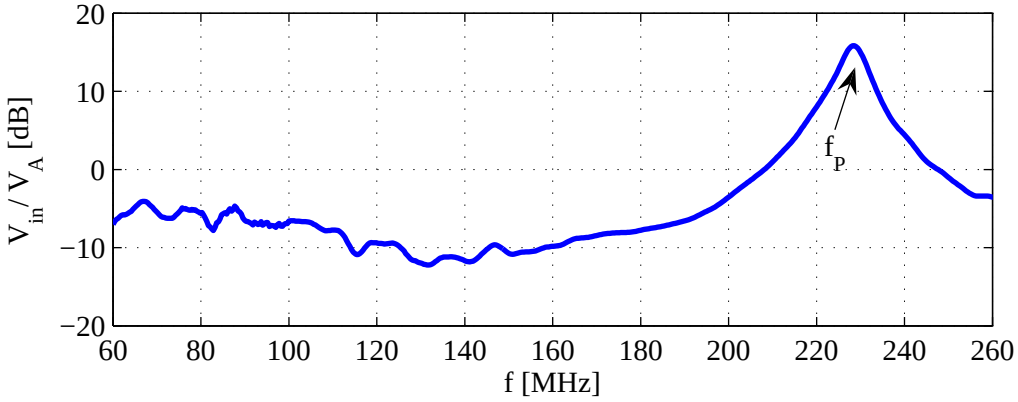

Fig. 7.2: Ratio between the amplifier input voltage $\underline{V}_{\text{in}}$ and CCHA antenna voltage $\underline{V}_{\text{A}}$ as a function of frequency.

element is replaced by its equivalent circuit consisting of the voltage source $\underline{V}_{\text{A}}$ and the antenna impedance $\underline{Z}_{\text{A}}$. The capacitance C_{par} sums up the capacitive parasitic effects which occur on the input path of the amplifier, including ESD protection.

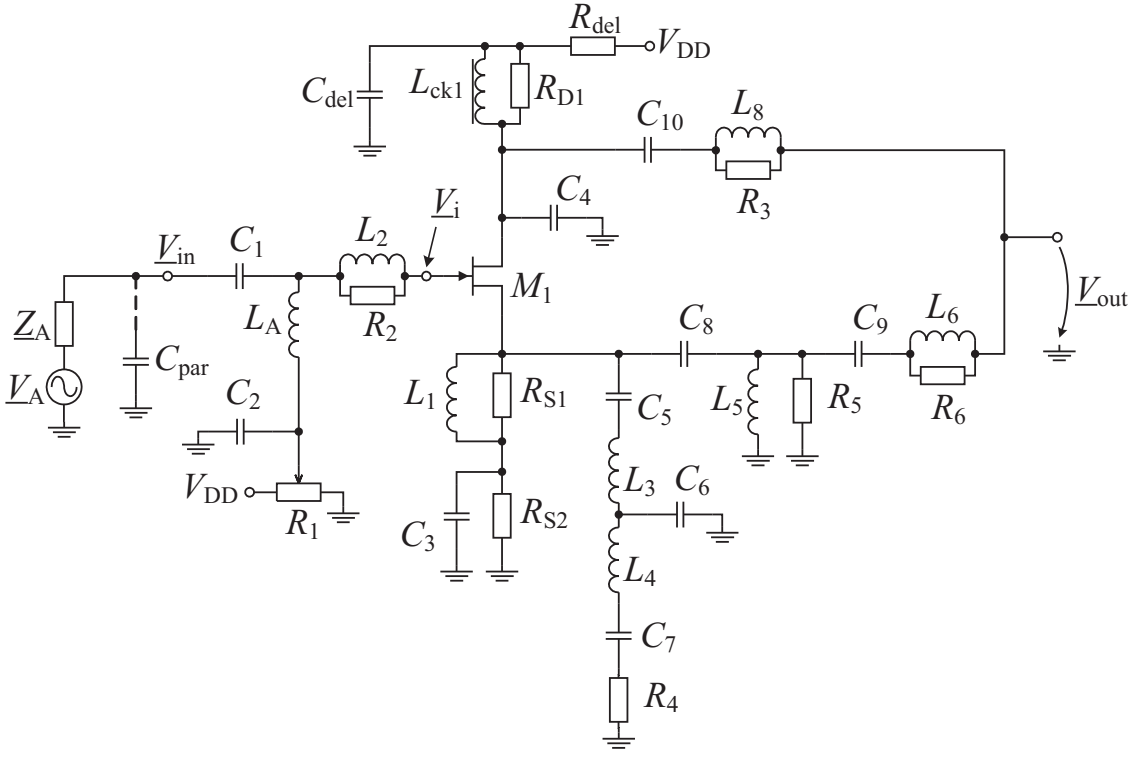

Fig. 7.3: Schematic of the single-transistor FM/DAB amplifier.

The signals in different bands follow different paths in the circuit in Fig. 7.3. The circuit can be seen as a common source configuration with degeneration for the FM

and Band-III, while in L-Band it acts like a source follower with resonant output transformation.

The amplifier is built around a GaAs HEMT transistor M_1 (type NE3508 [41]). Inductor L_{ck1} acts like a choke in the entire operating range, while R_{S2} together with the gate biasing voltage set by potentiometer R_1 determine the drain current. The L_2–R_2 and L_8–R_3 groups ensure the stability of the stage and are such dimensioned to have a minimal impact upon the working range. L_8–R_3 also blocks the L-Band signal from entering the FM/Band-III path. The decoupling capacitors C_2, C_3 and C_{10} can be considered short-circuits for the entire operating range. R_{del}, C_{del}, R_1 and C_2 have to address the start-up transient issue in a similar manner to the one described in Chapter 5.

7.2.1 FM Amplifier Path

The FM part of the amplifier is shown in Fig. 7.4. It is, basically, a common source stage with degeneration, very similar to the one used in Section 5.4.1. Capacitor C_3 short-circuits R_{S2} in AC, so that the degeneration is formed by the L_1–R_{S1} group and has an inductive character. The impedance is thus frequency dependent, but it features less noise than a broadband resistive degeneration does.

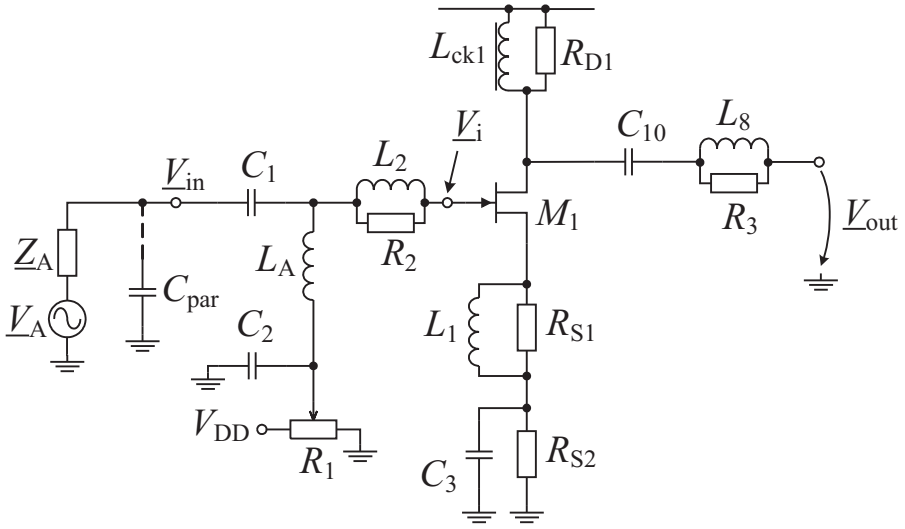

Fig. 7.4: Schematic of the FM path in the FM/DAB amplifier.

The components are such dimensioned in order to obtain about 6 dB voltage gain $A_{V,T}$ at 100 MHz. The Band-III and L-band paths connected at the transistor's source and omitted in Fig. 7.4 have little impact upon the FM range. The simulated voltage gain $A_{V,T}$, total voltage gain $A_{V,tot} = |\underline{V}_{out}/\underline{V}_A|$ and the output noise voltage $V_{out,N}$ are shown in Fig. 7.5. The output noise voltage is increasing at lower frequencies, as the voltage gain also increases.

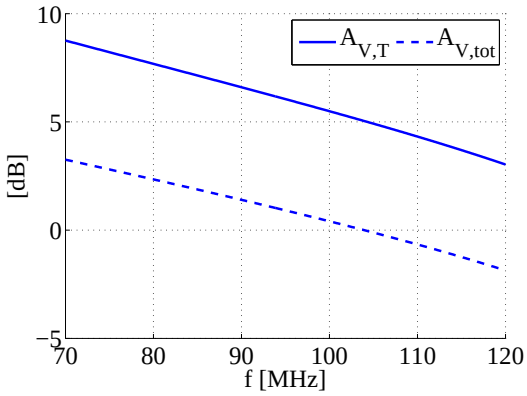

(a) Simulated FM voltage gain.

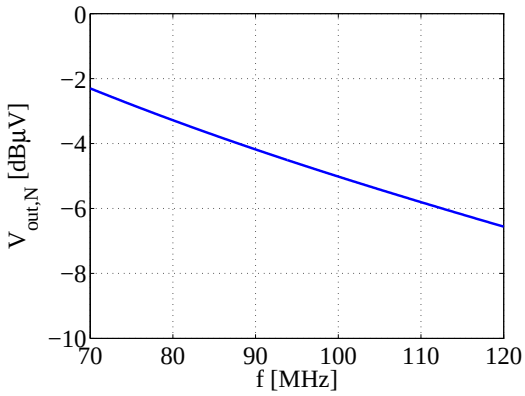

(b) Simulated FM output noise voltage for 120 kHz bandwidth, with $\underline{Z}_\mathrm{A}$ connected at the amplifier's input.

Fig. 7.5: Simulated FM gain and output noise voltage.

7.2.2 Band-III Amplifier Path

The Band-III part of the amplifier is shown in Fig. 7.6, which is also a common source stage with degeneration. To the FM degeneration previously described is now added a frequency selective network C_5–L_3–C_6–L_4–C_7–R_4, with the purpose of flattening the DAB resonance. This network consists actually from two coupled resonant circuits, and its impedance has to exhibit the maximum at the frequency where the antenna parallel resonance occurs.

The frequency dependent degeneration alters the input impedance of the stage, so that the frequency where the antenna resonance occurs varies too.

Let us first evaluate the case in which the transistor would be employed in a common source configuration, thus yielding the maximum voltage gain. The load it sees is about $|\underline{Z}'_\mathrm{L}| \simeq 60\,\Omega$ when a $50\,\Omega$ impedance loads the output, so that using values from Table 5.1 we get $|\underline{A}_\mathrm{V}| \simeq 7 = 16.9\,\mathrm{dB}$. Together with the antenna element, because of its resonance, the transfer function has now a ripple of about 20 dB. The amplifier should now compensate for at least 10 dB at the resonance. Calculating the required degeneration by solving eq. (5.2) for $|\underline{A}_\mathrm{V,csd}| = 2.2$ one gets $|\underline{Z}_\mathrm{S}| = 17.5\,\Omega$.

The use of a simple parallel resonant circuit as selective degeneration is not practical, because it poses difficulties in accommodating the FM degeneration. This is because the value required in FM is too large for the parallel resonant circuit that should be employed in Band-III, and a different approach is being used.

The input impedance of the two capacitive coupled series resonant circuits C_5–L_3–C_6–L_4–C_7–R_4 is plotted in red ($\diamond$) in Fig. 7.7. The presence of the FM degeneration (L_1–R_S1) shifts the impedance loop, as shown by the blue curve ($\triangle$) in Fig. 7.7. This has the disadvantage of increasing the degeneration impedance at the lower end of the frequency range; at the same time, however, it decreases the "peak" – an

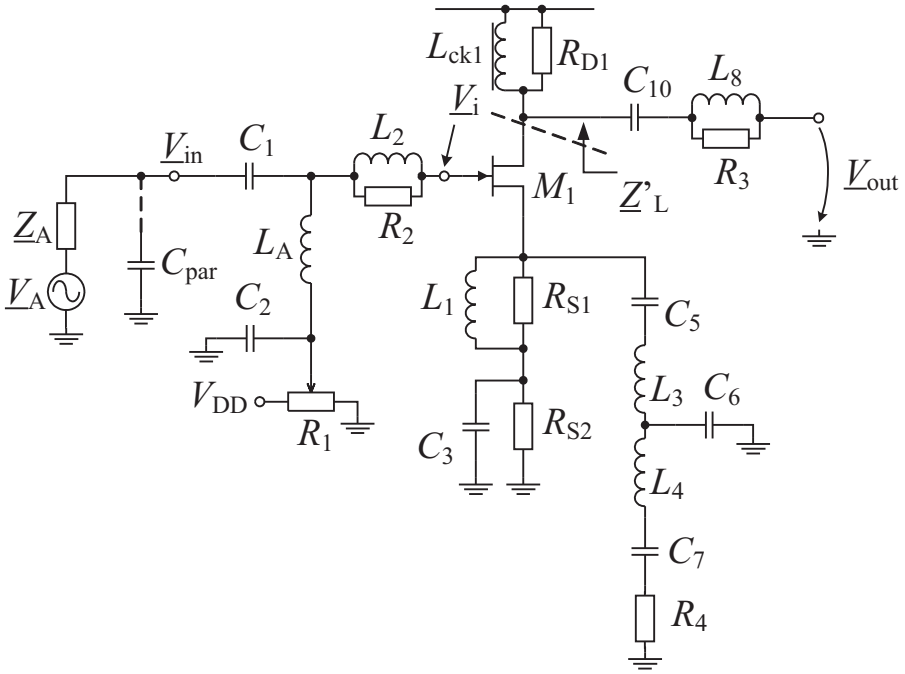

Fig. 7.6: Schematic of the Band-III path in the FM/DAB amplifier.

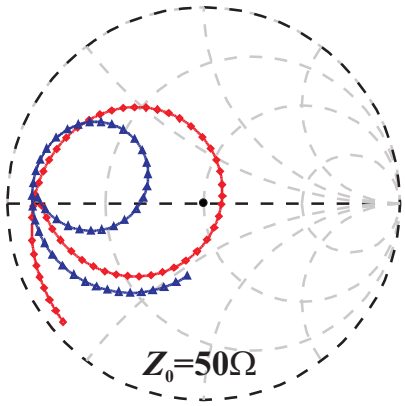

Fig. 7.7: Impedance of the Band-III degeneration: (◇) without FM degeneration; (△) FM degeneration connected in parallel.

obvious result of connecting two impedances in parallel.

The simulated voltage gain $A_{V,T} = |\underline{V}_{out}/\underline{V}_{in}|$ of the amplifier core can be seen in Fig. 7.8(a) and the effect of the selective degeneration can be observed. The total voltage gain $A_{V,tot} = |\underline{V}_{out}/\underline{V}_A|$ (including $\underline{Z}_A$) is also plotted in Fig. 7.8(a), whereby the highest gain is achieved between 200 MHz and 230 MHz (channel blocks 8 to 12). As expected, the lower frequency range benefits from less amplification, as the degeneration impedance is quite large. For frequencies higher than 190 MHz a good flatness has also been achieved.

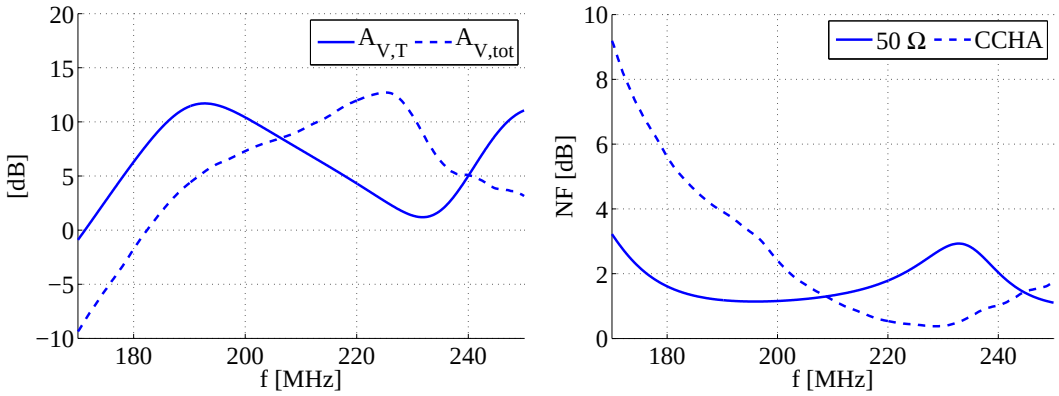

(a) Simulated Band-III voltage gain.

(b) Simulated *NF* with 50 Ω and $\underline{Z}_\mathrm{A}$ connected at the amplifier's input.

Fig. 7.8: Simulated Band-III gain and noise figure.

The simulated noise figure is shown in Fig. 7.8(b) for two cases: for a 50 Ω source impedance and for a $\underline{Z}_\mathrm{A}$ source impedance. In the first case the *NF* is almost overall lower than 2 dB and higher around the degeneration impedance peak. When the antenna element is connected, the best *NF* (about 0.4 dB) is attained around the parallel antenna resonance, with the noise performance decreasing towards lower frequencies because of lack of power gain.

7.2.3 L-Band Amplifier Path

The L-Band part of the amplifier is shown in Fig. 7.9. It is a source follower, in which the drain is not very "clean" grounded, because C_4 has a relative small value of 2.7 pF. In order to obtain voltage gain, the stage drives the L_5–C_8 network that boosts up the voltage level at its output.

The voltage gain of the core amplifier $\underline{A}_\mathrm{V} = \underline{V}_\mathrm{o}/\underline{V}_\mathrm{i}$ can be obtained with the help of the small-signal equivalent circuit in Fig. 7.10:

$$\underline{A}_\mathrm{V} = \frac{\underline{Z}_\mathrm{D} + r_\mathrm{o}(1 + \underline{Z}_\mathrm{gs} g_\mathrm{m})}{\underline{Z}_\mathrm{D} + \underline{Z}_\mathrm{gs}\left(1 + \frac{\underline{Z}_\mathrm{D}}{\underline{Z}_\mathrm{L}}\right) + r_\mathrm{o}\left(1 + \underline{Z}_\mathrm{gs} g_\mathrm{m} + \frac{\underline{Z}_\mathrm{gs}}{\underline{Z}_\mathrm{L}}\right)} \tag{7.1}$$

where $\underline{Z}_\mathrm{D}$ is the impedance in the transistor's drain, $\underline{Z}_\mathrm{L}$ the impedance in the transistor's source, $\underline{Z}_\mathrm{gs}$ the transistor's gate-source impedance and r_o the transistor's output resistance. At the L-Band frequency $\underline{Z}_\mathrm{D}$ consists mainly of C_4. Stability considerations are the reason for this "unclean" grounding of the common drain stage: experimental trials have shown that the stability of the stage is improved in the presence of a relatively small C_4.

The simulated voltage gain $A_\mathrm{V,T} = |\underline{V}_\mathrm{out}/\underline{V}_\mathrm{in}|$ of the amplifier core can be seen in Fig. 7.11(a). The total voltage gain $A_\mathrm{V,tot} = |\underline{V}_\mathrm{out}/\underline{V}_\mathrm{A}|$ (including $\underline{Z}_\mathrm{A}$) is also plotted in Fig. 7.11(a).

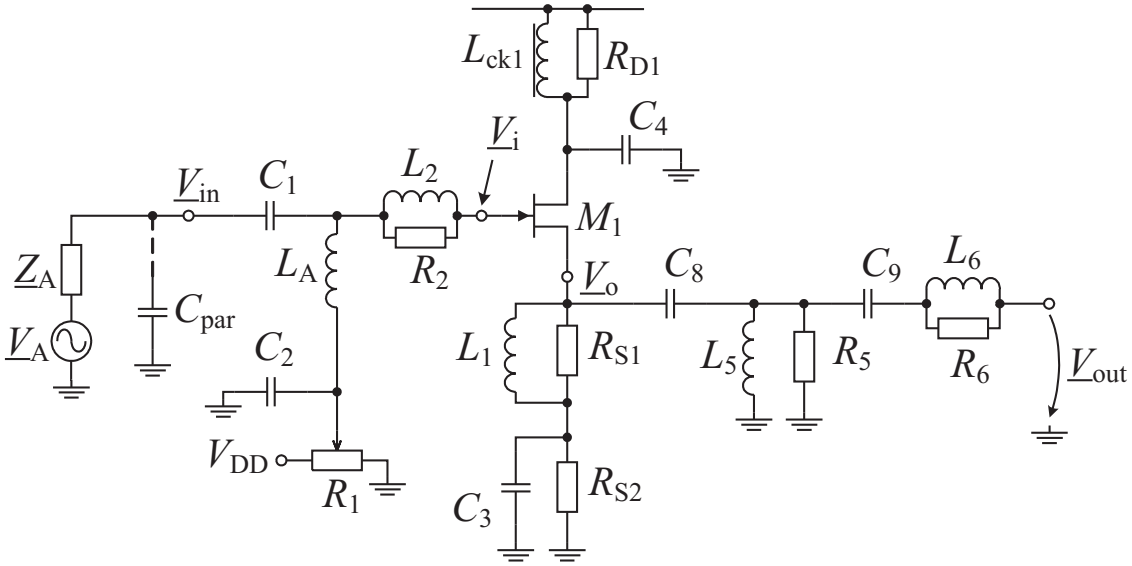

Fig. 7.9: Schematic of the L-Band path in the FM/DAB amplifier.

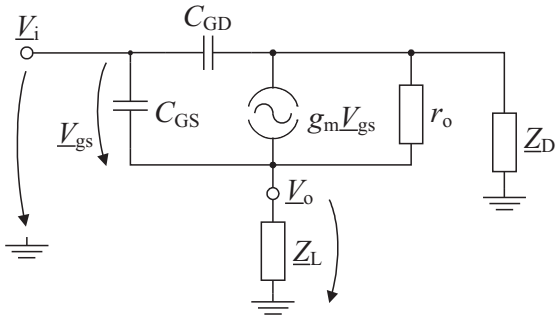

Fig. 7.10: AC small-signal equivalent circuit of the L-Band path in the FM/DAB amplifier.

The simulated noise figure is shown in Fig. 7.11(b) for two cases: for a 50 Ω source impedance and for a $\underline{Z}_A$ source impedance. In the first case the *NF* is overall about 1.3 dB, while when the antenna element is connected, the *NF* drops to about 0.8 dB.

7.2.4 Combining the FM and DAB Amplifier Paths

The different signal paths corresponding to each operating band are common at the input of the transistor, while at the output they are separated by means of filters. In Fig. 7.3 the L_8 – R_3 group prevents the L-Band signal from entering the FM/Band-III path, while the series resonance of C_9 and L_6 is tuned on the L-Band frequency and isolates it from FM and Band-III signals.

The intermodulation products occurring in one operating band and affecting the other are the main problem of this one-transistor amplifier. More specifically,

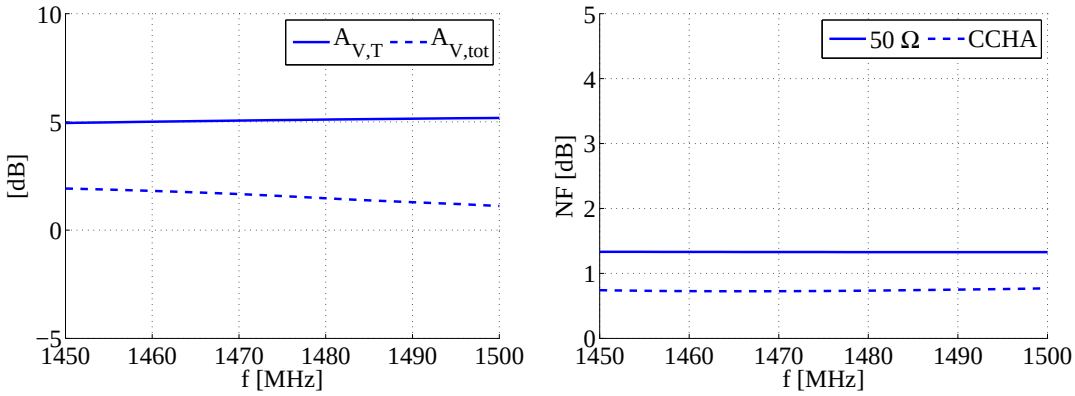

(a) Simulated L-Band voltage gain.

(b) Simulated NF with $50\,\Omega$ and $\underline{Z}_{\mathrm{A}}$ connected at the amplifier's input.

Fig. 7.11: Simulated L-Band gain and noise figure.

second order intermodulation products of strong FM stations will fall into the Band-III range.

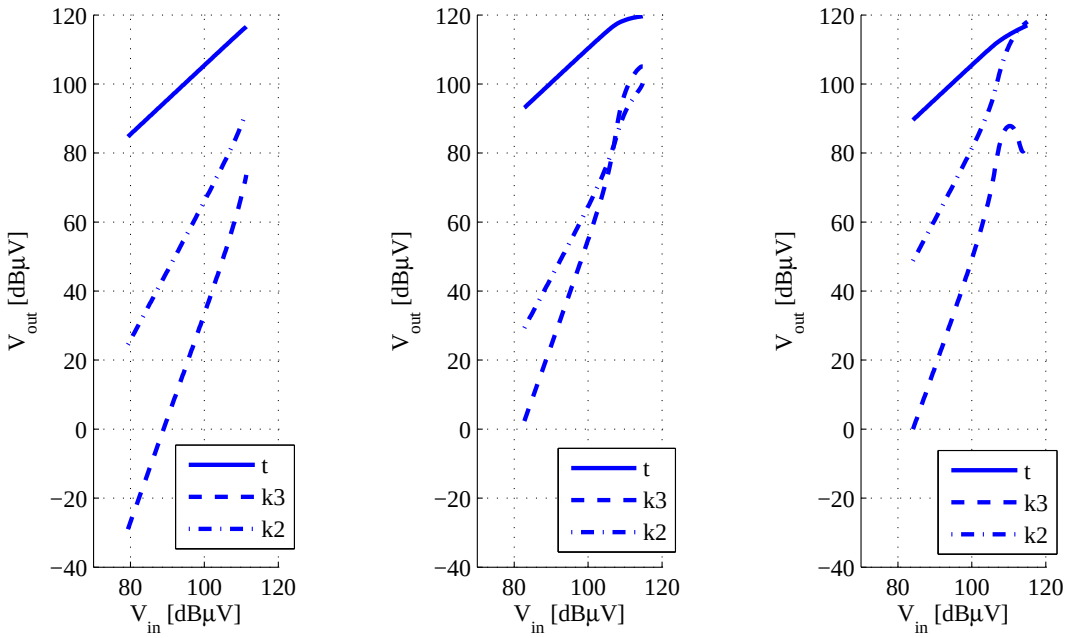

(a) FM.

(b) Band-III.

(c) L-Band.

Fig. 7.12: Simulated 2nd and 3rd order intermodulation products in FM and DAB range.

The simulated linearity performance is shown in Fig. 7.12 and the evaluated intermodulation distance is summarized in Table 7.1. As it can be seen, the specifications are fulfilled for all services as far as a_{k3} is concerned. However, as expected,

there is a serious issue concerning the FM a_{k2}.

	FM	Band-III	L-Band
a_{k3} [dB]	62.1	76.6	67.8
a_{k2} [dB]	34.6	56.6	29.8

Table 7.1: The simulated intermodulation performance achieved by the one-transistor amplifier for both FM and DAB services (110 dBµV output level for FM, 100 dBµV output level for DAB).

7.2.5 Experimental Results

The realization of the proposed FM/DAB active antenna is shown in Fig. 7.13. The transistor is biased at 30 mA. The antenna element can be mounted directly on the amplifier PCB. The layout design was aimed at minimizing any parasitic capacitance of the input node and generally ensuring the circuit's stability. Another important issue was the L-Band, because of its higher frequency which requires special attention when designing the layout.

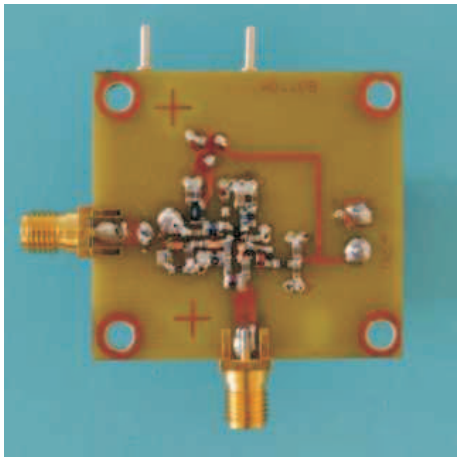

Fig. 7.13: Realized single transistor FM/DAB amplifier.

Frequency Characteristic

The voltage gain of the amplifier itself $A_{V,T} = |\underline{V}_{out}/\underline{V}_{in}|$ measured in the lab is plotted in Fig. 7.14, together with the simulation result for comparison. The experimental results fit the simulations well, especially in the FM band. In the Band-III there is a certain difference between the two curves, which is caused by the fine tuning of the realized circuit, in order to flatten the response obtained in combination with the real antenna element. The discrepancy in the L-Band is

mainly caused by the parasitic elements on the PCB that have not been fully taken into account in the simulation.

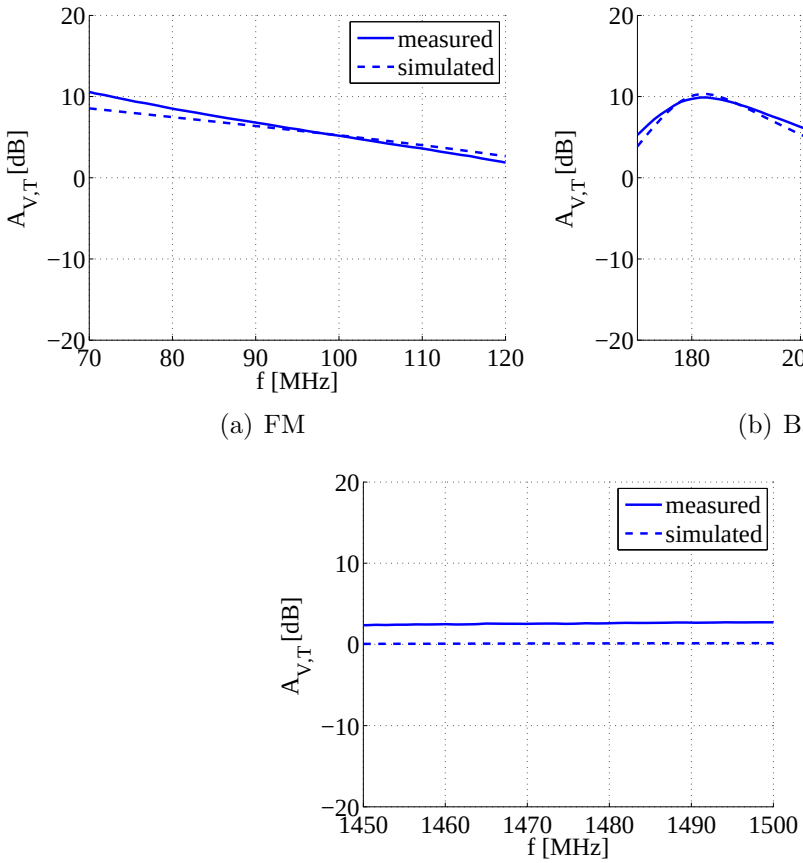

(a) FM

(b) Band-III

(c) L-Band

Fig. 7.14: FM and DAB voltage gain of the amplifier alone $A_{\mathrm{V,T}} = |\underline{V}_{\mathrm{out}}/\underline{V}_{\mathrm{in}}|$, measurement and simulation.

An indication of the achieved flatness in combination with the CCHA element can be seen in Fig. 7.32 for all three bands. The measurement took place in the lab and the results indicate the transmission between a passive sender antenna and the output of the active antenna. The single-transistor FM/DAB active antenna can be used all over the FM band, but delivers its best performance in the European range.

The frequency response in Band-III exhibits also a good flatness. In Fig. 7.32(c) depicting the L-Band range, the gain achievable with a passive 5 cm long monopole antenna is also plotted, so that it can be seen that the active FM/DAB antenna achieves in average 6 dB more signal.

Noise Performance

The measured FM output noise voltage $V_{\mathrm{out,N}}$ is depicted in Fig. 7.15 and is determined in an anechoic chamber, with the 14 cm long DAB-CCHA connected to the amplifier. For the European range the output noise level is below $-4.3\,\mathrm{dB\mu V}$, thus partially achieving the VDA recommendations[1]. The simulated values are found to provide a rather pessimistic estimate of the noise performance in the European range, as the comparison in Fig. 7.15 shows.

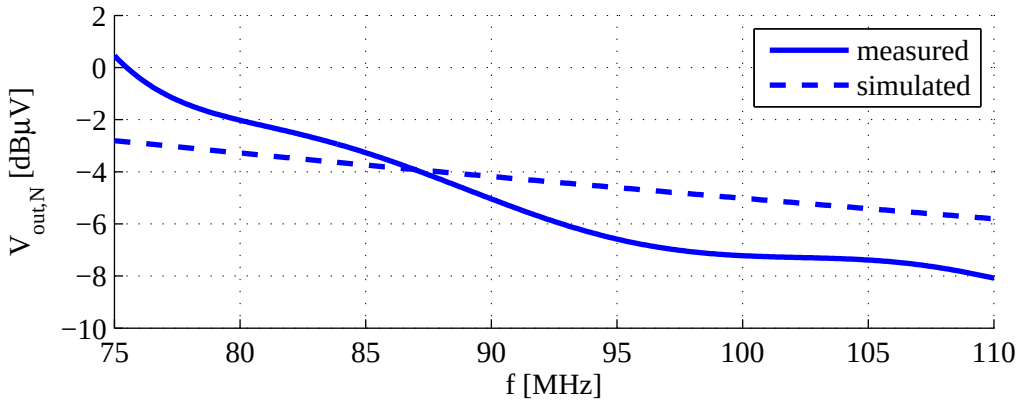

Fig. 7.15: Simulated and measured FM output noise voltage for 120 kHz bandwidth and $\underline{Z}_{\mathrm{A}}$ connected.

A comparison between the simulated and measured noise figure *NF* in Band-III and L-Band is shown in Fig. 7.16. Because the DAB requirements imposed to amplifiers are specified without the antenna element, both the simulation and the measurement took place in a $50\,\Omega$ system. Because of the tuning performed on the realized circuit, the simulated Band-III noise figure shows rather the trend of the measured data, while in the L-Band a very good agreement between measurement and simulation is obtained.

The sensitivity of the new active antenna is also measured in the anechoic chamber with the experimental setup explained in Section 4.3.4 and is referred to the sensitivity achievable under the same conditions with a passive 90 cm long rod antenna (reference antenna). The results depicted in Fig. 7.34 show that the sensitivity of the FM/DAB active helix antenna is in average 11.6 dB for the European FM range beneath the one of the reference rod.

[1]Because DAB is not planned to be introduced in Japan, a FM-DAB active antenna does not have to cover the Japanese FM range. However, the plots presented throughout this chapter include also this band, as it might be interesting from an academic point of view.

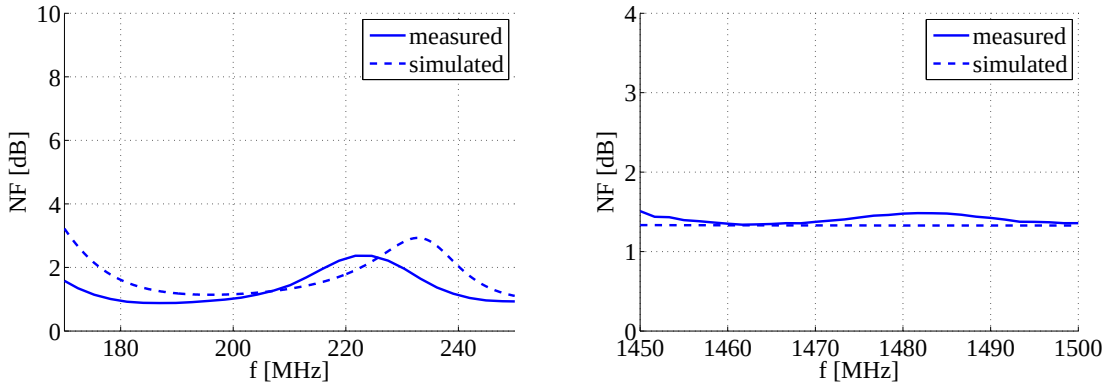

(a) Band-III. (b) L-Band.

Fig. 7.16: Simulated and measured Band-III and L-Band noise figure in a 50 Ω system.

Linearity

The linearity of the amplifier is measured in the lab in each of the operating bands and the results are plotted in Fig. 7.17. The tone frequencies used for the test and the achieved intermodulation distances are summarized in Table 7.2.

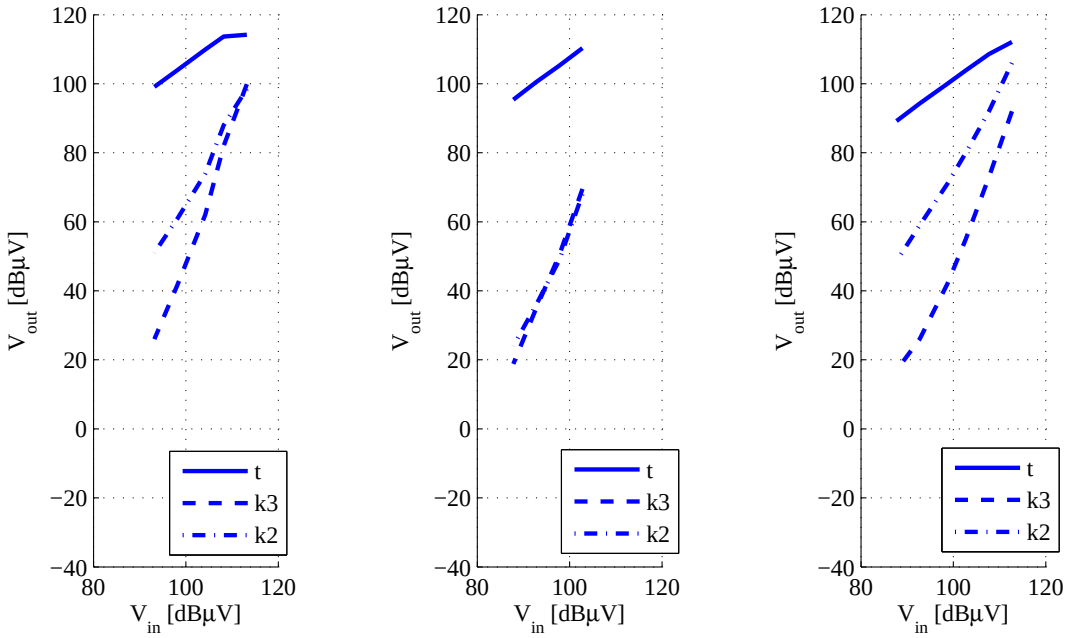

(a) FM. (b) Band-III. (c) L-Band.

Fig. 7.17: Measured 2nd and 3rd order intermodulation products in FM and DAB range.

As expected from the simulations (Table 7.1), the DAB values, with the exception

of the L-Band a_{k2}, are fulfilling the requirements. However, the 3rd and 2nd order FM intermodulation distances are poor and there is a serious issue concerning the FM-DAB interference. Additional AGC circuitry can help overcome this problem.

	FM	Band-III	L-Band
f_1 [MHz]	96	196	1470
f_2 [MHz]	98	200	1474
a_{k3} [dB]	48	68	58
a_{k2} [dB]	36	64	29

Table 7.2: The measured intermodulation performance achieved by the multipath amplifier for both FM and DAB services (110 dBμV output level for FM, 100 dBμV output level for DAB).

7.3 Multiple Transistor FM/DAB Antenna Amplifier

In order to overcome the difficulties caused by the intermodulation products affecting other bands, a solution is to process each radio band in a different amplifying path [53]. Such architecture has already been employed in the present work in Chapters 5 and 6 in order to avoid the FM-AM interference. Fig. 7.18 depicts a design in which the DAB Band-III and DAB Band-L paths are very similar to those in Fig. 7.3, but now contain different transistors: Band-III is directed towards M_2, while L-Band is amplified by M_1. The FM range is served by the M_1 and Q_1 transistors, thus having a common part with the L-Band path; this is possible, however, because FM and L-Band are not susceptible to mutual interference. The FM amplifier is very similar to the CD-CB architecture discussed in Chapter 6, but it performs no frequency flattening, since the DAB-CCHA element behaves as a capacitance in the FM range. The start-up issue is also similar to the one discussed in the previous chapters.

As it will become clear throughout this section, the main difficulty is to combine the amplifier paths in such a way, that the mutual influence is minimized.

7.3.1 FM Amplifier Path

The FM amplifier path is basically identical with the amplifier in Fig. 6.23, so that eq. (6.5) holds as well. In this new implementation the amplifier is no longer required to perform frequency equalization, so that the impedance between the common drain and the common base stage does not need to be resonant. Instead, inductor L_4 provides the required amount of feed-back to the first stage and improves the linearity. An inductor is preferred instead of a resistor in order to avoid further

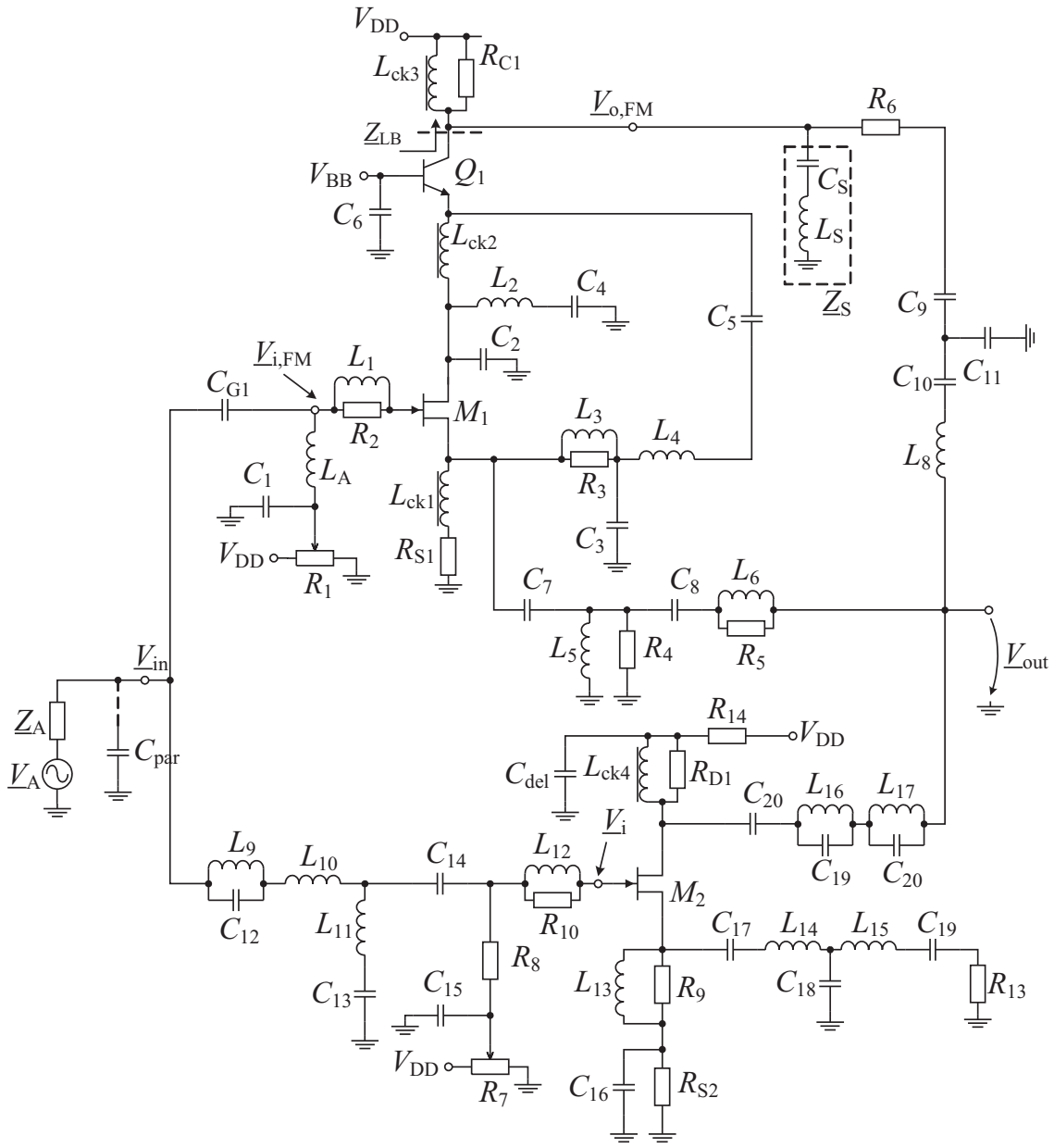

Fig. 7.18: Schematic of the three-transistor FM/DAB amplifier.

noise contribution to the circuit. When choosing L_4 a trade-off between the achieved voltage gain and linearity has to be made.

Because of the "unclean" grounding required for the L-Band path, a series resonant circuit L_2–C_4 tuned in the FM range ensures the grounding. Other aspects of the circuit, like the biasing, have already been discussed in Chapter 6.

7.3.2 Band-III Amplifier Path

The Band-III amplifier is similar to the single-transistor DAB amplifier; however, this time transistor M_2 serves only the DAB path. The gate biasing is now achieved with the help of the R_8 resistor, while resistor R_{14} shifts down the supply voltage.

7.3.3 L-Band Amplifier Path

The L-Band amplifier is also similar to the single-transistor DAB amplifier. In this implementation it shares the first FM stage transistor, as the L-Band signal is picked-up from the source of M_1 and further transformed by the C_7–L_5 network. The mutual influence between the FM and the L-Band amplifier is minimal.

7.3.4 Combining the FM and DAB Amplifier Paths

As already mentioned, the main difficulty is represented by the interconnection of the different amplifier paths. In brief, it is difficult to obtain filters with sufficient attenuation out of band and good performance in band, when both the signal source and the load are complex.

We are starting by combining the outputs, which is a more straightforward task due to the resistive terminations. Second order intermodulation products in the FM stage have to be attenuated at the output, in order to prevent them from mixing up with the Band-III signal. This means that the filter at the output of the FM path has to have a band-pass characteristic. The filter is implemented by C_9–C_{11}–C_{10}–L_8 and provides high impedance out of band, in order not to load the other paths, while achieving a return loss better than –11 dB in FM.

The filter structure on the Band-III output path has to block FM and L-Band, while letting the DAB-Band-III signals pass. A structure can be imagined like the L_{16}–C_{19}–L_{17}–C_{20} in Fig. 7.18, that produces two parallel resonances and a series one in between. The total impedance of the filter is:

$$\underline{Z} = j \cdot \frac{\omega(L_{16} + L_{17} - \omega^2 L_{16} L_{17}(C_{19} + C_{20}))}{(1 - \omega^2 L_{16} C_{19})(1 - \omega^2 L_{17} C_{20})} \tag{7.2}$$

so that the series resonance occurs at:

$$\omega_{\mathrm{S}} = \sqrt{\frac{L_{16} + L_{17}}{L_{16} L_{17}(C_{19} + C_{20})}} \tag{7.3}$$

while the parallel resonances are found at:

$$\omega_{\mathrm{P1}} = \frac{1}{\sqrt{L_{16} C_{19}}}; \quad \omega_{\mathrm{P2}} = \frac{1}{\sqrt{L_{17} C_{20}}} \tag{7.4}$$

Knowing the desired resonance frequencies, one of the components can be chosen as the independent variable, while all the others can be written as a function of it. For example, if L_{16} is the independent variable, then we have:

$$L_{17} = -L_{16} \cdot \frac{\omega_{\mathrm{P1}}^2(\omega_{\mathrm{P2}}^2 - \omega_{\mathrm{S}}^2)}{\omega_{\mathrm{P2}}^2(\omega_{\mathrm{P1}}^2 - \omega_{\mathrm{S}}^2)} \tag{7.5}$$

while the capacitances can be calculated from the parallel resonances. The value of L_{17} is dictated by the minimum practical value of C_{20}, because PCB parasitics make difficult the accommodation of capacitances lower than 1 pF. For $C_{20} = 1\,\mathrm{pF}$ we need $L_{17} = 12\,\mathrm{nH}$ in order to obtain the resonance in the L-Band range. As a consequence, $L_{16} = 56\,\mathrm{nH}$ and $C_{19} = 47\,\mathrm{pF}$.

The L-Band output is protected by the L_6–C_8 series resonant circuit tuned on the L-Band.

The input of the Band-III amplifier has to be prepared in a special way. The gate of the M_2 transistor is using the resistor R_8, which has a moderate value. This is done so in order to improve the stability, while still maintaining its high-impedance character.

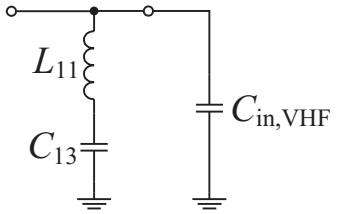

Fig. 7.19: Simplified representation of the Band-III input filter.

The next main concern is the strong FM signal: if it reaches the Band-III amplifier, then the intermodulation products occurring in M_2 will affect the DAB range. That is why the FM band has to be strongly attenuated. A parallel resonant circuit connected in series on the signal path proves to be inefficient for blocking FM, as the input of the Band-III amplifier is high-ohmic and thus the voltage division between the LC tank and the input is not effective. Better results are attained by connecting towards ground a series resonant circuit like L_{11}–C_{13} in Fig. 7.18, that is tuned on FM. As the resonant circuit behaves inductive beyond resonance, it can be used to produce a parallel resonance in the Band-III range. If $C_{\mathrm{in,VHF}}$ is the input capacitance of the Band-III amplifier, then this filter can be simplified represented as in Fig. 7.19. The filter input impedance can be written as:

$$\underline{Z} = \frac{1 - \omega^2 L_{11} C_{13}}{j\omega(C_{13} + C_{\mathrm{in,VHF}} - \omega^2 L_{11} C_{13} C_{\mathrm{in,VHF}})} \tag{7.6}$$

with the series and parallel resonances at:

$$\omega_{\mathrm{S}} = \frac{1}{\sqrt{L_{11} C_{13}}}; \quad \omega_{\mathrm{P}} = \sqrt{\frac{C_{13} + C_{\mathrm{in,VHF}}}{L_{11} C_{13} C_{\mathrm{in,VHF}}}} \tag{7.7}$$

which means that given $C_{\text{in,VHF}}$ and the resonance frequencies, the inductor value can be determined:

$$L_{11} = \frac{1}{C_{\text{in,VHF}}(\omega_{\text{P}}^2 - \omega_{\text{S}}^2)} \tag{7.8}$$

In our case, simulations show that $C_{\text{in,VHF}} \simeq 2.2\,\text{pF}$, so that we find $L_{11} = 384\,\text{nH}$ and $C_{13} = 6.6\,\text{pF}$. Simulations also indicate that inductance values larger than 100 nH have little impact upon the noise figure. For the practical realization, the calculated component values are rounded to the nearest standard value.

A parallel resonant circuit can now be inserted in order to mask the Band-III amplifier from the FM one (so that the FM signal is not short-circuited at the input of the FM amplifier). The main problem is now to determine how the Band-III path and filters affect the FM band. It is obvious that any capacitive loading from the Band-III path will attenuate the signal picked-up by the FM amplifier. Also, any resonant measure taken on the Band-III path will introduce a frequency dependence in the FM one.

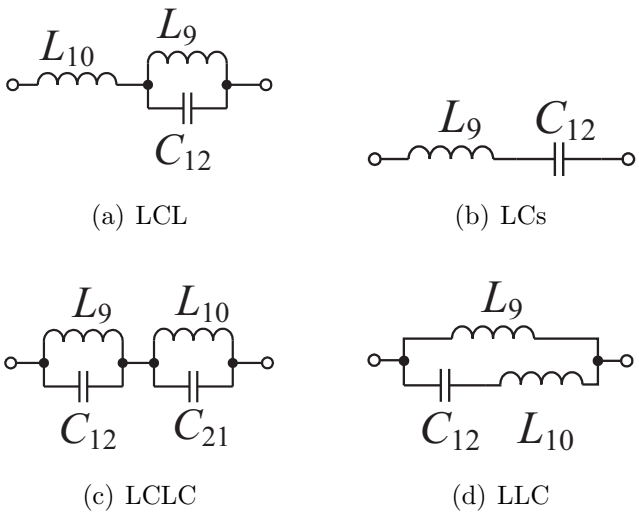

Fig. 7.20: Filter structures for the Band-III branch.

Fig. 7.20 depicts four possible input filters for the Band-III amplifier. The structures in Fig. 7.20(a) and Fig. 7.20(d) feature a parallel resonance in FM (at 100 MHz) and a series resonance in Band-III (at 200 MHz); the circuit in Fig. 7.20(b) is a simple resonant circuit tuned on the Band-III center frequency, whereby the precaution of choosing a small C_{12} has to be taken, in order to load the FM path with the smallest amount of additional capacitance possible. The structure in Fig. 7.20(c) is similar with the filter proposed for the output of the Band-III path, featuring parallel resonances in FM and L-Band and a series resonance for Band-III.

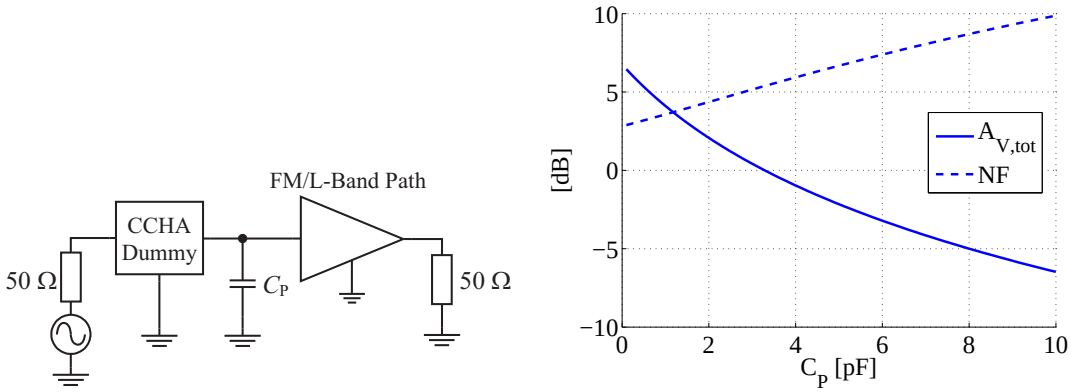

(a) Simplified schematic of the simulated circuit.

(b) Simulated voltage gain and *NF* at 100 MHz with $\underline{Z}_A$ connected at the amplifier's input.

Fig. 7.21: Estimation of the impact of C_P upon the circuit's gain and *NF* in the FM range.

LCs

We shall first investigate the effects of a direct capacitive loading upon the FM stage, as the circuit in Fig. 7.20(b) introduces. The L_9–C_{12} circuit has its resonance in Band-III and should introduce a high enough impedance in FM. Fig. 7.21(b) shows that for every pF additional capacitance on the FM input branch (simplified simulation schematic in Fig. 7.21(a)) both the voltage gain and the noise figure degrade considerably. Accepting an effective[2] additional capacitance C_P of 2 pF, then the DAB-filter can have $C_{12} \simeq 1.5\,\text{pF}$ and $L_9 \simeq 422\,\text{nH}$.

LCL

In Fig. 7.20(a) the parallel FM resonance is obtained with the help of L_9–C_{12}, while L_{10} is introduced to obtain a further series resonance in the Band-III range. The impedance of the filter can be written as:

$$\underline{Z} = j \cdot \frac{\omega(L_9 + L_{10} - \omega^2 L_9 L_{10} C_{12})}{1 - \omega^2 L_9 C_{12}} \tag{7.9}$$

so that the series and the parallel resonances occurs at:

$$\omega_S = \sqrt{\frac{L_9 + L_{10}}{L_9 L_{10} C_{12}}}; \quad \omega_P = \frac{1}{\sqrt{L_9 C_{12}}} \tag{7.10}$$

Which means that given the resonance frequencies, the inductor value L_{10} can be written as:

$$L_{10} = L_9 \cdot \frac{\omega_P^2}{\omega_S^2 - \omega_P^2} \tag{7.11}$$

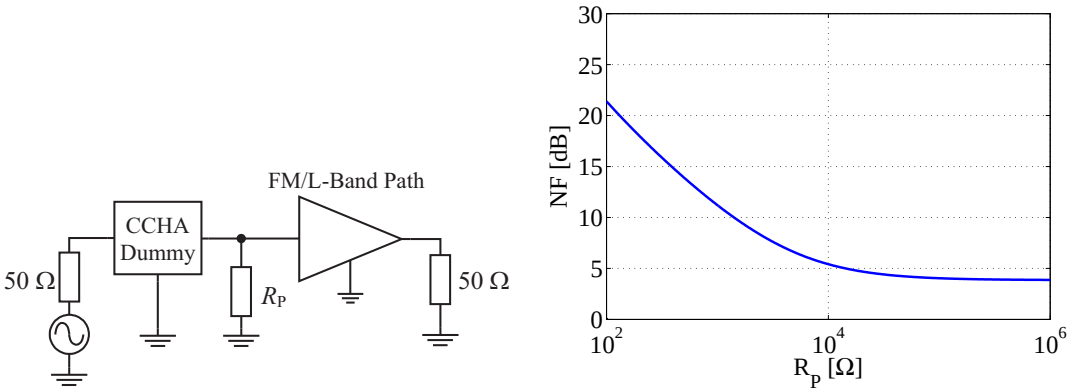

(a) Simplified schematic of the simulated circuit.

(b) Simulated *NF* at 100 MHz with $\underline{Z}_A$ connected at the amplifier's input.

Fig. 7.22: Estimation of the impact of R_P upon the circuit's *NF* in the FM range.

The required quality factor of the resonant circuit is next investigated. To do so, the tank circuit is represented at resonance only by its loss resistance R_P, as shown in Fig. 7.22(a). The value of R_P is swept and the resulted *NF* is plotted in Fig. 7.22(b). As it can be seen, R_P has to be larger than 16 kΩ in order to keep the *NF* increase below 1 dB. As $Q_P = R_P/(\omega L)$, large inductor values are required in order to keep the quality factor within a reasonable range. As for the signal behaviour alone, the inductor values should be at least 240 nH in order to keep the total impedance of the resonant circuit high enough all over European FM band. However, inductor values lower than 1 µH tend to favour a resonance in the European FM band, thus altering significantly the in-band ripple.

For $L_P = 1\,\mu H$ we get $Q_P = 25.5$, which is a practical value, and $C_P = 2.53\,pF$. Let us now investigate if there are any disadvantages concerning the other bands.

An interesting plot is obtained with the help of the circuit in Fig. 7.23, where the value of L_9 is being swept, R_P is kept constant, L_{10} is ideal and is always adjusted to obtain the series resonance at 200 MHz, while L_{11}–C_{13} consists of lossy elements. The Band-III amplifier is considered noiseless, in order to estimate only the noise contribution from the FM filter.

As expected, the noise performance in the DAB-Band-III range is better for lower values of L_9, due to the short-circuiting effect the capacitor has upon R_P. Lower L_9 values also require lower L_{10} inductances, thus allowing for a broader resonance and less losses in the Band-III range.

A compromise has to be made between the requirements for FM and those for Band-III: good FM reception demands larger L_9 values, while the reception in the Band-III requires smallest possible values for L_9. Experiment shows that $L_9 = 1\,\mu H$ is a tolerable trade-off; for the other elements we get then: $C_{12} \simeq 2.5\,pF$ and $L_{10} \simeq 330\,nH$.

[2]Equivalent capacitance of the resonant circuit in FM.

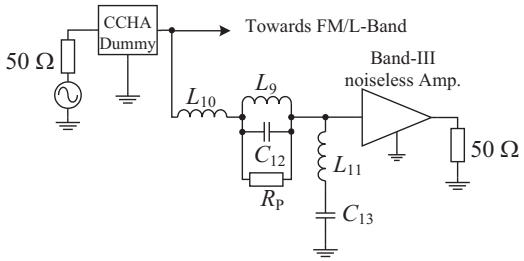

(a) Simplified schematic of the simulated circuit.

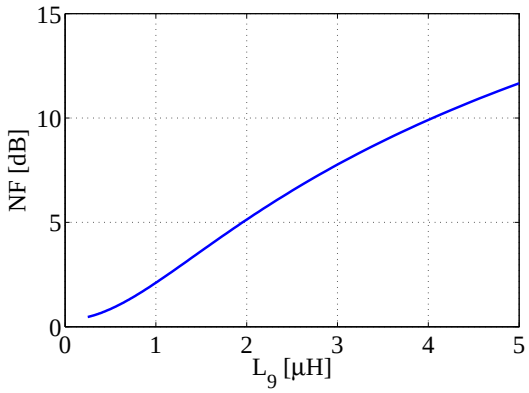

(b) Simulated *NF* at 200 MHz with $\underline{Z}_A$ connected at the amplifier's input.

Fig. 7.23: Estimation of the impact of L_9 upon the circuit's *NF* in the Band-III range.

LCLC

We shall now investigate the effects of the circuit in Fig. 7.20(c). The FM resonance introduces the same constrains like the one in Fig. 7.20(a). However, this time there are some additional constrains regarding the three resonances. The value of L_{10} is this time dictated by the minimum practical value of C_{21}: capacitances lower than 1 pF are difficult to accommodate on the PCB because of parasitics. That is why for $C_{21} = 1\,\text{pF}$ we need $L_{10} = 12\,\text{nH}$ in order to obtain the resonance in the L-Band range. As a consequence, $L_9 \simeq 56\,\text{nH}$ and $C_{12} \simeq 47\,\text{pF}$, so that the FM resonant circuit exhibits about $1.23\,\text{k}\Omega$ at resonance, if $Q_P = 35$. Consequently, the low value connected in parallel to the FM path will degrade its performance.

LLC

The impedance of the circuit in Fig. 7.20(d) can be written as:

$$\underline{Z} = \frac{j\omega L_9(1-\omega^2 L_{10}C_{12})}{\omega^2 C_{12}(L_9+L_{10})-1} \tag{7.12}$$

indicating a series and a parallel resonance:

$$\omega_S = \frac{1}{\sqrt{L_{10}C_{12}}}; \quad \omega_P = \frac{1}{\sqrt{C_{12}(L_9+L_{10})}} \tag{7.13}$$

so that capacitance C_{12} can be calculated when ω_S, ω_P and L_9 are given:

$$C_{12} = \frac{1-\left(\frac{\omega_P}{\omega_S}\right)^2}{L_9 \cdot \omega_P^2} \tag{7.14}$$

For our application with $L_9 = 1\,\mu\text{H}$ we get $L_{10} \simeq 330\,\text{nH}$ and $C_{12} \simeq 1.9\,\text{pF}$.

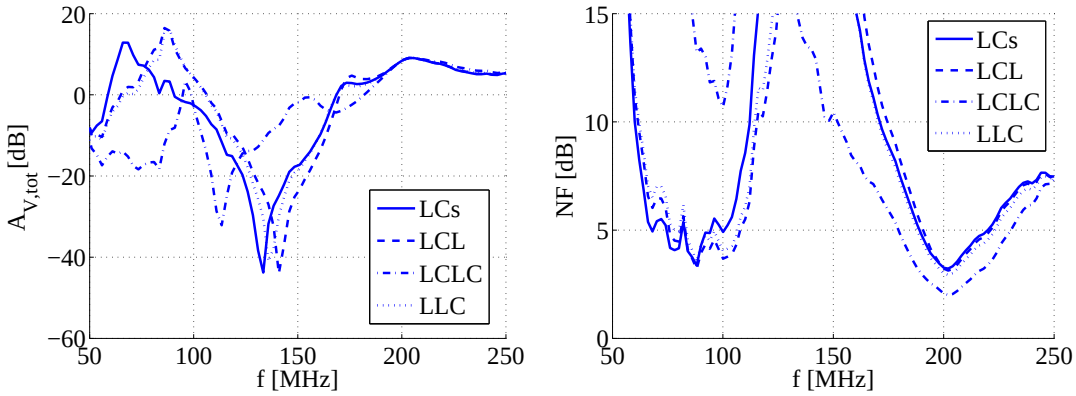

(a) Simulated total voltage gain.

(b) Simulated *NF* with $\underline{Z}_{\mathrm{A}}$ connected at the amplifier's input.

Fig. 7.24: Simulated voltage gain and noise figure for different filter configurations.

Comparison between the different filter implementations

A direct comparison between the performance achievable with these filter configurations is shown in Fig. 7.24. The configuration "LCs" (Fig. 7.20(b)) is the only one which provides a relatively flat FM response, since it loads the FM input mainly with a capacitance. However, it worsens the Band-III noise figure, and the FM voltage gain is significantly lowered. The Band-III *NF* can be improved by lowering L_9, but this measure requires a higher capacitance, which in turn further affects the FM path.

The "LCLC" filter does provide a good *NF* in Band-III, but it seriously affects FM, thus making it unusable. The "LCL" and "LLC" structures are very similar, the latter exhibiting marginally better noise figure in the Band-III range and somewhat poorer noise figure in the FM band.

The presence of the Band-III amplifier has little influence upon the L-Band one, and every filter implementation described so far offers about the same results. In Fig. 7.25 are shown the voltage gain and the noise figure attained in the presence of the "LCL" filter and it can be seen that a noise figure of about 0.7 dB can be thus obtained, when the DAB-CCHA is connected.

It is further assumed that the FM stage needs no protection against Band-III signals, since these are usually lower in magnitude and do not produce intermodulation products that may disturb FM. However, a high-pass filter action is taken by means of C_{G1}–L_{A} in order to protect the stage against strong AM signals.

The simulated linearity performance is shown in Fig. 7.26 and the evaluated intermodulation distance is summarized in Table 7.3. The 3$^{\mathrm{rd}}$ order FM intermodulation distance has a moderate value, indicating the trade-off between gain and linearity made when choosing the value of L_4. However, the FM-DAB intermodulation issue has now been alleviated, as a comparison with Table 7.1 reveals.

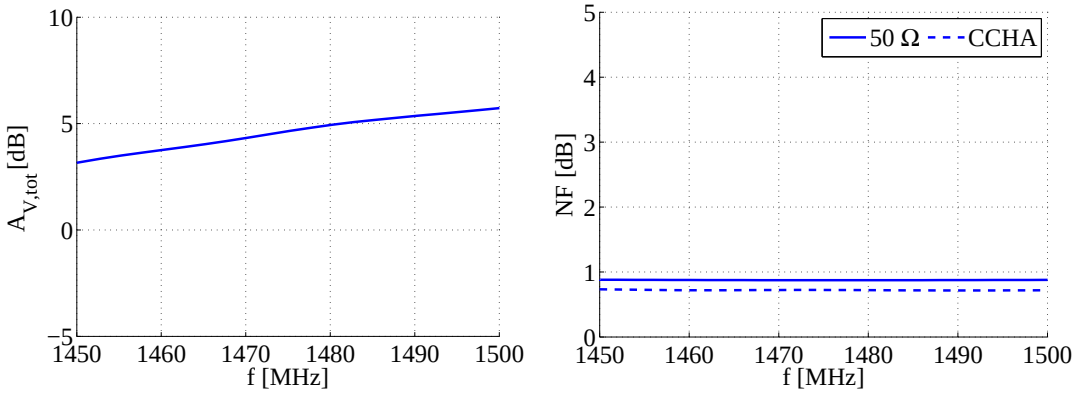

(a) Simulated L-Band total voltage gain.

(b) Simulated *NF* with 50 Ω and $\underline{Z}_A$ connected at the amplifier's input.

Fig. 7.25: Simulated L-Band gain and noise figure.

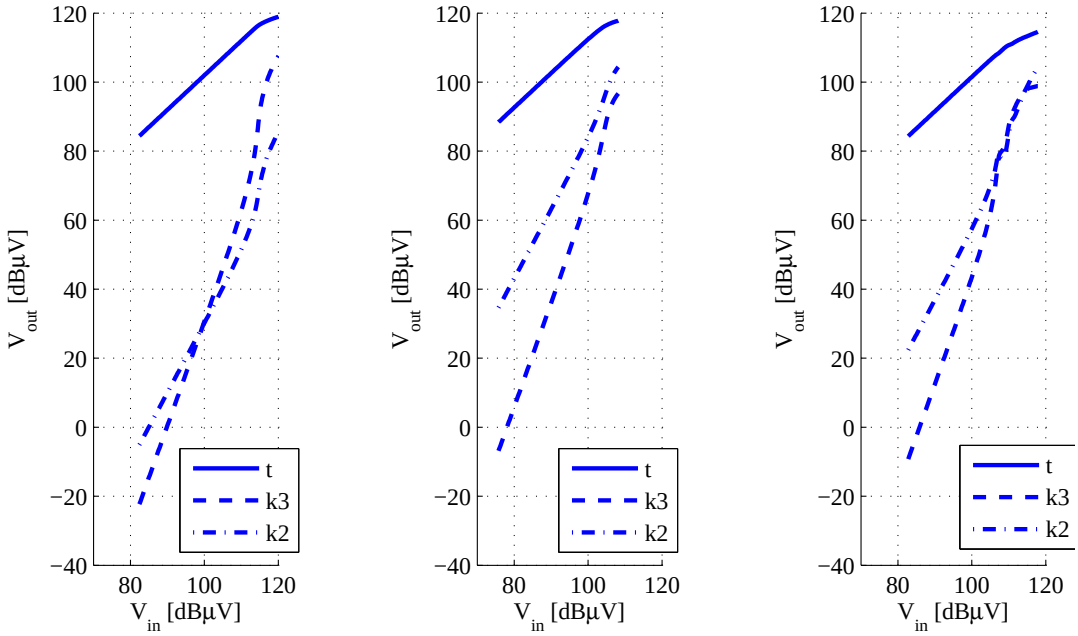

(a) FM.

(b) Band-III.

(c) L-Band.

Fig. 7.26: Simulated 2nd and 3rd order intermodulation products in FM and DAB range.

The specifications are fulfilled for the DAB services as far as a_{k3} is concerned, and almost fulfilled when it comes to a_{k2}.

	FM	Band-III	L-Band
a_{k3} [dB]	54	72	61.2
a_{k2} [dB]	63	42	45.6

Table 7.3: The simulated intermodulation performance achieved by the three-transistor amplifier for both FM and DAB services (110 dBμV output level for FM, 100 dBμV output level for DAB).

7.3.5 Experimental Results

The realization of the proposed FM/DAB active antenna is depicted in Fig. 7.27. The antenna element is mounted directly on the amplifier PCB, in order to avoid additional capacitive loading at the input node. The layout design was aimed at minimizing any parasitic capacitance of the input node and generally ensuring the circuit's stability.

Fig. 7.27: Realized 14 cm long DAB-CCHA antenna mounted on the three-path FM/DAB amplifier.

Frequency Characteristic

The voltage gain of the amplifier itself $A_{V,T} = |\underline{V}_{out}/\underline{V}_{in}|$ measured alone in the lab is plotted in Fig. 7.28, together with the simulation result for comparison. The experimental results fit the simulations well, especially in the FM band. The effect of the L_S–C_S resonance can be also observed well in Fig. 7.28(a). In the Band-III there is a certain difference between the two curves, which is caused by the fine tuning of

the realized circuit, in order to flatten the response obtained in combination with the real antenna element. The discrepancy in the L-Band is mainly caused by the parasitic elements on the PCB not fully taken into account in the simulation.

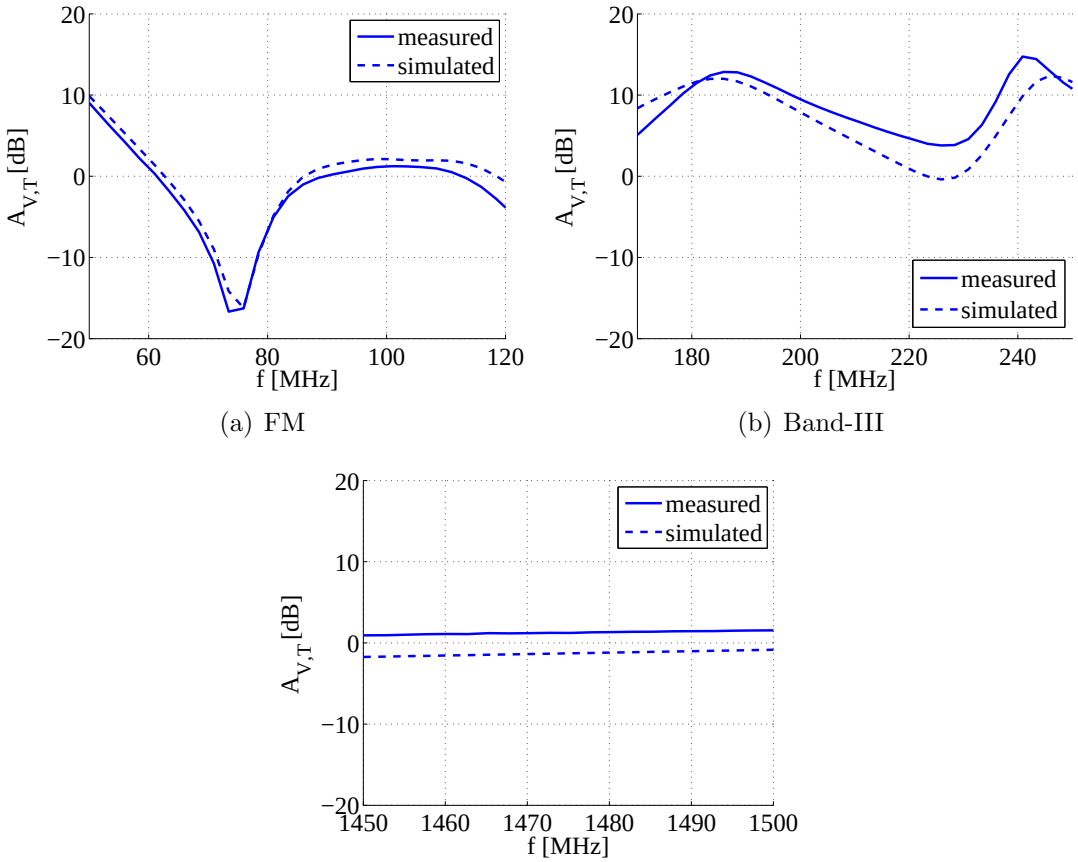

(a) FM

(b) Band-III

(c) L-Band

Fig. 7.28: FM, Band-III and L-Band voltage gain of the amplifier alone $A_{V,T} = |\underline{V}_{out}/\underline{V}_{in}|$, measurement and simulation.

An indication of the achieved flatness in combination with the CCHA element can be seen in Fig. 7.32 for all three bands. The measurement took place in the lab and the results indicate the transmission between a passive transmit antenna and the output of the active antenna. The three-transistor FM/DAB active antenna achieves good flatness in the European FM and Band-III ranges. In Fig. 7.32(c) depicting the L-Band range, the gain achievable with a passive 5 cm long monopole antenna is also plotted. The active antenna achieves in average 5.2 dB more signal than the passive counterpart.

Noise Performance

The measured FM output noise voltage $V_{\mathrm{out,N}}$ is depicted in Fig. 7.29 and is determined in an anechoic chamber, with the 14 cm long DAB-CCHA connected to the amplifier. For the European range the output noise level is below $-5.2\,\mathrm{dB\mu V}$, thus achieving the VDA recommendations. The simulated values are found to provide a rather pessimistic estimate of the noise performance, as the comparison in Fig. 7.29 shows.

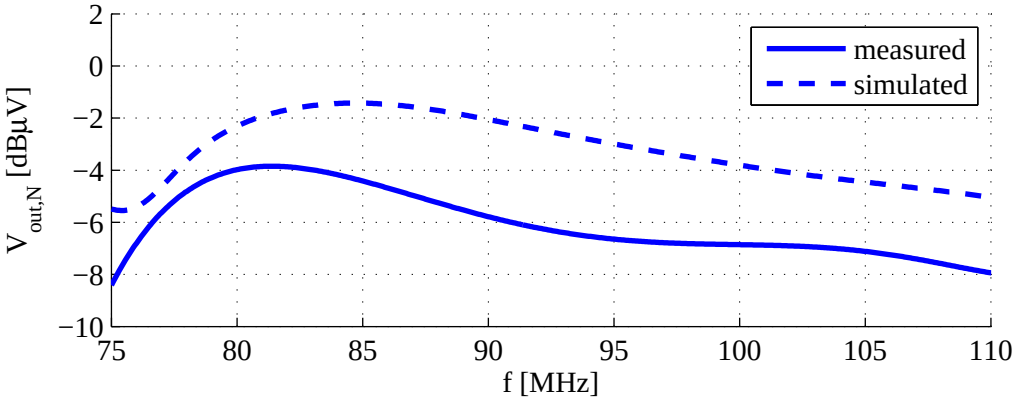

Fig. 7.29: Simulated and measured FM output noise voltage for 120 kHz bandwidth and $\underline{Z}_{\mathrm{A}}$ connected.

A comparison between the simulated and measured noise figure *NF* in Band-III and L-Band is shown in Fig. 7.30. Because the DAB requirements imposed to amplifiers are specified without the antenna element, both the simulation and the measurement took place in a $50\,\Omega$ system. As expected, the simulated Band-III noise figure shows rather the trend of the measured data, while in the L-Band a very good agreement between measurement and simulation is obtained.

The sensitivity of the new active antenna measured in the anechoic chamber with the same experimental setup so far employed is depicted in Fig. 7.34 and it shows that the FM sensitivity of the FM/DAB active helix antenna is in average 13.5 dB (European range) beneath the one of the reference rod, which is an important performance loss.

Linearity

The linearity of the amplifier is measured in the lab in each of the operating bands and the results are plotted in Fig. 7.31. The tone frequencies used for the test and the achieved intermodulation distances are summarized in Table 7.4.

As expected from the simulations (Table 7.3), the 3^{rd} and 2^{nd} order FM intermodulation distances have moderate values. The DAB values are somewhat lower than expected, but with the exception of the Band-III a_{k2}, all other requirements are almost fulfilled.

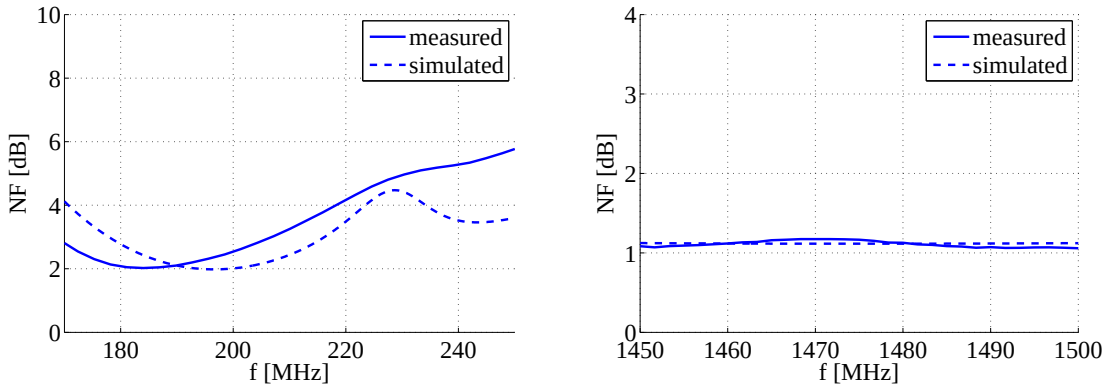

(a) Band-III. (b) L-Band.

Fig. 7.30: Simulated and measured Band-III and L-Band noise figure in a 50 Ω system.

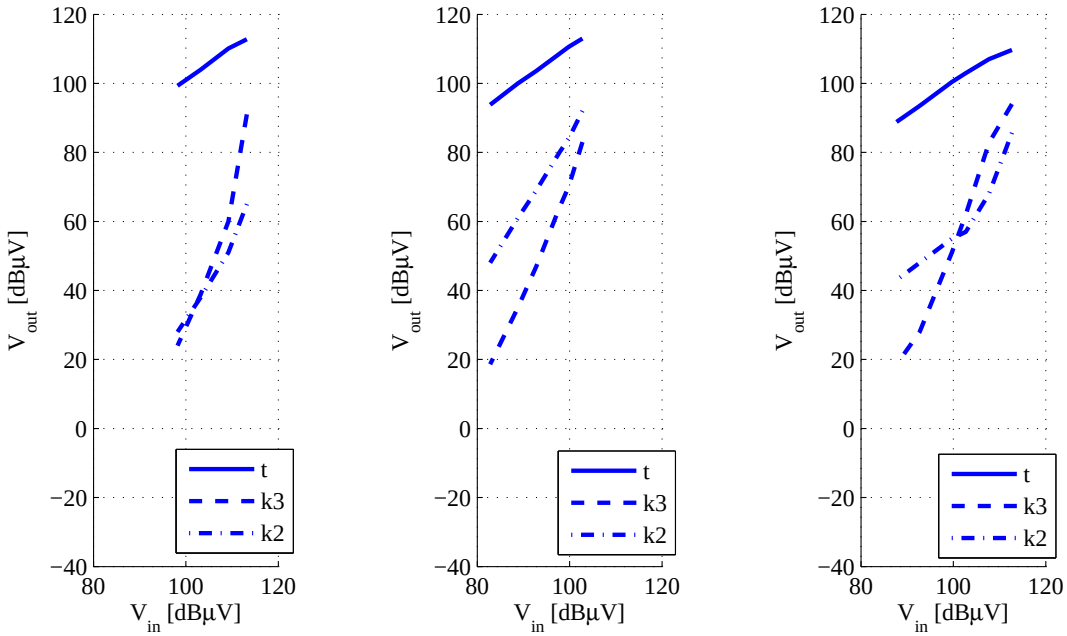

(a) FM. (b) Band-III. (c) L-Band.

Fig. 7.31: Measured 2nd and 3rd order intermodulation products in FM and DAB range.

	FM	Band-III	L-Band
f_1 [MHz]	96	196	1470
f_2 [MHz]	98	200	1474
a_{k3} [dB]	50	65	49
a_{k2} [dB]	59	39	45

Table 7.4: The measured intermodulation performance achieved by the three-transistor amplifier for both FM and DAB services (110 dBμV output level for FM, 100 dBμV output level for DAB).

7.4 One-Transistor Amplifier vs. Three-Transistor Amplifier for FM/DAB

A comparison of the signal performance of the two amplifier architectures (one-transistor and three-transistor respectively) is shown in Fig. 7.32. The measurement took place in the lab and the results indicate the transmission between a passive radiating antenna and the output of the considered active antenna (DUT). The same DAB-CCHA element has been used for both amplifiers.

Fig. 7.32(a) shows for comparison also the FM curve obtained with a simple AM/FM active CCHA, similar to the one described in Chapter 6, but not sufficient enough tuned in order to correct for the in band resonance; however, it shows that both FM/DAB active antennas have inferior performance. The FM performance of the one-transistor amplifier is better, because the signal is directly fed to the active device and no further paths load its input. The connection of a further Band-III amplifier, as the case is for the three-path architecture, cannot be such designed in order not to load the FM input. This aspect has already been discussed and analysed and now we can see its influence in a direct comparison.

In the Band-III range the three-path architecture achieves a more flat response, while in L-Band both amplifiers have in average about the same performance. Fig. 7.32(c) also shows a comparison with a passive 5 cm long monopole operating in the L-Band and it is obvious that the use of an active antenna, regardless its architecture, is improving the reception.

The FM output noise voltage of the two architectures is compared in Fig. 7.33 and it can be seen that in the European FM range the two circuits have in average similar performance.

The comparison of the measured sensitivity is shown in Fig. 7.34. Both FM/DAB active antennas have lower sensitivity than the AM/FM version discussed in Chapter 6. This is because of both the antenna element itself and the structure of the amplifier. When compared to the single transistor architecture, the three-path one has inferior sensitivity, mainly because of the loading caused by filters on the input path.

The noise performance of the three-path amplifier is inferior in the Band-III

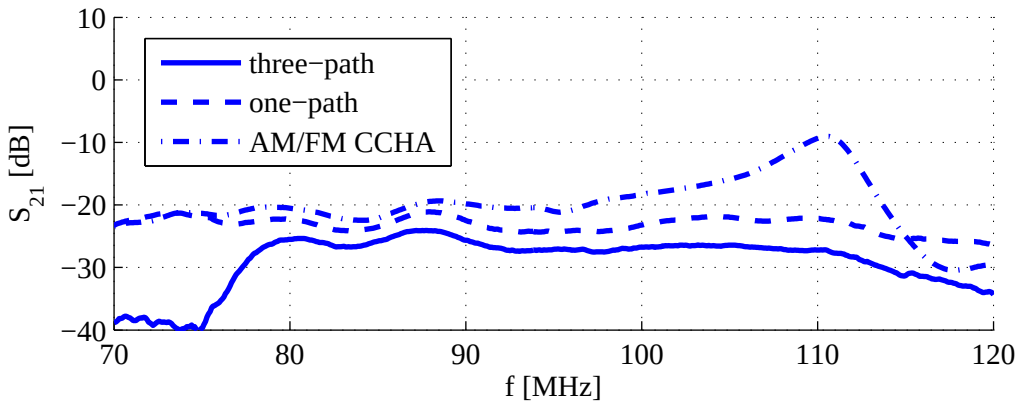

(a) FM

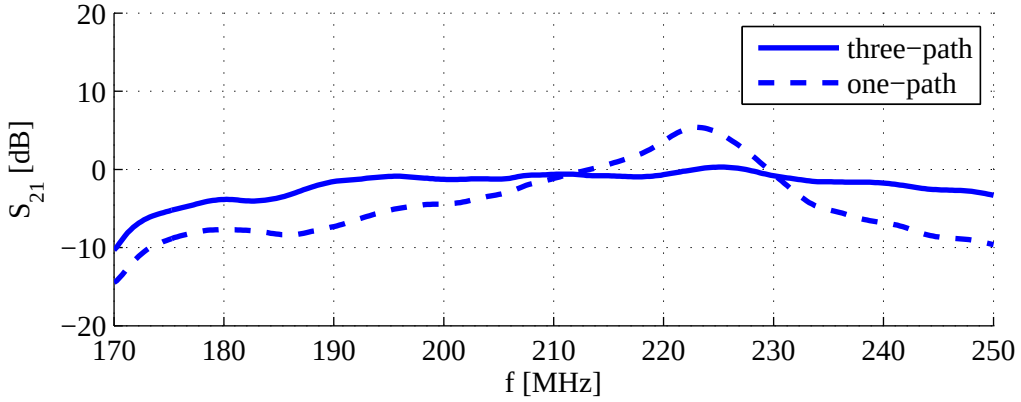

(b) Band-III

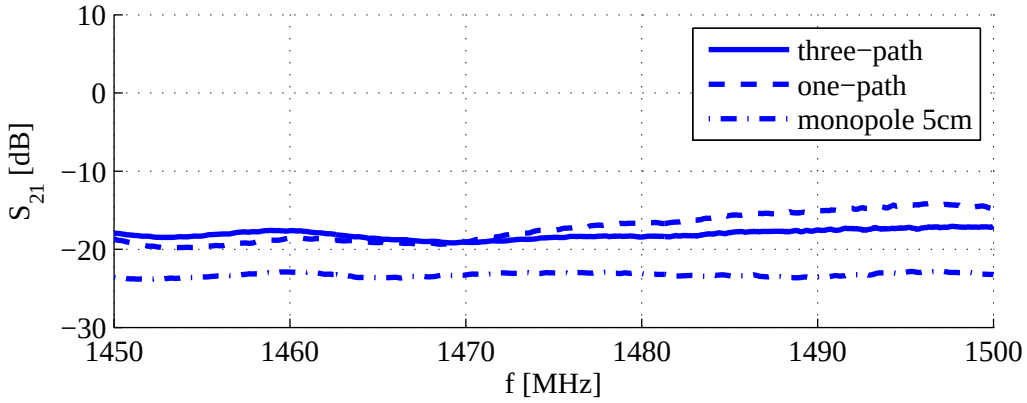

(c) L-Band

Fig. 7.32: Comparison between the signals delivered in lab field measurements by the one-transistor amplifier and the three-transistor amplifier in both FM and DAB range.

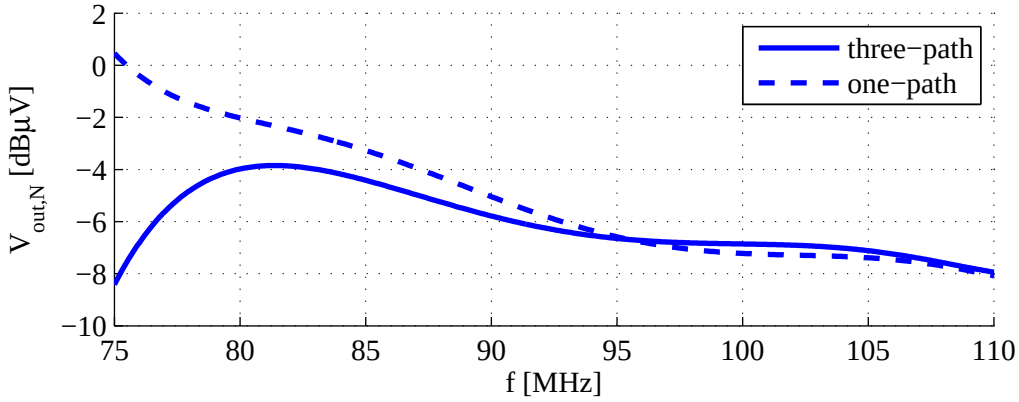

Fig. 7.33: Comparison between the measured output noise voltage achieved by the one-transistor amplifier and the three-transistor amplifier in FM range (120 kHz bandwidth, $\underline{Z}_{\mathrm{A}}$ connected).

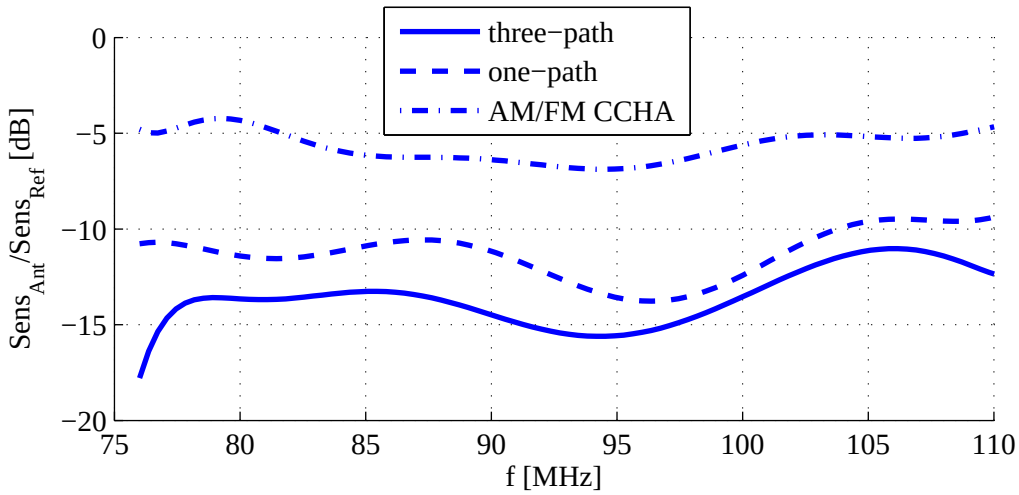

Fig. 7.34: Measured FM sensitivity and comparison between the one-transistor, three-transistor and the simple AM/FM amplifier. Results are referred to the 90 cm long passive reference rod antenna.

range, as depicted in Fig. 7.35(a). This is because of the losses and impedance transformations introduced by the filters separating the FM and DAB paths. However, in the L-Band the three-transistor amplifier exhibits marginally better noise performance.

Regarding the non-linear performance, a comparison can be made by inspecting Tables 7.2 and 7.4. The main advantage of the three-transistor architecture is a better suppression of the 2^{nd} order intermodulation products of FM signals affecting the Band-III (about 23 dB more in comparison to the one-transistor amplifier).

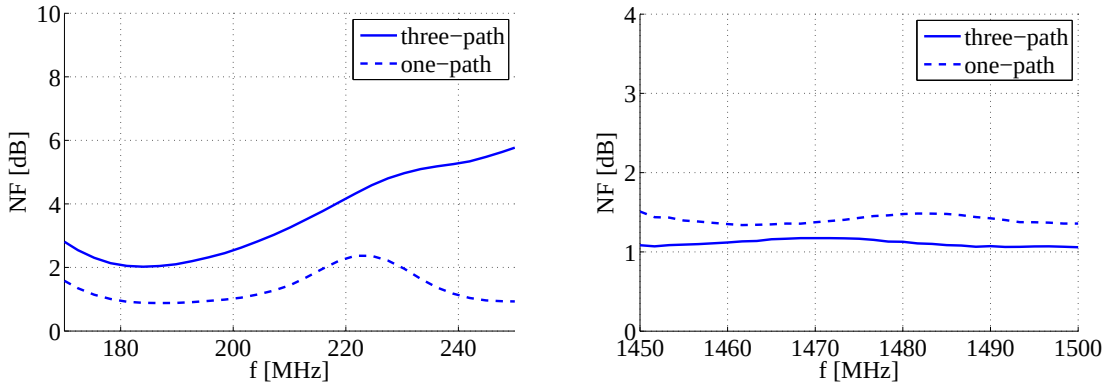

(a) Band-III. (b) L-Band.

Fig. 7.35: Comparison between the measured noise figure achieved by the one-transistor amplifier and the three-transistor amplifier in both Band-III and L-Band (50 Ω system).

7.5 Summary

The investigations performed throughout this chapter show that a capacitive coupled helical antenna (CCHA) element can be basically used for a multiservice AM/FM/DAB active antenna. In the AM and FM bands the antenna element behaves capacitive, while a resonance is tailored to arise in the Band-III. In the L-Band only a small portion of the antenna element is being used, which can be reduced to a simple $\lambda/4$ monopole. However, there are certain difficulties in implementing an appropriate multiservice amplifier.

The use of a single-transistor amplifier for the FM/DAB services has the appeal of an ultra-compact, low-cost solution, in combination with low demands imposed on the input path. However, the intermodulation issues, especially between FM and Band-III, cannot be overcome without the use of AGC circuitry.

In order to overcome the FM-DAB-Band-III intermodulation issue a separate amplifier path can be introduced for the Band-III, while the FM and L-Band can be partly processed together. However, this architecture poses some difficulties when it comes to separate the FM and DAB-Band-III signals on the input path. The filters required for this task have to introduce little losses and at the same time to mask well enough each path from the other, so that no additional loading degrades the signal. The implementation proposed here successfully splits and combines the different signal paths, however at the cost of a lower signal performance in the FM band and lower DAB-Band-III noise performance.

Chapter 8

Conclusions

Radio reception in cars belongs nowadays to everyday life. Over the years two antenna solutions have been preferred for the mass production: the active window-printed antenna and the short active rod antenna. While the first is usually met in high-end cars and achieves superior aesthetics, the latter is the usual choice for low-end cars.

In the quest for reducing the length of rod antennas, the boundaries of the available technology are reached fast. The passive version of long rod antennas, 90 cm in length, can be used for both AM and FM reception. However, further reducing the monopole length has dramatic effects upon the performance, because the antenna's capacitance, effective height, efficiency and attainable bandwidth decrease. Electrically very short monopoles are antennas whose physical length is lower than a tenth of the operating wavelength. Power matching is not possible for such monopoles and they cannot be combined with conventional techniques for broadband radio reception. The active antenna principle has to be employed, which combines the antenna element with a special designed amplifier that has to fulfil certain requirements concerning gain, noise and linearity.

The main goal of this work has been finding effective ways to deal with ultra-short rod antennas. An investigation has been performed in order to identify the active devices best suited for this task, whereby the device transconductance and noise performance are of main importance. The noise parameters of the transistors compared in this work have been experimentally measured and the resulting noise models are found to be more accurate in describing low frequency noise effects than standard simulation models do. It has been concluded that Si JFETs, due to their low flicker noise, are more appropriate for AM applications, while for FM, DAB-Band-III and DAB-L-Band the GaAs HEMT devices are preferred.

The first target has been the reduction of a simple monopole to only 20 cm height, which brings important difficulties in coping with the antenna impedance and the low effective height. A cost convenient one-transistor architecture which handles both AM and FM has been first investigated. This implementation has to address the high flicker noise issue of the HEMT transistors in the AM range.

However, due to the high transconductance of the active device, this active antenna still provides sufficient gain in the AM range. The main drawbacks are the poor sensitivity in FM and the pronounced FM to AM conversion, which occurs because of the nonlinear character of the device and the fact that both bands are amplified by the same transistor.

In order to elude this nonlinear issue, a two-path architecture is preferred, in which both AM and FM are processed separately. The AM amplifier consists of a low-noise JFET cascode which provides low input capacitance and thus achieves an outstanding measured SNR comparable to the one of the passive 90 cm reference. From an electrical point of view, all the antenna elements investigated throughout this work have in the AM range a similar behaviour to the simple monopole. As a result, this AM amplifier allows them to be used also for AM reception.

In the FM range the performance situates itself below the performance achievable with a 90 cm long passive whip antenna, because of the much reduced antenna effective height and the highly reactive character of the antenna impedance. However, this solution features sufficient linearity and can be seen as a low-cost option for AM/FM, provided that the FM sensitivity issue can be accepted.

The introduction of a novel capacitive coupled helical antenna (CCHA) allows the further reduction of the rod to only about 14 cm. Due to the more complex structure of the antenna element the effective height and the antenna impedance are improved for the operating band. The possibilities to use the CCHA for AM and FM reception have been investigated and it has been shown that the required performance can be attained in combination with a special designed high-impedance amplifier.

Such a resonant antenna structure produces very sharp resonances and is therefore difficult to be used in broadband applications. The investigation of two high input impedance amplifier configurations shows that a common-drain – common-base resonant amplifier topology can flatten the antenna frequency characteristic, while achieving low noise and low distortion. By combining the FM amplifier with an AM amplifier similar to the one previously discussed, the new active antenna can be used for automotive applications in both bands. At the same time, the overall amplifier complexity is just moderately increased.

Measurements confirm that the novel ultra-short 14 cm helical active antenna performs better than the 20 cm long active monopole antenna and achieves in average about the same signal level as a passive 90 cm long monopole antenna. Furthermore, this novel active antenna fulfills the linearity requirements and therefore does not need additional automatic gain control circuitry. The measured sensitivity is comparable to the one attained by 40 cm long active rod antennas and is sustained over the entire European and Japanese FM ranges. To the best of our knowledge, this is the first time when such short antenna elements achieve this sensitivity.

By modifying its resonant frequency, a capacitive coupled helical antenna can be used for the DAB service too. In this case the antenna element behaves capacitive

in the AM and FM bands, while a resonance is tailored to occur in the Band-III. In the L-Band only a small portion of the antenna element is used, which can be reduced to a simple $\lambda/4$ monopole.

It is however challenging to realize the right amplifier for a multiservice AM/ FM/ DAB antenna. A single-transistor amplifier has the appeal of an ultra-compact low-cost solution, in combination with the low demands imposed on the input path. However, the intermodulation issues, especially between FM and Band-III, cannot be overcome without the use of AGC circuitry.

An amplifier which separates the Band-III and processes partly together the FM and L-Band is able to alleviate the undesired FM-Band-III conversion. However, separating the FM and DAB-Band-III signals on the input path is challenging. The filters required for this have to introduce little losses and at the same time to separate well enough each path from the other, so that no additional loading degrades the signal. An extensive investigation had the purpose of finding the best suited filter topology. Besides the more complex structure, the realized active antenna shows some disadvantages concerning noise and gain in FM and Band-III when compared to the single-transistor version, but it succeeds in alleviating the linearity. The L-Band gain and noise performance is very good.

Preliminary analysis shows that the amplifier principle used in combination with the AM/FM CCHA element is also suited for other implementations of the helical architecture. Usually, the so-called "shark fin" mounted on the car roof above the rear window shelters antennas for higher frequency ranges, like GSM, GPS or Digital Satellite Radio (DSR). However, in order to enable also the reception of AM and FM without additional window-printed antennas, there are also some implementations available which make use of antenna elements with roof capacitance hidden inside the fin.

The AM/FM CCHA employed in this work can be also modified in order to fit inside a shark fin, by shortening its main body and adding a roof capacitance. Such an AM/FM antenna element can be further combined with a circular polarized ring antenna for the reception of DSR signals. The ring antenna type in [54] is able to receive the signals from both geostationary and geosynchronous highly elliptical orbit satellites. The CCHA element can be mounted in the centre of the ring antenna structure, as there arises no electromagnetic field in the DSR frequency range. In this way undesired couplings between the two antennas are avoided and the way towards a new generation of high performance highly integrated shark fin antennas is opened. In this context, except for some changes, the same amplifier architecture used in Chapter 6 can be basically employed.

Appendix A

Equivalent Noise Circuit for Two-Ports and Optimum Noise Impedance

The noise sources contained in a two-port can be various and numerous, so that an overview can become difficult, if not impossible. A good method to handle the complexity of this issue is to replace all these internal noise sources with a set of noise sources placed outside the two-port (now considered noiseless), so that the overall noise behaviour is preserved.

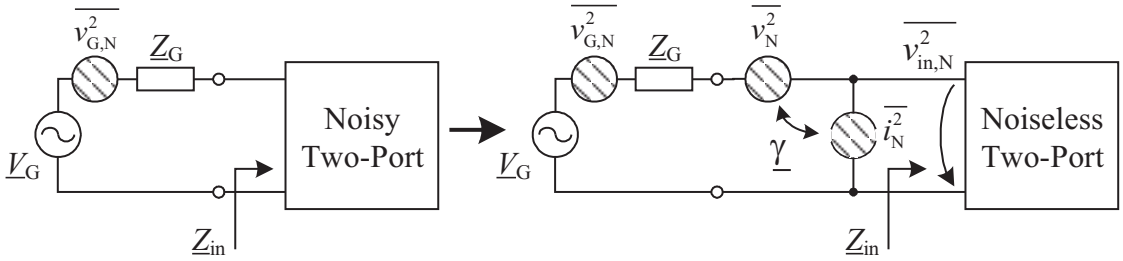

Fig. A.1: Equivalent noise circuit for a two-port.

Fig. A.1 depicts the most common way to achieve this. Two complex correlated equivalent noise sources – one voltage source and one current source – are placed before the two-port, now considered noiseless. The noise of the generator impedance $\underline{Z}_G$ is accounted for by the presence of $\overline{v_{G,N}^2}$. The two noise sources $\overline{v_N^2}$ and $\overline{i_N^2}$ are required in order to correctly describe the noise behaviour of the two-port for an arbitrary generator impedance $\underline{Z}_G$. For example, if the current source i_N were not included, then for $\underline{Z}_G \to \infty$ there would be no noise at the output port, because the entire v_N voltage would fall on $\underline{Z}_G$. This is of course incorrect, since the real two-port is always noisy. On the other hand, if the voltage source v_N were not included, then for $\underline{Z}_G \to 0$ there would be no noise at the output port, because the entire

i_N current would be short-circuited by $\underline{Z}_G$. This is again incorrect, since the real two-port is noisy also in this context. Therefore, the correct noise behaviour can be described for any $\underline{Z}_G$ only by using two noise sources at the input of the two-port.

The complex correlation coefficient $\underline{\gamma}$ arises from the fact that parts of v_N and i_N can have a common origin (i.e. the same physical cause) inside the real two-port. This correlation coefficient can be expressed analytically as [30]:

$$\underline{\gamma} = \frac{\overline{u_N i_N^*}}{\sqrt{\overline{u_N^2} \cdot \overline{i_N^2}}} \tag{A.1}$$

When calculating the noise voltage $v_{in,N}^2$ arising at the input of the two-port shown in Fig. A.1, one has to take $\underline{\gamma}$ into account. By superimposing the effects of the different noise generators we get:

$$\begin{aligned} \overline{v_{in,N}^2} &= \overline{v_{in,G}^2} + \overline{(v_{in1} + v_{in2})(v_{in1} + v_{in2})^*} = \overline{v_{in,G}^2} + \overline{v_{in1}^2} + \overline{v_{in2}^2} + \overline{v_{in1} v_{in2}^*} + \overline{v_{in1}^* v_{in2}} = \\ &= \overline{v_{in,G}^2} + \overline{v_{in1}^2} + \overline{v_{in2}^2} + 2\mathrm{Re}\{\overline{v_{in1} v_{in2}^*}\} \end{aligned} \tag{A.2}$$

where v_{in1} is the voltage at the two-port input in the absence of i_N and $v_{G,N}$, v_{in2} is the voltage at the two-port input in the absence of v_N and $v_{G,N}$, while $v_{in,G}$ is the voltage at the two-port input in the absence of v_N and i_N. After some algebra and substituting $\overline{u_N i_N^*}$ from eq. (A.1), we get:

$$\overline{v_{in,N}^2} = \frac{|\underline{Z}_{in}|^2}{|\underline{Z}_{in} + \underline{Z}_G|^2} \left(\overline{v_N^2} + \overline{v_{G,N}^2} + \overline{i_N^2} |\underline{Z}_G|^2 + 2\sqrt{\overline{u_N^2} \cdot \overline{i_N^2}} \cdot \mathrm{Re}\{\underline{\gamma} \cdot \underline{Z}_G^*\} \right) \tag{A.3}$$

When two random variables X and Y are partially correlated, then one of them can be split into two terms: the first fully correlated with the other variable, and the second fully uncorrelated [55]:

$$Y = aX + Z \tag{A.4}$$

where $\underline{a} = \underline{\gamma} \sqrt{\overline{Y^2} / \overline{X^2}}$ is a constant and $\overline{ZZ^*} = \overline{YY^*}(1 - |\underline{\gamma}|^2)$ is the uncorrelated part. This method is used for the Rothe and Dahlke noise model [30], in which a noiseless complex correlation impedance $\underline{Z}_{cor}$ is introduced to account for the correlation between $\overline{v_N^2}$ and $\overline{i_N^2}$. In this case, the noise voltage v_N can be expressed as:

$$v_N = v_N' + i_N \underline{Z}_{cor} \tag{A.5}$$

where v_N' is the uncorrelated part and $\underline{Z}_{cor}$ is in series with v_N'. The circuit noise analysis can be carried on using a superposition method like eq. (3.14). Obviously, i_N can be also decomposed instead of v_N, whereby a noiseless complex correlation admittance $\underline{Y}_{cor}$ in parallel with the noise generator eases the calculations.

Considering the equivalent noise circuit depicted in Fig. A.1, it is easy to observe that the noise applied at the two-port's input is a function of the generator impedance $\underline{Z}_{\mathrm{G}} = R_{\mathrm{G}} + j \cdot X_{\mathrm{G}}$. The noise factor can be written as:

$$F = 1 + \frac{\overline{v_{\mathrm{N}}^2} + \overline{i_{\mathrm{N}}^2} \left|\underline{Z}_{\mathrm{G}}\right|^2 + 2\sqrt{\overline{v_{\mathrm{N}}^2} \cdot \overline{i_{\mathrm{N}}^2}} \cdot \mathrm{Re}\left\{\underline{\gamma} \cdot \underline{Z}_{\mathrm{G}}^*\right\}}{4kTBR_{\mathrm{G}}} \tag{A.6}$$

It can be shown that there is a generator impedance $\underline{Z}_{\mathrm{G}} = \underline{Z}_{\mathrm{opt}}$ for which the noise factor of the two-port reaches its minimum value:

$$F_{\mathrm{min}} = 1 + 2\sqrt{\overline{v_{\mathrm{N}}^2} \cdot \overline{i_{\mathrm{N}}^2}} \cdot \frac{\gamma_{\mathrm{r}} + \sqrt{1 - \gamma_{\mathrm{i}}^2}}{4kTB} \tag{A.7}$$

where $\underline{\gamma} = \gamma_{\mathrm{r}} + j \cdot \gamma_{\mathrm{i}}$. This optimum impedance can be determined from the two noise sources and their correlation coefficient:

$$\underline{Z}_{\mathrm{opt}} = \sqrt{\frac{\overline{v_{\mathrm{n}}^2}}{\overline{i_{\mathrm{n}}^2}}} \cdot \left(\sqrt{1 - \gamma_{\mathrm{i}}^2} - j \cdot \gamma_{\mathrm{i}}\right) \tag{A.8}$$

For an arbitrary generator impedance $\underline{Z}_{\mathrm{G}}$ other than $\underline{Z}_{\mathrm{opt}}$ the noise factor will always be larger than F_{min}, as shown by eq. (3.22). This equation can be also expressed in terms of reflection coefficients [31]:

$$F = F_{\mathrm{min}} + 4R_{\mathrm{n}} \frac{\left|\underline{\Gamma}_{\mathrm{G}} - \underline{\Gamma}_{\mathrm{opt}}\right|^2}{\left(1 - \left|\underline{\Gamma}_{\mathrm{G}}\right|^2\right)\left|1 + \underline{\Gamma}_{\mathrm{opt}}\right|^2} \tag{A.9}$$

where $\underline{\Gamma}_{\mathrm{opt}}$ is the generator reflection coefficient at which minimum noise factor occurs and $\underline{\Gamma}_{\mathrm{G}}$ is the generator reflection coefficient presented to the input of the two-port.

If we represent eq. (3.22) in the Smith chart with F as parameter, we obtain a set of circles (denoted as constant noise circles) having their centers at [31]:

$$\underline{C}_{\mathrm{F}} = \frac{\underline{\Gamma}_{\mathrm{opt}}}{1 + n_{\mathrm{F}}} \tag{A.10}$$

and radii of:

$$r_{\mathrm{F}} = \frac{\sqrt{n_{\mathrm{F}}^2 + n_{\mathrm{F}}\left(1 - \left|\underline{\Gamma}_{\mathrm{opt}}\right|^2\right)}}{1 + n_{\mathrm{F}}} \tag{A.11}$$

where $n_{\mathrm{F}} = (F - F_{\mathrm{min}}) \cdot \left|1 + \underline{\Gamma}_{\mathrm{opt}}\right|^2 / (4R_{\mathrm{n}})$. Each circle represents the geometric locus of the generator impedances for which a given F is obtained. The larger the circle's radius, the larger is the noise mismatch and so the noise factor of the two-port.

Amplifiers designed around discrete active components do not offer many degrees of freedom when it comes to noise optimization. The designer can only choose a

type of active device featuring low enough noise factor and to bias the component accordingly. Next step is to provide the amplifier with the correct generator impedance $\underline{Z}_{\mathrm{opt}}$ in order to reach F_{min}. This is usually done with the help of some circuit techniques and the use of matching networks, which have to be as lossless as possible, as they are placed at the amplifier's input.

Appendix B

Types of Field Effect Transistors Used throughout this Work

This appendix overviews different types of transistors available nowadays and investigates their applicability for an active antenna. Their operation is briefly described, in order to emphasize the different features and particularities. Their small-signal equivalent circuits are presented in some detail and the noise properties are discussed, since the active device plays the major role in the output SNR of an active antenna.

B.1 Junction Field Effect Transistors (JFETs)

The silicon JFET is nowadays used mostly in discrete designs and only seldom for integrated circuits. A cross-section through a n-channel JFET is shown in Fig. B.1. A n-well is formed into the p-type substrate, and a heavily doped p^+ region is diffused into this well [56]. The p^+ and the n regions form together a p^+n junction. The p^+ diffusion is the gate of the transistor and is contacted with metal. Heavily doped n^+ wells allow for a low-resistivity contact between the n channel and the drain and source metal depositions. The substrate (bulk) is usually connected at the most negative supply voltage.

In order for the device to operate, the p^+n junction is reverse-biased. This produces a depletion layer which extends almost entirely into the n region and controls the current flow through the channel. When a high enough reverse-bias gate-source voltage has been applied, the depletion layer extends over the entire depth of the channel and the current flow between source and drain is no longer possible. This voltage is called the pinch-off voltage and is usually referred to as V_P.

In normal operation with $V_\mathrm{GS} > V_\mathrm{P}$ and $V_\mathrm{DS} > 0$, the depletion layer in the channel becomes tapered, due to the potential gradient along the channel. As long as the channel is not pinched-off at the drain end (where the reverse-bias voltage is the highest), which happens as long as $V_\mathrm{DS} \leq V_\mathrm{GS} - V_\mathrm{P}$, the transistor is said to

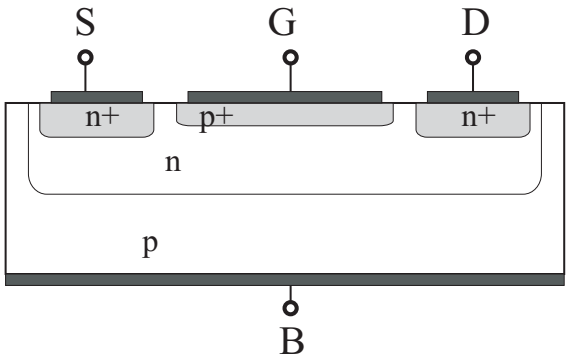

Fig. B.1: JFET cross-section

work in the *linear (triode) region*.

When the voltage between the drain end of the channel and the gate is below V_{P}, the channel is pinched-off at this point and the current saturates (remains approximately constant). The transistor operates in the *saturation region*, in which $V_{\mathrm{DS}} > V_{\mathrm{GS}} - V_{\mathrm{P}}$, and the current-voltage characteristic can be written as:

$$I_{\mathrm{D}} = I_{\mathrm{DSS}} \left(1 - \frac{V_{\mathrm{GS}}}{V_{\mathrm{P}}}\right)^2 (1 + \lambda V_{\mathrm{DS}}) \tag{B.1}$$

where I_{D} is the drain current, I_{DSS} is the drain saturation current, V_{GS} is the gate-source voltage and λ is the channel length modulation parameter. The latter can be related to the Early voltage[1] V_{A} to be $\lambda = 1/V_{\mathrm{A}}$. Because the p^+n junction is reverse biased, the gate leakage current is very small, in the range of nA.

Fig. B.2 depicts a simplified small-signal model for the JFET. R_{g}, R_{d} and R_{s} represent the parasitic ohmic contacts of the gate, drain and source, respectively. Inductive parasitic elements have been omitted. If the channel length modulation is neglected, the small-signal transconductance g_{m} can be computed by differentiating eq. (B.1):

$$g_{\mathrm{m}} = \frac{\partial I_{\mathrm{D}}}{\partial V_{\mathrm{GS}}} = \frac{2I_{\mathrm{DSS}}}{|V_{\mathrm{P}}|}\left(1 - \frac{V_{\mathrm{GS}}}{V_{\mathrm{P}}}\right) = \frac{2\sqrt{I_{\mathrm{DSS}} I_{\mathrm{D}}}}{|V_{\mathrm{P}}|} \tag{B.2}$$

The output resistance of the device can be expressed as function of the Early voltage V_{A}:

$$r_{\mathrm{o}} = \frac{1}{\lambda I_{\mathrm{D}}} = \frac{|V_{\mathrm{A}}|}{I_{\mathrm{D}}} \tag{B.3}$$

C_{GS}, C_{GD} and C_{DS} are the parasitic capacitances of the device.

[1]The Early effect describes the variation of the drain current I_{D} with the drain-source voltage V_{DS}. The Early voltage V_{A} is an intercept point obtained on the V_{DS} axis by the extrapolation of the I-V characteristic of the transistor in the saturation region (for FET). This effect holds also for bipolar transistors, if the I-V curves in the active region are extrapolated [39].

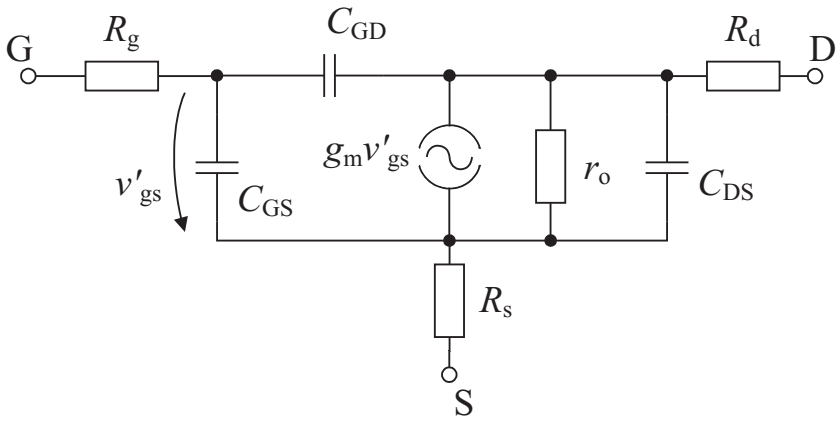

Fig. B.2: Simplified equivalent small-signal circuit for the JFET and MOSFET transistor.

B.2 Metal Oxide Field Effect Transistors (MOSFETs)

The silicon MOSFET is nowadays the natural choice for mixed-signal very large scale integration (VLSI) circuits. It allows extremely high integration density, while featuring low power consumption and low production costs [39]. Modern submicron technologies exhibit also excellent performance in the GHz range, competing with more expensive GaAs or InP processes [57] [58].

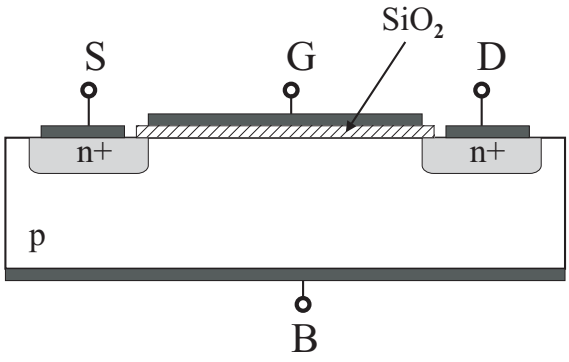

Fig. B.3: NMOS cross-section.

A cross-section through a n-channel MOSFET is shown in Fig. B.3. The device is formed in a p-type substrate. The gate consists of conductive material and is separated from the substrate by a very thin isolating layer of SiO_2. Heavily doped n^+ wells allow for a low-resistivity contact between the n channel and the drain and source metal depositions [39]. The substrate (bulk) is usually connected to the most negative supply voltage.

When no gate-source voltage V_{GS} is applied, the current flowing between drain

and source is negligible, since these regions are separated by back-to-back *pn* junctions. When a sufficient positive V_{GS} voltage is applied, a n channel is electrostatically induced by the gate in the p-type substrate and conduction between drain and source occurs. This phenomenon is called inversion and the required V_{GS} is denoted as *threshold voltage* V_T. After the inversion occurs ($V_{GS} > V_T$), the channel conductivity is controlled by V_{GS}.

Like in the case of JFET, the operation of the MOSFET also exhibits a *linear (triode) region* for $V_{DS} \leq V_{GS} - V_T$, and a *saturation region* for $V_{DS} > V_{GS} - V_T$. In the saturation region the drain end of the channel is pinched-off and the drain current I_D is ideally independent of V_{DS}. For this operation mode the current-voltage characteristic can be written as:

$$I_D = \frac{\mu_n C_{ox}}{2} \frac{W}{L} (V_{GS} - V_T)^2 (1 + \lambda V_{DS}) \tag{B.4}$$

where μ_n is the electron mobility, C_{ox} is the gate oxide capacitance per unit area, W is the gate width, L is the gate length and $\lambda = 1/V_A$ is the channel length modulation parameter (with V_A the Early voltage). A bit of algebraic manipulation reveals that this equation is very similar to eq. (B.1).

It is important to note that the gate current of MOSFETs is extremely small, in the range of a few pA, since the gate is virtually isolated from the channel.

Fig. B.2 depicts a simplified small-signal model for the MOSFET, in fact identical with the one for the JFET. The significance of the circuit elements has already been explained in section B.1. By differentiating eq. (B.4) (and neglecting the Early effect), the small-signal transconductance g_m is obtained:

$$g_m = \frac{\partial I_D}{\partial V_{GS}} = \mu_n C_{ox} \frac{W}{L} (V_{GS} - V_T) = \sqrt{2\mu_n C_{ox} \frac{W}{L} I_D} \tag{B.5}$$

B.3 Noise Models for JFETs and MOSFETs

Fig. B.4 depicts the noise model which applies for the JFET and MOSFET transistors. $\overline{v_{RgN}^2}$, $\overline{v_{RdN}^2}$ and $\overline{v_{RsN}^2}$ represent the thermal noise sources of the parasitic resistances. The drain noise current source $\overline{i_{DN}^2}$ incorporates the thermal noise exhibited by the channel and the flicker noise:

$$\overline{i_{DN}^2} = 4kT_0 P g_m B + K \frac{I_D^\alpha}{f} B \tag{B.6}$$

where $P = \frac{2}{3}$ for long channel devices and B is the bandwidth. The flicker noise is modeled with the help of the device-dependent constants K and α. The $1/f$ noise dominates the drain noise at low frequencies, while the thermal noise is predominant at high frequencies.

It should be mentioned here that P is found larger for submicron devices [39]. For both JFETs and MOSFETs, the flicker noise is caused by the existence of trapping

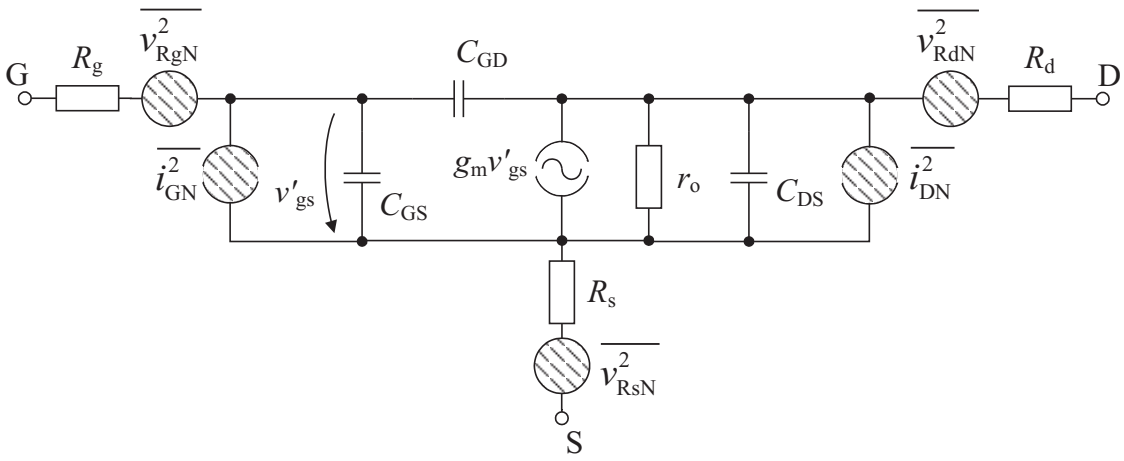

Fig. B.4: Simplified equivalent small-signal circuit for the JFET and MOSFET transistors, including the noise model.

centers, which trap and release carriers, making the channel current fluctuate. In MOSFETs, the trapping centers are located in the gate oxide or at the $Si - SiO_2$ interface. For JFETs, these centers are to be found in the depletion region and are caused by impurities and crystal defects. Devices with very low gate leakage current have also low $1/f$ noise, since the same traps are mainly responsible for both reverse current in pn junctions and $1/f$ noise [28].

The gate noise current source $\overline{i_{GN}^2}$ consists of the shot noise produced by the gate leakage current and a noise current induced on the gate by the channel thermal noise:

$$\overline{i_{GN}^2} = 2qI_G B + \frac{4kTB}{R_{eq}} \tag{B.7}$$

where I_G is the gate leakage current, and R_{eq} is an equivalent resistance which shows the amount of thermal noise "induced" from the channel on the gate through the Miller capacitor C_{GD}. This resistance can be estimated as [28]:

$$R_{eq} = \frac{1}{\omega^2 g_m (r_o || R_L)^2 C_{GD}(C_{DS} + C_L)} \tag{B.8}$$

where R_L and C_L represent the load connected to the drain of the transistor.

Concerning eq. (B.7), there are some comments to be made. The shot noise dominates at low frequencies and is normally very small for JFETs and MOSFETs, as the gate leakage current I_G is also very small. The induced gate noise increases rapidly with f^2 and is correlated with the thermal part of $\overline{i_{DN}^2}$, since both originate from the thermal noise of the channel.

B.4 Metal-Semiconductor Field Effect Transistors (MESFETs)

The GaAs MESFET is a transistor normally used for microwave applications. As a semiconductor material, the GaAs offers important speed advantages over the silicon, as the electron mobility is significantly higher.

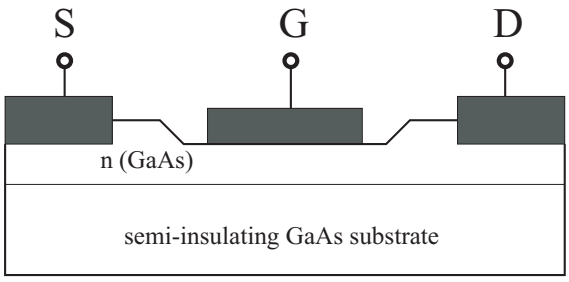

Fig. B.5: MESFET cross-section.

A cross-section through a n-channel MESFET is shown in Fig. B.5. A n-layer GaAs is diffused in an undoped (semi-insulating) GaAs substrate and a metal forming the gate is deposited on top of this layer [56]. The metal and the n-layer form together a Schottky-barrier diode. This structure is preferred, because pn-junctions are difficult to realize in materials like the GaAs. Heavily doped n^+ wells allow for a low-resistivity contact between the n channel and the drain and source metal depositions.

When the Schottky-barrier diode is reverse biased, the current in the GaAs channel is controlled by the V_{GS} voltage, like in the case of the JFET. The main difference between the operation of a MESFET and the one of a JFET consists in the way the saturation occurs. For the JFET this happens when the channel is pinched-off, while for the MESFET the electron drift velocity saturates. This phenomenon will result in the saturation of the drain current occurring at drain-source voltages lower than those for JFETs.

Since the amplifier operation requires the MESFET to be in the saturation region, we shall further discuss only this case. The current-voltage characteristic follows a square law and resembles the ones of the JFET and MOSFET [59]:

$$I_{\mathrm{D}} = \beta \left(V_{\mathrm{GS}} - V_{\mathrm{P}}\right)^2 \left(1 + \lambda V_{\mathrm{DS}}\right) \tag{B.9}$$

where β is a transconductance parameter which is device-dependent, V_{P} is the pinch-off voltage, $\lambda = 1/V_{\mathrm{A}}$ is the channel-length modulation factor and V_{A} is the Early voltage. The Early effect should be taken into account, since the output conductance of the MESFET is larger than the one of the JFET, because of current injection into the substrate [60]. Moreover, the output conductance tends to increase with the frequency.

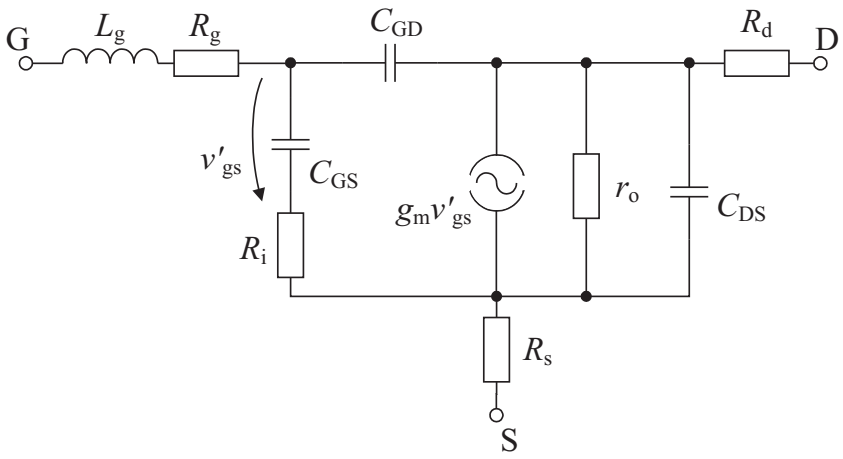

Fig. B.6: Simplified equivalent small-signal circuit for the MESFET transistor.

Fig. B.6 depicts a simplified small-signal model for the MESFET. Since the MESFET is a transistor type used for microwave frequencies, the modeling of the device is rather complex and we shall not enter into too much detail, since this is not the purpose of this work. Moreover, some of the elements shown in Fig. B.6 have different values for DC and microwave region.

As the gate signal propagates across the gate width, a delay will occur, which is accounted for by introducing the equivalent lumped elements L_g and R_g. R_i is the resistance of the channel section where the electrons drift with velocities lower than the saturation velocity. The current generator is controlled by the voltage v'_{gs} applied on the channel region with saturated velocity. The capacitance of the depletion layer will introduce a delay in the transconductance, $g_m(\omega) = g_{m0} \cdot e^{-j\omega\tau}$, where g_{m0} can be computed by differentiating eq. (B.9):

$$g_m = \frac{\partial I_D}{\partial V_{GS}} = 2\beta\,(V_{GS} - V_P)\,(1 + \lambda V_{DS}) = 2\sqrt{\beta\,(1 + \lambda V_{DS})\,I_D} \tag{B.10}$$

C_{GS}, C_{GD} and C_{DS} are the parasitic capacitances of the device. The gate-source capacitance C_{GS} is mainly determined by the depletion capacitance of the channel section with unsaturated drift velocity. The output resistance of the device is modeled with the help of r_o.

R_g, R_d and R_s represent the parasitic ohmic contacts of the gate, drain and source, respectively. Depending on the actual device geometry and packaging, geometric capacitances and inductances can be added to the basic equivalent circuit in order to make the model more accurate.

The substrate current I_{SUB} is a result of the channel current spreading into the semi-insulating substrate and is, as a consequence, gate-bias dependant. Moreover, r_o and g_{m0} are a function of I_{SUB}.

B.5 High Electron Mobility Transistors (HEMTs)

The GaAs HEMT is also used for microwave applications and it features excellent low-noise properties, combined with significant amplification.

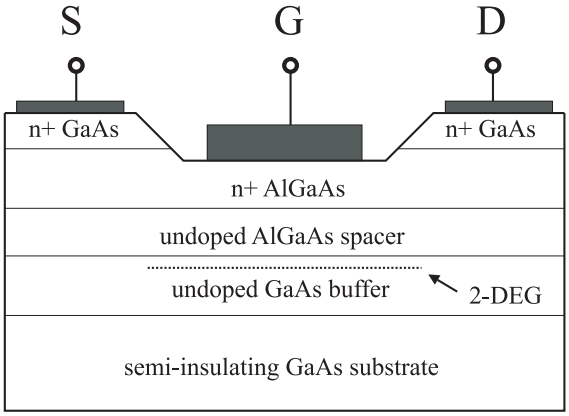

Fig. B.7: HEMT cross-section.

A cross-section through a n-channel HEMT is shown in Fig. B.7. The AlGaAs and the GaAs layers form a heterojunction in which the different band gap energies lead to a spatial separation of ions and electrons on both sides of the heterointerface. Thus an electron sheet (two-dimensional electron gas 2-DEG) is formed in the GaAs layer in the vicinity of the heterointerface. In contrast to a conventional MESFET, the scattering caused by ionized impurities is now much reduced, and the electrons contained in the 2-DEG display high mobility properties [61]. The undoped AlGaAs spacer serves the purpose to further separate the 2-DEG from the ionized donors.

Similar to the MESFET, the gate metallization and the n^+ AlGaAs layer form together a Schottky-barrier diode. Heavily doped n^+ wells allow for a low-resistivity contact to the drain and source metal depositions.

The carrier channel consists of the 2-DEG sheet and when the Schottky-barrier diode is reverse biased, the current in the channel is controlled by the V_{GS} voltage, like in the case of the MESFET. The device pinches-off by applying sufficient negative bias on the gate, so that the 2-DEG becomes completely depleted of carriers.

For a device operating in saturation, eq. (B.9) holds both for MESFETs and HEMTs. The gate leakage current of HEMTs can be significantly higher than that of MESFETs, so that it may be necessary to describe it more precisely [60]:

$$I_{\mathrm{G}} = I_{\mathrm{S}} \left(e^{\frac{q(V_{\mathrm{G}} - I_{\mathrm{G}} R_{\mathrm{g}})}{nkT}} - 1 \right) \tag{B.11}$$

where I_{S} is the Schottky diode saturation current, q the elementary charge, V_{G} the gate voltage, R_{g} the series gate resistance, n the ideality factor, k the Boltzmann constant and T the temperature.

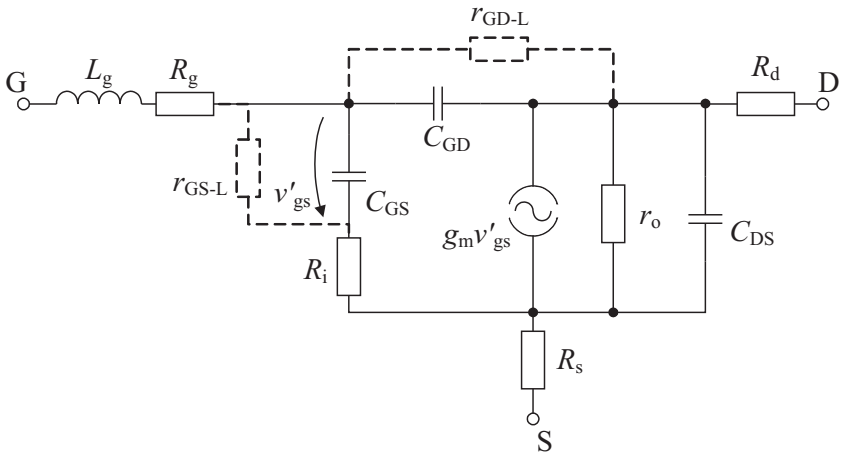

Fig. B.8: Simplified equivalent small-signal circuit for the HEMT transistor.

Fig. B.8 depicts a simplified small-signal model for the HEMT. The equivalent circuit is similar to the one presented for the MESFET, with the difference that in the case of HEMTs the gate leakage current should be taken into account by introducing the r_{GS-L} and r_{GD-L} resistors. The significance of the other circuit elements has already been explained in Section B.4. Unlike the MESFET, the well-defined 2-DEG channel allows the HEMT to sustain its transconductance g_m even at low drain current values [56].

B.6 Noise Models for MESFETs and HEMTs

Fig. B.9 depicts the noise model which applies to the GaAs MESFET and HEMT transistors. $\overline{v_{RgN}^2}$, $\overline{v_{RdN}^2}$ and $\overline{v_{RsN}^2}$ represent the thermal noise sources of the parasitic resistances. The drain noise current source $\overline{i_{DN}^2}$ incorporates the thermal noise exhibited by the unsaturated region of the channel, the diffusion noise in the saturated region and a flicker noise component [62]. Lengthy calculations can be reduced to the form:

$$\overline{i_{DN}^2} = 4kT_0 P g_m B + K\frac{I_D^\alpha}{f}B \tag{B.12}$$

where P is device dependent, B is the bandwidth, and K and α are flicker noise constants. The defects in the hetero-interface, such as they occur in HEMTs, cause an important generation-recombination noise, which dominates over the thermal noise even up to 100 MHz [61].

The gate noise current source $\overline{i_{GN}^2}$ consists of the shot noise produced by the gate leakage current and a noise current induced on the gate by the channel thermal

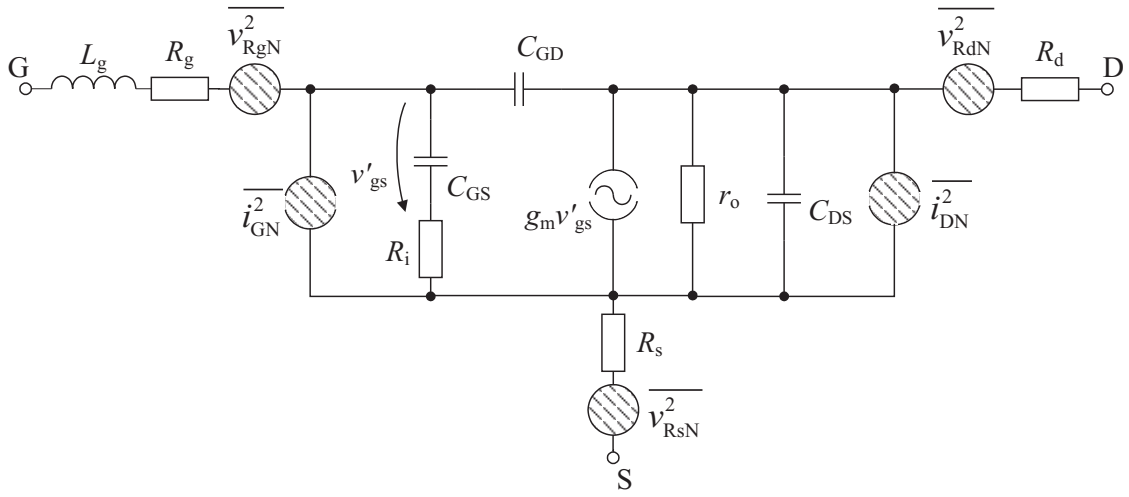

Fig. B.9: Simplified equivalent small-signal circuit for the MESFET and HEMT transistors, including the noise model.

noise. In a simplified fashion this can be written as:

$$\overline{i^2_{GN}} = 2qI_G B + 4kT_0 R \frac{(\omega C_{GS})^2}{g_m} B \tag{B.13}$$

where I_G is the gate leakage current and R is device dependent. The shot noise dominates at low frequencies and is not necessarily negligible, since the gate leakage current I_G of MESFETs and HEMTs is usually not negligible. The induced gate noise increases rapidly with f^2 and is correlated with the thermal part of $\overline{i^2_{DN}}$, since both originate from the noise of the channel.

The complex correlation coefficient between i_{DN} and i_{GN} can be expressed in a similar manner as eq. (A.1) and is imaginary and frequency independent when the induced gate noise dominates the gate noise current.

The better confinement of the channel allows the HEMT transistor to exhibit a lower noise figure than the MESFET, and this up to very high microwave frequencies [56].

Bibliography

[1] R. Mäusl, *Analoge Modulationsverfahren.* Heidelberg, Germany: Hüthig Buch Verlag, 1988, p. 175.

[2] H. Lindenmeier and J. Hopf, *Kurzwellenantennen.* Heidelberg, Germany: Hüthig Buch Verlag, 1992, p. 232.

[3] E. Armstrong, "A method of reducing disturbances in radio signaling by a system of frequency modulation," in *Proc. of the IRE*, vol. 24, 1936, pp. 689–740.

[4] L. Reiter, "Mobile Rundfunkempfangstechnik," Habilitationsschrift, Universität der Bundeswehr München, Germany, 1995.

[5] W. Fischer, *Digitale Fernsehtechnik in Theorie und Praxis.* Berlin, Germany: Springer Verlag, 2006, p. 562.

[6] World DAB, www.worlddab.org.

[7] U. Freyer, *DAB - digitaler Hörfunk.* Berlin, Germany: Verlag Technik, 1997, p. 132.

[8] H. Lindenmeier, J. Hopf, and L. Reiter, "Active AM-FM windshield antenna with equivalent performance to the whip now as standard equipment in car production," in *IEEE Antennas and Propagation Society International Symposium*, vol. 23, Vancouver, Canada, June 17–21, 1985, pp. 621–624.

[9] H. Lindenmeier, L. Reiter, J. Hopf, and A. Schwab, "Multiple FM window antenna system for scanning diversity with an integrated processor," in *IEEE 40th Vehicular Technology Conference*, May 6–9, 1990.

[10] H. Lindenmeier, J. Hopf, and L. Reiter, "Antenna and diversity techniques for broadcast reception in vehicles," in *IEEE Antennas and Propagation Society International Symposium*, vol. 2, June 18–25, 1992, pp. 1097–1100.

[11] K. Fujimoto and J. James, *Mobile Antenna Systems Handbook (Chapter 5).* Artech House, 1994, p. 617.

[12] L. Reiter, S. Lindenmeier, and A. Ramadan, "Compact antenna with novel high impedance amplifier diversity module for the common integration into narrow dielectric parts of a cars skin," in *XXVIII-th General Assembly of International Union of Radio Science (URSI)*, New Delhi, India, Oct. 23–29, 2005.

[13] H. Lindenmeier, "Relation between minimum antenna height and bandwidth of the signal-to-noise ratio in a receiving system," in *IEEE Antennas and Propagation Society International Symposium*, vol. 14, Amherst, Massachusetts, USA, Oct. 11–15, 1976, pp. 246–249.

[14] H. Lindenmeier, "Design of electrically small broadband receiving antennas under consideration of nonlinear distortions in amplifier elements," in *IEEE Antennas and Propagation Society International Symposium*, vol. 14, Amherst, Massachusetts, USA, Oct. 11–15, 1976, pp. 242–245.

[15] K. Warnick and M. Jensen, "Signal and noise analysis of small antennas terminated with high-impedance amplifiers," in *European Conference on Antennas and Propagation EUCAP 2007*, Edinburgh, UK, Nov. 11–16, 2007.

[16] P. Lindberg and A. Kaikkonen, "Internal active antenna for FM radio reception in mobile handsets," in *European Conference on Antennas and Propagation EUCAP 2007*, Edinburgh, UK, Nov. 11–16, 2007.

[17] P. Lindberg, S. Irmscher, and A. Kaikkonen, "Electrically small receive-only resonant antennas with wideband performance for FM radio reception in mobile phones," in *International Workshop on Antenna Technology iWAT 2010*, Lisbon, Portugal, Mar. 1–3, 2010.

[18] A. Ramadan, "Active antennas with high input impedance low noise and higly linear amplifiers," Ph.D. dissertation, Universität der Bundeswehr München, Germany, 2005.

[19] F. Bruccoleri, E. Klumperink, and B. Nauta, *Wideband low noise amplifiers exploiting thermal noise cancellation.* Dordrecht, The Netherlands: Springer-Verlag, 2005, p. 191.

[20] E. Nordholt and B. V. Eerden, "An integrated amplifier for an active car-radio antenna," *IEEE Journal of Solid-State Circuits*, vol. 17, pp. 591–593, 1982.

[21] Z. Chang and W. Sansen, "Low-noise, low-distortion CMOS AM wide-band amplifiers matching a capacitive source," *IEEE Journal of Solid-State Circuits*, vol. 25, pp. 833–840, 1990.

[22] E. Nordholt and D. V. Willigen, "A new approach to active antenna design," *IEEE Transactions on Antennas and Propagation*, vol. 28, pp. 904–910, 1980.

[23] "ATR4253 datasheet," Atmel Corporation, www.atmel.com.

[24] "MAX2180 datasheet," Maxim Integrated Products, www.maxim-ic.com.

[25] S. Treinies, J. Brose, J. Hopf, and S. Lindenmeier, "A method for evaluation of FM antenna diversity systems for cars," in *2010 IEEE Antennas and Propagation Society International Symposium*, Toronto, Ontario, Canada, July 11–17, 2010.

[26] G. Janzen, *Kurze Antennen*. Stuttgart, Germany: Franckh, 1986, p. 408.

[27] H. Meinke and F. W. Grundlach, *Taschenbuch der Hochfrequenztechnik*. Germany: Springer Verlag, 1968, p. 1667.

[28] C. D. Motchenbacher and J. A. Connelly, *Low-Noise Electronic System Design*. New York, USA: John Wiley, 1993, p. 422.

[29] W. W. Mumford and E. H. Scheibe, *Noise Performance Factors in Communication Systems*. Dedham, USA: Horizon House - Microwave, 1968, p. 89.

[30] G. Vasilescu, *Electronic Noise and Interfering Signals*. Germany: Springer Verlag, 2005, p. 520.

[31] G. Gonzalez, *Microwave Transistor Amplifiers - Analysis and Design*. New Jersey, USA: Prentice-Hall, 1984, p. 245.

[32] J. Rogers and C. Plett, *Radio Frequency Integrated Circuit Design*. Boston, USA: Artech House, 2003, p. 513.

[33] C. D. Motchenbacher and F. C. Fitchen, *Low-Noise Electronic Design*. New York, USA: John Wiley, 1973, p. 358.

[34] U. Rohde and T. Bucher, *Communications Receivers*. New York, USA: McGraw-Hill, 1988, p. 608.

[35] H. Meinke and F. W. Grundlach, *Taschenbuch der Hochfrequenztechnik*, 5th ed. Germany: Springer Verlag, 1992, p. 902.

[36] "VDA-Spezifikation für Fahrzeug-Antennen 240-200," Funktionsanforderungen und Messmethoden, Verband der Automobilindustrie, Jan. 2005.

[37] S. Cripps, *RF Power Amplifiers for Wireless Communications*. Boston, USA: Artech House, 1999, p. 337.

[38] H. Lindenmeier, "Optimum bandwidth of signal-to-noise ratio of receiving systems with small antennas," *AEÜ*, vol. 30, pp. 356–367, Sept. 1976.

[39] P. Gray, P. Hurst, S. Lewis, and R. Meyer, *Analysis and Design of Analog Integrated Circuits*, 4th ed. New York, USA: John Wiley, 2001, p. 875.

[40] "ATF-33143 datasheet," Avago Technologies, www.avagotech.com.

[41] "NE3508M04 datasheet," NEC Electronics Corporation, www.nec.com.

[42] A. Negut, L. Reiter, J. Hopf, and S. Lindenmeier, "Performance of a 20 cm short active AM/FM monopole antenna for automotive application," in *European Conference on Antennas and Propagation EUCAP 2009*, Berlin, Germany, Mar. 23–27, 2009, pp. 2708–2712.

[43] P. Heymann *et al.*, "Experimental evaluation of microwave filed-effect-transistor noise models," *IEEE Trans. Microwave Theory Tech.*, vol. 47, pp. 156–163, Feb. 1999.

[44] E. Perri, "Continously loaded mast antennas for vehicular applications," in *IEEE Antennas and Propagation Society International Symposium 2006*, Albuquerque, USA, July 9–14, 2006, pp. 2357–2360.

[45] A. Negut, L. Reiter, J. Hopf, and S. Lindenmeier, "High-impedance amplifier for a novel 14 cm short AM/FM automotive active antenna," in *European Conference on Antennas and Propagation EUCAP 2010*, Barcelona, Spain, Apr. 12–16, 2010.

[46] S. Klisch, "Simulation einer kapazitiv gekoppelten kurzen Helix FM-Antenne," Bachelor thesis, Universität der Bundeswehr München, Munich, Germany, Mar. 2010.

[47] "Stelco 0805 wire-wound inductors datasheet," Stelco GmbH, www.stelco.de.

[48] "Chip inductors – 0603cs series datasheet," Coilcraft Inc., www.coilcraft.com.

[49] S. Schlegel, "Optimierung von rauscharmen Hochimpedanzverstärkern für den FM-Bereich," Diploma thesis, Universität der Bundeswehr München, Munich, Germany, Nov. 2009.

[50] "BAV99 silicon switching diode datasheet," Infineon, www.infineon.com.

[51] "BFQ19 datasheet," NXP Semiconductors, www.nxp.com.

[52] "Noise figure measurement accuracy – the Y-factor method," Agilent Technologies, http://cp.literature.agilent.com/litweb/pdf/5952-3706E.pdf.

[53] S. Lindenmeier, L. Reiter, and A. Negut, "Ultra short active antenna with high impedance amplifier for AM, FM and DAB (VHF, L-Band)," in *German Microwave Conference GeMiC 2010*, Berlin, Germany, Mar. 15–17, 2010.

[54] J. Kammerer and S. Lindenmeier, "A compact car antenna with high efficiency for reception of heo- and geo-satellite signals," in *2011 IEEE APS-URSI International Symposium on Antennas and Propagation*, Spokane, Washington, USA, July 3–8, 2011, pp. 1205–1206.

[55] A. V. D. Ziel, *Noise in Solid State Devices and Circuits.* New York, USA: John Wiley and Sons, 1986, p. 306.

[56] P. Ladbrooke, *MMIC Design: GaAs FETs and HEMTs.* Boston, USA: Artech House, 1989, p. 396.

[57] L. Belostotski and J. Haslett, "Sub-0.2 dB noise figure wideband room-temperature CMOS LNA with non-50 Ohm signal-source impedance," *IEEE J. Solid-State Circuits*, vol. 42, pp. 2492–2502, Nov. 2007.

[58] E. Klumperink *et al.*, "Achieving wideband sub-1 dB noise figure and high gain with MOSFETs if input power matching is not required," in *IEEE Radio Frequency Integrated Circuits (RFIC) Symposium*, Honolulu, Hawaii, USA, June 3–5, 2007, pp. 673–676.

[59] M. Shur, *GaAs Devices and Circuits.* New York, USA: Plenum Press, 1987, p. 684.

[60] R. Anholt, *Electrical and Thermal Characterization of MESFETs, HEMTs and HBTs.* Boston, USA: Artech House, 1995, p. 324.

[61] F. Ali and A. Gupta, *HEMTs and HBTs: Devices, Fabrication and Circuits.* Boston, USA: Artech House, 1991, p. 392.

[62] R. Pucel, H. Haus, and H. Statz, *Advances in Electronics and Electron Physics*, L. Marton, Ed. New York, USA: Academic Press, 1975, vol. 38, p. 292.